

System Identification and High Performance Controllers of Active Magnetic Bearing Systems

Amin Noshadi

B.Sc., M.Sc.

Submitted in fulfillment of the requirements of the degree of

Doctor of Philosophy

(Electrical and Electronic Engineering)

College of Engineering and Science



December 2015

©Copyright by Amin Noshadi

All Rights Reserved

*To my beloved wife **MONA** and my parents
for their understanding, supports, and most of all, love.*

Abstract

In recent years, active magnetic bearing systems (AMBs) have attracted the attention of researchers as suitable replacements for conventional mechanical and hydrostatic bearings. The absence of mechanical frictions, high-precision and low maintenance costs have all made AMBs suitable technologies for high-speed and high-precision applications. However, along with the numerous advantages, several challenges have hindered the widespread applications of these systems. AMBs are inherently open-loop unstable and hence feedback controllers are essential for stabilisation of AMB equipped systems. The multiple-input multiple-output nature of AMBs and the presence of high-frequency resonant modes further exacerbate the problem of modelling and control design of such systems.

In the first step of this research, a closed-loop system identification is performed by collecting the frequency-domain response data of the system. A novel method is employed for single-input single-output (SISO) and multi-input multi-output (MIMO) modelling of the system. Next, robust controllers are designed on the basis of the obtained SISO and MIMO models. The main drawback of the available robust control algorithms is that the order of the synthesised controllers

is excessively high and hence difficult to implement. Therefore, several control design strategies are proposed to obtain lower-order robust controllers that are more reliable for implementation and product commissioning. The designed robust controllers are evaluated experimentally and it is shown that the performance of the system can be substantially improved by proper modelling and robust control design of the system compared to the conventional control design methods.

After the rotor shaft is successfully stabilised (levitated) between the magnetic bearings, it is desired to reduce the vibrations caused by the rotor imbalance, gyroscopic forces, and other unknown bounded disturbances while the rotor is spinning with the help of an attached air-turbine at one end of the rotor. A two-degrees-of-freedom (2DOF) control scheme comprising an outer-loop feedback stabiliser and an inner-loop disturbance observer-based controller (DOBC) is proposed to reduce the rotor vibrations while it is rotating at various speeds. It is observed that the presented algorithm significantly reduces the overall vibration of the system compared to single-loop control structures. Moreover, it is shown that the vibration of the rotor can be further reduced by combining the inner DOBC loop with the repetitive control structure. The proposed hybrid scheme is called repetitive disturbance observer-based control (RDOBC) throughout the thesis and the experimental results reveal the superior performance of the presented scheme over the single-loop control structures.

It is shown that the main difficulty with all “model-based” robust controllers is that an accurate model of the system is required at the control design stage. In the case of AMBs, an exceedingly high-order model is required to represent the

dynamics of the system accurately. Consequently, high-order controllers are to be designed on the basis of these high-order models. The real-time implementation of such high-order controllers is challenging and require advanced hardware. As an alternative, the design and implementation of “model-free” fuzzy logic controllers are investigated in the next step of the research. One significant advantage of the fuzzy logic controllers over the “model-based” control schemes is that an accurate model of the system is not required at the controller design stage. However, the difficulty with the design of fuzzy logic controllers is that the performance of these controllers depends highly on the proper selection of some design parameters which is usually obtained primarily based on engineering intuitions. In recent works, global optimisation algorithms are used to find optimal values of the design parameters more systematically. Yet, the performance of meta-heuristic algorithms depends not only on the size of optimisation search-domain, but also on the proper selection of the objective functions. Otherwise, the optimisation algorithm converges to undesirable values. To alleviate this problem, some novel objective functions are proposed in this thesis for the time-domain optimisation of fuzzy logic controllers. It is shown via simulation and experimental studies that by employing the presented objective functions the optimisation algorithm converges to relatively similar results regardless of the size of optimisation search-domain.

The last phase of the research investigates the idea of iterative identification and control of partially known systems and the AMBs in particular. On the one hand, the successful design of high-performance “model-based” controllers depends highly on the quality of the identified model. In order to obtain an accurate model of the system experimentally, the plant needs to be excited with

sufficiently rich probing signals. However, this is not always desirable in practice, because overly exciting the system for identification purposes may deteriorate the performance of the system and may even lead to system instability. On the other hand, the theoretical stability analysis of the “model-free” controllers is a challenging task and the stability of the closed-loop system can only be verified experimentally. In this thesis, a two-step control design algorithm is presented for the purpose of iterative identification and control of partially known systems. In the proposed algorithm, the open-loop unstable system is first stabilised by using minimum-weighted energy controllers that are designed on the basis of a rough model of the system that is only known in the low-frequency regions. Then, the closed-loop bandwidth of the stabilised system is increased cautiously and progressively until the closed-loop bandwidth cannot be further increased by the current controller. At this stage, a more accurate model of the system over an extended range of frequency is required. Once a better model is identified, new controllers can be designed on the basis of the re-identified model. The iteration can stop once the desired closed-loop bandwidth of the system is obtained. The presented algorithm allows more performance-oriented analysis of the interactions between identification and controller design stages.

Declaration

“I, Amin Noshadi, declare that the PhD thesis entitled ‘system identification and high performance controllers of active magnetic bearing systems’ is no more than 100,000 words in length including quotes and exclusive of tables, figures, appendices, bibliography, references and footnotes. This thesis contains no material that has been submitted previously, in whole or in part, for the award of any other academic degree or diploma. Except where otherwise indicated, this thesis is my own work”.



15/12/2015
Date

Acknowledgements

My first, and most earnest, acknowledgement in my doctoral studies must go to my respected supervisor, Associate Professor Dr. Juan Shi for countless discussions, invaluable guidance and support, and for encouraging me throughout my doctoral studies. I am indebted to Dr. Wee Sit Lee for his advice and directions which has enabled me not only to complete this research but also to become a better researcher. I would also like to sincerely thank Professor Peng Shi and Professor Akhtar Kalam for their constructive guidance, immense supports and the many helpful discussions during this journey.

I gratefully acknowledge the financial support provided through the Victoria University Postgraduate Research Scholarship for the whole duration of my doctoral studies. I would like to thank Ms. Elizabeth Smith for her continuous assistance and guidance throughout my studies. I would also like to thank the staff of Graduate Research Office for processing and approving my scholarship applications for attending several refereed international conferences.

I would also like to express my sincere gratitude to the entire members of staff of the College of Engineering and Science, Victoria University and all those who

provided me with the needed assistance while doing this research. A special thanks and gratitude to the Senior Technical Officers, Mr. Abdulrahman Hadbah, Mr. Takyin Chan, and Mr. Amitedo (Nitesh) Gunooory for their technical assistance and valuable supports during my doctoral studies at Victoria University.

Published/submitted papers during the author's candidature

Most of the research results reported in this thesis have been published as academic articles in refereed journals, presented as conference papers, or have been submitted as academic papers to refereed journals. A list of the published/submitted papers are:

Journal Papers

- 1) Amin Noshadi, Juan Shi, Wee Sit Lee, Peng Shi, and Akhtar Kalam “System Identification and Robust Control of Multi-Input Multi-Output Active Magnetic Bearing Systems”. *IEEE Transactions on Control Systems Technology*, (Q1 with I.F. 2.521), DOI: 10.1109/TCST.2015.2480009, 2015.
- 2) Amin Noshadi, Juan Shi, Wee Sit Lee, Peng Shi, and Akhtar Kalam “Optimal PID-type Fuzzy Logic Controller for Multi-Input Multi-Output Active Magnetic

Bearing System”, *Neural Computing and Applications*, (Q2 with I.F. 1.569), DOI: 10.1007/s00521-015-1996-7, 2015.

- 3) Amin Noshadi, Juan Shi, Wee Sit Lee, Peng Shi, and Akhtar Kalam “Robust Control of an Active Magnetic Bearing System Using H_∞ and Disturbance Observer Based Control”, *Journal of Vibration and Control*, (Q2 with I.F. 4.355), DOI: 10.1177/1077546315602421, 2015.
- 4) Amin Noshadi, Juan Shi, Wee Sit Lee, Peng Shi, and Akhtar Kalam “Synchronous Disturbance Attenuation in an Active Magnetic Bearing System Using H_∞ Controller and Repetitive Disturbance Observer-based Controller”, to be submitted.
- 5) Amin Noshadi, Juan Shi, Wee Sit Lee, Peng Shi, and Akhtar Kalam “Application of Full-Order and low-Order μ -Synthesis Controls for Robust Stabilisation of an Active Magnetic Bearing System”, to be submitted.
- 6) Amin Noshadi, Juan Shi, Wee Sit Lee, Peng Shi, and Akhtar Kalam “A Literature Review on Modelling and Control of Active Magnetic Bearing Systems”, to be submitted.

Conference Papers

- 1) Amin Noshadi, Juan Shi, Wee Sit Lee, Peng Shi, and Akhtar Kalam “Genetic Algorithm-Based System Identification of Active Magnetic Bearing System: A Frequency-Domain Approach”, *in the Proceedings of International Conference of Control and Automation*, Taiwan, pp. 1281-1286, 2014.
- 2) Amin Noshadi, Juan Shi, Wee Sit Lee, and Akhtar Kalam, “PID-type Fuzzy Logic Controller for Active Magnetic Bearing System”, *in the Proceedings of the 40th Annual Conference of IEEE Industrial Electronics*, USA, pp. 241-247, 2014.
- 3) Amin Noshadi, Juan Shi, Wee Sit Lee, Peng Shi, and Akhtar Kalam, “High Performance H_∞ Control of Non-Minimum Phase Active Magnetic Bearing System”, *in the Proceedings of the 40th Annual Conference of IEEE Industrial Electronics*, USA, pp. 183-189, 2014.
- 4) Amin Noshadi, Juan Shi, Sam Poolton, Wee Sit Lee, and Akhtar Kalam, “Comprehensive Experimental Study on the Stabilization of Active Magnetic Bearing System”, *in the Proceedings of Australasian Universities Power Engineering Conference*, Australia, pp. 1-7 2014.
- 5) Amin Noshadi, Juan Shi, Wee Sit Lee, Peng Shi, and Akhtar Kalam, “On Two-Step Controller Design for Partially Unknown Unstable Systems”, *in the Proceedings of European Control Conference*, Austria, pp. 485-490, 2015.

- 6) Edward Whittle, Amin Noshadi, Juan Shi, and Akhtar Kalam, “Experimental Study on Servo Linear Quadratic Gaussian and Observer-Based Sliding Mode Control for Active Magnetic Bearing System”, *in the Proceedings of Australian Universities Power Engineering Conference*, Australia, 2015.

- 7) Amin Noshadi, Juan Shi, Wee Sit Lee, Peng Shi, and Akhtar Kalam, “Repetitive Disturbance Observer-based Control for an Active Magnetic Bearing System”, *in the Proceedings of Australian Control Conference*, Australia, 2015.

The contents of some of the chapters have been adopted from the published/submitted papers. The detailed list of the included papers in each chapter is given in the table.

Chapter No.	Paper Title	Publication Details	Publication Status
2&3	System Identification and Robust Control of Multi-Input Multi-Output Active Magnetic Bearing Systems	IEEE Transactions on Control Systems Technology	Article in Press
	Genetic Algorithm-Based System Identification of Active Magnetic Bearing System: a Frequency-Domain Approach	IEEE International Conference of Control and Automation	Available in <i>IEEEExplore</i>
4	Application of Full-Order and Fixed-Order μ -Synthesis Controls for Robust Stabilization of an Active Magnetic Bearing System	-	To be Submitted
5	Optimal PID-type Fuzzy Logic Controller for Multi-Input Multi-Output Active Magnetic Bearing System	Neural Computing and Applications	Article in Press
	PID-type Fuzzy Logic Controller for Active Magnetic Bearing System	the 40th Annual Conference of IEEE Industrial Electronics	Available in <i>IEEEExplore</i>
6	Robust Control of an Active Magnetic Bearing System Using H_∞ and Disturbance Observer Based Control	Journal of Vibration and Control	Article in Press
7	Repetitive Disturbance Observer-based Control for an Active Magnetic Bearing System	Australian Control Conference	Available in <i>IEEEExplore</i>
8	On Two-Step Controller Design for Partially Unknown Unstable Systems	European Control Conference	Available in <i>IEEEExplore</i>

List of Abbreviations

ADC	Analog to Digital Converter
AMB	Active Magnetic Bearing
BFGS	Broyden-Fletcher-Golfarb-Shanno
BNC	Bayonet Neill-Concelman
DAC	Digital to Analog Converter
DFT	Discrete Fourier Transform
DOBC	Disturbance Observer-based Controller
DOF	Degrees of Freedom
DSP	Digital Signal Processing
FLC	Fuzzy Logic Controller
GA	Genetic Algorithm
GWO	Grey Wolves Optimisation

ICA	Imperialist Competitive Algorithm
IAE	Integral of Absolute of Error
ISE	Integral of Squares of Error
ITAE	Integral of Time Multiplied by Absolute of Error
ITAU	Integral of Time Multiplied by Absolute of Control Signal ($U(t)$)
IVM	Instrumental Variable Method
LFT	Lower Fractional Transformation
LQG	Linear Quadratic Gaussian
LQR	Linear Quadratic Regulator
LTI	Linear Time-Invariant
MIMO	Multi-Input Multi-Output
N4SID	Numerical Sub-Space State-Space Identification
NS	Nominal Stability
OEM	Output Error Method
PEM	Prediction Error Method
PID	Proportional Integral Derivative
PIP	Parity Interlacing Property
PSO	Particle Swarm Optimisation
RDOBC	Repetitive Disturbance Observer-based Controller

RHP	Right Half-Plane
RS	Robust Stability
RP	Robust Performance
SAE	Sum of Absolute of Error
SISO	Single-Input Single-Output
SSE	Sum of Squares of Error
UFT	Upper Fractional Transformation
WLS	Weighted Least Squares

List of Symbols

CHAPTER 2

$F_{y_1}-F_{y_4}$	Magnetic forces
i_{bias}	Bias current
I_0	Moment of inertia of the rotor
l	Distance from bearings to the end
l_2	Distance from hall-effect sensors to the end of the rotor
L	Total length of the rotor
y_{airgap}	Air-gap between the bearings and the rotor
Y_1-Y_4	Displacement of the rotor (location of sensors)
y_1-y_4	Location of actuators
θ	Angle of rotation
k	Electromagnetic constant
A,B,C,D	System state-space matrices

R	Probing signals
ξ	Measurement noise
$G(s)$	Transfer function representation of the system
$K(s)$	Feedback controller
$Y(s)$	System output
$U(s)$	Control Signal
$\hat{G}(s)$	Estimated model
e	Error in estimation
$*$	Complex-conjugate transpose
J	Cost function
W	Frequency weighting matrix
α, β	Weighting scaling factors
I	Identity matrix
$diag$	Block-diagonal matrix

Chapter 3

$\ \cdot \ _{\infty}$	H_{∞} -norm
sup	Supremum
S	Sensitivity function
T	Complementary sensitivity function
P	Generalised (augmented) system

\mathcal{F}_l	Lower Fractional Transformation
W_P, W_U, W_T	Mixed-sensitivity weighting functions
ζ	Damping ratio of notch filter
b	Bandwidth of notch filter
β, γ	Lead-lag compensator gain factors

CHAPTER 4

μ	Structured singular value
$\Delta(s)$	Stable proper transfer-function
$W_I(s)$	Multiplicative input uncertainty
$D(s)$	Stable minimum-phase scaling
\mathcal{F}_u	Upper Fractional Transformation
$\bar{\sigma}$	Maximum singular value
α	Spectral abscissa

CHAPTER 5

$e(t)$	Error signal
$\Delta e(t)$	Rate of change of error signal
$\Sigma e(t)$	Sum of the error signal
$\hat{e}(t)$	Normalised error signal
\hat{U}_{PD-FLC}	Normalised PD-type control signal
\hat{U}_{PI-FLC}	Normalised PI-type control signal

T_1-T_4	Fuzzy logic controller normalising factors
S_1-S_{11}	Scalings for distribution of membership functions
$x_{i,d}^t$	Current position of the i^{th} particle
$x_{i,d}^{t+1}$	Future position of the i^{th} particle
v_i^t	Current velocity of the particle
w	Weighting on the velocity of the particle
$p_{i,d}$	Best current solution of the i^{th} particle
$p_{g,d}$	Best current global solution
r_1, r_2	Random numbers between $[0, 1]$
α, β, δ	First, second, and third best solutions
X_p	Position of the prey
$X(t)$	Current position of the grey wolf
$X(t + 1)$	Future position of the grey wolf
C_n	Normalised cost of the n^{th} imperialist
c_i	Cost of each imperialist
N_{col}	Initial number of colonies
Q, R	Weightings on optimisation objective function

CHAPTER 6

$G_n(s)$	Nominal System
u_a	Input signal to DOBC loop

d	External disturbance
ξ	Sensor noise
$Q(s)$	DOBC loop filter
$G^{-1}(s)$	Inverse of the system
$G_{dy}(s)$	Transfer function from disturbance to output
$G_{uay}(s)$	Transfer function from input of DOBC loop to output
$G_{\xi y}(s)$	Transfer function from sensor noise to output
r	Relative degree of Q-filter
τ	Cut-off frequency of Q-filter

CHAPTER 7

$G_{n-mp}(s)$	Minimum-phase factor of nominal system
$G_{n-ap}(s)$	All-pass factor of nominal system
z^{-m}	m-step time-delay
α	Bandwidth of repetitive disturbance rejecter

CHAPTER 8

K_{reg}	State-feedback regulator
J_{LQR}	Linear Quadratic Regulator cost function
P	Solution to algebraic Riccati equation
$G_{closed-loop}$	Closed-loop stable transfer function

L	State observer gain
\hat{x}	Estimated states
\hat{y}	Estimated output
$F(s)$	IMC filter
α, γ, λ	IMC filter parameters
$G_{initial}(s)$	Initial model of system
$G_{re-identified}(s)$	Re-identified model of system

Contents

List of figures	xxx
List of tables	xl
1 Introduction	2
1.1 Motivation and Background	2
1.2 Objective and Scope of the Thesis	5
1.3 Main Scientific Contributions	7
1.3.1 System Identification	9
1.3.2 SISO and MIMO H_2 and H_∞ Optimal Controllers	10
1.3.3 Full-Order and low-Order μ -Optimal Controllers	11
1.3.4 PID-Type Fuzzy Logic Controller	12
1.3.5 Disturbance Observer-Based Controller	14
1.3.6 Repetitive Disturbance Observer-Based Controller	15
1.3.7 Iterative Identification and Two-Step Controller Design	16
1.4 Organisation of the Thesis	18

2	Modelling and System Identification of the AMB System	22
2.1	Introduction	22
2.2	System Description	26
2.3	Analytical Modelling	28
2.4	Experimental System Identification	36
2.5	Conclusion	56
3	SISO and MIMO Robust Controllers	57
3.1	Introduction	57
3.2	H_∞ Controller Design	61
3.3	Lead-Lag Compensator Design	75
3.4	MIMO H_2 and H_∞ Controllers	78
3.5	Experimental Validation	79
3.6	Conclusion	86
4	Full-Order and Fixed-Order μ-Optimal Controllers	88
4.1	Introduction	88
4.2	Full-order H_∞ -optimisation and μ -Synthesis	94
4.3	Fixed-order H_∞ -optimisation and μ -synthesis	100
4.3.1	Fixed-Order μ -Synthesis	101
4.4	Simulation Results	105
4.4.1	Approach (1): μ -synthesis based on the full-order model of the system	105
4.4.2	Approach (2): Full-order μ -synthesis by considering the high- frequency dynamics as multiplicative input uncertainties	107

4.4.3	Approach (3): Direct synthesis of Fixed-order μ -optimal controllers	112
4.5	Experimental Results	114
4.6	Conclusion	119
5	Optimal PID-type Fuzzy Logic Control of AMB System	121
5.1	Introduction	121
5.2	PID-Type Fuzzy Logic Controllers	122
5.3	Review of Some Optimisation Algorithms	126
5.3.1	Genetic Algorithm (GA)	127
5.3.2	Particle Swarm Optimisation (PSO)	128
5.3.3	Grey Wolf Optimisation (GWO)	129
5.3.4	Imperialist Competitive Algorithm (ICA)	131
5.4	Choice of an Objective Function	134
5.4.1	Example: Stabilisation of a Time-Varying System Using the PID-Type Fuzzy Logic Controller	135
5.5	Two-Level Tuning of the PID-Type Fuzzy Logic Controller and Application to Robust Stabilisation of Active Magnetic Bearing System	141
5.6	Real-Time Implementation of the Optimal PID-type Fuzzy Logic Controller on AMB System	145
5.7	Conclusion	154
6	Disturbance Observer-Based Control of AMB System	156
6.1	Introduction	156
6.2	Disturbance Observer-Based Control (DOBC)	159

6.3	Stability Analysis of the Closed-loop System Using Hybrid H_∞ – <i>DOBC</i> Scheme	161
6.4	DOBC Design for Non-minimum Phase Systems	166
6.4.1	Design Procedure of H_∞ – <i>DOBC</i>	167
6.5	Simulation and Experimental Validations	168
6.6	Conclusion	178
7	Repetitive Disturbance Observer-Based Controller of AMB Sys- tem	181
7.1	Introduction	181
7.2	Repetitive Disturbance Observer-based Control	182
7.2.1	Robust Stability of the Repetitive Disturbance Observer- based Control	186
7.2.2	Design of RDOBC for Non-minimum Phase Systems	187
7.3	Simulation and Experimental Validations	188
7.4	Conclusion	194
8	Two-Step Controller Design for AMB System	197
8.1	Introduction	197
8.2	Two-Step Controller Design Approach	200
8.2.1	First Step: Linear Quadratic Regulator (LQR)	201
8.2.2	Second Step: Mixed-Sensitivity H_∞ Controller	203
8.3	Numerical Example and Experimental Validation	206
8.3.1	Difficulties with One-Step Control Design Approach	206
8.3.2	Verification by Experiment: Time-domain Response of Non- Minimum Phase AMB System	212

8.4 Conclusion	216
9 Summary and Future Work	218
9.1 Summary	218
9.2 Future Works	226
References	229

List of figures

2.1	Active magnetic bearing (AMB) system.	27
2.2	Front panel of the experimental AMB system.	28
2.3	Free-body diagram of the system for channels Y_1 and Y_3 (horizontal direction).	29
2.4	Bode diagrams of the rigid-body and total-body models of the system (in the horizontal direction).	35
2.5	Power spectrum of input chirp signal.	40
2.6	Power spectrum of control signal.	41
2.7	Power spectrum of output signal.	41

2.8	Frequency-domain response data of the MIMO AMB system.	42
2.9	Convergence of GA.	48
2.10	A snapshot of GA optimisation.	49
2.11	Bode (magnitude) diagrams of the measure experimental data and the identified SISO models of the system using the presented algorithm, PEM, and N4SID, (a) Channel Y_1 , (b) Channel Y_2 , (c) Channel Y_3 , (d) Channel Y_4	50
2.12	The identified 4×4 MIMO model of the system and the experimental frequency response data.	52
3.1	Mixed S/T/KS sensitivity problem.	62
3.2	Singular values of S , T , $1/W_P$, and $1/W_T$ of all four channels, (a) Channel Y_1 , (b) Channel Y_2 , (c) Channel Y_3 , (d) Channel Y_4	73
3.3	Singular values of the closed-loop sensitivity functions $S(s)$ and the complementary sensitivity functions $T(s)$ using the MIMO H_2 and H_∞ optimal controllers.	80
3.4	Step responses of all four channels using the SISO controllers in the presence of unit-step disturbances.	81

3.5	Control signals of all four channels using the SISO controllers in the presence of unit-step disturbances on all four channels.	82
3.6	Step responses of all four channels using the MIMO controllers in the presence of unit-step disturbances.	83
3.7	Control signals of all four channels using the MIMO controllers in the presence of unit-step disturbances.	83
3.8	Trajectory of the geometrical center of the rotor (at both ends) using the SISO and MIMO controllers. Blue lines represent: analog on-board controllers, green lines: SISO lead-lag compensators, red lines: SISO H_∞ controllers, purple lines: MIMO H_2 controllers, black lines: MIMO H_∞ controllers, (a) air pressure of 20 <i>psi</i> , (b) air pressure of 30 <i>psi</i> , (c) air pressure of 40 <i>psi</i> , (d) air pressure of 50 <i>psi</i> , (e) air pressure of 60 <i>psi</i> , (f) air pressure of 80 <i>psi</i> , (g) air pressure of 100 <i>psi</i> . 85	85
3.9	Rotational speed of the rotor using the SISO and MIMO controllers. 86	86
4.1	(a) General control configuration for controller synthesis, (b) $N - \Delta$ structure for μ -synthesis (or analysis).	97
4.2	Translation on D-scaling, (a) original D-scaling, (b) translation of D-scaling into feedback form, (c) combination of the D-scaling with the controller.	103

4.3	Bode-diagram (magnitude) of the full-order μ -optimal controller and the reduced-order controller.	107
4.4	Nominal system (solid red line) and a set of uncertain systems (dashed blue lines).	109
4.5	Upper-bound on the structured singular value μ for robust stability and robust performance.	111
4.6	Bode-diagram of the full-order controller and the reduced-order controllers.	111
4.7	Closed-loop step response of a set of uncertain systems.	112
4.8	Closed-loop robust stability and robust performance for the fixed-order μ -optimal controller.	113
4.9	Closed-loop step response of some random uncertain systems.	114
4.10	Step response of the system using the full-order and fixed-order H_∞ - and μ -optimal controllers in the presence of disturbance, (a) Displacement of channel Y_1 , (b) Displacement of channel Y_3 , (c) Control Signal of channel Y_1 , (d) Control Signal of channel Y_3	117

4.11	Displacement and control signals of channels Y_1 and Y_3 as rotational speed of the shaft increases over time, (a) Displacement of channel Y_1 , (b) Displacement of channel Y_3 , (c) Control Signal of channel Y_1 , (d) Control Signal of channel Y_3	118
4.12	Transient rotational speed of the rotor using the full-order and fixed-order H_∞ - and μ -optimal controllers.	119
5.1	Common PID-type fuzzy logic controllers, (a) Two-input PID-type FLC with error and sum of the error signals as inputs, (b) Two-input PID-type FLC with error and rate of change of the error signals as inputs, (c) Three-input PID-type FLC with error, rate of change of error and the second derivative of the error signals as inputs, (d) Three-input PID-type FLC with error, rate of change of error and sum of the error signals as inputs.	123
5.2	Alternative PID-type fuzzy logic controller.	124
5.3	Initial distribution of the inputs/output membership functions, (a) Distribution of the error input membership function, (b) Distribution of the rate of change of error input membership function, (c) Distribution of the output membership function.	125
5.4	Closed-loop step responses of the system using different objective functions (Table 5.2).	136

5.5	Closed-loop step responses of the system using ITAE as the objective function with different optimisation search-domains (Table 5.3).	138
5.6	Closed-loop step responses of the system by using equation (5.15) as the objective function (Table 5.4).	140
5.7	Closed-loop step responses of the system by using equation (5.15) as the objective function and different Q and R (Table 5.5).	141
5.8	Closed-loop step responses of the system using different scaling factors $T_{1,2,3,4}$ (Table 5.6).	143
5.9	(a) Optimal distribution of error input membership function, (b) Optimal distribution of rate of change of error input membership function, (c) Optimal distribution of output membership function, (d) The closed-loop response of the system using different optimisation algorithms.	145
5.10	Closed-loop step response of the simulation model and the actual AMB system.	146
5.11	Displacement of the geometrical centres of the rotor over 120 <i>seconds</i> (left end).	148
5.12	Displacement of the geometrical centres of the rotor over 120 <i>seconds</i> (right end).	148

5.13	Control signals using the optimal PID-type fuzzy logic controllers and the analog on-board controllers over 120 <i>seconds</i> , (a) Control signal on channel Y_1 , (b) Control signal on channel Y_2 , (c) Control signal on channel Y_3 , (d) Control signal on channel Y_4	149
5.14	Step response of the system using the PID-FLC controller and the lead-lag compensator in the presence of disturbance.	150
5.15	Step response of the system using the PID-FLC controller and the on-board analog controller in the presence of disturbance.	150
5.16	Trajectory of the rotor using PD-FLC, LQG, and the on-board analog controllers at 2500 <i>rpm</i>	151
5.17	Trajectory of the rotor using PD-FLC, LQG, and the on-board analog controllers at 8000 <i>rpm</i>	152
5.18	Trajectory of the rotor using PID-FLC and H_∞ controllers at 2500 <i>rpm</i>	153
5.19	Trajectory of the rotor using PID-FLC and H_∞ controllers at 8000 <i>rpm</i>	153
5.20	Rotational speed of the rotor under PD-FLCs and PID-FLCs.	154
6.1	Standard framework of the disturbance observer-based controller.	159

6.2	(a) Equivalent DOBC structure with the outer-loop controller $K(s)$, (b) robust stability analysis.	163
6.3	Overall $H_\infty - DOBC$ control structure.	167
6.4	Sensitivity and complementary sensitivity functions of the DOBC ($1 - Q(s)$ and $Q(s)$), single-loop H_∞ controller ($S(s)$, $T(s)$), and the hybrid $H_\infty - DOBC$ ($S_d(s)$, $T_d(s)$).	172
6.5	Displacement and control signal in the presence of step disturbance, (a) Displacement, (b) Control signal.	173
6.6	Displacement and control signal in the presence of sinusoidal distur- bance, $d(t) = 0.2 \sin(10\pi t)$, (a) Displacement, (b) Control signal. . .	174
6.7	Displacement and control signal in the presence of sinusoidal distur- bance, $d(t) = 0.2 \sin(40\pi t)$, (a) Displacement, (b) Control signal. . .	175
6.8	Displacement and control signal in the presence of sinusoidal distur- bance, $d(t) = 0.2 \sin(200\pi t)$, (a) Displacement, (b) Control signal. .	176
6.9	Closed-loop sensitivity functions of the single-loop H_∞ controller and hybrid $H_\infty - DOBC$	177

6.10	Trajectory of the geometrical centres of the rotor at different speeds using $H_\infty - DOBC$, H_∞ , and the analog on-board controllers, (a) Channel Y_1 , (b) Channel Y_2 , (c) Channel Y_3 , (d) Channel Y_4	179
7.1	Schematic diagram of the repetitive disturbance observer-based control.	184
7.2	Closed-loop sensitivity functions using the single-loop H_∞ controller and the hybrid H_∞ -RDOBC with $\alpha = 0.999$	191
7.3	Closed-loop sensitivity functions using the single-loop H_∞ controller and the hybrid H_∞ -RDOBC with $\alpha = 0.995$	192
7.4	Rotor Displacement at 3000 <i>rpm</i>	192
7.5	Spectra of the rotor displacement with and without RDOBC loop.	193
7.6	Displacement of the rotor on first channel over 180 seconds.	195
7.7	Rotational speed of the rotor over 180 seconds.	195
8.1	Proposed two-step controller design structure.	204
8.2	Step response of the system and the control signal using 1DOF IMC.	208
8.3	Magnitude of $1/W_P$, S , $1/W_T$, T , and $G_{stable}K_\infty$	211

8.4	Step response of the system and the control signal (input signal to the plant) using the proposed controller.	211
8.5	Initial and re-identified model of AMB system.	213
8.6	Step response of the system using the proposed 2DOF controller, 1DOF H_∞ controller, and servo LQR.	215
8.7	Control signal using the proposed 2DOF controller, 1DOF H_∞ controller, and servo LQR.	215
8.8	Trajectory of the geometrical center of the rotor at 10000 <i>rpm</i> using the proposed 2DOF controller, 1DOF H_∞ controller, and servo LQR.	216

List of tables

2.1	AMB System Parameters	28
2.2	Chirp Signal Inputs	39
4.1	Achieved μ -value and the controller order using the standard <i>DK</i> - iteration	107
4.2	Achieved μ -value and the controller order using the standard <i>DK</i> - iteration	110
4.3	The order of synthesised controllers using various methods	114
5.1	5×5 FLC rule-base in tabular form	126
5.2	Optimal scaling factors using different objective functions	136

5.3	Optimal scaling factors using ITAE as the objective function and different bounds on the optimisation search-domain	137
5.4	Optimal scaling factors using the presented objective function (ITAE+ITAU) in equation (5.15)	139
5.5	Effect of Q and R on the optimal scaling factors	140
5.6	Optimal scaling factors using ITAE+ITAU equation (5.15) as the objective function and different optimisation algorithms	142
5.7	The optimisations runtime and the best objective function values	144

“Imagination is more important than knowledge...”

— Albert Einstein (1879 - 1955)

Chapter 1

Introduction

This chapter provides an overview of the research reported in this thesis. The motivations for the work is presented and previous progresses made by other researchers are reviewed. The objectives of the research are identified and the main scientific contributions made through this research are highlighted.

1.1 Motivation and Background

The application of active magnetic bearing systems (AMBs) as a suitable technology for high speed rotating machines such as energy storage flywheels, pumps, compressors and tool-machining spindles has been growing rapidly in recent years. The AMB equipped components have notable advantages over their mechanical

and hydrostatic counterparts. The contactless suspension of the rotatory component by attractive forces that are produced by electromagnets allow the AMBs to attain high rotational speeds. The absence of physical contacts and mechanical frictions between the bearings and the rotatory components eliminate the needs of lubrication. As the rotor of AMBs is levitated between the electromagnets without any frictions, the wear of components is almost absent and the rotational speed of the rotor is only limited by the proper design of the rotatory component. Also, AMBs have considerably longer lifetime compared to the mechanical and hydrostatic bearings. These characteristics of the AMBs offer a unique capability for operating in the vacuum or clean environments [1, 2]. AMBs can provide clean means for suspending rotors in ventricular assist devices that are used to partially or entirely replace a failing heart in humans [1, 2]. AMBs can be utilised in many other industrial applications where fast and precise operations are desired such as linear induction motors and turbo-molecular vacuum pumps [3, 4].

Some recent studies show that if AMBs are utilised in wind turbines, they will be able to start-up with substantially lower wind-speed and hence they can increase the wind power capacity [5, 6, 7]. The use of magnetic bearings can also significantly reduce the weight of structural material needed in direct-drive generators by allowing the use of flexible structures [5]. In reference [8], a novel motor with a magnetically levitated rotor is designed and its dynamic characteristics are simulated. The proposed motor is shown to have successfully achieved five degrees-of-freedom active control. The work in reference [9] studies active surge control of a centrifugal compressor where thrust active magnetic bearings are employed. The results demonstrate the potential application of AMB-based compressor surge controllers.

In reference [10], an AMB is utilised as an actuator to guarantee chatter-free cutting operations in high-speed milling processes. The work in reference [11] investigates the application of active radial magnetic bearings for agile satellite systems. As a result, the control current and the associated power losses are considerably reduced. With these exceptional properties, the AMBs are paving the way for design and production of new rotating machines with much higher speeds and much lower power dissipation in comparison to the common mechanical bearing equipped systems.

Along with the numerous advantages, AMBs have certain drawbacks that have hindered the widespread commercial and industrial applications of these systems. AMBs are inherently open-loop unstable and thus a feedback stabiliser is essential in all AMB equipped systems [12, 13]. In order to design high-performance “model-based” feedback controllers for AMBs, accurate models of the system need to be identified first. Since AMBs are open-loop unstable, closed loop system identification procedures are necessary. The existence of high-frequency noise and structural resonant frequencies make the modelling and control design tasks even more challenging. The dynamics of AMBs are also influenced by the rotor speed. These speed dependent dynamics such as rotor mass-imbalance, gyroscopic effects and centrifugal forces not only complicate the modelling process, but also necessitate the development of high-performance control strategies for system operating over a wide range of speeds. The presence of cross-couplings between different channels, gyroscopic forces, and other structural interactions further exacerbate the problem. Additional uncertainties are introduced through the dynamics of amplifiers, sensors, and digital controllers. As AMBs are subject to several sources

of uncertainties, the robustness of the closed-loop system against uncertainties can be considered as the primary requirement in the feedback control design of these systems. Consequently, better models and high-performance controllers are needed to address these challenges. All the aforementioned reasons have motivated us to investigate the current gaps between the theory and challenges involved in system identification and real-time implementation of robust controllers on AMBs.

1.2 Objective and Scope of the Thesis

The aim of this thesis is to design and implement advanced control algorithms on a laboratory scale AMB system. The main interests of the thesis can be classified into two parts, namely, system identification and advanced controllers design. Firstly, novel algorithms are developed for identification of SISO and MIMO models of the AMB system using the frequency-domain response of the system. Next, several linear and nonlinear controllers are designed to maximise the robust performance of the system in the presence of unmodelled dynamics and external disturbances over a wide operating speeds. Extensive experimental studies on the performance of the designed controllers are conducted throughout the thesis.

The objectives of the thesis are as follows:

- I) Analytical modelling of the AMB system including the rigid-body and flexible-body models of the system.

-
- II) SISO modelling of the system by using the experimental frequency-domain data and the proposed GA-based weighted least squares method.
 - III) MIMO modelling of the system by using the experimental frequency-domain data and the proposed extended GA-based weighted least squares method.
 - IV) Real-time implementation of several robust controllers that are designed on the basis of the SISO models of the system.
 - V) Real-time implementation of several robust controllers that are designed on the basis of the MIMO model of the system.
 - VI) Performance comparison of full-order and reduced-order robust H_∞ - and μ -optimal controllers.
 - VII) Real-time implementation of nonlinear fuzzy logic controllers.
 - VIII) Vibration reduction of the system while the rotor is rotating at different speeds by introducing a second degree-of-freedom control scheme into the overall feedback loop.
 - IX) Comparative study and sensitivity analysis of the proposed control methods.
 - X) Improvements on the idea of iterative identification and control of partially unknown unstable systems.

1.3 Main Scientific Contributions

This research strives to enhance the performance of the AMB system while the rotor is stationary as well as while it is rotating at various speeds. The original contributions of the thesis may be divided into two parts, the first of which is concerned with the modelling and identification of the AMB system. Since most of the available identification methods can model the system in the low-frequency regions, but fail to accurately model the high-frequency resonant modes of the system, a novel system identification method is presented in which the SISO and MIMO models of the system can be identified very accurately in both low and high frequency regions. The application of the presented algorithm is not limited only to the modelling of AMB systems, but it can be employed to the identification of any systems with “slow” and “fast” dynamics that need to be modelled accurately.

The second area of contribution of the thesis is concerned with the robust control design of the AMB system. With respect to this problem, there are two issues to be addressed thoroughly, namely, the robust stabilisation of the system while the rotor is stationary, and disturbance rejection capabilities of the system while the rotor is rotating at various speeds. For the robust stabilisation of the system while the rotor is stationary, in the most of reported works in the literature, the order of the synthesised robust controllers are found to be excessively high. The real-time implementation of such high-order controllers is very challenging and it requires expensive hardware. Therefore, some controller design strategies are proposed in this thesis that will result in much lower-order robust controllers

that are more reliable for implementation and product commissioning. After the performance requirements are satisfied while the rotor is stationary, it is desired for the system to reject the disturbances caused by the rotor mass-imbalance, centrifugal forces, and other unknown but bounded disturbances while the rotor is rotating. It is shown that most of the available methods in the literature require the speed of the rotor to be continuously measured in order for the control algorithm to reject these disturbances. However, successful implementation of these control schemes requires the installation of an additional speed sensor on the system. To alleviate this problem, two design structures based on disturbance observer-based control (DOBC) and repetitive disturbance observer-based control (RDOBC) are proposed in this thesis for the rejection of unknown but bounded disturbances while the rotor is rotating. It is shown via simulation and experimental studies that the presented algorithms are very effective in rejecting disturbances without having to continuously measure the speed of the rotor.

Although several works can be found on the system identification and robust control of AMBs, the results presented in the recent works have many shortcomings. This is the main motivation of this thesis to address the current gaps between the theory and challenges in designing robust controllers for AMBs. In the sequel, some of the original contributions to be presented in the thesis are introduced briefly.

1.3.1 System Identification

It is well-known that the combination of magnetic bearings and a flexible rotatory shaft results in an MIMO system that contains both “slow” and “fast” dynamics [14, 15, 16, 17]. The slow dynamics come from the rigid-body model of the system including the model of the electromagnets, sensors, and amplifiers. Whereas, the fast dynamics result from the flexible modes of the rotor. In order to ensure the robust performance of the system over a wide operating range, the dominant flexible modes need to be modelled accurately. It is shown that the problem with most of the common identification methods is that an accurate model of the system is obtained in the low-frequency regions, but these algorithms fail to model the high-frequency flexible modes (resonant frequencies) accurately enough.

In Chapter 2, a novel system identification method based on weighted least squares method is presented for SISO and MIMO modelling of the system using the frequency-domain response data of the system. To this end, appropriate frequency weightings are required to ensure that the flexible modes are modelled accurately. Hence, Genetic Algorithm is employed in combination with the weighted least squares method to iteratively find the required weighting factors that appropriately scale up certain frequency ranges of interest. The iterations continue until the difference (in the least-squares sense) between the frequency response of the model and the experimental data is found to be less than a predefined value (or the maximum number of iterations is reached). The obtained models are compared with the prediction error method (PEM) and the numerical subspace state-space

identification (N4SID) method. The results show that much more accurate models of the AMB system are obtained by using the presented algorithm.

1.3.2 SISO and MIMO H_2 and H_∞ Optimal Controllers

Robust control of active magnetic bearing systems has been an active topic of many recent research works. In Chapter 3, it is shown that the results presented in the recent works have many shortcomings. For instance, in some works, the MIMO system is modelled as a family of SISO subsystems by neglecting the . The robust controllers are designed on the basis of the SISO models and the cross-coupling effects between the channels are neglected [12, 13, 18, 19]. This approach is practical if low-order controllers are to be designed and if the system is stationary or it is operating at low rotational speeds. However, the effects caused by the cross-coupling between channels, centrifugal forces, and other unmodelled dynamics become more significant at higher speeds. Therefore, multivariable robust controllers need to be designed on the basis of MIMO models of the system including the models of the cross-coupling channels. However, most of the recent published works are limited to the simulation studies of robust multivariable controllers on AMBs while the difficulties with the real-time implementation of robust MIMO controllers on AMBs can be seen in references [20, 21, 22, 23]. In fact, it is observed in the results provided in references [20, 21, 22, 23] that the designed stabilising controllers were found to be unstable themselves. More importantly, these controllers with right-half plane poles failed to stabilise the actual system which clearly means that the identified model of system was not acquired accurately and hence the

designed controllers failed to stabilise the actual system. It should also be noted that there are examples in the literature that stabilising controllers are found to be *unstable* [24], but this is not the case for AMBs, as there exist *stable* controllers for stabilising the AMBs. Thus, implementation of *unstable* stabilising controllers should be avoided at all cost, unless no *stable* controllers are found for stabilising the system.

In this thesis, several SISO and MIMO controllers, namely, lead-lag type compensators, SISO H_∞ -optimal controllers, and MIMO H_2 - and H_∞ -optimal controllers are designed on the basis of the obtained models and successfully implemented for robust stabilisation of the AMB system. It is shown that the proper modelling of the system will result in stable high-performance controllers that can be implemented on the actual system directly and safely without any additional modifications.

1.3.3 Full-Order and low-Order μ -Optimal Controllers

It is observed in Chapter 4 that most of the existing multivariable control design approaches for robust stabilisation of active magnetic bearing systems (AMBs) are either based on the rigid-body dynamics of the system or a decoupled model of the system after neglecting the cross-coupling effects between the channels [12, 13, 18, 19]. In recent works, inclusion of the cross-coupling effects between the channels and high-frequency dynamics resulting from the rotor flexible modes in the model are attempted. Clearly, a higher-order model is required to successfully

represent the cross-coupling effects and high-frequency dynamics of the system. Robust controllers can then be designed by using for instance, H_∞ optimisation methods or μ -synthesis algorithms so that the robust performance of the closed-loop system is achieved in the presence of uncertainties and unmodelled dynamics. However, it can be clearly seen from the reported results that the order of such controllers is exceedingly high and hence demands expensive hardware for successful implementation [25, 26]. On the other hand, many industrial controllers are constrained in their order/structure and still are required to meet high performance and robustness demands. In Chapter 4, some control design strategies are provided that lead to much lower-order robust H_∞ - and μ -optimal controllers that not only satisfy the design requirements, but also they are found to be more efficient and reliable for product commissioning.

1.3.4 PID-Type Fuzzy Logic Controller

In Chapter 5, it is shown that the main difficulty with the “model-based” robust controllers is that an accurate model of the system is required at the control design stage. As an alternative to the “model-based” controllers, the so-called “model-free” controllers such as fuzzy logic controllers have emerged. For the latter, only a low-order linear model of the system is required at the control design stage. However, there are two challenges in designing fuzzy logic controllers. The first one is regarding the structure of fuzzy logic controllers. There exist several structures in the literature which some of them are computationally involved and hence not efficient for implementation [27]. One of the contribution of the thesis is to provide

a simple but effective PID-type fuzzy logic control scheme that can be generalised to control of linear and nonlinear systems whose approximate model (low-order model of one channel in the case of AMB system) is only available. Another challenge in designing fuzzy logic controllers is that the performance of the designed controllers is highly dependent on the proper selection of some design parameters which is usually obtained heuristically without a systematic method. With the recent developments in the area of global optimisation [28], it is possible to obtain near to “optimal” values of the design parameters more systematically.

In Chapter 5, it is shown that the performance of most of the meta-heuristic algorithms depends not only on the size of optimisation search-domain, but also on the proper selection of the optimisation objective function. Otherwise, the algorithm converges to undesirably large values which may lead to large control signals and hence saturation of actuators. To alleviate this problem, novel objective functions are proposed for the optimisation of the design parameters of the fuzzy logic controllers. It is shown that by employing the presented objective functions, regardless of the size of the optimisation search-domain, the optimisation algorithms converge to relatively similar results in terms of time-domain performance of the closed-loop system. Finally, the optimal fuzzy logic controllers are coded in *C* and successfully implemented on the AMB system. The experimental results are compared with those of linear controllers and it is shown that the fuzzy logic controllers provide much better performance compared to the linear controllers.

1.3.5 Disturbance Observer-Based Controller

After the control design requirements are satisfied for robust stabilisation of the rotor, the flexible shaft is rotated with the help of an attached air-turbine at one end of the rotor while it is levitated between the bearings. The AMBs are usually subject to harmonic disturbances with frequencies that vary according to the speed of the rotor [29, 30]. Several methods such as varying notch filters, gain scheduling controllers, and linear parameter varying (LPV) controllers have been reported in the literature to reject these disturbances while the system is rotating at different speeds. Although the gain-scheduling and LPV controllers show appealing results when applied to several simulation models, the real-time implementation of such controllers appears to have many practical issues. For instance, the experiments reported in references [31, 32] were carried out for a limited speed range of ($[4000, 5000]$ rpm), because the optimisation problem was found to be infeasible for other operating speeds.

In Chapter 6, a control scheme is proposed to ensure the rejection of unknown but bounded disturbances while the rotor shaft is rotating at various speeds. In the proposed scheme, the rotor is first levitated between the bearings by using outer-loop feedback stabilisers. Then, the inner-loop disturbance observer-based controllers (DOBC) are included in the overall feedback to reduce the effects of disturbances. One advantage of the proposed two-degrees-of-freedom (2DOF) control scheme is that the inner-loop achieves a faster dynamic response than the outer-loop stabiliser and hence it is more effective than single-loop control structures in rejecting disturbances. Motivated by the frequency-domain loop-

shaping properties of H_∞ controllers and the disturbance rejection capabilities of DOBCs, the two methods have been combined into a hybrid H_∞ -DOBC scheme for robust stabilisation of the AMB system while the rotor is stationary as well as while it is rotating at various speeds.

1.3.6 Repetitive Disturbance Observer-Based Controller

It is observed that the proposed 2DOF control structure (H_∞ -DOBC) significantly reduces the effects of unknown but bounded disturbances compared to the single-loop structures while the shaft is rotating. However, if there exists a repetitive disturbance with known fundamental frequency, it turns out that the repetitive control (RC) provides significant improvements in rejecting the repetitive disturbances [33]. However, the main drawback of the repetitive controllers is that, along with the rejection of periodic disturbances, there will be undesirable gain amplifications of non-periodic disturbances. In Chapter 7, it is shown that the repetitive controller can be reformulated as a disturbance observer-based control structure. It is demonstrated via simulation and experimental studies that the presented repetitive disturbance observer-based control (RDOBC) scheme not only greatly reduces the gain amplification of repetitive disturbances, it also reduces the effects caused by non-repetitive disturbances substantially. The stability analysis of the overall 2DOF control scheme is provided and some guidelines are given for designing RDOBC scheme for systems with right half-plane zeros.

1.3.7 Iterative Identification and Two-Step Controller

Design

In order to obtain accurate models of the system experimentally, the system needs to be excited with sufficiently rich probing signals. On the one hand, this is not always possible in practice, because overly exciting the system may deteriorate the performance of the system or may even lead to system instability. On the other hand, poor probing signals result in poor signal to noise ratios and hence may fail to provide enough information about the dynamics of the system. Although relatively strong probing signals have been used in this research to excite the laboratory scale AMB system for the system identification purposes, a strategy that can be generalised for identification of systems without having to overly excite the system over a wide range of frequencies needs to be developed. In Chapter 8, a two-step controller design algorithm is proposed that can be considered as an improvement to the idea of iterative identification and control of partially known unstable systems [34]. In the first step of the design, a low-bandwidth controller is designed on the basis of a crude model of the system (a known model in low-frequency regions) and implemented on the system. The bandwidth of the controller is increased progressively and cautiously until the actual closed-loop bandwidth of the system can no longer be increase by the current controller. At this stage, a more accurate model of the system over an extended range of frequencies is required. Once a better model of the plant is identified, new controllers can be designed on the basis of the re-identified model. The iterative identification and control design scheme can be viewed as an indirect adaptive control scheme with a time-scale separation

between the closed loop identification and controller redesign [35]. This allows more performance-oriented analysis of the interaction between identification and controller design stages [36, 37]. As the control objective here is to increase the bandwidth of the closed-loop system cautiously, it is desirable to have a control method in which a single parameter can be used to describe the bandwidth of the closed-loop system. If the system is open-loop stable, the internal model control (IMC) method is found to have this desirable property. In the IMC method, the closed-loop bandwidth of the system can be altered by a single design parameter (known as λ of the IMC filter) [38, 39, 40]. However, if the plant is open-loop unstable, the controller design based on the standard IMC methods is found to be very challenging [40] and undesirable closed-loop performances maybe achieved by using the IMC method [34].

Chapter 8 provides a systematic two-step control design approach for open-loop unstable systems for iterative identification and control purposes [41]. In the first step of the proposed algorithm, a minor-loop (or inner-loop) is designed to stabilise the open-loop unstable system with minimum weighted energy (“expensive energy control strategy”). It is desirable to stabilise the system without exciting the high-frequency regions where the model of the plant is highly uncertain. Next, a major-loop (or outer-loop) is designed on the basis of the stabilised system. In order to progressively increase the closed-loop bandwidth of the system, a mixed-sensitivity H_∞ optimisation procedure is applied to the stabilised plant. The advantage of using the mixed-sensitivity H_∞ controller design over the standard IMC method is that the bandwidth of the closed-loop system can be expanded by proper selection of the design frequency weighting functions and re-synthesising

the H_∞ controller. Furthermore, special attentions can be paid to the magnitude of control signal and the high-frequency roll-off at the control design stage.

1.4 Organisation of the Thesis

This thesis is presented in nine Chapters. The organisation of the remaining Chapters is as follows:

Chapter 2 provides a general description of the AMB system under study. A detailed analysis of the mathematical modelling and experimental system identification are given. Both SISO and MIMO models of the system are obtained by using a proposed GA-based iterative weighted least squares method. The obtained SISO and MIMO models are used in later Chapters for “model-based” robust control design.

Chapter 3 presents some theoretical backgrounds on modern robust control approaches. A brief overview of the H_2 and H_∞ optimisation methods are given and some useful remarks for design of robust controllers for unstable non-minimum phase systems are provided. Next, several H_2 and H_∞ optimal controllers are designed on the basis of the SISO and MIMO models of the system and the performances of the designed SISO and MIMO controllers are evaluated through simulation and experimental studies.

Chapter 4 studies beyond the robust stability of the nominal system and it investigates the robust performance of the system in the presence of modelling uncertainties and unmodelled dynamics. It shows that μ -optimal controllers can be designed such that not only the nominal system remain stable with the designed controllers, but also all possible uncertain systems in the uncertainty set remain robustly stable. The main drawback of control design based on the standard algorithms is that the order of the final controllers is excessively high. Therefore, some control design strategies are provided that ultimately result in much lower-order H_∞ - and μ -optimal controllers than those controllers that are designed by using the standard *DK*-iteration methods.

Chapter 5 examines the design and optimisation of the PID-type fuzzy logic controllers (PID-FLC). Several structures that are equivalent to PID-type fuzzy logic controllers are studied and a simple but effective structure that requires minimum number of design parameters is presented. Several meta-heuristic optimisation algorithms are then employed to obtain the optimal values of the design parameters. It is shown via simulation studies that the “optimal” values obtained by using the meta-heuristic algorithms depend highly on the predefined optimisation objective function and this may result in undesirable values. Therefore, some conflicting objective functions are presented for the time-domain optimisation of the fuzzy logic controllers. The simulation results show that the presented optimisation objective function is much more effective than the common time-domain objective functions used for obtaining optimal design parameters of the fuzzy logic controllers. It is shown that when the presented objective function is employed, most of the meta-heuristic algorithms converge to similar values regardless of the size of search-

domain. A similar procedure is used to obtain the optimal tuning parameters of the PID-type fuzzy logic controllers for stabilisation of the laboratory AMB system. The final designed controllers are coded in C and implemented on the AMB system. The experimental results are also compared with linear controllers.

Chapter 6 focuses on vibration reduction and disturbance rejection of the system while it is rotating at various speeds. This is achieved by including a secondary loop into the overall feedback. The secondary (inner) loop that is a disturbance observer-based controller is combined with an outer-loop feedback stabiliser to improve the performance of the system in terms of disturbance rejection and vibration attenuation while the system is stationary as well as while it is rotating. The performance of the resulting hybrid control scheme is compared with those of single-loop structures and the on-board analog controllers via experiments.

Chapter 7 combines the features of the disturbance observer-based controllers with the repetitive controllers, and presents a hybrid scheme that not only greatly reduces the gain amplifications of harmonic disturbances, but also reduces the gain amplification of the non-repetitive disturbances. Similar to the disturbance observer-based control structure, an outer-loop feedback controller is required for the stabilisation of the open-loop unstable system. The inner-loop repetitive disturbance observer-based controller is then introduced to the overall feedback to result in a two degrees-of-freedom (2DOF) scheme. The stability analysis of the overall 2DOF scheme is provided and the effectiveness of the proposed structure is verified via simulations and real-time experiments on the AMB system.

Chapter 8 proposes a systematic two-step control design approach for improving the stability and system performance of open-loop unstable systems via iterative identification and control. In this approach, the unstable system is first stabilised by a parallel feedback stabiliser with the minimum-weighted energy. In the second step of the design, a mixed-sensitivity H_∞ controller is designed on the basis of the closed-loop stable system to gradually improve the overall performance of the closed-loop system. The advantage of the proposed two-step control design scheme for open-loop unstable systems over the available one-step design approach is studied via a simulation example. Next, a similar approach is utilised for the iterative identification and control design of the AMB system. It is shown that accurate models of the system in a wide range of frequencies can be obtained from the initial partially known models by using the presented algorithm and hence the overall performance of the system can be improved by controllers that are designed on the basis of the re-identified models of the system.

Chapter 9 summarises the research work and presents the conclusions drawn from the study along with some recommendations for possible future research opportunities.

Chapter 2

Modelling and System

Identification of the AMB System

2.1 Introduction

In order to design high performance “model-based” controllers, sufficiently accurate models of the system are required for the control design stage. Since the AMBs are open-loop unstable, closed-loop system identification is inevitable over the standard open-loop identification methods. The most commonly used techniques for open-loop identification of systems are prediction error methods (PEM), instrumental variable method (IVM), and output error methods (OEM) [42]. Recently, numerical subspace state space system identification (N4SID) methods have attracted the at-

tention of many researchers [43, 44, 45] for identification of multi-input multi-output (MIMO) systems. Although these methods have shown to provide satisfactory results in system identification of MIMO systems, their efficiency on identification of open-loop unstable AMBs are investigated in this thesis. Artificial intelligence (AI) techniques, on the other hand are suitable alternatives for parameter identification of systems. Genetic Algorithm (GA) has been widely used in optimisation problems with several local minima where conventional search algorithms fail to provide optimal solutions [46, 47]. The work in reference [48] proposes a method for parametric identification of poles and zeros of both continuous- and discrete-time transfer functions by using GA. The provided results show that the GA is able to converge to the actual values of the parameters after few iterations. However, the authors show that the convergence of the proposed method is slow in some cases like identification of zeros, because of the insensitivity of the objective function to small changes in zeros. In reference [49], GA is utilised to identify the model of a power plant. The results show the successful identification of a high order model of the de-superheating process and hence improvement in the performance of the steam temperature controller. The work in reference [50] employs GA to identify the parameters of the transfer function of a rectangular flexible plate system. A novel algorithm for truncation-based selection of the GA is used that shows a faster convergence to the global optimum solution compared to the conventional methods. However, the drawback of utilising GA for parametric identification of a transfer function is that increasing the model order will subsequently increase the number of parameters to be identified by GA. Furthermore, the algorithm may not converge to the optimal values if the system is high-order or ill-conditioned (systems with large condition numbers).

For the AMB system under study, the two flexible (resonant) modes of the rotor need to be modelled accurately, as they are within the bandwidth of the system. The problem with the most of available identification methods is that these algorithms find an accurate model of the system in the low-frequency regions, but they fail to model the high frequency flexible modes accurately. The aim here is to find a model of the system that is as simple as possible, and yet capable of capturing all important characteristics of the system. In this thesis, weighted least squares (WLS) method is combined with GA to iteratively find the best model of the system in the frequency range of interest with a predefined model-order. It is well-known that the least-squares (LS) problems can be solved analytically and have unique solutions. Moreover, the weighted least squares (WLS) methods can be used if more attentions need to be paid to certain range of frequencies. These weightings can be obtained using the iteratively re-weighted least squares algorithms [51]. In this research, the frequency weightings are used to emphasise particular ranges of frequencies which are more of interest in controller design stage. In fact, we need to ensure that the system is modelled accurately not only in the low-frequency regions, but also the high frequency flexible modes are modelled accurately. In this Chapter, GA is combined with weighted least squares (WLS) to alter the frequency weightings (fictitious noise components) required in the WLS method and perform an iterative re-weighted least squares algorithm until the best model fit is obtained. This iterative approach can be summarised into four steps: 1) GA generates a population of weight vectors, 2) WLS is solved explicitly by utilising the constructed weight vectors, 3) GA alters the weight vectors by changing the range and the corresponding scaling factors, and 4) the iteration continues until the minimum difference between the frequency response of the measured data and

the fitted model is achieved. The advantage of this method is that regardless of the order of the system, the number of parameters to be optimised by GA remains unchanged.

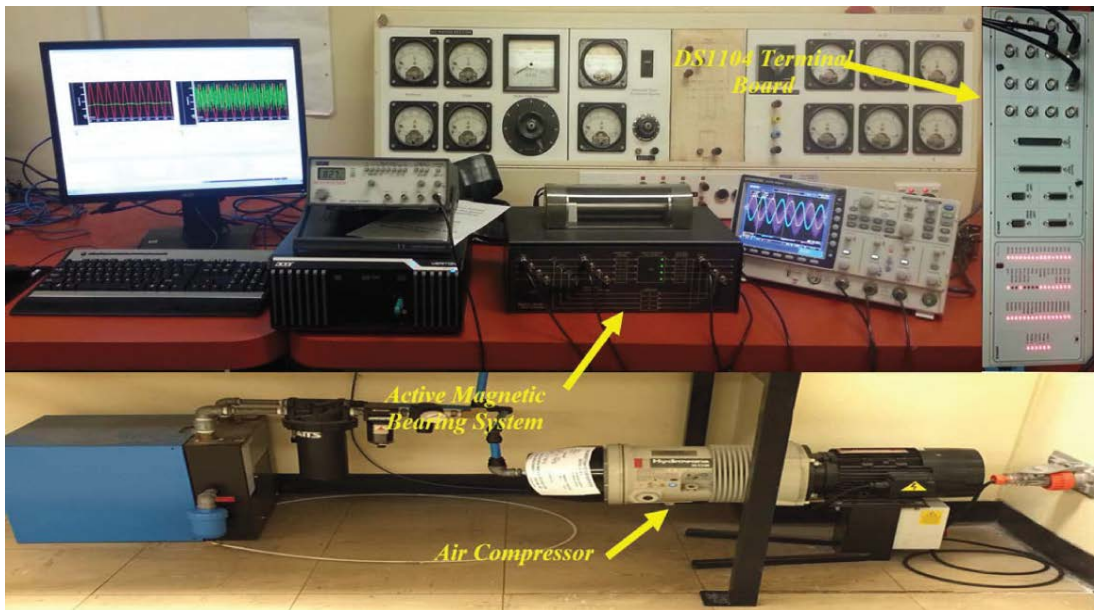
In the first section of this Chapter, the analytical model of the AMB system is obtained by using the first principles. The model of the system in the horizontal direction is linearised around the system's operating point. In addition, the linearised models of the sensors and amplifiers are included in the final model. Finally, the obtained rigid-body model of the system is combined with the first two bending-modes of the rotor shaft and the overall state-space representation of the system is presented. The second section is devoted to the system identification of the AMB system by using the recorded responses of the system to the input chirp signals. The captured time-domain signals are first converted into frequency-domain by employing the Discrete Fourier Transformation (DFT) and the GA-WLS is employed to obtain the SISO and MIMO models of the system. If low-order (low-complexity) controllers are to be designed for the system, the cross-coupling effects between the channels are neglected and the MIMO system is treated as four SISO subsystems and the model of each subsystem is obtained individually. The advantage of obtaining the SISO models is that low-order (low-complexity) SISO controllers can be designed on the basis of the identified SISO models, and their performance is comparable to the analog on-board controllers. To strive for a better performance, the proposed GA-WLS algorithm is extended to obtain the MIMO model of the system that includes the models of all four channels and the coupling effects between different channels. High performance MIMO controllers can then be designed on the basis of the MIMO model of the system.

2.2 System Description

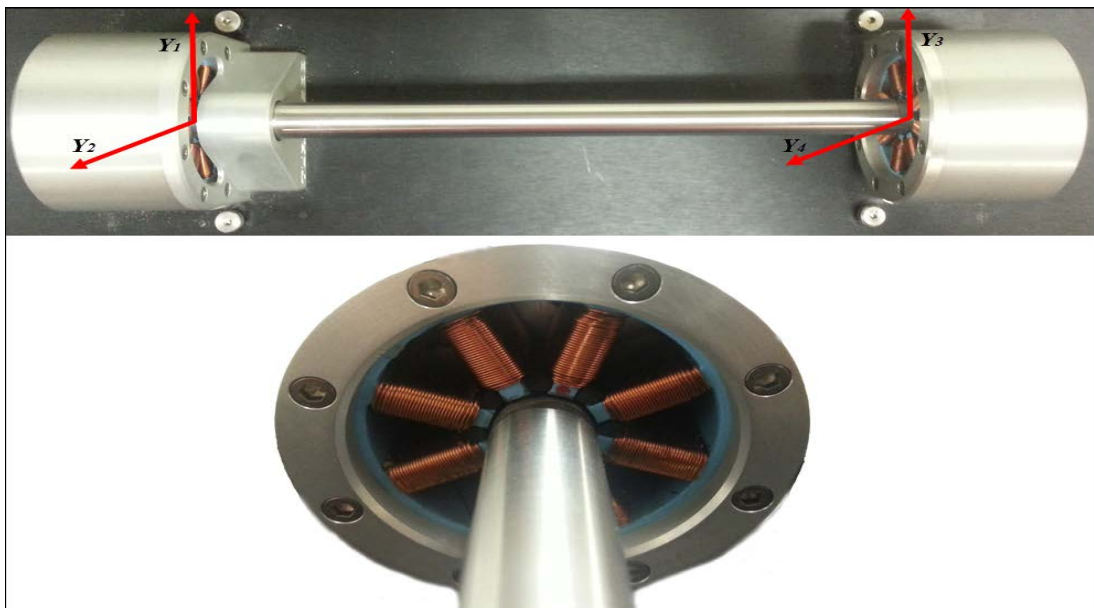
The laboratory experimental AMB system is shown in Fig. 2.1. The system includes a rotor shaft, four pairs of horseshoe electromagnets (two pairs at each end), an air-turbine that can be driven by compressed air, four hall-effect sensors, four linear current-amplifiers, and four analog on-board controllers. The rotor is levitated with magnetic forces provided by the electromagnets, and the rotational speed of the rotor shaft can reach up to 10000 *rpm*. The rotor shaft has four degrees of freedom (4DOF) which are labeled as $Y_1 - Y_4$ in Fig. 2.1. Y_1 and Y_2 correspond to the horizontal and vertical displacements of the rotor at one end. Whereas, channels Y_3 and Y_4 correspond to the horizontal and vertical displacements of the rotor at the other end of the system, respectively. A digital signal processing card (DS1104) is used for the data acquisition and real-time implementation of the control algorithms.

The schematic diagram of the front panel of the AMB system is depicted in Fig. 2.2. The front panel consists 12 Bayonet NeillConcelman (BNC) connections for easy access to the system's inputs and outputs. There are four switches in the feedback loops and these switches allow the user to replace the on-board analog controllers with digital controllers. If only one loop is switched off, the user can perform SISO control design experiments. By switching off all four loops, the decoupled analog on-board controllers can be replaced by four digital SISO controllers or a single MIMO controller.

The system parameters are described in Table 2.1.



(a)



(b)

Figure 2.1: Active magnetic bearing (AMB) system.

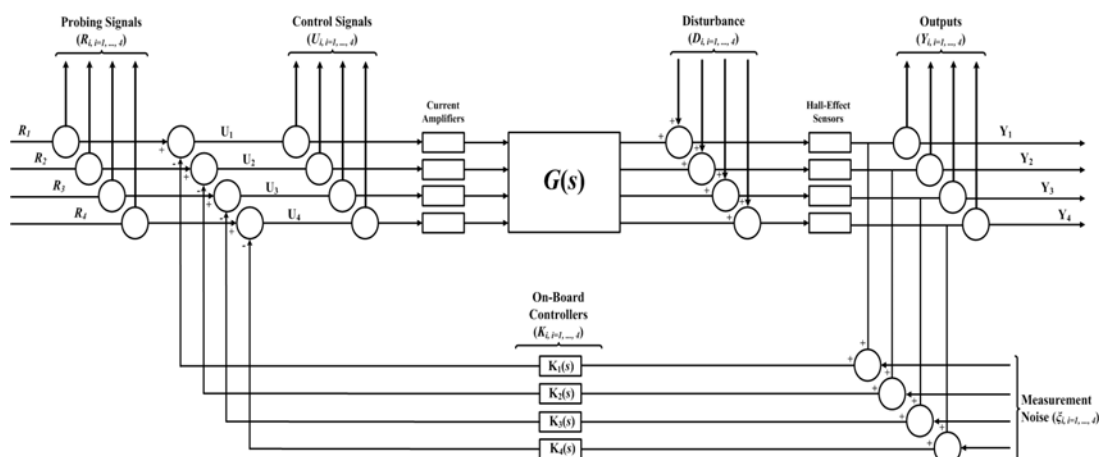


Figure 2.2: Front panel of the experimental AMB system.

Table 2.1: AMB System Parameters

Description	Value
Total length of the rotor (L)	0.269 m
Mass of the rotor (m)	0.2629 kg
Air-gap between the bearings and the rotor (y_{airgap})	0.4 mm
Bias current (i_{bias})	0.5 A
Moment of inertia of the rotor (I_0)	$1.5884 \times 10^{-3} \text{kgm}^2$
Distance from bearings to the end (l)	0.024m
Distance from Hall-effect sensors to the end (l_2)	0.0028m

2.3 Analytical Modelling

The analytical modelling gives an intuition about the dynamic behaviour of the system and helps with the experimental identification of the system. The free-body diagram of the system in the horizontal direction is depicted in Fig. 2.3. When the electromagnets are arranged in perpendicular planes as shown in Fig. 2.1, the horizontal and vertical plane dynamics can be considered to be independent of each

other. In this case, the 4×4 MIMO system can be regarded as two independent subsystems, each having 2 inputs and 2 outputs. Thus, robust controllers can be designed for the horizontal and vertical planes separately.

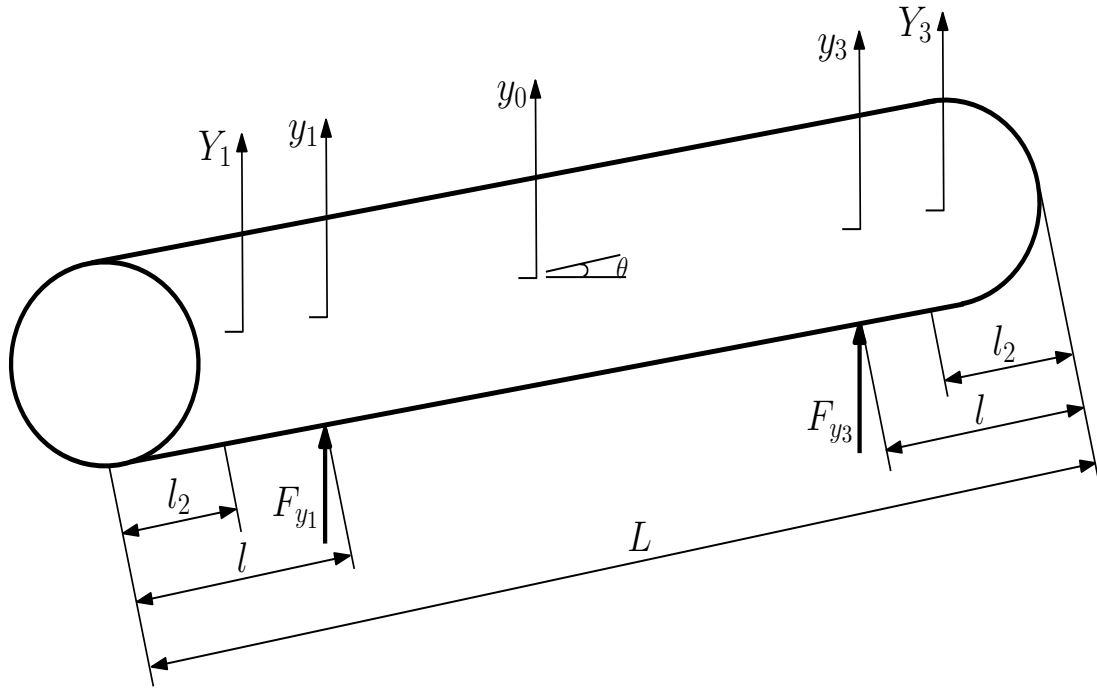


Figure 2.3: Free-body diagram of the system for channels Y_1 and Y_3 (horizontal direction).

Firstly, the rigid-body dynamics of the system can be obtained while the system is stationary. The system is assumed to be symmetrical at both ends. The geometrical analysis of the rotor yields the following relationship between the

translational and rotational motions of the rotor.

$$\begin{aligned}
y_1 &= y_0 - \left(\frac{L}{2} - l\right) \sin \theta \approx y_0 - \left(\frac{L}{2} - l\right) \theta \\
y_3 &= y_0 + \left(\frac{L}{2} - l\right) \sin \theta \approx y_0 + \left(\frac{L}{2} - l\right) \theta \\
Y_1 &= y_0 - \left(\frac{L}{2} - l_2\right) \sin \theta \approx y_0 - \left(\frac{L}{2} - l_2\right) \theta \\
Y_3 &= y_0 + \left(\frac{L}{2} - l_2\right) \sin \theta \approx y_0 + \left(\frac{L}{2} - l_2\right) \theta
\end{aligned} \tag{2.1}$$

The equations of motions governing the AMB system around the center of gravity can be expressed as follows:

$$\sum F_y = m\ddot{y} = F_{y_1} + F_{y_3} \tag{2.2}$$

$$\sum M_y = I_0\ddot{\theta} = F_{y_3} \left(\frac{L}{2} - l\right) \cos \theta - F_{y_1} \left(\frac{L}{2} - l\right) \cos \theta \tag{2.3}$$

Note that for small variations of θ about the equilibrium point, it can be assumed that $\sin \theta_i \approx \theta_i$. The generated electromagnetic force by each pair of horseshoe electromagnets can be formulated as:

$$F_{y_i} = \frac{k(i_{control_i} + i_{bias})^2}{(y_i - y_{airgap})^2} - \frac{k(i_{control_i} - i_{bias})^2}{(y_i + y_{airgap})^2} \tag{2.4}$$

where, $k = 2.8 \times 10^{-7}$, the current bias $i_{bias} = 0.5$ A, and the air-gap between the rotor and the electromagnets $y_{airgap} = 0.4$ mm. In equation (2.3), $i_{control_i}$ is

the current supplied by the current amplifiers and x_i is the displacement of the shaft inside the bearings at each end of the rotor. The nonlinear magnetic force in equation (2.3) can be linearised about the equilibrium point $(0, 0)$ by linear Taylor series approximation in equation (2.5).

$$F(y_i, i_{control_i}) = F_i(0, 0) + \left[\frac{\partial F_i}{\partial y_i}(0, 0) \right] (y_i - 0) + \left[\frac{\partial F_i}{\partial i_i}(0, 0) \right] (i_{control_i} - 0) \quad (2.5)$$

The linearised magnetic force in equation (2.5) can be expressed as in equation (2.6).

$$F_{y_i} = 4375y_i + 3.5i_{control_i} \quad (2.6)$$

Combining equations (2.1) and (2.6) results in:

$$\begin{aligned} F_{y_1} &= 4375y_0 - 4375 \left(\frac{L}{2} - l \right) \theta + 3.5i_{control_1} \\ F_{y_3} &= 4375y_0 + 4375 \left(\frac{L}{2} - l \right) \theta + 3.5i_{control_2} \end{aligned} \quad (2.7)$$

The nonlinear models of the hall-effect sensors also need to be linearised about the equilibrium point $(0, 0)$ by using the Taylor series approximation. The nonlinear model of the sensors is given as:

$$V_{sensor_i} = 5000Y_i + (25 \times 10^9) Y_i^3 \quad (2.8)$$

Thus, the linear model of the sensors can be described as in equation (2.9).

$$V_{sensor_i} = V_{sensor_i}(0) + \left[\frac{\partial V_{sensor_i}}{\partial Y_i}(0) \right] (Y_i - 0) = 5000Y_i \quad (2.9)$$

The linear model of the current amplifiers is given as in equation (2.10).

$$\frac{d}{dt}(i_{control_i}) = -\frac{1}{2.2 \times 10^{-4}} i_{control_i} + \frac{0.25}{2.2 \times 10^{-4}} V_{control_i} \quad (2.10)$$

The state-space representation of the rigid-body motion of the system is obtained by combining equations (2.1)-(2.10) in the form of:

$$\begin{cases} \dot{x} = Ax + Bu, & x \in R^n, \quad u \in R^k \\ y = Cx, & y \in R^m \end{cases} \quad (2.11)$$

In equation (2.11), x is the state vector that is chosen to be $x = [y_0, \dot{y}_0, \theta, \dot{\theta}, i, \dot{i}]^T$, u is the control signal vector of $u = [V_{control_1}, V_{control_2}]^T$, and y is the output vector of $y = [V_{sensor_1}, V_{sensor_2}]^T$. The 6th-order state-space representation of the system

is shown in equations (2.12) and (2.13).

$$\dot{x} = \begin{bmatrix} 0 & 1 & 0 & 0 & 0 & 0 \\ \frac{8750}{m} & 0 & 0 & 0 & \frac{3.5}{m} & \frac{3.5}{m} \\ 0 & 0 & 0 & 1 & 0 & 0 \\ 0 & 0 & \frac{8750}{I_0} \left(\frac{L}{2} - l\right)^2 & 0 & -\frac{3.5}{I_0} \left(\frac{L}{2} - l\right) & \frac{3.5}{I_0} \left(\frac{L}{2} - l\right) \\ 0 & 0 & 0 & 0 & \frac{-1}{2.2 \times 10^{-4}} & 0 \\ 0 & 0 & 0 & 0 & 0 & \frac{-1}{2.2 \times 10^{-4}} \end{bmatrix} x + \begin{bmatrix} 0 & 0 \\ 0 & 0 \\ 0 & 0 \\ 0 & 0 \\ \frac{0.25}{2.2 \times 10^{-4}} & 0 \\ 0 & \frac{0.25}{2.2 \times 10^{-4}} \end{bmatrix} \begin{bmatrix} V_{control_1} \\ V_{control_2} \end{bmatrix} \quad (2.12)$$

$$\begin{bmatrix} V_{sensor_1} \\ V_{sensor_2} \end{bmatrix} = 5000 \begin{bmatrix} 1 & 0 & -\left(\frac{L}{2} - l_2\right) & 0 & 0 & 0 \\ 1 & 0 & -\left(\frac{L}{2} - l_2\right) & 0 & 0 & 0 \end{bmatrix} x \quad (2.13)$$

The bending-body motion of the rotor can also be included into the model. A second-order model is required to represent each flexible-mode of the rotor. Since the first two modes are within the rotor's operating range, the order of the rigid-body motion is increased by 4. The final 10th-order state-space representation of the system in the horizontal direction is found to be in the form of equation (2.14).

$$A = \begin{bmatrix} 0 & 1 & 0 & 0 & 0 & 0 & 0 & 0 & 0 & 0 \\ \frac{8750}{m} & 0 & 0 & 0 & \frac{-8750 \times 1.19029}{m} & 0 & 0 & 0 & \frac{3.5}{m} & \frac{3.5}{m} \\ 0 & 0 & 0 & 1 & 0 & 0 & 0 & 0 & 0 & 0 \\ 0 & 0 & \frac{8750}{I_0} \left(\frac{L}{2} - l\right)^2 & 0 & 0 & \frac{1}{I_0} \left(\frac{L}{2} - l\right) \times 8750 \times 0.608354 & 0 & 0 & -\frac{3.5}{I_0} \left(\frac{L}{2} - l\right) & -\frac{3.5}{I_0} \left(\frac{L}{2} - l\right) \\ 0 & 0 & 0 & 0 & 0 & 0 & 1 & 0 & 0 & 0 \\ 0 & 0 & 0 & 0 & 0 & 0 & 0 & 1 & 0 & 0 \\ \frac{-8750 \times 1.19029}{0.272146} & 0 & 0 & 0 & \frac{-6.05762e6 + 8750 \times 1.19029^2}{0.272146} & 0 & 0 & 0 & \frac{-3.5 \times 1.19029}{0.272145} & \frac{-3.5 \times 1.19029}{0.272145} \\ 0 & 0 & \frac{\left(\frac{L}{2} - l\right) \times 8750 \times 0.608354}{0.262297} & 0 & 0 & \frac{-4.4363e7 + 8750 \times 0.608354^2}{0.262297} & 0 & 0 & \frac{-3.5 \times 0.608354}{0.262297} & \frac{-3.5 \times 0.608354}{0.262297} \\ 0 & 0 & 0 & 0 & 0 & 0 & 0 & 0 & -\frac{1}{2.2e-4} & 0 \\ 0 & 0 & 0 & 0 & 0 & 0 & 0 & 0 & 0 & -\frac{1}{2.2e-4} \end{bmatrix}$$

$$B^T = \begin{bmatrix} 0 & 0 & 0 & 0 & 0 & 0 & 0 & 0 & \frac{0.25}{2.2e-4} & 0 \\ 0 & 0 & 0 & 0 & 0 & 0 & 0 & 0 & 0 & \frac{0.25}{2.2e-4} \end{bmatrix}$$

$$C = 5000 \begin{bmatrix} 1 & 0 & -\left(\frac{L}{2} - l_2\right) & 0 & -1.93745 & -1.83546 & 0 & 0 & 0 & 0 \\ 1 & 0 & -\left(\frac{L}{2} - l_2\right) & 0 & -1.93745 & 1.83546 & 0 & 0 & 0 & 0 \end{bmatrix}$$

$$D = \begin{bmatrix} 0 & 0 \\ 0 & 0 \end{bmatrix} \quad (2.14)$$

The Bode diagrams of the rigid-body model of the system and the full-body model of the system (including the rigid-body and the flexible modes of the system) in the horizontal direction are depicted in Fig. 2.4.

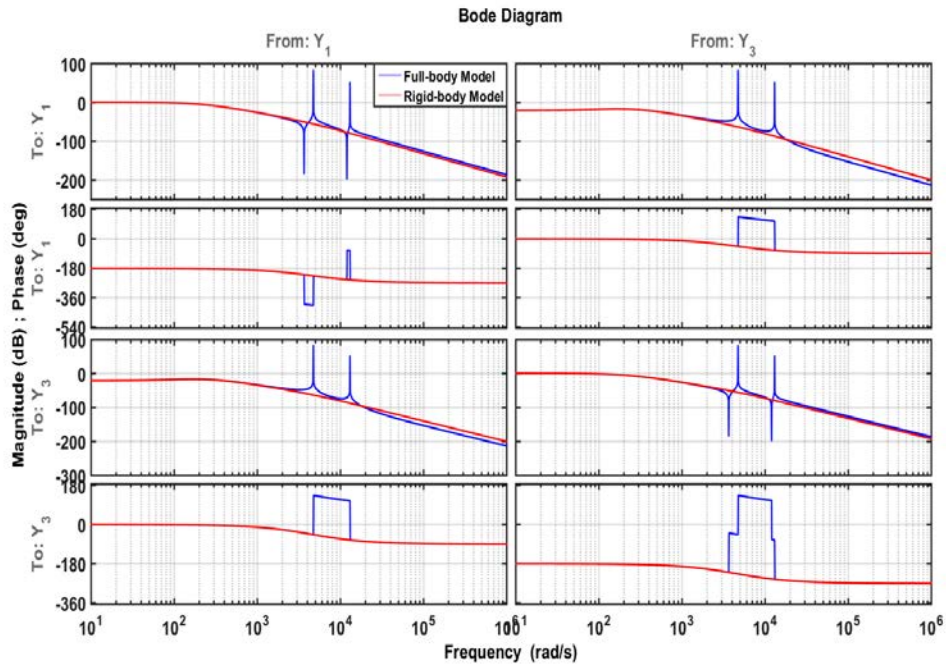


Figure 2.4: Bode diagrams of the rigid-body and total-body models of the system (in the horizontal direction).

2.4 Experimental System Identification

As AMBs are inherently open-loop unstable, closed-loop system identification must be performed instead of more common open-loop identification techniques [52, 53]. Although time-domain and frequency-domain data can be used for the system identification procedure, the use of frequency-domain data is preferred here over time-domain data because of the many advantages that frequency-domain data offer:

- I) noisy data can be detected and eliminated;
- II) it is easy to combine data from different experiments of various frequency ranges;
- III) using multi-frequency excitation, the system's behaviour in a wide range of frequencies can be observed;
- IV) no initial state estimation of the system is required;
- V) it can be ensured that the dynamics associated with the rigid-body and flexible-body motions of the system are carefully modelled.

Fig. 2.2 shows the block diagram of the setup that is used to collect the required data for the system identification stage. The data are taken while the rotor is stationary and stabilised with the four analog on-board controllers under the

assumption that no disturbance is acting on the system. A control-relevant system identification procedure on the AMB system is described here. Assuming that the closed-loop system is stable and it is not subject to any external disturbances, the relationship between the system outputs $Y = [Y_1, Y_2, Y_3, Y_4]^T$, the probing signals $R = [R_1, R_2, R_3, R_4]^T$, and the measurement noise $\xi = [\xi_1, \xi_2, \xi_3, \xi_4]^T$ is given in equation (2.15).

$$\begin{aligned} Y(s) &= \left(I + G(s)K(s) \right)^{-1} G(s)R(s) \\ &\quad - \left(I + G(s)K(s) \right)^{-1} G(s)K(s)\xi(s) \end{aligned} \quad (2.15)$$

Similarly, the relationship between the control signals $U = [U_1, U_2, U_3, U_4]^T$, the probing signals $R = [R_1, R_2, R_3, R_4]^T$, and the measurement noise $\xi = [\xi_1, \xi_2, \xi_3, \xi_4]^T$ can be obtained as in equation (2.16).

$$\begin{aligned} U(s) &= \left(I + K(s)G(s) \right)^{-1} R(s) \\ &\quad - \left(I + K(s)G(s) \right)^{-1} K(s)\xi(s) \end{aligned} \quad (2.16)$$

Since the probing signals R and the measurement noise (with zero mean) ξ are uncorrelated, the transfer functions between the system outputs Y and the probing signals R can be obtained as in equation (2.17). For matrices of appropriate dimensions, equation (2.17) should follow the push-through rule:

Push-through rule: Assuming that the transfer matrices G and K are invertible, and both G and K are such matrices that GK and KG are defined:

$$G(I + KG)^{-1} = (I + GK)^{-1}G$$

Proof: Multiplying both sides of the equation by $(I + KG)$ results in:

$$\begin{aligned} G(I + KG)^{-1}(I + KG) &= (I + GK)^{-1}G(I + KG) \Leftrightarrow \\ G &= (I + GK)^{-1}(G + GK) \Leftrightarrow G = (I + GK)^{-1}(I + GK)G \Leftrightarrow G = G \end{aligned}$$

According to the push-through rule, the transfer function between the output signal Y and the probing signal R can be written as in equation (2.17).

$$T_{YR}(s) \approx \left(I + G(s)K(s) \right)^{-1} G(s) = G(s) \left(I + K(s)G(s) \right)^{-1} \quad (2.17)$$

Similarly, the transfer function between the control signals U and the probing signals R can be simplified as in equation (2.18).

$$T_{UR}(s) \approx \left(I + K(s)G(s) \right)^{-1} \quad (2.18)$$

By using equations (2.17) and (2.18), the open-loop unstable SISO transfer functions of the system can be estimated from the closed-loop system identification as:

$$G(s) = T_{YR}(s)T_{UR}(s)^{-1} \quad (2.19)$$

Chirp signals are employed as the probing signals to the system for the purpose of collecting frequency response data. Initial frequency, target time, and the frequency at the target time of the chirp signals are chosen in such a way that the frequency does not increase too fast, so that the system has enough time to attain its steady-state response. A fixed sample time of 0.000049 seconds that corresponds to sampling frequency of approximately 20 kHz is used for the system identification process. A higher sampling frequency may result in aliasing effects. In order not to overly excite the resonant frequencies, several sets of measurements have to be taken, each one within a certain range of frequency and amplitude. This problem is solved by taking several measurements with different amplitudes and frequencies and combining them in MATLAB. The amplitude and frequency range of each chirp signal are depicted in Table 2.2.

Table 2.2: Chirp Signal Inputs

Measurement	Low Freq.	First Resonance	Middle Freq.	Second Resonance	High Freq.
Chirp Start freq. (Hz)	1	610	975	1880	2220
Chirp End freq. (Hz)	610	975	1880	2220	5000
Amplitude (Volts)	0.6	0.4	0.6	0.1	0.2

The MIMO measurements are taken in 20 individual experiments. In each experiment, five different chirp signals with different amplitudes and frequencies (shown in Table 2.2) are sent to one input channel and the responses of four output channels are collected. The experimental power spectrum of the input chirp signal and the resulting control and output signals for the first channel are shown in Figs. 2.5 - 2.7.

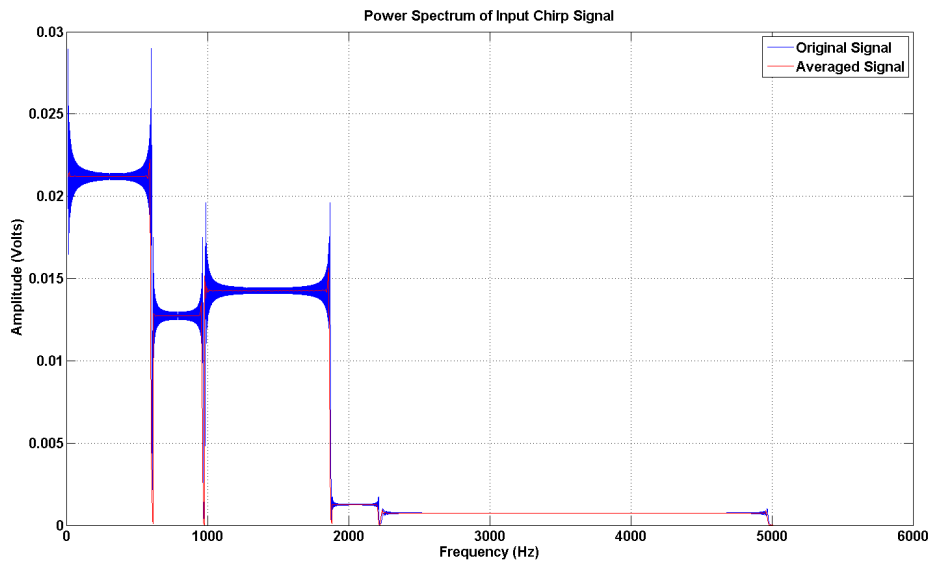


Figure 2.5: Power spectrum of input chirp signal.

The MIMO measurements are taken by sending chirp signals to the input channels R and collecting the control signals U and the system output responses Y . The time-domain response of the system is collected using the dSPACE ControlDesk software and then exported to MATLAB for Discrete Fourier Transform (DFT) analysis. The obtained frequency-domain response (magnitude) of the system is shown in Fig. 2.8. The diagonal terms in Fig. 2.8 represent the frequency response

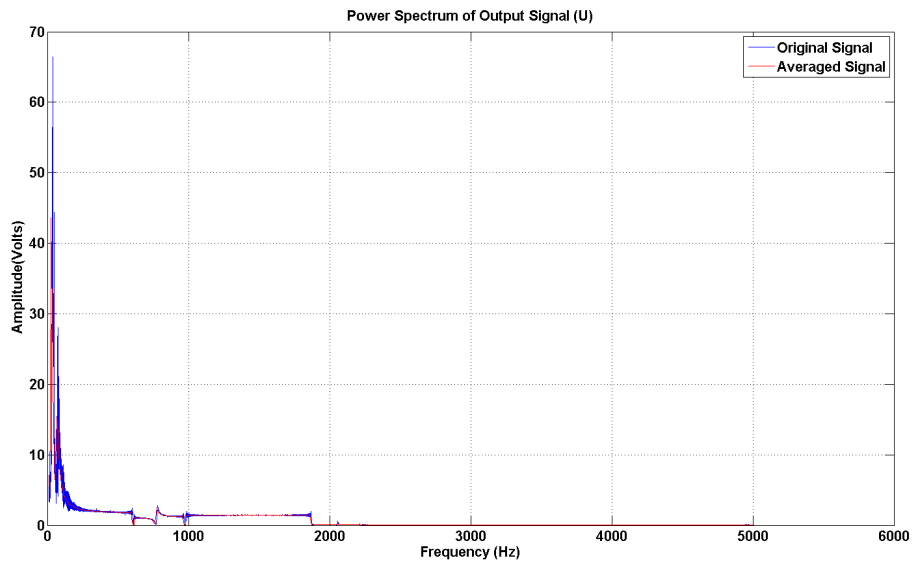


Figure 2.6: Power spectrum of control signal.

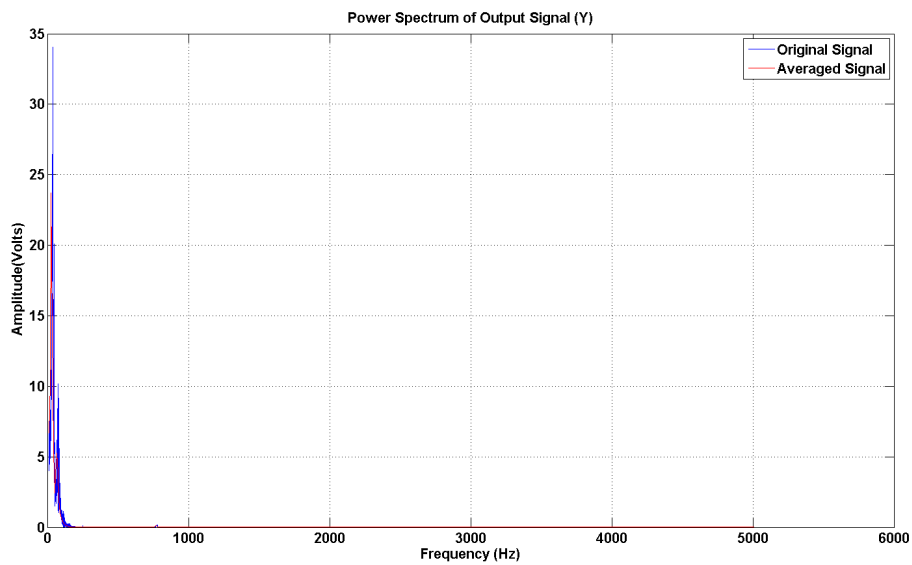


Figure 2.7: Power spectrum of output signal.

between the input and output of the same channel. The off-diagonal terms, on the other hand, represent the cross-coupling effects between different channels. It can

be seen from Fig. 2.8 that the gain contribution of the off-diagonal terms is small in the low-frequency region, i.e., a dc-gain of about -20 dB or less. Therefore, if low-order (low-complexity) controllers are to be designed for the system, the MIMO system can be treated as four SISO subsystems and the model of each subsystem can be obtained individually.

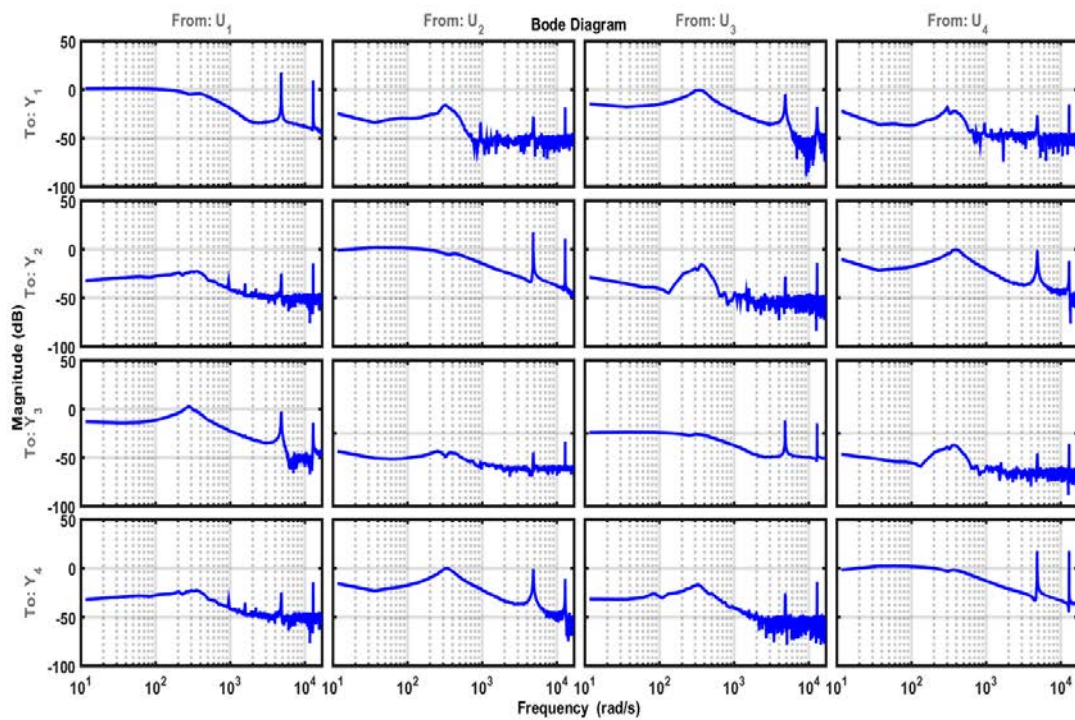


Figure 2.8: Frequency-domain response data of the MIMO AMB system.

The SISO models of the system can be represented as linear time-invariant transfer functions of the form:

$$G(s) = \frac{N(s)}{D(s)} \quad (2.20)$$

where,

$$\begin{aligned} N(s) &= n_0 + n_1(s) + n_2(s)^2 + \dots + n_k(s)^k, & \forall s = j\omega \\ D(s) &= 1 + d_1(s) + d_2(s)^2 + \dots + d_l(s)^l, & \forall s = j\omega \end{aligned}$$

In order to have a proper system, the order of the numerator (k) has to be less than or equal to the order of the denominator (l). From the DFT analysis of the input and output signals of the system at all experimental frequencies ($\omega_1, \omega_2, \dots, \omega_N$), a non-parametric model of the system can be obtained as $\hat{G}(j\omega)$. The operator $\hat{\cdot}$ is used because there are always unavoidable errors in the measurement. Since it is assumed that $\hat{G}(j\omega) = N(j\omega)/D(j\omega)$, we have:

$$D(j\omega)\hat{G}(j\omega) = N(j\omega) \quad (2.21)$$

The unknown coefficients (n_0, n_1, \dots, n_k), and ($1, d_1, \dots, d_l$) can be evaluated by minimising the sum of squared of moduli of the errors between the frequency response of the fitted transfer function $N(s)/D(s)$ and the collected frequency response data $\hat{G}(j\omega)$ [54]:

$$J = \sum_{i=1}^N e_i^* e_i \quad (2.22)$$

where, $e_i = D(j\omega_i)\hat{G}(j\omega_i) - N(j\omega_i)$, and $*$ denotes complex-conjugate transpose.

The term e_i can be expressed as:

$$e_i = \begin{bmatrix} 1 + d_1(j\omega_i) + \cdots + d_l(j\omega_i)^l \\ - [n_0 + n_1(j\omega_i) + \cdots + n_k(j\omega_i)^k] \end{bmatrix} \hat{G}(j\omega_i) \quad (2.23)$$

or alternatively,

$$e_i = \begin{bmatrix} \hat{G}(j\omega_i) - [- (j\omega_i)\hat{G}(j\omega_i), \dots, -(j\omega_i)^l\hat{G}(j\omega_i), \\ 1, j\omega_i, \dots, (j\omega_i)^k] \theta \end{bmatrix} \quad (2.24)$$

where $\theta = [d_1, d_2, \dots, d_l, n_0, n_1, \dots, n_k]^T$ is a vector of unknown parameters. The cost function J can now be expressed as:

$$J = \sum_{i=1}^N e_i^* e_i = (Y - X\theta)^*(Y - X\theta) \quad (2.25)$$

where,

$$\theta = \begin{bmatrix} d_1, d_2, \dots, d_l, n_0, n_1, \dots, n_k \end{bmatrix}^T$$

$$Y = \begin{bmatrix} \hat{G}(j\omega_1), \hat{G}(j\omega_2), \dots, \hat{G}(j\omega_N) \end{bmatrix}^T$$

$$X = \begin{bmatrix} -j\omega_1\hat{G}(j\omega_1) & \cdots & -(j\omega_1)^l\hat{G}(j\omega_1) & 1 & j\omega_1 & \cdots & (j\omega_1)^k \\ \vdots & & & & & & \vdots \\ -j\omega_N\hat{G}(j\omega_N) & \cdots & -(j\omega_N)^l\hat{G}(j\omega_N) & 1 & j\omega_N & \cdots & (j\omega_N)^k \end{bmatrix}$$

The cost function J as a function of θ can be minimised by differentiating J with respect to each unknown parameter in θ and setting the result to zero. The value of θ that minimises J can be obtained as:

$$\theta = \left(X^* X \right)^{-1} \left(X^* Y \right) \quad (2.26)$$

In a standard least-squares problem, it is assumed that the collected response data are of equal quality and hence have a constant noise variance. However, if this assumption does not hold, the quality of the fitted model can be influenced by poor quality data. To improve the model at certain ranges of frequencies, one can use weighted least-squares where the frequency weighting is used to emphasise certain frequencies of interest. The weighted least-squares minimises the sum squared of the weighted error:

$$J = \sum_{i=0}^N w_i e_i^* e_i \quad (2.27)$$

The weights w_i determine how much each response value influences the final parameter estimates. Note that the weights w_i are positive definite and they are

given as the diagonal elements of the weight matrix W :

$$W = \begin{bmatrix} w_1 & 0 & \dots & 0 \\ 0 & w_2 & \dots & 0 \\ \vdots & \vdots & \ddots & \vdots \\ 0 & 0 & \dots & w_N \end{bmatrix} \quad (2.28)$$

The unique solution to the weighted least-squares problem is known to be in the form of equation (2.29).

$$\theta = \left(X^* W X \right)^{-1} \left(X^* W Y \right) \quad (2.29)$$

For the AMB system under study, the two flexible (resonant) modes of the rotor need to be modelled accurately, as they are within the bandwidth of the system. The problem with the most of available identification methods is that these algorithms find an accurate model of the system in the low-frequency region, but they fail to model the resonant modes. The aim here is to find a model of the system that is as simple as possible, and yet capable of capturing all the important characteristics of the plant. To overcome this problem, genetic algorithm (GA) [46, 47] is employed to find the required frequency weightings (fictitious noise components) automatically, and perform an iterative re-weighted least squares algorithm to identify the system model. In this approach, GA generates a random vector of $w_i > 0$ to be the diagonal elements of the weight matrix W . Then, GA

alters the weights by changing the range and scaling factors in the vector w_i . The WLS is solved on the basis of the updated weight matrix, and the iteration continues until the minimum difference between the frequency response of the model and the experimental data and a predefined value is achieved (or the maximum number of iterations is reached). In order to scale up the errors around the two resonant modes, six variables are defined. These parameters are mainly the lower and upper frequency ranges of interest ($[\omega_{1-start}, \omega_{1-end}]$, and $[\omega_{2-start}, \omega_{2-end}]$), and their corresponding scaling factors (α and β) as shown in equation (2.30). The optimum value of (α and β) are to be found by the GA to heavily penalise the fitting error in a particular range of frequencies where the modelling accuracy is important.

$$w_i = \begin{bmatrix} 1, \dots, 1, \alpha\omega_{1-start}, \dots, \alpha\omega_{1-end}, 1, \dots, 1, \\ \beta\omega_{2-start}, \dots, \beta\omega_{2-end}, 1, \dots, 1 \end{bmatrix} \quad (2.30)$$

Figs. 2.9 and 2.10 show the convergence of GA and the effect of the frequency weighting on the explicit solution of the least-squares problem and hence on the frequency response of the modelled transfer function. It should be noted that the optimisation process is only illustrated for the first channel, and relatively similar results are obtained for the other three channels.

It is important to note that the desired order of the model has to be assigned before the optimisation process is initiated. Since the total order of four is required to model the two flexible (resonant) modes of the rotor, it can be deduced that models with order less than five will fail to accurately model the behavior of the

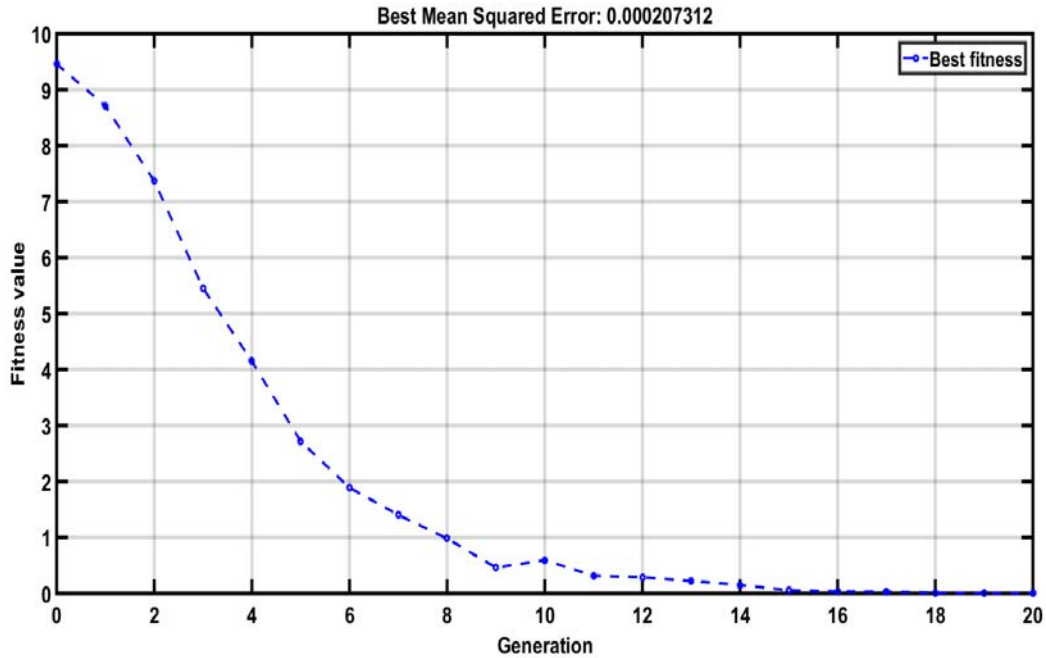


Figure 2.9: Convergence of GA.

actual system. Therefore, a sixth-order model is chosen to ensure the accurate modelling of the system at the frequency ranges of interest. The obtained SISO models of all four channels using the proposed methods are compared with two common methods, namely, the prediction error method (PEM) and the numerical subspace state-space (N4SID) identification method in Fig. 2.11. The results show the effectiveness of the proposed method in the identification of systems that include both slow and fast dynamics. The resulting transfer functions of all four channels are presented in equations (2.31)-(2.34).

$$\begin{aligned}
 G_1(s) &= \frac{-0.0054872(s+1.72 \times 10^4)(s-2075)}{(s+374.4)(s-310.2)} \\
 &\times \frac{(s^2+4240s+2.127 \times 10^7)(s^2+3305s+1.637 \times 10^8)}{(s^2+0.96s+2.344 \times 10^7)(s^2+0.37s+1.668 \times 10^8)} \quad (2.31)
 \end{aligned}$$

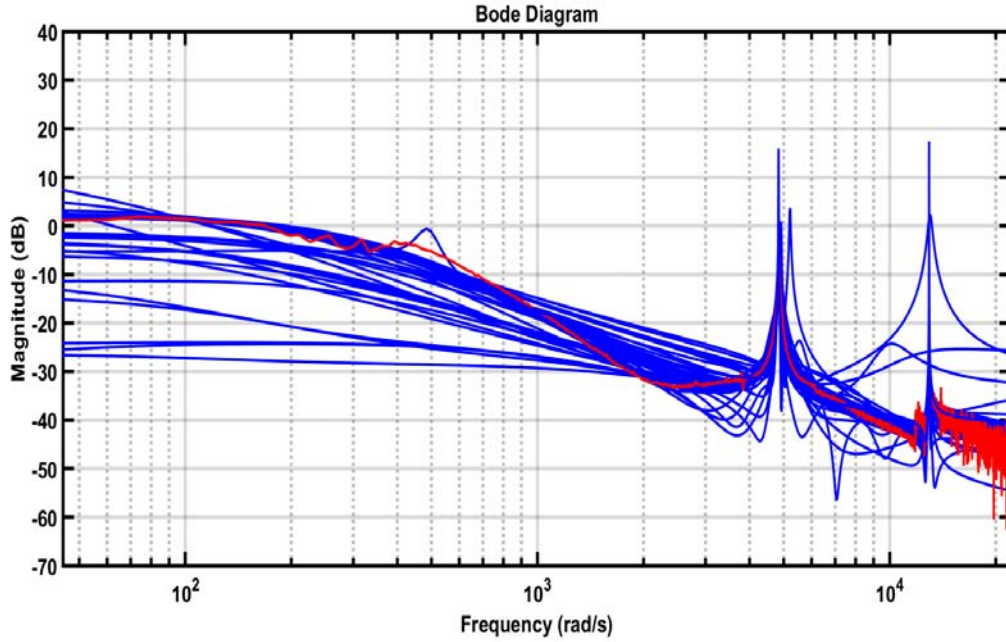


Figure 2.10: A snapshot of GA optimisation.

$$\begin{aligned}
 G_2(s) &= \frac{-0.0205(s+5699)(s-1588)}{(s+433.4)(s-233.4)} \\
 &\times \frac{(s^2+4168s+2.127 \times 10^7)(s^2+3140s+1.631 \times 10^8)}{(s^2+0.27s+2.307 \times 10^7)(s^2+0.3s+1.673 \times 10^8)} \quad (2.32)
 \end{aligned}$$

$$\begin{aligned}
 G_3(s) &= \frac{-0.01993(s+5178)(s-2135)}{(s+628.1)(s-215.5)} \\
 &\times \frac{(s^2+4083s+2.329 \times 10^7)(s^2+5183s+1.631 \times 10^8)}{(s^2+0.31s+2.399 \times 10^7)(s^2+0.35s+1.673 \times 10^8)} \quad (2.33)
 \end{aligned}$$

$$\begin{aligned}
 G_4(s) &= \frac{-0.04793(s+3912)(s-1189)}{(s+388.4)(s-246.7)} \\
 &\times \frac{(s^2+4022.66s+1.947 \times 10^7)(s^2+3743s+1.631 \times 10^8)}{(s^2+0.529s+2.3 \times 10^7)(s^2+0.726s+1.65 \times 10^8)} \quad (2.34)
 \end{aligned}$$

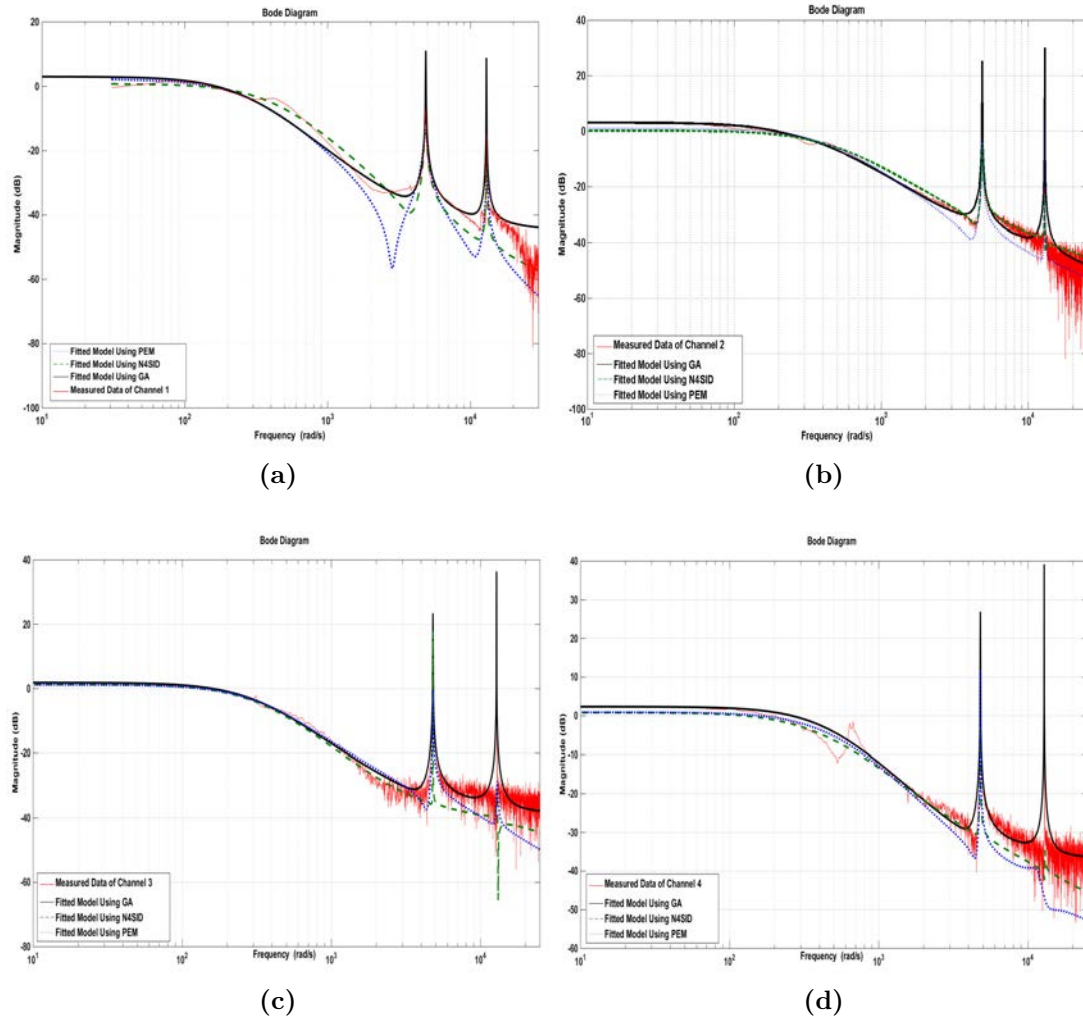


Figure 2.11: Bode (magnitude) diagrams of the measure experimental data and the identified SISO models of the system using the presented algorithm, PEM, and N4SID, (a) Channel Y_1 , (b) Channel Y_2 , (c) Channel Y_3 , (d) Channel Y_4 .

The described approach for the SISO modelling of the system can be extended to estimate the MIMO model of the system (including the cross-coupling effects between the channels in Fig. 2.8) if a high-order MIMO controller is to be designed on the basis of the MIMO model of the system. Suppose that the model is represented in the state-space form (assuming that the feed-through term D is

zero):

$$\begin{aligned}\dot{x}(t) &= Ax(t) + Bu(t), \quad x \in R^n, \quad u \in R^k \\ y &= Cx(t), \quad y \in R^m\end{aligned}\tag{2.35}$$

It is assumed that the system has k inputs, m outputs, and n states. A transfer function representation of the system can be obtained as:

$$G(s) = C(sI - A)^{-1}B, \quad \forall s = j\omega\tag{2.36}$$

Similar to the SISO case, the vector of unknown parameters

$$\theta = \left[\text{vec}(A)^T, \text{vec}(B)^T, \text{vec}(C)^T \right]$$

can be estimated by minimising the weighted sum of the squared errors between the frequency response of the state-space model $G(s)$ and the experimental data at all experimental points $\hat{G}(j\omega)$:

$$J = \sum_{i=1}^N w_i \|\hat{G}(j\omega_i) - G(j\omega_i)\|^2\tag{2.37}$$

Again, GA is utilised to obtain the best weighting vector that minimises the cost function J over the unknown parameter vector θ . Note that a higher-order model is required to successfully describe the dynamics of the MIMO system including

the cross-couplings. After some trials, an eighteenth-order state-space model of the system is found to have a fair representation of the actual system dynamics. The frequency response of the MIMO model is shown in Fig. 2.12, and it is compared with the collected frequency-domain data. The state-space representation of the obtained eighteenth-order MIMO model of the system is given in equation (2.38), and it is used for the synthesis of the MIMO H_2 and H_∞ controllers.

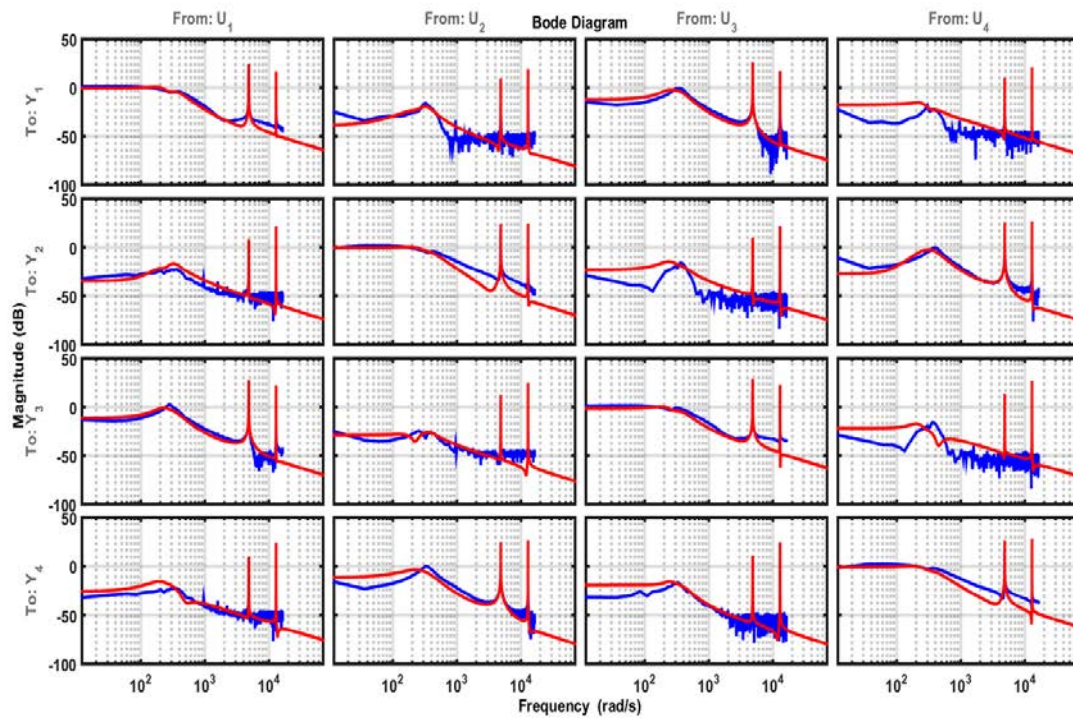


Figure 2.12: The identified 4×4 MIMO model of the system and the experimental frequency response data.

$$A = \text{diag} \left\{ \begin{pmatrix} -0.0359 & 12900 \\ -12900 & -0.0359 \end{pmatrix}, \begin{pmatrix} -0.55 & 4826 \\ -4826 & -0.55 \end{pmatrix}, \right. \\ \begin{pmatrix} -0.69 & 4835 \\ -4835 & -0.69 \end{pmatrix}, \begin{pmatrix} -152 & 335.8 \\ -335.8 & -152.9 \end{pmatrix}, \\ \begin{pmatrix} -120.9 & 341.8 \\ -341.8 & -120.9 \end{pmatrix}, \begin{pmatrix} -111.8 & 228.2 \\ -228.2 & -111.8 \end{pmatrix}, \\ \left. \begin{pmatrix} -70.51 & 212.4 \\ -212.4 & -70.51 \end{pmatrix}, 191.4, 243.4, 272.4, 284.5 \right\}$$

$$B = \begin{pmatrix} -0.0243 & 0.0176 & -0.0235 & -0.0193 \\ 0.0453 & -0.0672 & 0.0486 & 0.0839 \\ 0.5450 & 0.0348 & -0.5991 & 0.0686 \\ -1.4730 & 0.2672 & 1.7560 & 0.3069 \\ -0.1713 & -1.4250 & 0.2059 & -1.7710 \\ 0.0820 & -0.7334 & -0.0522 & -0.8909 \\ -5.2730 & 4.2650 & -4.8140 & -3.4230 \\ -1.7190 & -3.8070 & 3.0520 & 9.5530 \\ -5.1950 & 2.4130 & -8.4050 & -3.1360 \\ -1.4100 & 1.6070 & 1.4170 & -3.6310 \\ -2.0850 & -1.2980 & -0.3873 & 4.2370 \\ -2.0320 & 5.3700 & -1.7270 & 5.5080 \\ 7.4800 & -0.7283 & -5.0160 & -1.0070 \\ 1.1000 & 0.9193 & 1.7110 & 1.5220 \\ 8.7810 & -21.0600 & 0.5281 & 33.6300 \\ -44.7700 & -16.0000 & -53.4300 & 1.0640 \\ -50.9400 & -8.0200 & 65.9800 & 13.8900 \\ 34.1700 & -55.9100 & -50.3000 & -44.6800 \end{pmatrix}$$

$$C^T = \begin{pmatrix} -7.2300 & -2.1590 & -1.5950 & 6.9340 \\ -5.5360 & 16.7600 & -18.1900 & -20.8700 \\ -10.4100 & 0.5644 & 16.4900 & 1.6760 \\ -5.5310 & 1.7130 & 3.7640 & 1.2470 \\ -1.2190 & -6.6440 & 1.9040 & -1.9720 \\ 0.7982 & 11.4200 & -1.7800 & 14.4700 \\ -1.3220 & -15.4500 & 0.3159 & 9.0980 \\ 6.2330 & 9.8390 & 4.5670 & -3.8710 \\ 12.8700 & 16.3700 & 9.2420 & -3.2940 \\ 8.9640 & -0.9097 & 3.0000 & 1.0810 \\ 3.3940 & 1.7800 & 1.0590 & -15.4300 \\ -3.4690 & -17.5500 & 3.2230 & -10.5200 \\ -8.5000 & -1.9170 & 10.1500 & -1.3500 \\ 4.0930 & -2.0230 & -8.2030 & -2.2680 \\ 0.6677 & -2.5790 & 0.3406 & 3.1050 \\ -2.1520 & -0.2261 & -1.9370 & 0.4813 \\ -1.1260 & -1.9160 & 1.4620 & -0.5211 \\ 0.6849 & -1.9850 & 0.2637 & -1.0290 \end{pmatrix} \quad (2.38)$$

2.5 Conclusion

AMBs are ideal for extremely fast and accurate operations. However, the systems resonant modes could threaten the stability of the system and need to be accurately modelled. In this Chapter, both analytical and experimental models of the system were obtained. GA was employed in conjunction with WLS for closed-loop identification of the AMB system in frequency-domain. Frequency windows were defined in order to improve the models in certain ranges of frequencies. Compared with some widely known identification techniques, GA performed very well or even better in terms of mean squared error (MSE) between the frequency response of the identified model and the real system. A similar approach was utilised to obtain both SISO and MIMO models of the AMB system. In the remaining of the thesis, the SISO models of the system shown in equations (2.31)-(2.34) are used when SISO controllers are to be designed. Whereas, the 4×4 MIMO model in equation (2.38) is used to design MIMO controllers.

Chapter 3

SISO and MIMO Robust Controllers

3.1 Introduction

Although several works can be found on the analytical modelling and simulation of H_∞ controllers on AMBs [55, 56, 57, 58], real-time application of robust control methods on AMBs is a relatively recent development [18, 19, 20, 21, 22, 23, 59, 60, 61, 62, 63]. Furthermore, the results presented in the recent works have many shortcomings to consider this problem as solved. This gives reasonable motivations to address the current gaps between the theory and the challenges involved in real-time application of robust controllers on AMB systems. In the sequel, some

of the shortcomings in the recent works are discussed in more details. The work in reference [19] reports a single-input single-output (SISO) modelling and real-time implementation of H_∞ controller of an AMB system. An SISO controller is designed on the basis of the second-order model of the electromagnets. While low-bandwidth (low-performance) controllers can always be designed on the basis of a low-order model of the system for stabilisation purposes, the effects caused by the cross-couplings between the channels, flexible modes of the rotor, the rotor mass-imbalance, and centrifugal forces in high speeds could lead to system instability. The difficulties that may arise when more accurate (and higher-order) models of the system are used to design the robust controllers can be clearly seen in the recently published works. For instance, the frequency-domain results presented in reference [18] clearly show that the synthesised controllers fail to reject the effects caused by the flexible modes of the rotor. It is dangerous to implement such non-robust controllers on the system, as it could lead to system instability. To alleviate the problem, the work in reference [59] suggests to manually add additional notch filters to the final designed controllers to ensure that the resonant modes of the rotor are not excited. However, it should be noted that the closed-loop stability of the overall system is no longer guaranteed. More recently, the MIMO identification and H_∞ control synthesis of AMBs are investigated in references [20, 21, 22, 23]. Firstly, a high-order MIMO model of the system, including the cross-couplings between all inputs and outputs is obtained from the frequency-domain response data of the system. Next, the identified model is used to synthesise the MIMO H_∞ controllers. However, all the synthesised controllers are found to be *unstable* themselves and impossible to implement on the actual system. The fact that the designed *unstable* controllers fail to stabilise the system implies that the identified

model may not represent the characteristics of the actual system being controlled. The authors proceed to implement the unstable controllers by first stabilising the system using low-performance *stable* controllers that are synthesised on the basis of a low-order model of the system and gradually switching to the unstable controllers (in a time-span of five seconds). The successful switching between the controllers depends highly on the slow transition between the stable and unstable controllers. It should also be noted that the order of the MIMO H_∞ controllers are very high and the presented Youla parametrisation of the switching controllers further increases the order of the final controllers. This approach is not only impractical in the industrial applications, it is also extremely challenging to implement such excessively high-order controllers in real-time.

The synthesis of *unstable* H_∞ controllers that are not directly implementable on the system is not a trivial issue, and it may occur in the control synthesis of systems other than AMBs. The authors in references [22, 23] claim that synthesising unstable controllers is not a surprise, as the H_∞ synthesis algorithms tend to cancel the right-half plane (RHP) complex-conjugate zeros in the model of AMBs with RHP poles in the controller. Although several examples on *unstable* controllers can be found in the literature, it should be noted that unstable controllers should be accepted only if the system model does not possess the parity interlacing property (PIP) [24, 64]. The PIP condition only applies to the poles and zeros on the real-axis. Therefore, regardless of the location of the complex-conjugate poles and zeros in the model, as long as the PIP conditions are satisfied (which is the case for AMBs), there should exist *stable* controllers that guarantee the internal stability of the system-controller interconnection and hence no switching is required between the

controllers. It is also emphasised in reference [24] that unstable controllers should only be used in special circumstances where stabilisation with stable controllers is infeasible and should be avoided at all cost.

This Chapter is devoted to the synthesis of controllers that are designed on the basis of the identified SISO and MIMO models of the system. Firstly, four SISO H_∞ optimal controllers are designed on the basis of the SISO models and some useful remarks are given for the design of the weighting functions required in the H_∞ controller design procedure. To demonstrate the advantages of the H_∞ optimisation algorithms over the classical control design methods, four lead-lag type compensators are also designed on the basis of the identified SISO models. In order to investigate the effects of the cross-coupling channels on the overall performance of the system, MIMO H_2 and H_∞ optimal controllers are synthesised on the basis of the 4×4 MIMO model. Similar time- and frequency-domain requirements are chosen for the design of both SISO and MIMO controllers. This ensures that the conditions of all SISO and MIMO controllers are similar and hence the comparison between the performance of these controllers is fair. It is shown that the proper modelling of the system results in *stable* high-performance controllers that can be implemented on the system directly and safely without any additional modification or switching between the controllers.

3.2 H_∞ Controller Design

The H_∞ norm of a function is defined as the least upper bound (supremum) of the function over frequency [65]:

$$\|F\|_\infty = \sup_{\omega \in \mathbb{R}} |F(j\omega)| \quad (3.1)$$

In the mixed-sensitivity H_∞ control synthesis approach, three weighting functions can be designed to shape the closed-loop behaviour of the system (see Fig. 3.1). In fact, W_P is designed to shape the closed-loop sensitivity function ($S = (I + GK)^{-1}$) to improve the steady-state error of the system as well as the disturbance rejection capabilities. Whereas, W_T bounds the closed-loop complementary sensitivity function ($T = GK(I + GK)^{-1}$) to increase the system's robustness against uncertainties and to reject the high-frequency measurement noise. Furthermore, W_U is a weighting function to penalise the control signal ($KS = K(I + GK)^{-1}$) and to avoid the actuators saturation. The requirements can be absorbed into a stacked H_∞ optimisation problem and the feedback system can be rearranged as a linear fractional transformation (LFT). The weighting functions (W_P , W_T , and W_U) can be easily combined with the system and represented as a generalised plant $P(s)$.

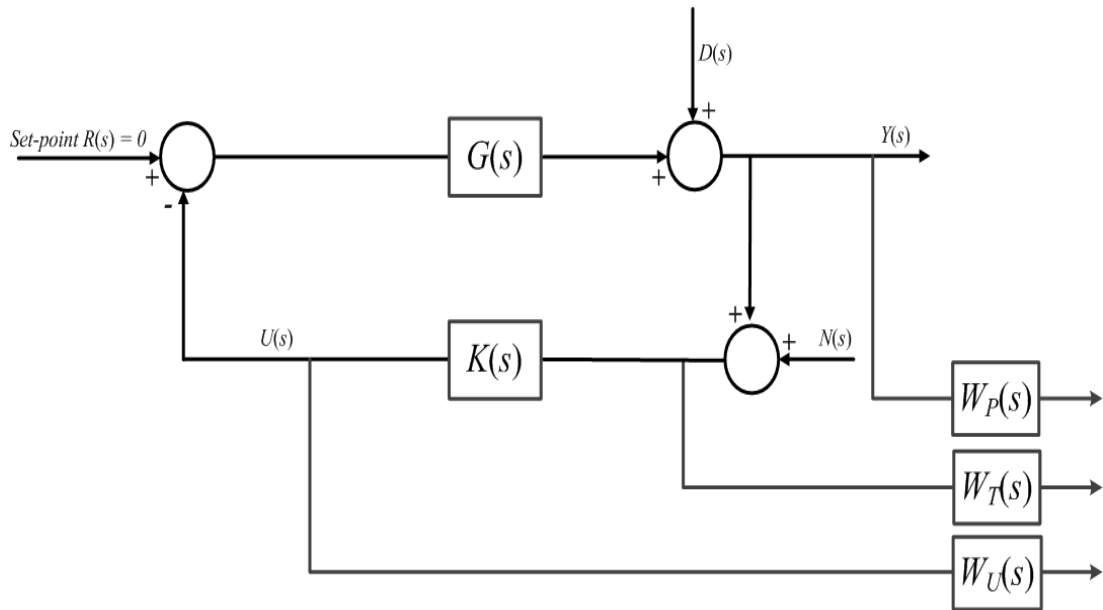


Figure 3.1: Mixed S/T/KS sensitivity problem.

The state-space realisation of the generalised plant $P(s)$ in equation (3.2) can be found as:

$$P = \left[\begin{array}{c|cc} A & B_1 & B_2 \\ \hline C_1 & D_{11} & D_{12} \\ C_2 & D_{21} & D_{22} \end{array} \right] \quad (3.2)$$

The closed-loop transfer function of the system can be found as an LFT of the generalised plant with respect to the controller as shown in equation (3.3).

$$N := \mathcal{F}_l(P, K_\infty) = P_{11} + P_{12}K_\infty(I - P_{22}K_\infty)^{-1}P_{21} \quad (3.3)$$

In equation (3.3), $\mathcal{F}_l(P, K_\infty)$ is the lower LFT of $P(s)$ with respect to $K_\infty(s)$. Also, $P_{11} = [0, 0, W_P I]^T$, $P_{12} = [W_U I, W_T G, W_P G]^T$, $P_{21} = -I$, and $P_{22} = -G$. The H_∞ mixed-sensitivity synthesis problem is to find a controller K_∞ which stabilises the system and minimises the H_∞ -norm of the closed-loop transfer function of the augmented plant $P(s)$:

$$\min_{K \text{ stabilising}} \|\mathcal{F}_l(P, K)\|_\infty \quad (3.4)$$

where,

$$\|\mathcal{F}_l(P, K)\|_\infty = \left\| \begin{array}{c} W_P S \\ W_U K S \\ W_T T \end{array} \right\|_\infty \quad (3.5)$$

It is assumed that the plant P and the controller K are proper and real rational. Their corresponding state-space realisations are also assumed to be stabilisable and detectable. The objective of sub-optimal H_∞ problem is to find an admissible (internally stabilisable) controller $K(s)$, such that the H_∞ norm of the closed-loop transfer function, i.e., $\|\mathcal{F}_l(P, K)\|_\infty < \gamma$ is minimised. The weighting functions W_P , W_U and W_T are chosen to reflect the design objectives. The solution to the H_∞ optimisation problem based on the Ricatti approach involves optimisation of two

Hamiltonian matrices [65]:

$$H_\infty = \begin{bmatrix} A & \gamma^{-2}B_1B_1^* - B_2B_2^* \\ -C_1^*C_1 & -A^* \end{bmatrix} \quad (3.6)$$

$$J_\infty = \begin{bmatrix} A^* & \gamma^{-2}C_1^*C_1 - C_2^*C_2 \\ -B_1B_1^* & -A \end{bmatrix} \quad (3.7)$$

There exists a stabilising controller such that the $\|T\|_\infty < \gamma$ if and only if the following three conditions hold:

- 1) $H_\infty \in \text{dom}(\text{Ric})$ and $X_\infty := \text{Ric}(H_\infty) \geq 0$
- 2) $J_\infty \in \text{dom}(\text{Ric})$ and $Y_\infty := \text{Ric}(J_\infty) \geq 0$
- 3) $\rho(X_\infty Y_\infty) < \gamma^2$

If the three conditions hold, one such controller can be formulated as in equation (3.8).

$$K_{sub}(s) := \left[\begin{array}{c|c} \hat{A}_\infty & Z_\infty L_\infty \\ \hline F_\infty & 0 \end{array} \right] \quad (3.8)$$

where,

$$\begin{aligned} \hat{A}_\infty &:= A + \gamma^{-2} B_1 B_1^* X_\infty + B_2 F_\infty + Z_\infty L_\infty C_2 \\ F_\infty &:= -B_2^* X_\infty, \quad L_\infty := -Y_\infty C_2^*, \quad Z_\infty := (\mathbf{I} - \gamma^{-2} Y_\infty X_\infty)^{-1} \end{aligned} \quad (3.9)$$

The work in reference [66] shows that the regular H_∞ problem can be reformulated as linear matrix inequalities (LMI) rather than the usual dual Riccati equations. Then, efficient convex optimisation techniques can be employed to solve the problem. The H_∞ optimisation using LMIs not only offers an efficient numerical solution, but also it has several advantages over the regular Riccati-based H_∞ optimisation. For instance, it prevents undesirable control-plant pole-zero cancellations. It is further shown that the proposed approach can be introduced for low-order H_∞ synthesis.

Assuming that the pairs (A, B_2) and (A, C_2) in equation (3.2) are stabilisable and detectable, and $D_{22} = 0$, a feedback controller $K(s)$ in the form of

$$K(s) = \begin{bmatrix} A_K & B_K \\ C_K & D_K \end{bmatrix} := C_K (sI - A_K)^{-1} B_K + D_K$$

exists that stabilises the system. If such a controller is found, the closed-loop transfer function from the exogenous inputs to the controlled outputs is obtained as:

$$T_{cl}(s) = C_{cl}(sI - A_{cl})^{-1} B_{cl} + D_{cl} \quad (3.10)$$

where,

$$\begin{aligned} A_{cl} &= \begin{bmatrix} A + B_2 D_K C_2 & B_2 C_K \\ B_K C_2 & A_K \end{bmatrix}, & B_{cl} &= \begin{bmatrix} B_1 + B_2 D_K D_{21} \\ B_K D_{21} \end{bmatrix}, \\ C_{cl} &= \begin{bmatrix} C_1 + D_{12} D_K C_2 & D_{12} C_K \end{bmatrix}, & D_{cl} &= D_{11} + D_{12} D_K D_{21} \end{aligned} \quad (3.11)$$

In order to derive the LMI-based H_∞ control synthesis, two lemmas need to be recalled first.

Lemma 1. Bounded Real Lemma: *Consider a linear time-invariant system . The following statements are equivalent.*

- (i) *there exists a symmetric positive definite matrix X such that the following LMI has a solution.*

$$\begin{pmatrix} A_{cl}^T + X A_{cl} & X B_{cl} & C_{cl}^T \\ B_{cl}^T X & -\gamma I & D_{cl}^T \\ C_{cl} & D_{cl} & -\gamma I \end{pmatrix} < 0 \quad (3.12)$$

- (ii) $\|D_{cl} + C_{cl}(sI - A_{cl})^{-1}B_{cl}\|_\infty < \gamma$ and A_{cl} is stable, i.e., $Re(\lambda_i(A_{cl})) < 0$.

Lemma 2. *Given a symmetric matrix $\Psi \in \mathbf{R}^{m \times m}$ and two matrices P, Q of column dimension m , then the inequality:*

$$\Psi + P^T \Theta^T Q + Q^T \Theta P < 0$$

is solvable for Θ if and only if:

$$\begin{cases} W_P^T \Psi W_P^T < 0 \\ W_Q^T \Psi W_Q^T < 0 \end{cases} \quad (3.13)$$

where, W_P and W_Q are any matrices whose columns form bases of the null spaces of P and Q .

By combining the two lemmas, reference [66] shows that the H_∞ control synthesis problem has a solution, if and only if, there exist two symmetric matrices of R and S that satisfy the following system of LMIs:

$$\begin{pmatrix} \mathcal{N}_R & 0 \\ 0 & I \end{pmatrix}^T \begin{pmatrix} AR + RA^T & RC_1^T & B_1 \\ C_1 R & -\gamma I & D_{11} \\ B_1^T & D_{11}^T & -\gamma I \end{pmatrix} \begin{pmatrix} \mathcal{N}_R & 0 \\ 0 & I \end{pmatrix} < 0 \quad (3.14)$$

$$\begin{pmatrix} \mathcal{N}_S & 0 \\ 0 & I \end{pmatrix}^T \begin{pmatrix} A^T S + SA & SB_1 & C_1^T \\ B_1^T S & -\gamma I & D_{11}^T \\ C_1 & D_{11} & -\gamma I \end{pmatrix} \begin{pmatrix} \mathcal{N}_S & 0 \\ 0 & I \end{pmatrix} < 0 \quad (3.15)$$

$$\begin{pmatrix} R & I \\ I & S \end{pmatrix} \geq 0 \quad (3.16)$$

where, \mathcal{N}_R and \mathcal{N}_S denote bases of the null spaces of $\begin{pmatrix} B_2^T & D_{12}^T \end{pmatrix}$ and $\begin{pmatrix} C_2 & D_{21} \end{pmatrix}$. Such bases can be obtained via singular value decomposition (SVD) of $\begin{pmatrix} B_2^T & D_{12}^T \end{pmatrix}$ and $\begin{pmatrix} C_2 & D_{21} \end{pmatrix}$. In addition, the H_∞ -norm between the exogenous inputs and the controlled output (γ) can be minimised by solving a convex optimisation problem of the form:

$$\begin{aligned} & \min_{R=R^T, S=S^T} \gamma \\ \text{s.t.} & \text{ equations (3.14) – (3.16)} \end{aligned} \quad (3.17)$$

In this research, the output feedback controllers are designed to satisfy the control design requirements. For instance, the first design requirement is to make the steady-state error as small as possible (to levitate the rotor at its geometrical center). It implies that $|S(j\omega)| \ll 1$ to achieve good reference signal tracking and also good disturbance rejection. On the other hand, attenuation of measurement noise requires $|T(j\omega)| \ll 1$, especially at higher frequencies where the model of the system is uncertain. However, these are impossible to achieve simultaneously over all frequency ranges, because of the algebraic constraint that $S + T = I$. The aim is to minimise the sensitivity function S and the complementary sensitivity function T over appropriate frequency ranges while satisfying the constraints. The desired closed-loop performance of the system can be specified through the use of weighting functions imposed on the magnitude of the sensitivity and complementary sensitivity functions in the frequency domain. The nominal performance of the system can be defined by equation (3.18).

$$|W_P(j\omega)S(j\omega)| < 1, \forall \omega \iff \|W_P S\|_\infty < 1 \quad (3.18)$$

It is clear that over the frequency range where the magnitude of W_P is large, the magnitude of S will be small. However, in order to secure stability robustness and reduce sensitivity to high frequency noise, the bandwidth of the system has to be limited. Therefore, another weighting function W_T will be specified to ensure that the magnitude of the complementary sensitivity function T decays appropriately at high frequencies, where the plant model is poor. This can be achieved by imposing

another condition as equation (3.19).

$$|W_T(j\omega)T(j\omega)| < 1, \forall \omega \iff \|W_T T\|_\infty < 1 \quad (3.19)$$

Another weighting function W_U can be optionally imposed to limit the magnitude and the rate of change of the control signal as indicated in Fig. (3.1). W_U is chosen to be constant here implying the limits on the maximum allowed voltage on the digital signal processing card. It should be noted that the AMB system under study is open-loop unstable and the presence of the *RHP*-zeros makes the stabilisation more difficult. The structural resonant modes bring an additional degree of difficulty to the problem. In order to provide a guideline for designing proper weighting functions, some useful remarks concerning the design of H_∞ controller for unstable non-minimum phase systems are provided in reference [67]:

Remark 1: Although it is desirable that $|S(j\omega)| \ll 1, \forall j\omega$ and $|T(j\omega)| \ll 1, \forall j\omega$, it is important to note that the presence of unstable poles/zeros increases the peak of sensitivity functions. It implies that the peak values of $S(s)$ and $T(s)$ exceed one and this is unavoidable. For a system with RHP-zero ($s = z$) and RHP-pole ($s = p$), the sensitivity peaks can be evaluated as in (3.20).

$$\|S\|_\infty > c, \|T\|_\infty > c, c = \frac{|z + p|}{|z - p|} \quad (3.20)$$

Remark 2: In the presence of RHP-pole ($s = p$), a high gain controller is required to stabilise the open-loop unstable system. However, it is impossible to

employ large loop gain in the frequency range close to the location of RHP-zero ($s = z$) while maintaining stability. It implies that for a system with RHP poles and zeros, a closed-loop bandwidth of $2p < \omega_c < z$ is expected.

Remark 3: The peak values of the sensitivity functions (M_P and M_T) are very closely related to the gain and phase margins and hence the following conditions are very useful for the performance analysis of the system:

$$GM \geq \frac{M_P}{M_P - 1}, PM \geq 2 \arcsin\left(\frac{1}{2M_P}\right)(rad) \quad (3.21)$$

$$GM \geq \frac{M_T}{M_T - 1}, PM \geq 2 \arcsin\left(\frac{1}{2M_T}\right)(rad) \quad (3.22)$$

Following the given remarks, a first-order low-pass filter (W_P) is designed as the weighting function on sensitivity function and a second-order high-pass filter (W_T) is designed as the weighting function on complementary sensitivity function. A second-order W_T is designed in order to ensure a faster decay of the open-loop transfer function (GK) at high frequencies and hence to reduce the high frequency noise. It is worth noting that choosing a second-order W_T results in a robust controller that completely removes the effect of the resonant frequencies (the flexible modes of the rotor). As the model of the system is relatively similar in all four channels, relatively similar closed-loop bandwidths and high frequency roll-offs are expected for all four channels. However, from the location of the *RHP*-zero in channel Y_4 , a lower closed-loop bandwidth is expected in channel Y_4 . Therefore, the

bandwidth of the design performance weighting filter (W_{P_4}) is chosen to be lower compared to the other three channels. The designed weighting functions (given in equations (3.23)-(3.26)) need to be augmented to the model $G(s)$ for control synthesis. There are several methods available to solve H_∞ problems depending on which optimisation algorithm is employed. The H_∞ synthesis based on the solution of the Ricatti equations is adopted in this Chapter. The designed weighting functions (W_P and W_T) and the resulting closed-loop sensitivity functions (S and T) for all four channels are illustrated in Fig. 3.2 (a)-(d). As it can be seen from the simulation results, the weighting functions are designed in such a way that $1/W_P$ and $1/W_T$ be the upper bounds on the closed-loop sensitivity functions (S and T), respectively. The synthesised continuous-time controllers for all four channels are given in equations (3.27)-(3.30).

$$W_{P_1}(s) = \frac{0.3333(s + 500)}{(s + 0.00333)}, \quad W_{T_1}(s) = \frac{10^4(s + 1500)^2}{(s + 3 \times 10^5)^2} \quad (3.23)$$

$$W_{P_2}(s) = \frac{0.3333(s + 700)}{(s + 0.00333)}, \quad W_{T_2}(s) = \frac{10^6(s + 2000)^2}{(s + 4 \times 10^6)^2} \quad (3.24)$$

$$W_{P_3}(s) = \frac{0.3333(s + 800)}{(s + 0.00333)}, \quad W_{T_3}(s) = \frac{10^4(s + 1500)^2}{(s + 3 \times 10^5)^2} \quad (3.25)$$

$$W_{P_4}(s) = \frac{0.3333(s + 300)}{(s + 0.00333)}, \quad W_{T_4}(s) = \frac{10^4(s + 1600)^2}{(s + 3.2 \times 10^5)^2} \quad (3.26)$$

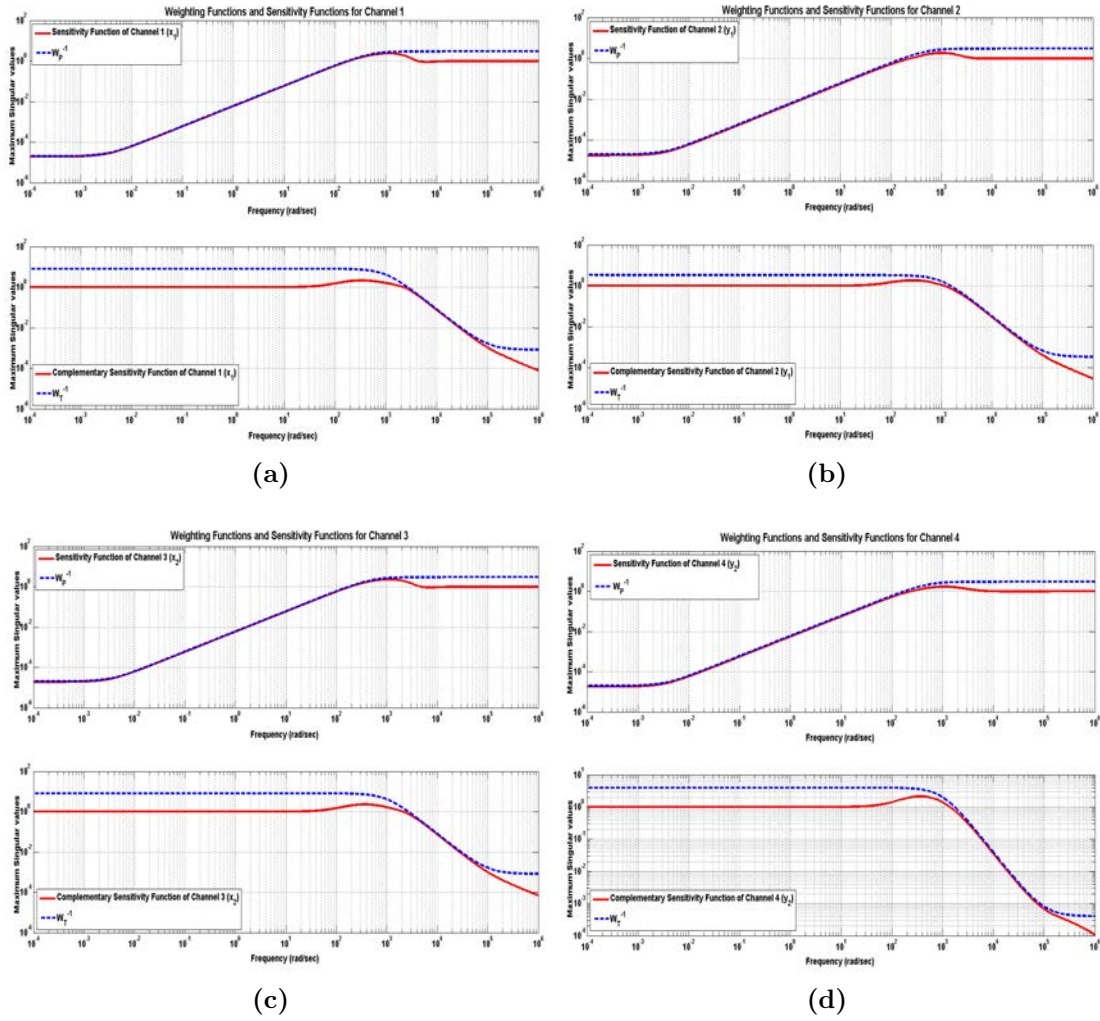


Figure 3.2: Singular values of S , T , $1/W_P$, and $1/W_T$ of all four channels, (a) Channel Y_1 , (b) Channel Y_2 , (c) Channel Y_3 , (d) Channel Y_4 .

$$K_{\infty_1}(s) = \frac{7986.2(s + 3 \times 10^5)^2(s + 374.4)}{(s + 4.822 \times 10^5)(s + 1.717 \times 10^4)(s + 0.003333)} \\ \frac{(s + 77.94)(s^2 + 0.96s + 2.344 \times 10^7)(s^2 + 0.37s + 1.668 \times 10^8)}{(s^2 + 6429s + 2.328 \times 10^7)(s^2 + 5087s + 2.191 \times 10^7)(s^2 + 5297s + 1.637 \times 10^8)} \quad (3.27)$$

$$K_{\infty_2}(s) = \frac{923.21(s + 3 \times 10^5)^2(s + 433.4)}{(s + 4.822 \times 10^5)(s + 1.717 \times 10^4)(s + 0.003333)} \\ \frac{(s + 71.86)(s^2 + 0.27s + 2.307 \times 10^7)(s^2 + 0.37s + 1.673 \times 10^8)}{(s^2 + 5755s + 2.002 \times 10^7)(s^2 + 5755s + 2.002 \times 10^7)(s^2 + 5139s + 1.631 \times 10^8)} \quad (3.28)$$

$$K_{\infty_3}(s) = \frac{718.62(s + 3 \times 10^5)^2(s + 628.1)(s + 91.89)}{(s + 1.739 \times 10^5)(s + 5125)(s + 0.003333)(s^2 + 6464s + 2.443 \times 10^7)} \\ \frac{(s^2 + 0.031s + 2.344 \times 10^7)(s^2 + 0.037s + 1.668 \times 10^8)}{(s^2 + 4983s + 2.136 \times 10^7)(s^2 + 5139s + 1.637 \times 10^8)} \quad (3.29)$$

$$K_{\infty_4}(s) = \frac{1321(s + 388.4)(s + 50.52)(s^2 + 6.4 \times 10^5s + 1.024 \times 10^{11})}{((s + 6.884 \times 10^5)(s + 3892)(s + 0.003333)(s^2 + 4977s + 1.99 \times 10^7)} \\ \frac{(s^2 + 0.0529s + 2.3 \times 10^7)(s^2 + 0.0726s + 1.65 \times 10^8)}{(s^2 + 5473s + 2.134 \times 10^7)(s^2 + 4743s + 1.661 \times 10^8)} \quad (3.30)$$

3.3 Lead-Lag Compensator Design

In order to design classical controllers, two notch filters need to be designed first to completely remove the effects caused by the resonant frequencies. Then, the reduced-order models of the system can be obtained by removing the poles and zeros corresponding to the resonant modes from the model transfer functions and keeping their dc-gains in the reduced-order models. Note that the unstable poles and RHP-zeros must be retained in the reduced-order models, as unstable poles and RHP-zeros introduce fundamental limitations on the system closed-loop bandwidth and hence have to remain in the model. The lead-lag type compensators are designed on the basis of the reduced-order models of all four channels. The following structure is used to design the two notch filters for each channel:

$$N(s) = \frac{s^2 + \zeta b \omega_n s + \omega_n^2}{s^2 + b \omega_n s + \omega_n^2} \quad (3.31)$$

In equation (3.31), ω_n is the notch frequency, ζ is the damping ratio and b bandwidth of the filter. After designing the notch filters required for the first two structural resonant modes, a lead-lag compensator is designed for the reduced order model:

$$K_{lead-lag} = K_{lead} K_{lag} \frac{(s+a)}{(s+\gamma a)} \frac{(s+\beta b)}{(s+b)}, \text{ with } \beta, \gamma > 1 \quad (3.32)$$

In the design of a lead compensator, the dc-gain is smaller than the high-frequency gain (by a factor of γ) and hence it shifts the low frequency gains by a factor of (K_{lead}/γ) and the high-frequencies by K_{lead} . Since lead compensator introduces phase-lead around the corner frequencies, it is used to increase the closed-loop bandwidth of the system. The largest phase-lead and the crossover frequency provided by the lead compensator can be written as equations (3.33) and (3.34).

$$\phi_{max-lead} = \tan^{-1}\left(\frac{\sqrt{\gamma} - \frac{1}{\sqrt{\gamma}}}{2}\right) \quad (3.33)$$

$$\omega_{max-lead} = a\sqrt{\gamma} \quad (3.34)$$

The lag part of the compensator is to recover the low-frequency gain and to reduce the steady-state errors to input signals. The key property of the lag compensator is that the dc-gain is larger than high-frequency gains by factor of β . Hence, it shifts the low-frequency region up by a factor of $K_{lag}\beta$ and high-frequency by K_{lag} . The maximum phase-lag introduced by the lag compensator is given by equation (3.35) and the corner frequency by equation (3.36).

$$\phi_{max-lag} = \tan^{-1}\left(\frac{\frac{1}{\sqrt{\beta}} - \sqrt{\beta}}{2}\right) \quad (3.35)$$

$$\omega_{max-lag} = b\sqrt{\beta} \quad (3.36)$$

The corner frequency of the lag compensator must be well below the lead compensator crossover frequency (usually a factor of 10 is recommended). Finally, a low-pass filter can be added to the controller to increase the high-frequency roll-off and hence attenuate the undesired high-frequency noise signals. The final designed controllers for all four channels are shown in equations (3.37)-(3.40).

$$K_{lead-lag_1} = \frac{1.0994 \times 10^{10}(s + 379.5)(s + 120)}{(s + 2.5 \times 10^4)^2(s + 3795)(s + 32.85)} \frac{(s^2 + 0.2449s + 2.344 \times 10^7)(s^2 + 0.1194s + 1.668 \times 10^8)}{(s^2 + 5421s + 2.344 \times 10^7)(s^2 + 3775s + 1.668 \times 10^8)} \quad (3.37)$$

$$K_{lead-lag_2} = \frac{7.9158 \times 10^9(s + 406.7)(s + 120)}{(s + 2.5 \times 10^4)^2(s + 2927)(s + 32.85)} \frac{(s^2 + 0.0708s + 2.307 \times 10^7)(s^2 + 0.107s + 1.673 \times 10^8)}{(s^2 + 4955s + 2.307 \times 10^7)(s^2 + 3384s + 1.673 \times 10^8)} \quad (3.38)$$

$$K_{lead-lag_3} = \frac{8.7532 \times 10^9(s + 459.8)(s + 132.2)}{(s + 2.5 \times 10^4)^2(s + 3310)(s + 21.06)} \frac{(s^2 + 4.165 \times 10^{-6}s + 2.344 \times 10^7)(s^2 + 5.214 \times 10^{-7}s + 1.668 \times 10^8)}{(s^2 + 4220s + 2.344 \times 10^7)(s^2 + 5214s + 1.668 \times 10^8)} \quad (3.39)$$

$$K_{lead-lag_4} = \frac{6.6619 \times 10^9(s + 308.2)(s + 116.9)}{(s + 2.5 \times 10^4)^2(s + 3346)(s + 19.63)} \frac{(s^2 + 2.85 \times 10^{-4}s + 2.3 \times 10^7)(s^2 + 8.927 \times 10^{-7}s + 1.65 \times 10^8)}{(s^2 + 6466s + 2.3 \times 10^7)(s^2 + 8927s + 1.65 \times 10^8)} \quad (3.40)$$

3.4 MIMO H_2 and H_∞ Controllers

In order to investigate the effects of cross-coupling channels on the overall performance of the system, MIMO H_2 and H_∞ optimal controllers are synthesised on the basis of the high-order MIMO model of the system (given in equation (2.38)). Again, similar weighting functions are employed for the synthesis of the MIMO controllers (similar to equations (3.23)-(3.26)). This ensures that the conditions of all SISO and MIMO controllers are similar and hence the comparison between the performance of these controllers is fair.

$$\begin{aligned}\mathbf{W}_P(s) &= \text{diag}\{W_{P_1}(s), W_{P_2}(s), W_{P_3}(s), W_{P_4}(s)\}, \\ \mathbf{W}_T(s) &= \text{diag}\{W_{T_1}(s), W_{T_2}(s), W_{T_3}(s), W_{T_4}(s)\}\end{aligned}\quad (3.41)$$

The diagonal weighting matrices ($\mathbf{W}_P(s)$, $\mathbf{W}_U(s)$, and $\mathbf{W}_T(s)$) are augmented with the MIMO model of the system, and the mixed-sensitivity H_2 and H_∞ optimisation procedures are performed on the generalised plant, respectively. Note also that the standard mixed-sensitivity H_2 loop-shaping problem is to find a stabilising controller K that minimises the H_2 -norm of the closed-loop system as

in equation (3.42) (see references [68, 69] for details on the H_2 optimisations).

$$\min_{K \text{ stabilising}} \left\| \begin{array}{c} \mathbf{W}_P S \\ \mathbf{W}_U K S \\ \mathbf{W}_T T \end{array} \right\|_2 \quad (3.42)$$

Fig. 3.3 shows the frequency response plot of the resulting closed-loop sensitivity and complementary sensitivity functions ($S(s)$ and $T(s)$) using the MIMO H_2 and H_∞ controllers. Since similar weighting functions are used for the synthesis of the H_2 and H_∞ controllers, similar performances are expected from the two controllers. However, the real-time experiments reveal some interesting results in the next section.

3.5 Experimental Validation

To evaluate the performance of the SISO and MIMO controllers experimentally, the designed continuous-time controllers are discretised using the Bilinear transformation with a sampling frequency of $20kHz$. The discrete-time controllers are implemented in real-time using an ADC/DAC converter and the dSPACE DS1104 digital signal processing board. In the first part of the experiment, the performance of the designed controllers is evaluated while the rotor is stationary and in the presence of constant disturbances. In order to investigate the disturbance rejection

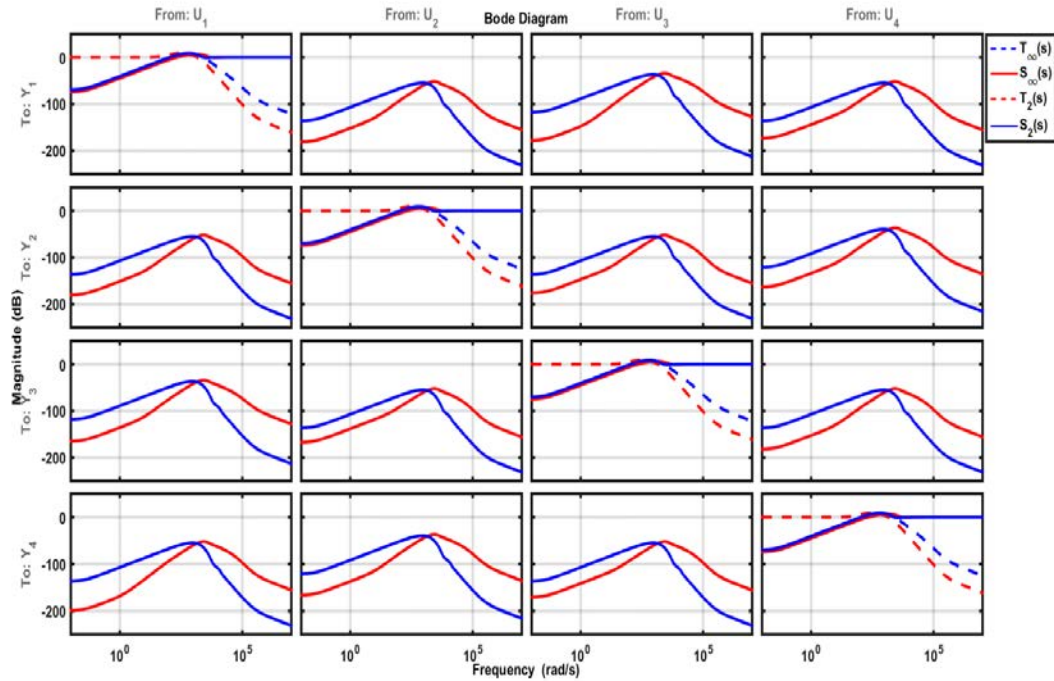


Figure 3.3: Singular values of the closed-loop sensitivity functions $S(s)$ and the complementary sensitivity functions $T(s)$ using the MIMO H_2 and H_∞ optimal controllers.

properties of the controllers, four unit-step disturbances are introduced to the system. The first disturbance is added to the first channel (Y_1) at approximately one second, followed by the second disturbance to the second channel (Y_2) after two seconds. The other two disturbances are introduced to the third and fourth channels (Y_3 and Y_4) after three and four seconds, respectively. For a fair comparison, the performance of the SISO and MIMO controllers are compared separately. The results from the SISO controllers, namely, the SISO H_∞ controllers, the lead-lag type compensators, and the analog on-board controllers are depicted in Figs. 3.4 and 3.5. Note that the analog on-board controllers are in the form of lead compensators

with first-order low-pass filters and with the transfer functions of:

$$K_{on-board_{1-4}} = \frac{1.7218 \times 10^5 (s + 1128)}{(s + 3030)(s + 4.545 \times 10^4)} \quad (3.43)$$

It is clear from the results in Figs. 3.4 and 3.5 that the SISO H_∞ controllers certainly outperform the analog on-board controllers. On the other hand, a relatively similar performance can be achieved by the carefully designed lead-lag type compensators. However, in contrast to the classical design methods, the H_∞ synthesis procedure includes the required components (compensators, notch filters, and the high-frequency low-pass filters) automatically if the weighting functions are chosen properly.

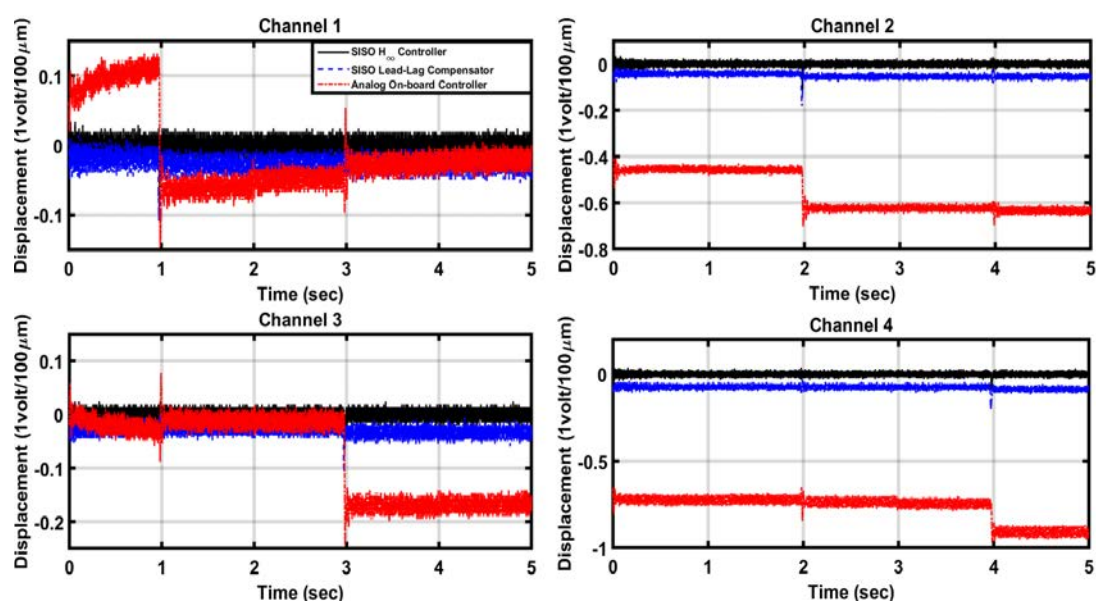


Figure 3.4: Step responses of all four channels using the SISO controllers in the presence of unit-step disturbances.

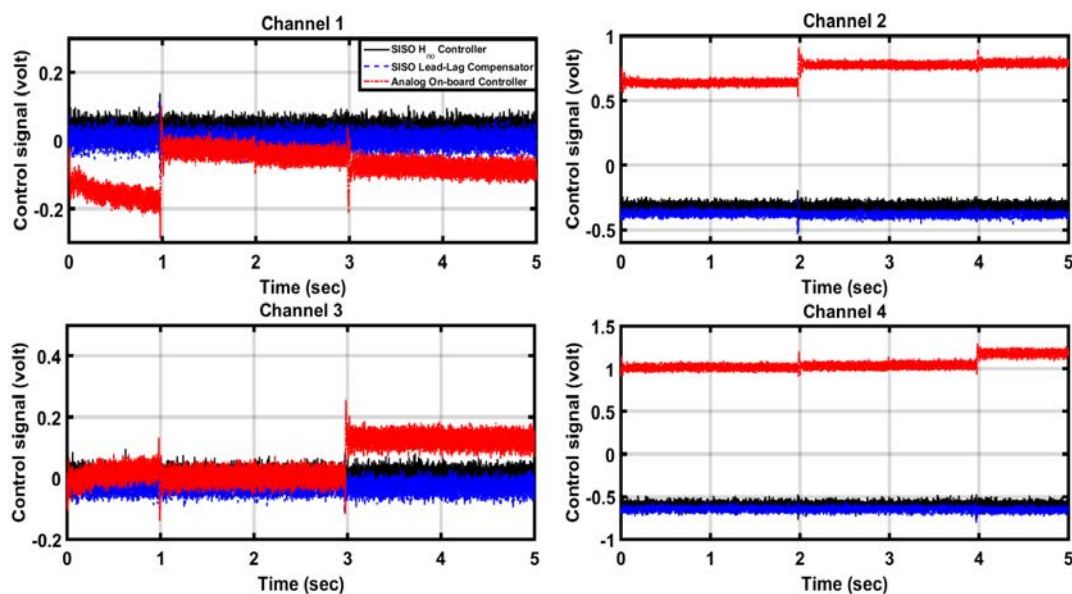


Figure 3.5: Control signals of all four channels using the SISO controllers in the presence of unit-step disturbances on all four channels.

The performance of the MIMO H_2 and H_∞ optimal controllers are also depicted in Figs. 3.6 and 3.7. Similar behaviours in terms of transient- and steady-state response can be seen from the two controllers in Fig. 3.6. However, from the control signals in Fig. 3.7, it can be deduced that the high-frequency measurement noises are much better attenuated by the H_2 controllers compared to the H_∞ controllers.

The AMB system under study consists of an internal air turbine attached to one end of the rotor that allows the spinning of the rotor up to 10000 *rpm*. In order to evaluate the performance of the SISO and MIMO controllers while the rotor is in rotation, the air-pressure supplied by the air compressor is increased gradually, and the displacements of the geometrical center of the rotor at both ends of the rotor are captured. The displacements of the rotor at all four channels are depicted

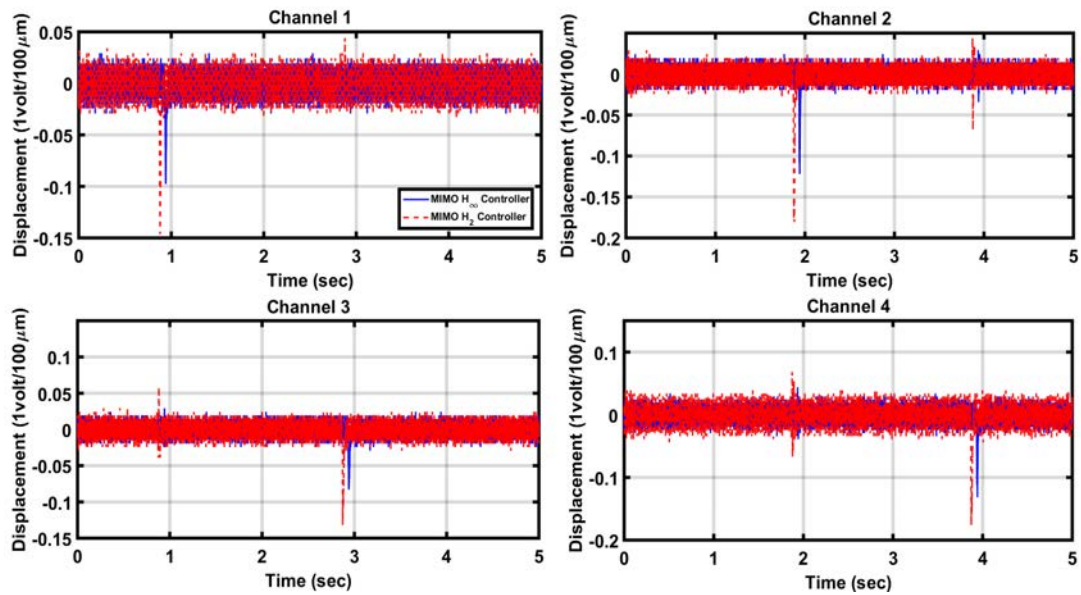


Figure 3.6: Step responses of all four channels using the MIMO controllers in the presence of unit-step disturbances.

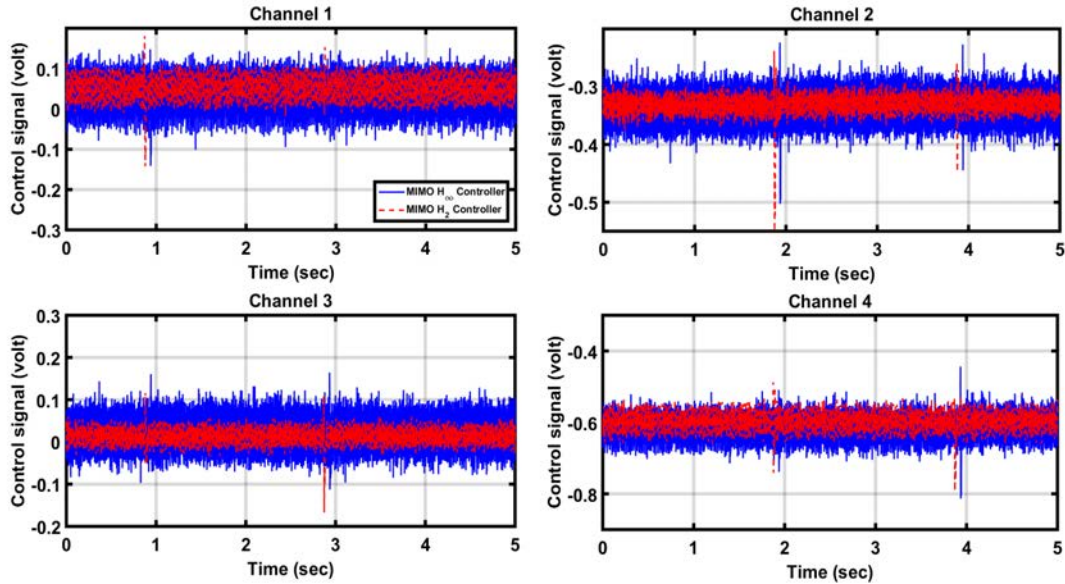


Figure 3.7: Control signals of all four channels using the MIMO controllers in the presence of unit-step disturbances.

in Fig. 3.8. As the rotational speed of the rotor increases, it can be seen that the overall performance of the MIMO H_∞ controller remain significantly better than all other controllers. Furthermore, unlike the stationary case, the MIMO H_2 controller shows a very poor performance compared to the MIMO H_∞ controller at high rotational speeds. Finally, the SISO H_∞ controllers show a convincing performance compared to the lead-lag type compensators and the analog on-board controllers.

More interestingly, the rotor achieves different steady-state rotational speeds using the designed controllers while constant air-pressure of 100 *psi* is supplied to the system. The transient speed responses of the system using the designed controllers are depicted in Fig. 3.9. The highest steady-state speed is achieved by using the MIMO H_∞ controller. This is because the effects caused by the rotor mass-imbalance and centrifugal forces are better rejected by the MIMO H_∞ controller, allowing the rotor to obtain higher rotational speeds compared to the other controllers. As it is expected, the system achieves very low steady-state speed by the MIMO H_2 controller due to the poor performance of the H_2 controllers at high rotational speeds. Furthermore, the SISO H_∞ controllers show better performance among the other SISO controllers. Last but not least, it can be deduced from the results that the high-order H_∞ controllers show better performance compared to the low-order H_∞ controllers. However, the price to pay is to implement excessively high-order controllers that demand more powerful hardware for a successful real-time implementation.

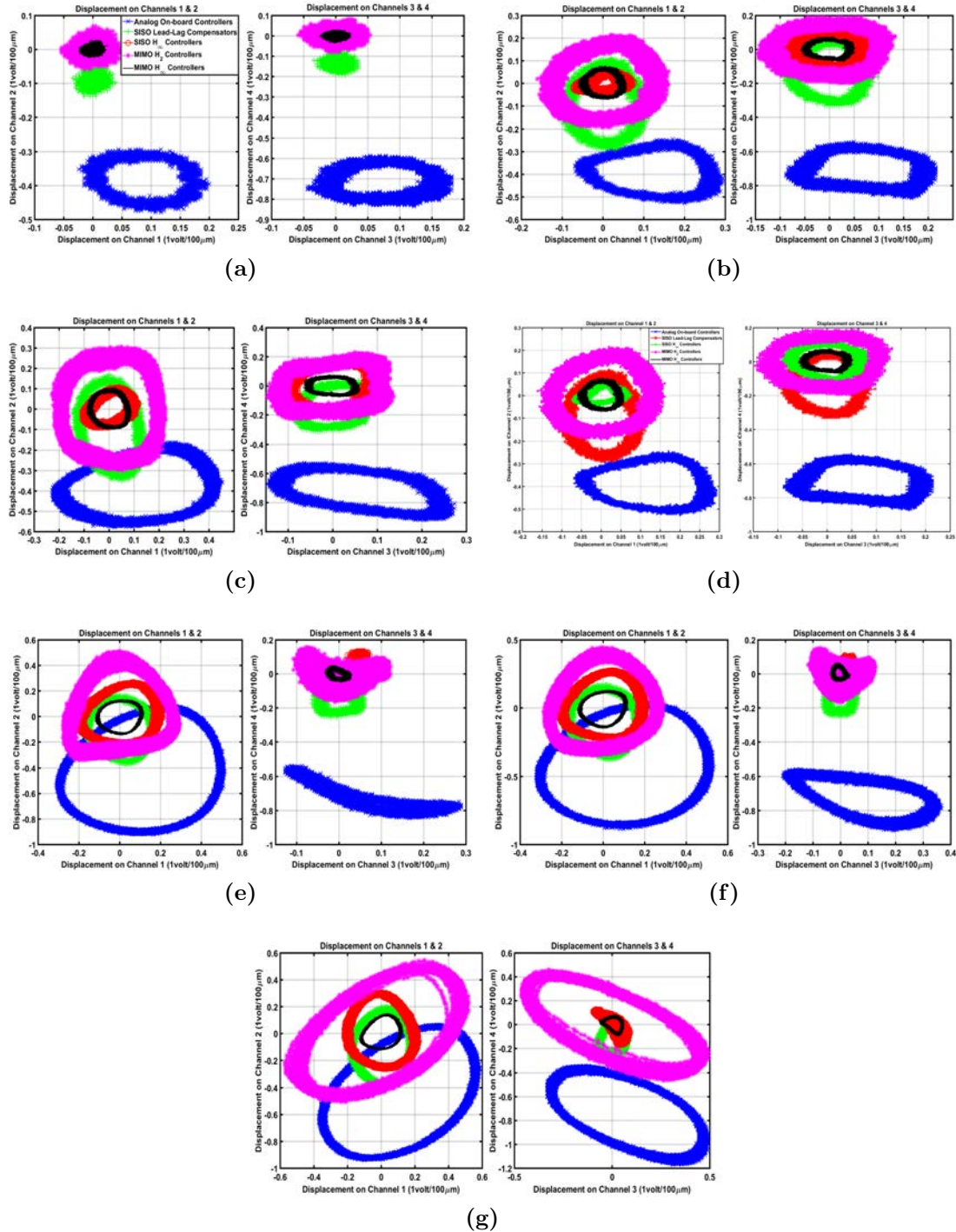


Figure 3.8: Trajectory of the geometrical center of the rotor (at both ends) using the SISO and MIMO controllers. Blue lines represent: analog on-board controllers, green lines: SISO lead-lag compensators, red lines: SISO H_∞ controllers, purple lines: MIMO H_2 controllers, black lines: MIMO H_∞ controllers, (a) air pressure of 20 *psi*, (b) air pressure of 30 *psi*, (c) air pressure of 40 *psi*, (d) air pressure of 50 *psi*, (e) air pressure of 60 *psi*, (f) air pressure of 80 *psi*, (g) air pressure of 100 *psi*.

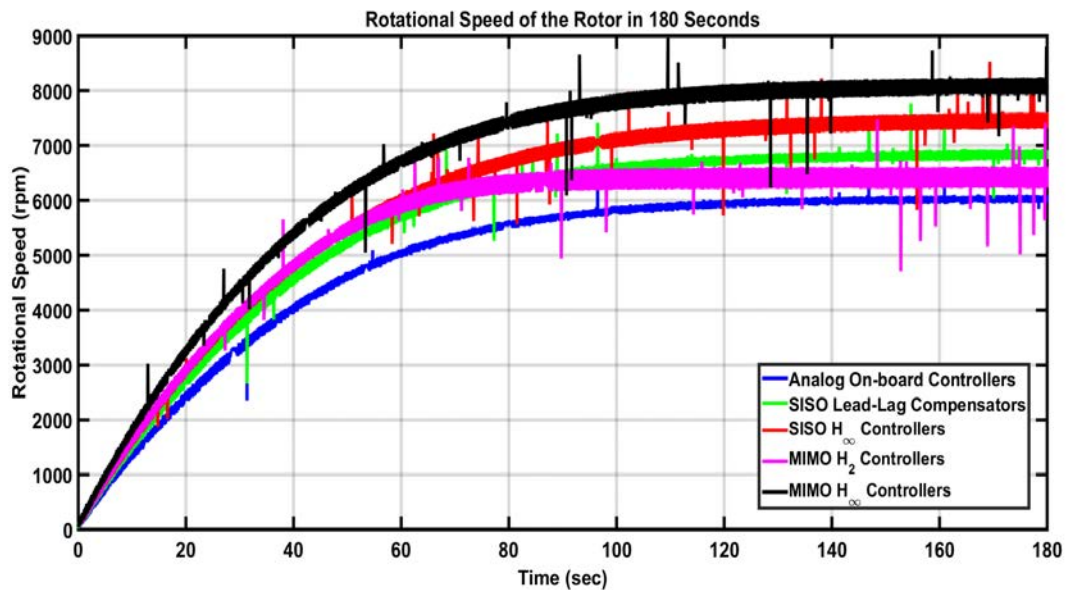


Figure 3.9: Rotational speed of the rotor using the SISO and MIMO controllers.

3.6 Conclusion

This Chapter dealt with high-performance controller design of the AMB system. Both SISO and MIMO controllers were designed on the basis of the identified models of the system. The designed controllers were discretised and implemented on the AMB system for real-time experimental analysis. The performance of the designed controllers was examined while the rotor was stationary as well as while it was operating at several rotational speeds. All the designed controllers showed much superior performances compared to the analog on-board controllers. Moreover, it was shown that the performance of the MIMO H_2 controller was not satisfactory at high speeds where the modelling uncertainties were more significant. Although the performance of the system was further improved by using the MIMO

H_∞ controllers over the SISO controllers, but the price to pay was to implement excessively high-order controllers that demanded powerful and expensive hardware.

Chapter 4

Full-Order and Fixed-Order μ -Optimal Controllers

4.1 Introduction

The differences between the obtained models of a system and the actual plant can result in degradation of the closed-loop system performance and in certain circumstances it could even lead to system instability. In the robust control synthesis approach, there are two design issues, namely, stability robustness and performance robustness. The former guarantees the closed-loop stability of the system in the presence of a specified class of uncertainties. However, more often than not, it is desirable to ensure that not only all the possible uncertain systems remain stable in

the presence of uncertainties, but also the uncertain systems to have an acceptable closed-loop performance. In the past decade, considerable amount of research has been devoted on finding stabilising controllers that not only guarantee the robustness of the system in the presence of uncertainties, but they ensure that the closed-loop performance requirements are satisfied for the family of uncertain systems in the uncertainty set. Several design methodologies have been proposed in the literature, such as synthesising all stabilising controllers using Youla Parametrisation [24], state-space based H_2 and H_∞ loop-shaping [64, 65, 68, 69, 70, 71], L_1 control design [72], linear matrix inequality (LMI) approach to H_2 and H_∞ control design [66, 73], and μ -synthesis and DK -iteration [74, 75].

With the recent developments in the robust control synthesis algorithms, robust multivariable controllers can be designed for the AMBs using readily available algorithms. For instance, the stabilising controllers can be designed using H_∞ -optimisation methods. Then, the upper-bound on the structured singular value (μ) can be evaluated for the robust performance analysis of the designed controllers in the presence of modelling uncertainties. As there is no available method for direct synthesis of μ -optimal controllers, the so-called DK -iteration method which combines the H_∞ controller synthesis and the μ -analysis approach can be employed in an iterative manner to find a μ -optimal controller. However, the major problem with the most of robust control techniques is that the order of such controllers is exceedingly high and hence demand expensive hardware for successful implementation. On the other hand, many industrial controllers are constrained in their order/structure and still are required to meet high performance and robustness demands.

Unfortunately, the problem of directly synthesising low-order (fixed-order/structure) controllers is very hard. In the early attempts to direct design of low-order robust controllers, optimal projection equations were developed. In this approach, the low-order (fixed-order/structure) controllers are characterised from a set of coupled Riccati and Lyapunov equations, each containing a projection matrix [76, 77, 78, 79]. The fixed-order decentralised H_2 -optimal controllers are introduced in references [80, 81, 82, 83]. The drawback of these methods is that the structure of the controller cannot be predefined (for instance PID or lead-lag type structures). With the development of linear matrix inequalities (LMI), the work in reference [66] shows that the regular H_2 and H_∞ problems can be reformulated as LMIs rather than the usual dual Riccati equations. Hence, efficient convex optimisation techniques can be employed to solve the problem. The H_∞ optimisation using LMIs not only offers an efficient numerical solution, but also it has several advantages over the regular Riccati-based H_∞ optimisation. For instance, it prevents undesirable control-plant pole-zero cancellations. However, it is shown in reference [84] that the scenario changes dramatically as soon as constraints are added into the order or structure of the controller. In fact, the problem of fixed-structure robust controllers is not convex and the problem may no longer be transformed into a convex optimisation problem and hence the global convergence of the problem is not guaranteed. However, in practice, the local optimisation methods have shown to result in acceptable controllers efficiently [84, 85, 86, 87, 88, 89, 90, 91, 92]. This motivated us to evaluate the performance of the locally optimal fixed-order controllers on the stabilisation of the AMB systems.

The challenge here is to arrive at minimal complexity controllers that remain robust in the presence of modelling errors and the closed-loop performance requirements are satisfied for all uncertain systems. In the early works, in order to design lower-order controllers, the system was modelled as a family of single-input single-output (SISO) subsystems and low-order controllers were designed on the basis of the SISO (decoupled) models of the system [93, 94, 95, 96, 97, 98, 99]. This strategy is suitable if the system is stationary. The reason is because the effects caused by the rotor flexible modes, cross-couplings between different channels, centrifugal forces, and other unmodelled dynamics may not be significant when the system is stationary. However, these effects become more significant when the rotor is rotating at high speeds and hence more accurate models are required to represent the high-frequency dynamics.

In the more recent works, more accurate models of the AMBs are attempted to be obtained by taking into account the cross-coupling effects between the different channels and high-frequency dynamics resulting from the flexible nature of the rotating shaft in the model. Clearly, higher-order models are required to successfully represent these dynamics. Consequently, the controller design using the classical methods may be found inefficient and cumbersome. Even though conventional controllers and in particular PID controllers are easy to implement, there are critical performance limitations associated with the PID controllers that prevent more advanced applications of AMBs that usually require stronger robustness and performance offered by modern robust control methods [100, 101]. To improve the performance and robustness of the closed-loop systems, some recently published works can be found on simulation studies and real-time applications of the μ -

synthesis approach on the AMBs [25, 26, 102, 103, 104, 105, 106]. It is worth noting that in the so-called “ μ -analysis” approach, the controllers are designed using any available methods and the robust performance is evaluated by computing the bounds on the structured singular value (μ) of the closed-loop system. Alternatively, the robust controllers can be designed directly using the “ μ -synthesis” approach [107, 108].

The aforementioned problem of arriving at very high-order controllers can be clearly seen in the recent published works. For instance, in reference [25], the μ -synthesis approach is employed for designing stabilising controllers for a laboratory AMB system. The performance of the designed μ -optimal controllers is compared with the conventional PID controllers. The experimental results show that the μ -optimal controllers provide much better performances in comparison with the conventional PID controllers. However, it should be noted that the designed μ -optimal controllers are found to have an order of 48 (after order reduction). In another example, a μ -synthesis approach is employed in reference [26] to design robust controllers for tool-tip tracking in an AMB spindle application. Similarly, the standard μ -synthesis approach (using the DK -iteration) is utilised for the synthesis of the μ -optimal controllers. The order of the designed μ -optimal controller is found to be 106. In order to implement the designed controller using the available hardware, the order of the controller is reduced to 44 by using the balanced truncation method. It is clear from these examples that the problem of designing robust controllers for high-order models of AMBs constitutes significant challenges which, at the same time, addresses fundamental issues in the practical implementation of feedback control systems.

The focus of this Chapter is on the design and real-time implementation of low-order MIMO H_∞ - and μ -optimal controllers for robust stabilisation of the laboratory AMB system. It shows the challenges concerning the design and real-time implementation of robust controllers for stabilisation of the MIMO active magnetic bearing system and presents some alternative approaches that result in lower-order and more reliable controllers. It is further shown that the emergence of new optimisation tools enable us to get around the issue of high-order controllers by synthesising the reduced-order controllers directly. Extensive experimental studies are conducted to compare the performance and effectiveness of the designed robust controllers in real-time. Mainly, three different approaches are considered in this Chapter to arrive at lower-order robust controllers for the MIMO AMB system under study:

- 1) the common approach used in the literature is investigated, i.e., “full-order” H_∞ - and μ -optimal controllers are synthesised on the basis of the high-order model of the system, followed by a controller-order reduction;
- 2) the order of the plant model is first reduced by keeping the “slow” dynamics in the reduced-order model while the “fast” dynamics are included in the design weighting functions;
- 3) low-order controllers are designed directly using fixed-order H_∞ optimisation and μ synthesis methods.

From the best of our knowledge, only approach (1) has been investigated in the literature for obtaining lower-order robust controllers for stabilisation of the AMB system. Therefore, the second approach is presented and studied in this Chapter. It is shown that the presented strategy results in much lower-order robust controllers and the effectiveness of the designed controllers is compared with the controllers that are designed using the common μ approach (1). Since there is no report on the direct synthesis of fixed-order (structure) H_∞ and μ optimal controllers for stabilisation of AMBs in the literature, approach (3) which is based on the direct synthesis of fixed-order controllers is also investigated here for the completeness of the study. The next section provides a brief introduction into the μ -synthesis approach.

4.2 Full-order H_∞ -optimisation and μ -Synthesis

In the μ -synthesis approach, the principal objective is to synthesise controllers that guarantee the robust stability and robust performance of the system in the presence of uncertainties and unmodelled dynamics. These requirements are satisfied by means of some lower and upper bounds involving frequency-dependent scales which account for the structure of the real and complex uncertainties [109, 110]. The closed-loop stability analysis can be broken into robust stability analysis and robust performance analysis [111, 112, 113]. The H_∞ optimisation can be utilised to design robust controllers so that the closed-loop system remain robustly stable for all modelling uncertainties. Furthermore, μ -analysis can be used to ensure that the

performance objectives are satisfied for all possible plants in the uncertainty set, even the worst-case plant. On the other hand, μ -optimal controllers can be designed directly using the so-called *DK*-iteration. In this method, the controller is designed iteratively (H_∞ synthesis and μ analysis) until the upper-bound on the closed-loop structured singular value (μ) is found to be less than 1.

In the standard mixed-sensitivity H_∞ synthesis problem, the objective is to design a stabilising controller so that the H_∞ -norm of the closed-loop transfer function is minimised. Several weighting functions can be designed to impose the design performance requirements such as reference tracking, disturbance rejection capabilities, and the high-frequency roll-off. As it was described in Section 3.2, the weighting functions can be combined with the system and the overall system can be represented as a generalised plant $P(s)$ [65]:

$$P(s) : \begin{bmatrix} P_{11} & P_{12} \\ P_{21} & P_{22} \end{bmatrix} = \begin{bmatrix} 0 & 0 & W_I(s)G(s) \\ -W_P(s) & W_P(s) & -W_P(s)G(s) \\ -I & I & -G(s) \end{bmatrix} \quad (4.1)$$

The H_∞ optimisation problem is to find a controller $K(s)$ which robustly stabilises the system, and minimises the H_∞ -norm of the closed-loop transfer

function of the augmented plant $P(s)$.

$$\min_{K \text{ stabilising}} \left\| \mathcal{F}_l(P, K) \right\|_{\infty} \quad (4.2)$$

In equation (4.2), $N := \mathcal{F}_l(P, K) = P_{11} + P_{12}K(I - P_{22}K)^{-1}P_{21}$ is the lower linear fractional transformation (LFT) of the generalised plant P with respect to the controller K . The signals in Fig. 4.1 are: u the control signals, y the measured outputs, w the exogenous input signals, and z are the weighted signals that need to be minimised. For robust stability analysis of the closed-loop system (assuming the nominal stability of the closed-loop system), it is sufficient to show that the closed-loop system remains stable for all plants in the uncertainty set, i.e., N is stable $\forall \Delta, \|\Delta\|_{\infty} \leq 1$. Whereas, to ensure the robust performance of the system, again assuming that the closed-loop system is nominally stable and robustly stable, it is required that all the performance objectives are satisfied for all possible plants in the uncertainty set, even the worst-case plant.

Assuming that the internal stability of the nominal system is achieved by the designed H_{∞} controller (H_{∞} -norm of the closed-loop system is minimised), the idea of μ -synthesis is to find a stabilising controller that minimises not only the H_{∞} -norm of the nominal system, but also the H_{∞} -norm of uncertain systems in the uncertainty set, i.e.:

$$\min_{K \text{ stabilising}} \left\| \mathcal{F}_u(\mathcal{F}_l(P, K), \Delta) \right\|_{\infty} \quad (4.3)$$

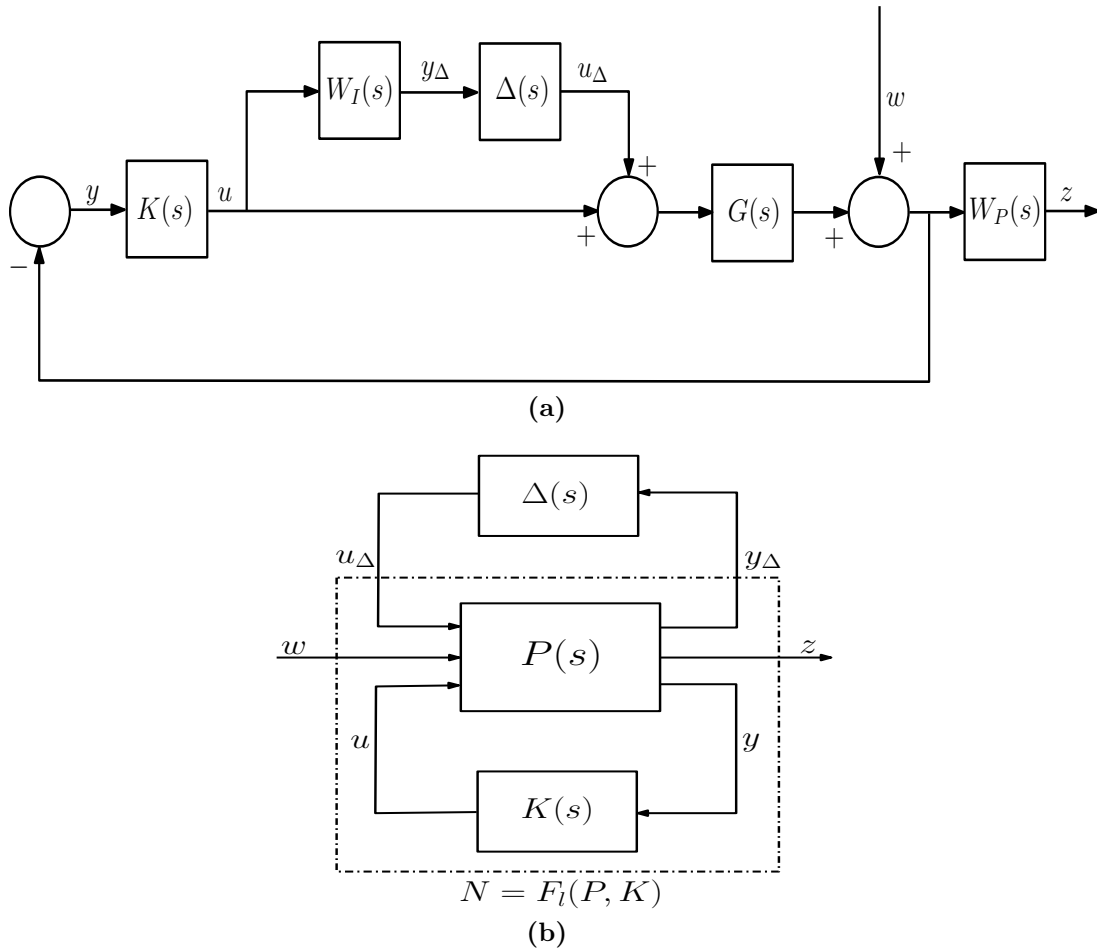


Figure 4.1: (a) General control configuration for controller synthesis, (b) $N-\Delta$ structure for μ -synthesis (or analysis).

where, $\mathcal{F}_u(\mathcal{F}_l(P, K))$ is the upper LFT of the closed-loop system $N =: \mathcal{F}_l(P, K)$ with respect to the modelling uncertainties. The robust performance of all possible uncertain systems is satisfied, if and only if:

$$\mu_\Delta(\mathcal{F}_l(P, K)) < 1 \tag{4.4}$$

The uncertainty block $\Delta(s)$ is stable, satisfies $\|\Delta(s)\|_\infty < 1$, and has a certain structure $\mathbf{\Delta}$. Here, μ_Δ is the structured singular value:

$$\mu_\Delta(\mathcal{F}_l(P, K)) := \frac{1}{\min_{\Delta \in \mathbf{\Delta}, \det(I - N\Delta) = 0} \bar{\sigma}(\Delta)}$$

The problem here is the computation of the structured singular value μ . The μ -synthesis approach in its general form is not tractable. However, by introducing stable and minimum-phase scaling matrices D that satisfy $D\Delta = \Delta D$, the structured singular value μ can be approximated by its upper bound which remains an optimally scaled maximum singular value [114]:

$$\mu_\Delta(N) \leq \inf_{D \in \mathcal{D}} \bar{\sigma}(D\mathcal{F}_l(P, K)D^{-1}) \quad (4.5)$$

Hence, the μ -synthesis problem can be cast into finding a controller that iteratively minimises:

$$\min_K \inf_D \|DND^{-1}\|_\infty \quad (4.6)$$

In the first step of this iterative approach, equation (4.6) becomes a standard H_∞ problem with arbitrary chosen initial values of D scales (usually identity matrix of appropriate dimension). After obtaining the controller that minimises equation (4.6) for fixed D scales, the controller K is fixed and one tries to minimise D and searches for a stable minimum-phase representation of D over the predefined

frequency grid. This means that we can obtain robust performance of the closed-loop system by minimising the upper-bound of μ over the frequency range of interest. From equation (4.4), the peak value of the μ -plot represents the inverse of the size of the uncertainties in which the robust performance of the closed-loop system remains satisfactory.

The standard μ -synthesis using so-called *DK*-iteration can be summarised as follows:

- 1) an H_∞ optimised controller is synthesised that minimises $\|DND^{-1}\|_\infty$ with fixed $D(s)$ scales,
- 2) a stable minimum-phase $D(s)$ is found such that it minimises the maximum structured singular value of $\bar{\sigma}(DND^{-1}(j\omega))$ at each frequency with fixed controller $K(s)$,
- 3) the controller synthesis is repeated with the updated $D(s)$ scales, and the iteration continues until a satisfactory robust performance is achieved, i.e.:

$$\mu_\Delta(N) \leq \min_{D \in \mathcal{D}} \bar{\sigma}(DND^{-1}) < 1 \quad (4.7)$$

For a thorough derivation and discussion of μ -synthesis, the interested readers are referred to [65, 69, 114]. One major drawback of the standard *DK*-iteration is that the order of the final controllers is excessively high. In fact, in each iteration, the order of the synthesised controller is equal to the sum of the order of the system,

the design weighting functions, and twice the order of the D scales. One way to overcome this problem is to use model/controller order reduction techniques to reduce the order of the final designed controller. Another way to overcome excessively high-order controllers is to use fixed-order (fixed-structure) μ -synthesis. This motivated us to investigate the recent non-smooth optimisation techniques to solve fixed-order (structure) H_∞ and μ synthesis problems. The next section provides an introduction to the idea of fixed-order (structure) H_∞ -synthesis and how it can be turned into fixed-order μ -synthesis problem.

4.3 Fixed-order H_∞ -optimisation and μ -synthesis

It is well known that the problem of directly synthesising fixed-order/structure) controllers is very hard and this is due to the fact the the problem is no longer convex and there is no guarantee for the optimisation problem to converge to the optimal solution [84]. Since finding the global minimum of this non-convex optimisation problem is hard, most of the available optimisation algorithms search only for the local minima. Recently, several methods have been proposed in the literature for solving these non-convex optimisation problems. A modified steepest descent method has been proposed in [84, 85, 86, 87], where Clarke sub-differential of the H_∞ -norm has been computed for the optimisation problem. Several examples on successful synthesis of fixed-order H_∞ -optimal controllers using the modified steepest descent method are provided in references [84, 87]. The problem of synthesising fixed-order H_∞ -optimal controller has also been solved via a special

class of quasi-Newton algorithms (Broyden-Fletcher-Goldfarb-Shanno (BFGS)) in references [88, 89]. Since the Newton's method and the BFGS methods are based on the first and second derivatives of the function, the global convergence of these methods is guaranteed only if the function has a quadratic Taylor approximation near the optimum. However, the results in references [88, 89] show that in practice, the BFGS algorithm provides acceptable results even for non-smooth, non-convex optimisation problems. The presented algorithm in references [88, 89] is called "HANSO" (Hybrid Algorithm for Non-smooth Optimisation) and it is freely available¹ and the algorithm for designing fixed-order H_∞ -optimal controller HIFOO (H_∞ Fixed Order Optimisation) for linear dynamical systems can be found in² references [90, 91, 92]. The fixed-structure H_∞ -synthesis based on the modified steepest descent method [84, 85, 86, 87] is utilised in this Chapter to obtain fixed-order (fixed-structure) H_∞ controllers. The derivations are rather long and are skipped here due to page limitations, but the details can be found in references [84, 85, 86, 87].

4.3.1 Fixed-Order μ -Synthesis

Similar to the full-order μ -synthesis approach, robust fixed-order μ -optimal controllers can be obtained by performing the fixed-order H_∞ optimisation and fixed-order dynamic D -scalings. Again, it is desired to minimise the structured singular value (μ) of the scaled LFT of the generalised plant with respect to the fixed structure controller over the set of uncertainties. Since the μ -synthesis approach

¹<http://www.cs.nyu.edu/overton/software/hanso/>

²<http://www.cs.nyu.edu/overton/software/hifoo/>

comprises two steps, namely the synthesis of the H_∞ -optimal controllers and minimising the upper-bound of μ using the D -scalings, it is necessary to ensure that the D scalings are of fixed-order as well. For complex uncertainties $\hat{\Delta} \in \text{diag}(\Delta, \Delta_P)$, the work in reference [115] shows that the synthesis procedure can be accomplished in one step rather than the two step optimisation process in the standard DK -iteration method. This is achieved by synthesising the fixed-order controllers and the D scalings in one step. The general interconnection for standard DK -iteration in Fig. 4.1 is rearranged as depicted in Fig. 4.2, so that the fixed-structure controller and the D scalings can be optimised at the same time.

Consider the new scaling $\tilde{D} = D - I$ in such a way that $\tilde{D}\Delta = \Delta\tilde{D}$ (see 4.2), the problem of synthesising the controller and minimising the D -scalings in two separate steps can be cast into an LFT of the fixed structure controller $\hat{K}(s)$ and the shifted scaling \tilde{D} which can be solved in one step:

$$D\mathcal{F}_l(P, K)D^{-1} = \mathcal{F}_l\left(P_c, \begin{bmatrix} K & 0 & 0 \\ 0 & \tilde{D} & 0 \\ 0 & 0 & \tilde{D} \end{bmatrix}\right) \quad (4.8)$$

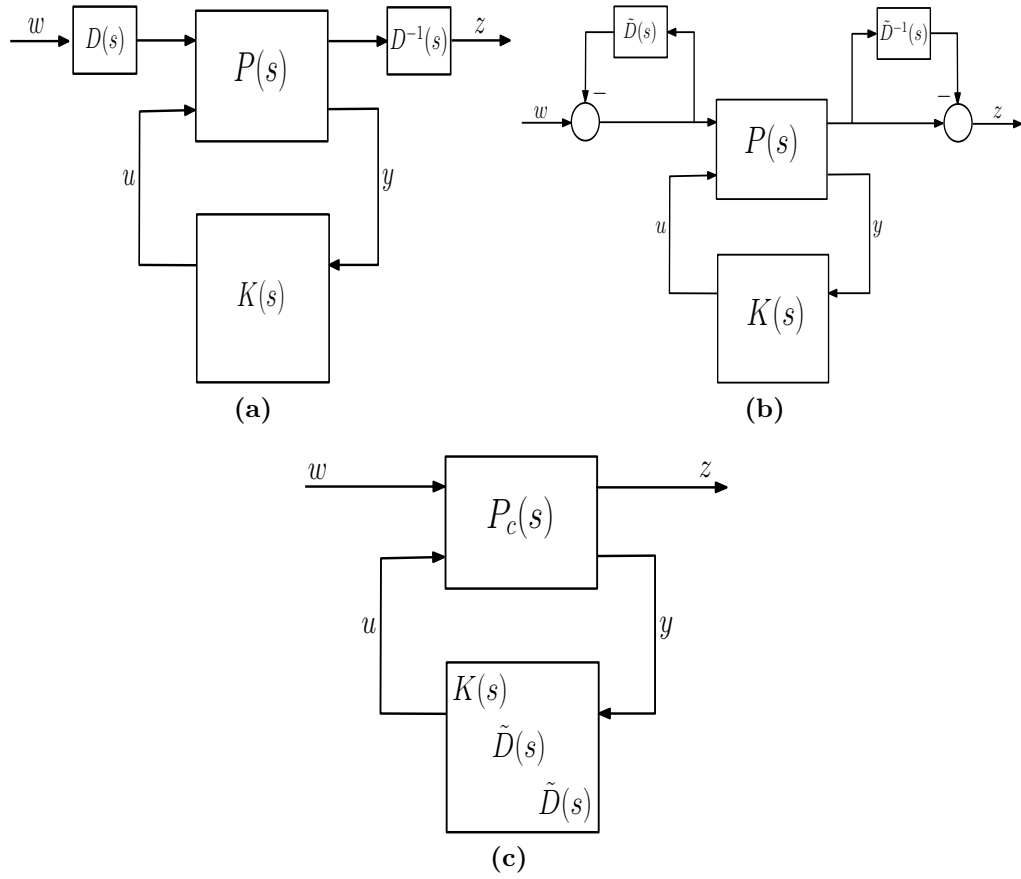


Figure 4.2: Translation on D-scaling, (a) original D-scaling, (b) translation of D-scaling into feedback form, (c) combination of the D-scaling with the controller.

where,

$$P_c(s) = \begin{bmatrix} I_N & 0 \\ 0 & I_{p2} \\ 0 & 0 \\ I_N & 0 \end{bmatrix} P(s) \begin{bmatrix} I_N & 0 & -I_N & 0 \\ 0 & I_{m2} & 0 & 0 \end{bmatrix} + \begin{bmatrix} 0 & 0 & 0 & I \\ 0 & 0 & 0 & 0 \\ I & 0 & -I & 0 \\ 0 & 0 & 0 & 0 \end{bmatrix} \quad (4.9)$$

The fixed-order μ -synthesis can then be performed using the available non-smooth optimisation approach [115, 116]:

$$\min_K \sup_{s=j\omega} \bar{\sigma} \left(\mathcal{F}_l(P_c, K) \right), P_c = DPD^{-1}$$

$$K := \begin{bmatrix} K & 0 & 0 \\ 0 & \tilde{D} & 0 \\ 0 & 0 & \tilde{D} \end{bmatrix}, \tilde{D} \in \tilde{\mathbf{D}}_{\Delta} \quad (4.10)$$

Inclusion of an additional constraint on the spectral abscissa of the closed-loop system can ensure the nominal stability of the closed-loop system:

$$\alpha\{A(G(s), K(s))\} \leq -\epsilon \quad (4.11)$$

where, $A(G(s), K(s))$ denotes the state-space A -matrix resulting from the feedback loop of $G(s)$ and $K(s)$. It should be noted that setting \tilde{D} to zero leads to standard H_{∞} control synthesis and keeping the controller K fixed results in μ -analysis problem. More details on non-smooth optimisation can be found in references [115, 116].

4.4 Simulation Results

4.4.1 Approach (1): μ -synthesis based on the full-order model of the system

In the first attempt, the analytical 10^{th} -order model of the system (shown in equation (2.14)) including both slow and fast dynamics is used for the synthesis of μ -optimal controllers. A first-order performance weight W_P is designed as shown in equation (4.12) to be the upper-bound on the closed-loop sensitivity function. Furthermore, an uncertainty of less than 10% is expected for low frequency regions. The uncertainties reach to more than 200% at frequencies beyond the rotor flexible modes (above 5000 rad/s). Subsequently, a second-order weight W_I is designed to be the upper-bound on the input multiplicative uncertainties and it is presented in equation (4.13).

$$W_P = \frac{0.3333(s + 600)}{(s + 0.03333)} \times \mathbf{I}_{(2 \times 2)} \quad (4.12)$$

$$W_I = \frac{5.59(s^2 + 995.5s + 9.727 \times 10^5)}{(s^2 + 1.364 \times 10^4s + 1.623 \times 10^8)} \times \mathbf{I}_{(2 \times 2)} \quad (4.13)$$

The standard DK -iteration procedure is employed to obtain the μ -optimal controller that robustly stabilises the 10^{th} -order system and satisfies the performance requirement for all possible systems in the uncertainty set. A peak μ -value of 1.158

is achieved with a controller of order 80. A lower peak μ -value maybe achieved by further limiting the bandwidth of the performance weight W_P in equation (4.12). It should be noted that with our available digital signal processing card, controllers with order higher than 22 fail to implement on the hardware. Therefore, the order of the designed controllers that are found to be higher than 22^{nd} needs to be reduced to 22^{nd} or less to be implementable on the available hardware. Here, Hankel singular value based model-order reduction is employed to reduce the order of the synthesised controller to 22. The Bode-diagram (magnitude) of the full-order and reduced-order controllers are depicted in Fig. 4.3. It is clear from the results that the excessively high-order controller is resulted from the numerical issues in the D -scaling stage. Nevertheless, the reduced-order controller is relatively identical to the full-order controller. It is also clear from the results that the controllers fail to completely remove the effects caused by the two dominant resonant frequencies. The real-time implementation of such controller is dangerous, as it could lead to system instability.

In this simulation study, the standard DK -iteration converges in three iterations. The achieved upper-bound on the structured singular value μ at each iteration and the order of the synthesised controllers along with the order of the D -scales are listed in Table 4.1.

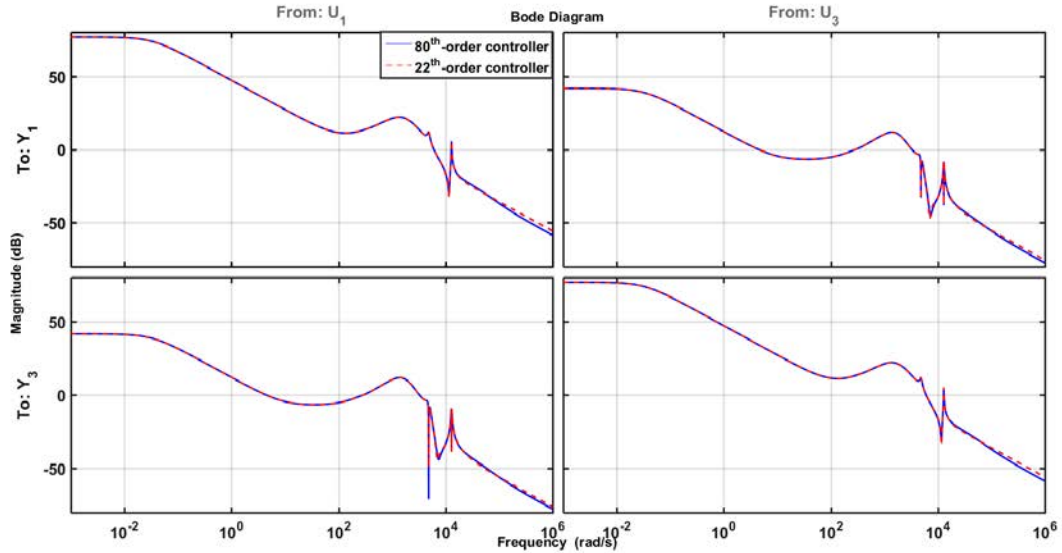


Figure 4.3: Bode-diagram (magnitude) of the full-order μ -optimal controller and the reduced-order controller.

Table 4.1: Achieved μ -value and the controller order using the standard DK -iteration

Iteration	1	2	3
Controller Order	18	26	80
Total D-scale Order	0	8	60
Peak μ -value	3.012	1.765	1.158

4.4.2 Approach (2): Full-order μ -synthesis by considering the high-frequency dynamics as multiplicative input uncertainties

As it was demonstrated in the previous Section, the system includes both “slow” and “fast” dynamics. The slow dynamics correspond to the dynamics of the electromagnets, hall-effect sensors, and the current amplifiers. Whereas, the fast

dynamics are related to the rotor flexible modes and other high-frequency unmodelled dynamics. The main cause of the numerical issues in synthesising optimal controllers in the previous Section was because of the presence of both “slow” and “fast” dynamics in the model. This increases the condition number (the ratio of the largest singular value to the smallest singular value) of the system and results in high-order controllers. From the acquired knowledge about the dynamics of the system, the rigid-body model of the system (slow-dynamics model) is used as the nominal model of the system for controller synthesis while the two flexible modes of the system are treated as structured modelling uncertainties and hence their models are included in the design weighting functions instead of the system model. This substantially improves the condition number of the overall system (i.e., 1.4384 compared to 1.6912×10^8 for the full-order model) and hence eliminates the numerical issues in the synthesis of robust controllers.

A similar first-order weighting function as shown in equation (4.12) is designed to ensure that the performance requirements are satisfied. Whereas, a sixth-order weighting W_I is designed to be the upper-bound on the modelling uncertainties. To this end, the stable minimum-phase weighting function in equation (4.13) is combined with two extracted resonant frequencies from the analytical model of the system to be represented as the modelling uncertainties:

$$\begin{aligned}
 W_I = & \frac{5.59(s^2 + 995.5s + 9.727 \times 10^5)}{(s^2 + 1.364 \times 10^4 s + 1.623 \times 10^8)} \times \frac{(s^2 + 10240s + 2.127 \times 10^7)}{(s^2 + 9.6 \times 10^{-5} s + 2.344 \times 10^7)} \\
 & \times \frac{(s^2 + 1.031 \times 10^4 s + 1.637 \times 10^8)}{(s^2 + 3.7 \times 10^{-5} s + 1.668 \times 10^8)} \times \mathbf{I}_{(2 \times 2)} \quad (4.14)
 \end{aligned}$$

Fig. 4.4 shows the rigid-body model of the system as the nominal system in red. Assuming the resonant modes and unknown high-frequency dynamics as multiplicative uncertainties, the set of uncertain systems can be represented in the form of $G(s)(1 + \Delta(s)W_I(s))$, where $\|\Delta(s)\|_\infty < 1$. In order to graphically demonstrate the nominal system and the uncertain systems, Δ is altered and some uncertain systems in the uncertainty set are depicted in Fig. 4.4.

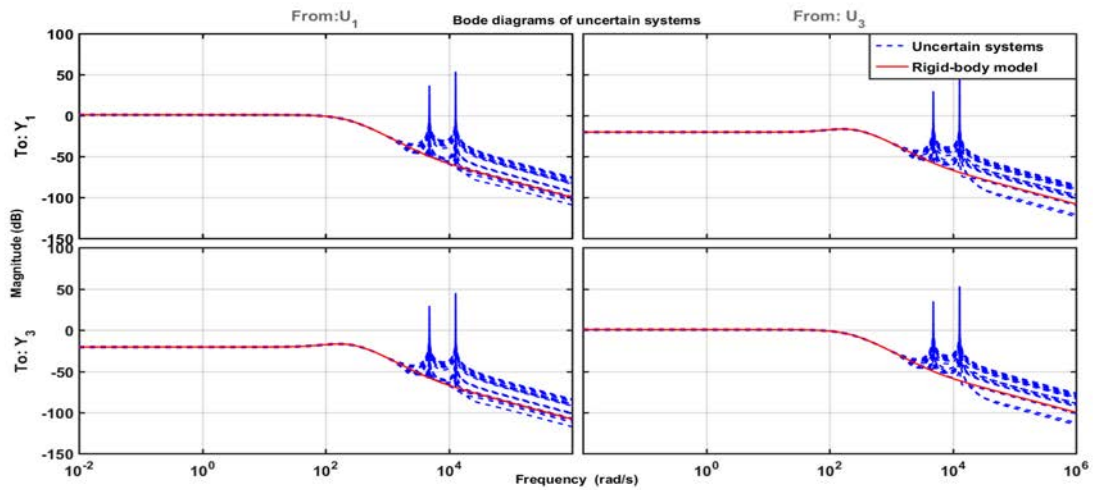


Figure 4.4: Nominal system (solid red line) and a set of uncertain systems (dashed blue lines).

Again, the standard μ -synthesis approach is carried out and the achieved peak μ -value and the controller orders using the standard DK -iteration are given in Table 4.2. In comparison to the results from previous Section where the full-order model of the system is utilised for the μ synthesis procedure, the order of the synthesised controller is found to be 32 which is much less than the 80th-order controller. Furthermore, the upper-bound on the structured singular value (μ) in Fig. 4.5 shows that the robust stability and robust performance of the uncertain

closed-loop systems are satisfied, i.e. $\mu_{\Delta}N(s) < 1$. furthermore, the bode-diagram (magnitude) of the synthesised controller is depicted in Fig. 4.6. Unlike the results obtained from the synthesis of μ -optimal controller using the full-order model of the system (Fig. 4.3), it can be seen that two notch filters are resulted in the controller which ensure the complete rejection of the two resonant frequencies. However, the order of the synthesised controller needs to be reduced to 22 or less to be implemented on the available hardware. Although there exist several numerical methods for order-reduction in the literature, it is crucial to keep the two notch filters in the reduced-order controller. The results in Fig. 4.6 clearly show the significant impact of different order-reduction methods on the final reduced-order controller. The Hankel singular value order reduction method is found to reduce the order of the original 32nd-order controller to 22nd-order by keeping the *dc*-gain and the two notch filters unchanged in the final controller.

Table 4.2: Achieved μ -value and the controller order using the standard *DK*-iteration

Iteration	1	2	3
Controller Order	20	28	32
Total D-scale Order	0	8	12
Peak μ -value	2.256	1.171	0.978

The closed-loop step responses of some uncertain systems are depicted in Fig. 4.7.

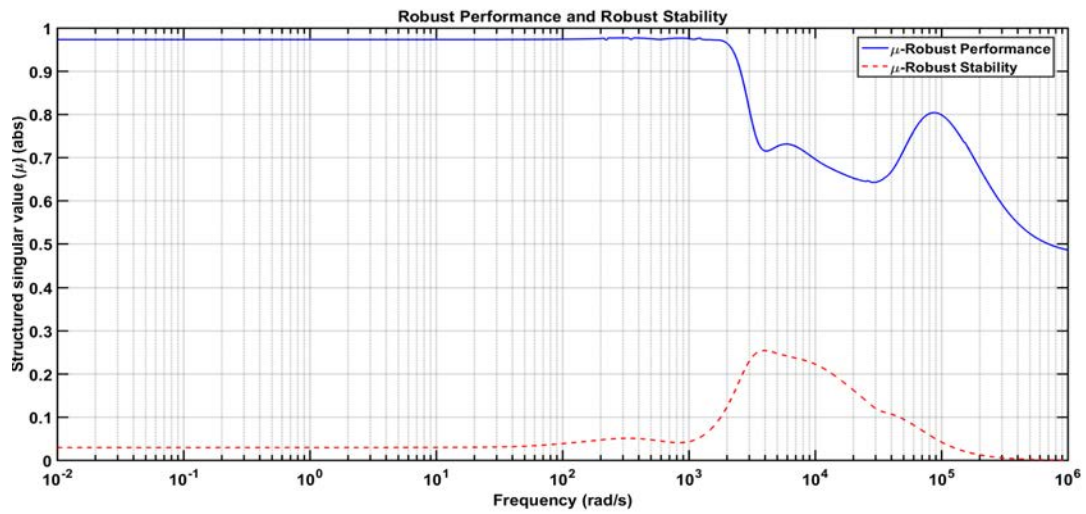


Figure 4.5: Upper-bound on the structured singular value μ for robust stability and robust performance.

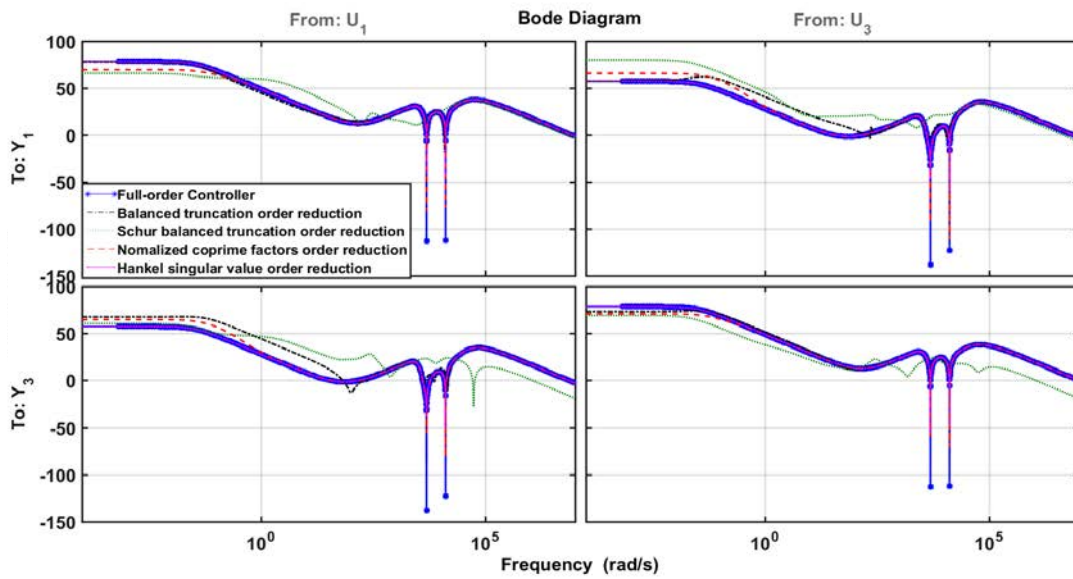


Figure 4.6: Bode-diagram of the full-order controller and the reduced-order controllers.

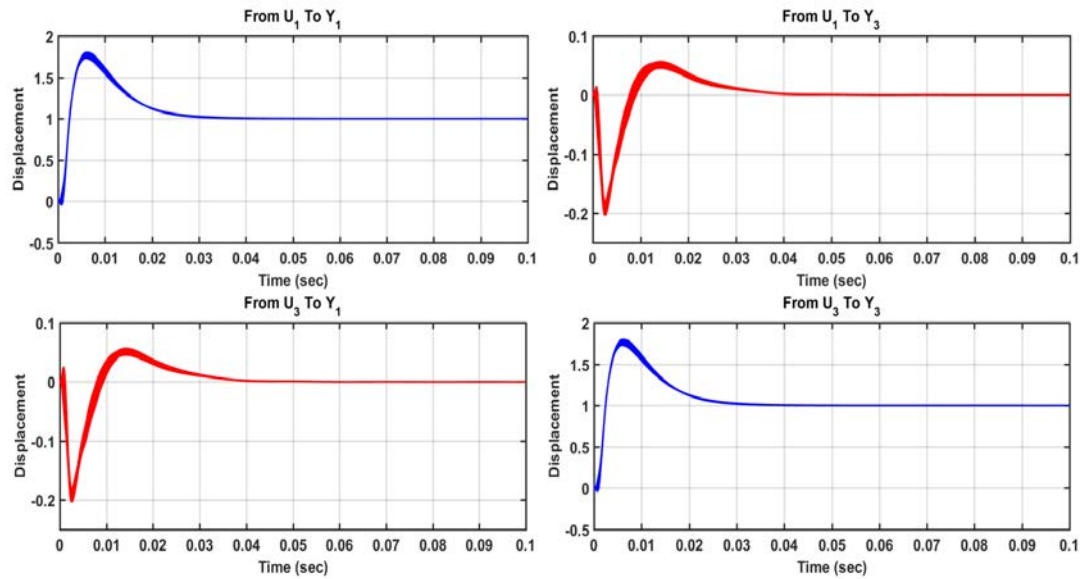


Figure 4.7: Closed-loop step response of a set of uncertain systems.

4.4.3 Approach (3): Direct synthesis of Fixed-order μ -optimal controllers

In order to synthesise a fixed-order H_∞ - or μ -optimal controller, the order (or structure) of the controller needs to be assigned *a priori*. This may sometimes become challenging, as robust stability and robust performance of the closed-loop system may not be satisfied with a specific fixed-order controller. In the case of our laboratory AMB system, if the 6th-order rigid-body model of the system (shown in equations (2.12) and (2.13)) is used for the synthesis of the robust controllers, it is found that controllers with order less than 4 fail to satisfy the robust stability and robust performance requirements. Furthermore, with the 10th-order full-body model of the system, controllers with order less than 8 are found not to robustly stabilise the closed-loop system. The non-smooth optimisation algorithm available

in MATLAB software package is utilised to tune the parameters of the controller and to ensure that the structured singular value μ is minimised over the frequency range of interest. The upper-bound on the structured singular value (μ) in Fig. 4.8 shows that the robust performance requirements of the uncertain systems are met, i.e. $\mu_{\Delta}N(s) = 0.92 < 1$.

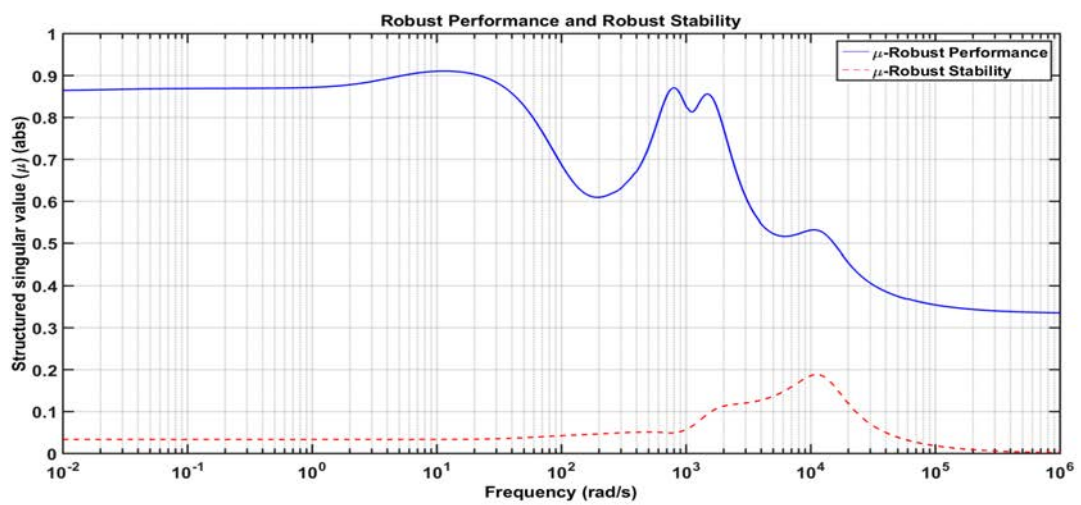


Figure 4.8: Closed-loop robust stability and robust performance for the fixed-order μ -optimal controller.

Finally, Table 4.3 summarises the order of the final synthesised controllers using the three approaches described in the previous Sections.

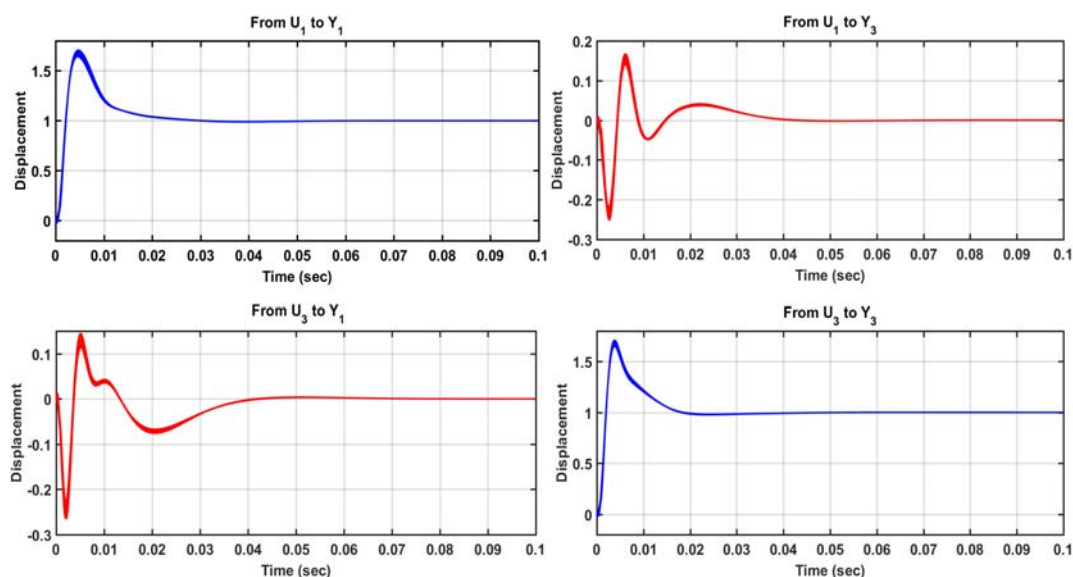


Figure 4.9: Closed-loop step response of some random uncertain systems.

Table 4.3: The order of synthesised controllers using various methods

Controller	Order
Standard μ -synthesis with full-body model	80
Standard μ -synthesis with rigid-body model	32
Fixed-order μ -synthesis with full-body model	8
Full-order H_∞ controller with full-body model	10
Fixed-order H_∞ controller with full-body model	8

4.5 Experimental Results

This section is devoted to real-time implementation of the synthesised full-order and fixed-order H_∞ - and μ -optimal controllers on the laboratory AMB system. The synthesised continuous-time controllers are discretised using the Bilinear transformation with a sampling frequency of 20 kHz . The discrete-time controllers are implemented using an analog-to-digital/digital-to-analog converter and the

dSPACE DS1104 digital signal processing board. In the first experiment, the rotor is stationary and the analog on-board controllers are replaced by the digital controllers for the stabilisation of the rotor between the bearings. To investigate the disturbance rejection capabilities of the designed controllers, two unit-step disturbances are introduced to the system. The first unit-step disturbance is introduced to the first channel (horizontal channel at one end) after approximately 1 s, followed by the second unit-step disturbance applied to the second channel (horizontal channel at the other end) after approximately 2 s. The disturbances are introduced at slightly different instances of time, so that the results can be evaluated clearly. As the cross-coupling effects between the same plane channels (*horizontal/horizontal* and *vertical/vertical* planes) are more significant than the different plane channels (*horizontal/vertical* planes), the results for the horizontal channels are demonstrated here. It should be noted that the full-order H_∞ - and μ -optimal controller that are designed on the basis of the full-order model (approach (1), see Fig. 4.3) failed to stabilise the system. This is because the designed controllers failed to completely reject the effects caused by the resonant frequencies. However, the full-order H_∞ - and μ -optimal controllers that are designed based on the proposed procedure described as approach (2) are successfully implemented on the system and the obtained results are compared with the fixed-order robust controllers (approach (3)) in Figs. 4.10-4.12. The unit-step responses of the horizontal channels are depicted in Figs. 4.10a and 4.10b. Furthermore, the required control signals are shown in Figs. 4.10c and 4.10d, respectively. From the obtained results, it can be deduced that the 8th-order μ -optimal controller shows a relatively similar performance compared to the 32th-order μ -optimal controller. Moreover, all the designed controllers provide much superior performance than the analog on-board

controllers. Note that the analog on-board controllers are of lead-type compensators and hence incapable of rejecting disturbances. Therefore, the step-response of the system with the analog on-board controllers are not included here (see references [53, 61, 63, 117] for example). It is also observed from the results in Figs. 4.10c and 4.10d that the control signals of the fixed-order H_∞ - and μ -optimal controllers are much noisier than the other robust controllers. An inclusion of a low-pass filter could reduce the effects of high-frequency measurement noise.

In order to further investigate the performance of the designed controllers in the presence of uncertainties and unmodelled dynamics, the shaft is rotated with the help of the internal air-turbine attached to one end of the rotor. The air-pressure supplied by the air-compressor is increased gradually and the displacements of the geometrical center of the rotor at both ends (horizontal channels) are depicted in Figs. 4.11a and 4.11b. Moreover, the corresponding control signals are depicted in Figs. 4.11c and 4.11d, respectively. It can be deduced from the results that all designed MIMO controllers provide much better performance in terms of unknown disturbance rejection and vibration attenuations compared to the on-board analog controllers. The rotor remains at its geometrical center for the entire operating range for all designed controllers, and the maximum magnitude of vibration in the system remain below $0.2\text{volts}/0.02\text{mm}$. It should be noted that the reduced-order μ -optimal controller that is designed on the basis of the high-order model of the system outperforms the other designed controllers. It should be further noted that at the analytical modelling stage the system is assumed to be symmetrical at both ends. However, it can be clearly seen from the results in Figs. 4.11a and 4.11b that

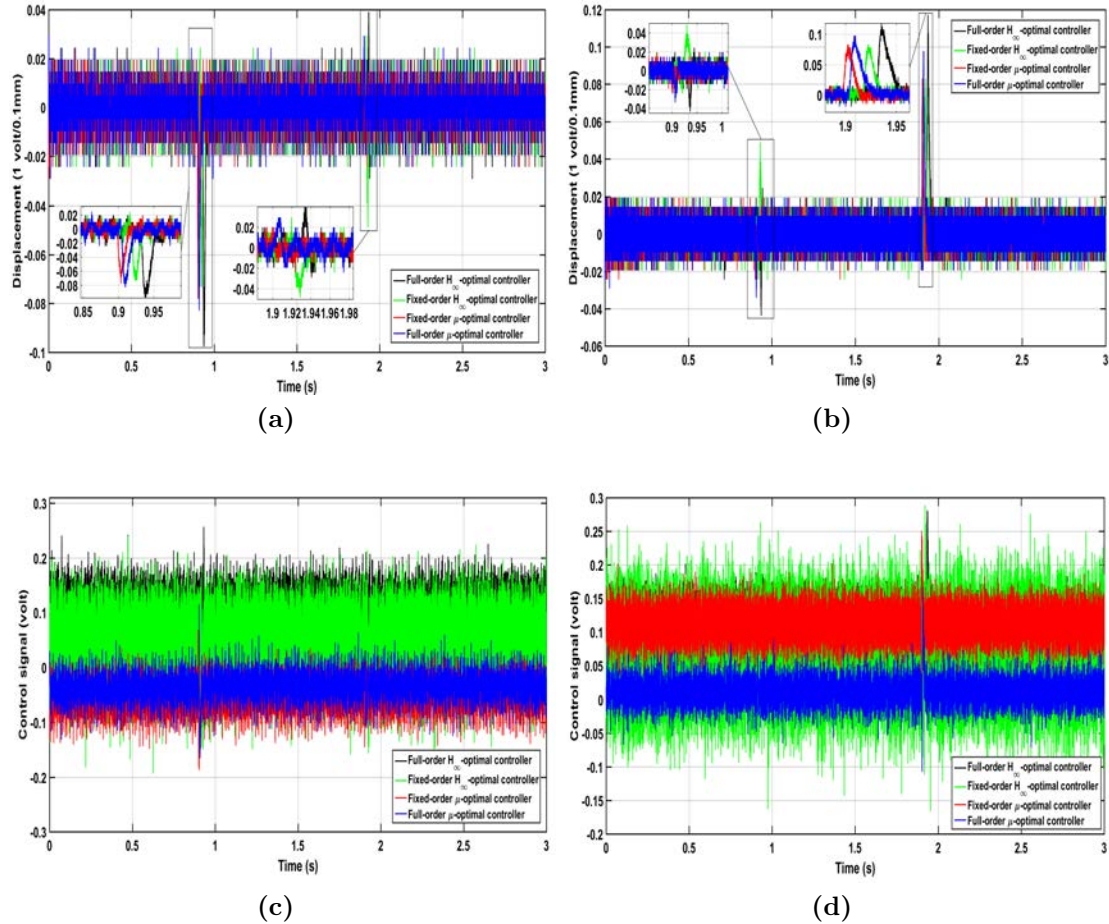


Figure 4.10: Step response of the system using the full-order and fixed-order H_∞ - and μ -optimal controllers in the presence of disturbance, (a) Displacement of channel Y_1 , (b) Displacement of channel Y_3 , (c) Control Signal of channel Y_1 , (d) Control Signal of channel Y_3 .

the effects caused by the internal air-turbine is more severe at one end of the rotor where the air-turbine is attached than the other end.

In the final set of experiments, constant air-pressure is provided to the rotor by the air-compressor and the transient-response of the system is recorded for 120 s. From the results in Fig. 4.12, the rotor reaches the highest rotational speed using

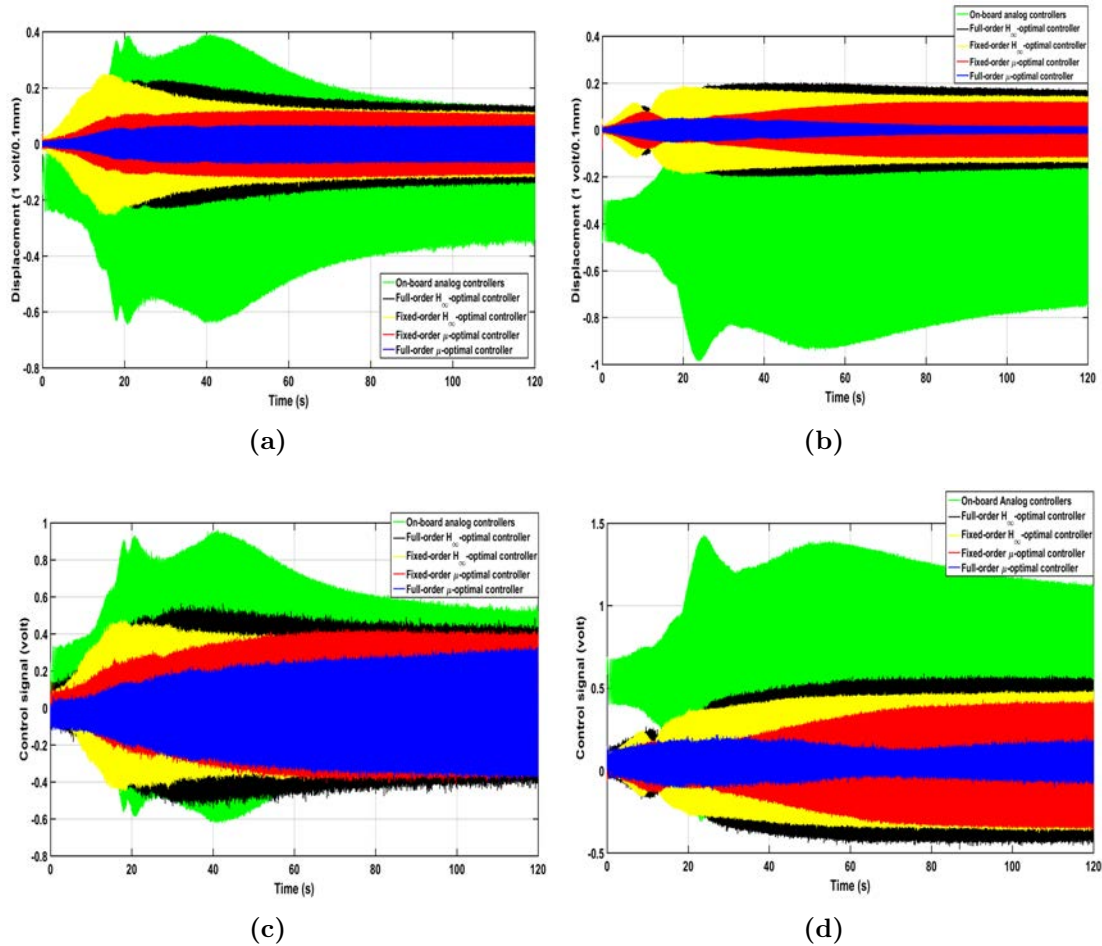


Figure 4.11: Displacement and control signals of channels Y_1 and Y_3 as rotational speed of the shaft increases over time, (a) Displacement of channel Y_1 , (b) Displacement of channel Y_3 , (c) Control Signal of channel Y_1 , (d) Control Signal of channel Y_3 .

the full-order μ -optimal controller among all other designed controllers. Whereas, the system reaches the lowest steady-state rotational speed (compared with the other synthesised controller) when the fixed-order H_∞ controller is employed. The other H_∞ - and μ -optimal controllers show relatively similar performances. It should also be noted that the on-board analog controllers do not show consistent results in terms of the steady-state speed. It can be seen from the results that the rotor

has achieved much lower steady-state speed here compared to the results presented in [63].

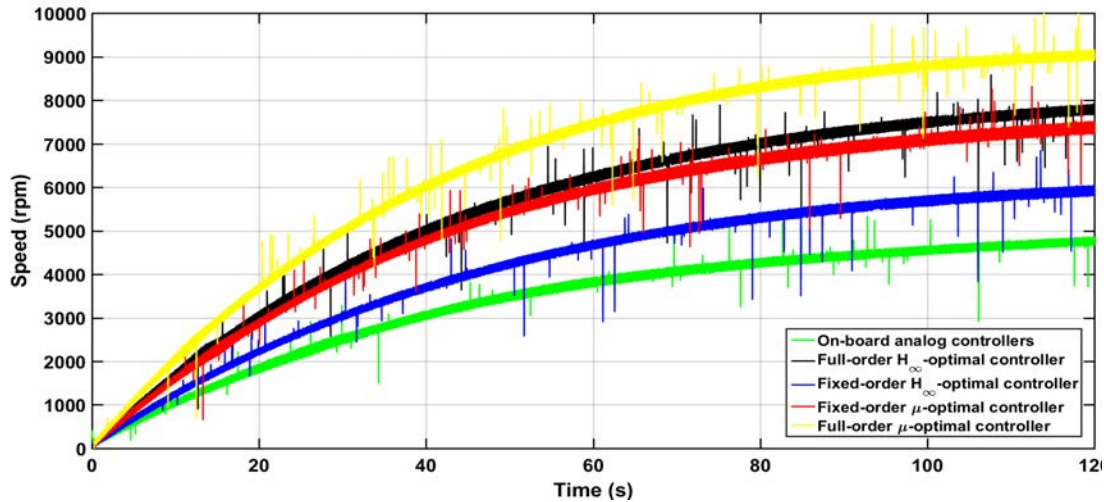


Figure 4.12: Transient rotational speed of the rotor using the full-order and fixed-order H_{∞} - and μ -optimal controllers.

4.6 Conclusion

In this Chapter, it is shown that the order of the μ -optimal controller that is synthesised on the basis of the full-order model of the system is found to be excessively large. This is because the system consists both "slow" and "fast" dynamics and this causes numerical issues at the D -scaling stage. On the other hand, a much lower-order μ -optimal controller can be designed by considering only the slow dynamics in the model and treating the fast dynamics as modelling uncertainties. The experimental results have confirmed that the designed controllers

based on the proposed procedure provide promising performances in terms of stabilisation and disturbance rejection of the AMB system. Furthermore, although there is no guarantee on the convergence of non-smooth non-convex optimisation of fixed-order (or structure) H_∞ and μ synthesis problems, the simulation and experimental results verified that the acceptable controllers can be obtained using the described algorithms. Also, the order of the fixed-order controllers is much less than the controllers that are designed using the standard DK -iteration algorithm. Last but not least, it should be noted that the non-smooth optimisation algorithms available in MATLAB software package for fixed-order control synthesis have been significantly improved over the last few years after the first commercial distributions as part of the Robust Control Toolbox 3.5 in MATLAB R2010b [118]. This is observed after synthesising the fixed-order controllers in MATLAB R2011b and compared the results with the synthesised controllers that are obtained in MATLAB R2014b [119]. In fact, the control synthesis algorithms had to be run multiple times in MATLAB R2011b in order to obtain satisfactory results. Furthermore, neither the upper-bound on the structured singular value μ nor the final obtained controllers were found to be consistent in multiple runs. However, this problem appears to have been resolved in the recent versions.

Chapter 5

Optimal PID-type Fuzzy Logic Control of AMB System

5.1 Introduction

This Chapter aims to provide a simple but effective PID-type fuzzy logic controller structure that can be generalised for control of linear and nonlinear systems where only an approximate model of the system is available. The design parameters are optimised using several meta-heuristic optimisation algorithms. It is shown via a simulation example that the performance of most of the meta-heuristic algorithms depends highly on the proper selection of the optimisation objective function. The problem with the most of time-domain optimisation objective functions is

that an accurate information is necessary about the optimisation search-domain. Otherwise, the algorithm converges to undesirables solutions which may lead to large control signals and hence saturation of actuators. To alleviate this problem, some alternative objective functions are proposed in this Chapter for the time-domain optimisation of control system design. It is shown that by employing the presented objective functions, regardless of the size of optimisation search-domain, the algorithm converges to a relatively similar result. Several meta-heuristic algorithms are utilised to ensure that the optimal values of the design parameters are obtained. Ultimately, the same procedure is used to design optimal PID-type fuzzy logic controllers for the robust stabilisation of the active magnetic bearing system. The designed optimal controllers are coded in *C* for real-time implementation on the system and the performance of the designed controllers is investigated while the system is stationary as well as while it is operating at various speeds.

5.2 PID-Type Fuzzy Logic Controllers

Several forms of fuzzy logic controllers can be found in the literature [27, 67, 120, 121]. It should be noted that the focus of this Chapter is on so-called “direct action” fuzzy logic controller. This structure will be called PID-type fuzzy logic controller or PID-FLC in short throughout this Chapter. On the other hand, the name fuzzy PID controller (or FLC-PID) refers to the so-called “gain-scheduling” type PID controllers where the fuzzy logic is used to produce the required K_P , K_I , and K_D gains of the linear PID controller [122, 123], and it is not studied here. The

PID-type fuzzy logic controllers are usually classified based on the number of inputs to the controller. Generally, two- and three- input fuzzy logic controllers are the most common structures, in which a nonlinear PID-like performance is expected from the controller. Some of the most commonly used structures are illustrated in Fig. 5.1. It should be noted that the input/output variables of the fuzzy logic controllers are normalised within the range of $[-1, 1]$. Therefore, six scaling factors are required to be properly chosen for the first two structures (see Figs. 5.1a and 5.1b), whereas, four scaling factors are required for the last two structures (see Figs. 5.1c and 5.1d).

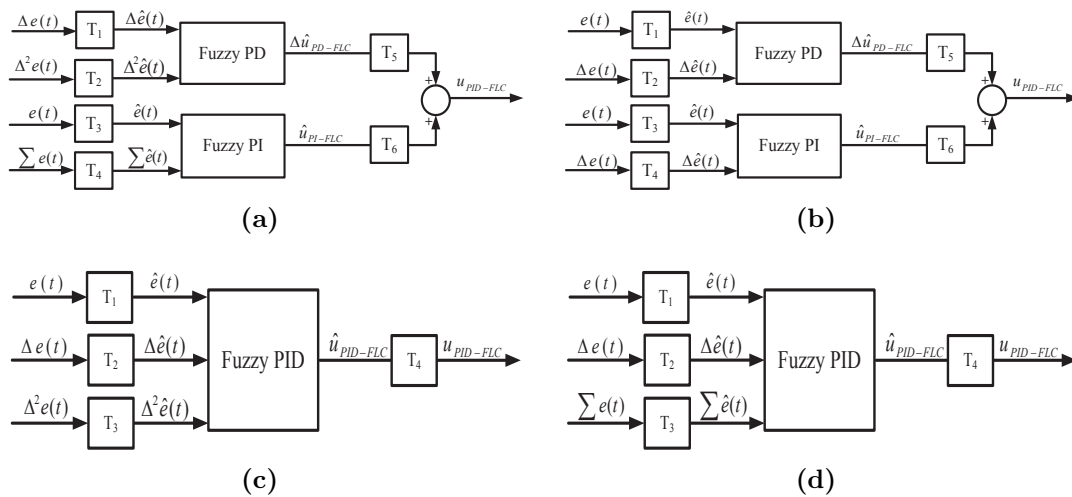


Figure 5.1: Common PID-type fuzzy logic controllers, (a) Two-input PID-type FLC with error and sum of the error signals as inputs, (b) Two-input PID-type FLC with error and rate of change of the error signals as inputs, (c) Three-input PID-type FLC with error, rate of change of error and the second derivative of the error signals as inputs, (d) Three-input PID-type FLC with error, rate of change of error and sum of the error signals as inputs.

An alternative structure is employed in this thesis and it is depicted in Fig. 5.2. The advantage of the presented structure over those of in Fig. 5.1 is that it

consists of a single two-input fuzzy logic controller that makes it computationally more efficient for real-time implementation. As two inputs are supplied to the fuzzy logic controller, less number of rules is required to be designed compared to the three-input structures.

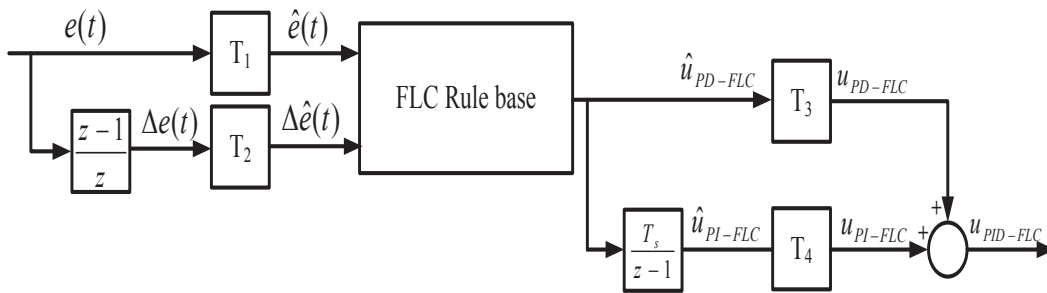


Figure 5.2: Alternative PID-type fuzzy logic controller.

It should also be mentioned that the processing time of the Sugeno-type fuzzy logic controllers is much faster than their Mamdani-type counterparts, as the area of the output membership functions is not required to be calculated in the Sugeno-type controllers. This makes the Sugeno-type fuzzy logic controllers more reliable for real-time implementation. Therefore, this study is restricted to the Sugeno-type fuzzy logic controllers. We first define a simple structure for the fuzzy logic controller with twenty five rules (see Fig. 5.3). Next, several optimisation methods are used to tune the design parameters in two levels. It is clear from Fig. 5.2 that the parameters $(T_{1,2,3,4})$ are the scaling factors to transform the input/output variables into the range of $[-1, 1]$. Therefore, in the first level of tuning, the optimal value of the scaling factors $(T_{1,2,3,4})$ are obtained. In the second level of tuning, the distribution of the input/output membership functions are

altered by varying the base and centroid locations ($S_{1,2,\dots,11}$) of the membership functions.

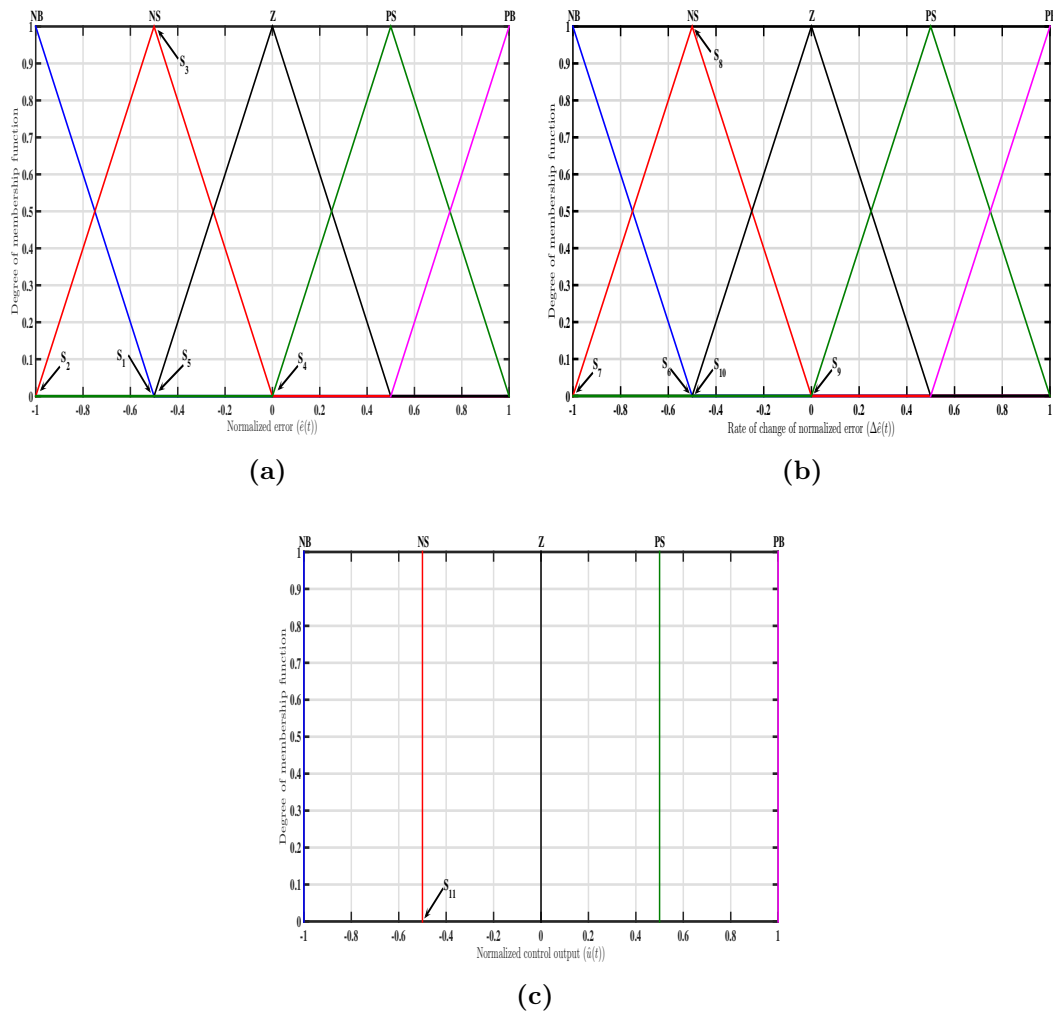


Figure 5.3: Initial distribution of the inputs/output membership functions, (a) Distribution of the error input membership function, (b) Distribution of the rate of change of error input membership function, (c) Distribution of the output membership function.

The inputs/outputs of the fuzzy logic controller are transformed into five linguistic variables, namely *NB* (negative big), *NS* (negative small), *Z* (zero), *PS*

(positive small), *PB* (positive big). The total number of twenty five rules is required to complete the fuzzy rule-base. The rule-base table can be designed based on the expected response of the system to a particular input to the system. For instance, the gray cells in Table 5.1 represent the required magnitude of the control signals in the transient stage of the system response to a unit-step input. Furthermore, the red cells show the required magnitude of the control signals in the settling stage, and the expected magnitude of the control signals in the steady-state stage are represented in white.

Table 5.1: 5×5 FLC rule-base in tabular form

$\Delta\hat{e}(t)$ $\hat{e}(t)$	NB	NS	Z	PS	PB
NB	NB	NB	NB	NS	Z
NS	NB	NB	NS	Z	PS
Z	NB	NS	Z	PS	PB
PS	NS	Z	PS	PB	PB
PB	Z	PS	PB	PB	PB

5.3 Review of Some Optimisation Algorithms

In recent years, various meta-heuristic optimisation algorithms have been proposed and some have shown promising performances on the optimisation of multi-dimensional mathematical problems. However, according to “no free lunch” theorem [124], it is impossible to find an algorithm that works the best on all optimisation

problems. Consequently, several optimisation algorithms are employed in this Chapter to analyse the sensitivity of the PID-type fuzzy logic controller to the design parameters.

5.3.1 Genetic Algorithm (GA)

Genetic Algorithm (GA) is a well known meta-heuristic algorithm based on the genetic evolution of the population. GA has been extensively used in the past and current research works for optimisation of single- and multi-objective problems [47, 53, 125, 126]. GA starts the optimisation process with a set of randomly generated solutions (population). In each iteration, the best individuals are selected to be the “parents”, and the next generation (“children”) are produced by crossover and mutation of the parents. Over an evolutionary algorithm, a better generation is produced from the past generation, and the solutions evolve towards the optimal value. A simple pseudo-code for GA is given below:

- 1) create a random initial population;
- 2) evaluate the fitness value of each individual;
- 3) select the best individuals;
- 4) while the stopping criteria are not reached:

- 4-1) generate new population using mutation and cross-over;
- 4-2) replace the worst individuals by the best individuals;
- 4-3) go to the next iteration.

5.3.2 Particle Swarm Optimisation (PSO)

Particle Swarm Optimisation (PSO) is another well-known global optimisation algorithm inspired by the flocking behaviour of birds [127, 128]. The algorithm starts by randomly generated particles within the search space. In each iteration, particles fly around the search-space with their assigned velocities in hope to find the best solution. The velocity of each particle updates based on the current velocity of the particle, the particle's individual best solution, and the global best solution that have been obtained so far. Then, the location of the particles updates iteratively based on the new velocities, until the stopping criteria are reached. The equations that emulate the described characteristics are given in equations (5.1) and (5.2) [127].

$$v_i^{t+1} = w \times v_i^t + c_1 \times r_1 \times (p_{i,d} - x_{i,d}^t) + c_2 \times r_2 \times (p_{g,d} - x_{i,d}^t) \quad (5.1)$$

$$x_{i,d}^{t+1} = x_{i,d}^t + v_i^{t+1} \quad (5.2)$$

In equations (5.1) and (5.2), $x_{i,d}^t$ and $x_{i,d}^{t+1}$ are the current and the future positions of the i^{th} particle. The parameter v_i^t is the current velocity of the particle, and w is a weighting function to control the effect of the particle's current velocity on its future velocity. The variable $p_{i,d}$ represents the best solution of the particle i at iteration t , and $p_{g,d}$ is the best global solution so far. The two weighting factors c_1 and c_2 determine the importance of the current local and global best solutions. Finally, r_1 and r_2 are two random numbers within the range of $[0, 1]$ to further encourage the stochastic exploration of the particles throughout the search space.

5.3.3 Grey Wolf Optimisation (GWO)

Grey Wolf Optimisation (GWO) is a recent meta-heuristic algorithm based on the natural hunting behaviour of grey wolves [129, 130, 131]. The solution candidates are made up of four different types of wolves (α , β , δ and ω). The wolves α , β and δ can be considered as the first, second, and third best solutions. There is only one candidate within each of α , β and δ dimensions, however, the ω can consist of multiple candidates. The algorithm starts with randomly generated solutions. All candidates are considered as ω at the start of the algorithm. Upon the end of the first iteration, the three wolves (α , β , and δ) are assigned to the best three solutions. The optimiser then continues to move the candidates towards the best scoring solution (α), as well as a random placement of some candidates throughout the

search space to promote exploration. The optimiser continues with an “encircling prey” algorithm which focuses on the surrounding of the prospective best solution. The encircling algorithm can be formulated as in equations (5.3) and (5.4) [129].

$$\vec{D} = |\vec{C} \times \vec{X}_p(t) - \vec{X}(t)| \quad (5.3)$$

$$\vec{X}(t+1) = \vec{X}_p(t) - \vec{A} \times \vec{D} \quad (5.4)$$

where X_p is the position of the prey, $X(t)$ and $X(t+1)$ represent the current and the future positions of a grey wolf. \vec{A} and \vec{C} are given in equations (5.5) and (5.6).

$$\vec{A} = 2 \cdot \vec{a} \cdot r_1 - \vec{a} \quad (5.5)$$

$$\vec{C} = 2 \cdot \vec{r}_2 \quad (5.6)$$

In equations (5.5) and (5.6), r_1 and r_2 are random set of vectors between $[0, 1]$. The parameter a is used to mathematically model the attacking stage when the prey stops moving. In fact, a decreases linearly from 2 to 0 over the course of iterations. GWO continues the algorithm by storing the best three solutions and updating their positions according to equations (5.7)-(5.9), and the iteration

continues until the stopping criteria are reached.

$$\begin{aligned}\vec{D}_\alpha &= |\vec{C}_1 \cdot \vec{X}_\alpha - \vec{X}|, \\ \vec{D}_\beta &= |\vec{C}_2 \cdot \vec{X}_\beta - \vec{X}|, \\ \vec{D}_\delta &= |\vec{C}_3 \cdot \vec{X}_\delta - \vec{X}|\end{aligned}\quad (5.7)$$

$$\begin{aligned}\vec{X}_1 &= \vec{X}_\alpha - \vec{A}_1 \cdot \vec{D}_\alpha, \\ \vec{X}_2 &= \vec{X}_\beta - \vec{A}_2 \cdot \vec{D}_\beta, \\ \vec{X}_3 &= \vec{X}_\delta - \vec{A}_3 \cdot \vec{D}_\delta\end{aligned}\quad (5.8)$$

$$\vec{X}(t+1) = \frac{\vec{X}_1 + \vec{X}_2 + \vec{X}_3}{3}\quad (5.9)$$

5.3.4 Imperialist Competitive Algorithm (ICA)

Imperialist Competitive Algorithm (ICA) is another recent meta-heuristic algorithm inspired by the social behaviour of imperialist countries [132, 133]. The algorithm starts with a randomly generated solutions (countries). Some of the best individuals are selected to be the initial imperialists while the rest of candidates are possessed by the imperialists as their colonies. The number of colonies under the control of each imperialist depends on the power of the corresponding imperialist (power is calculated as the reciprocal of the fitness value). To ensure the normal distribution of the colonies among the imperialists, the normalised cost of each imperialist is

defined as in equation (5.10) [132].

$$C_n = c_n - \max_i c_i \quad (5.10)$$

where, C_n is the normalised cost of the n^{th} imperialist, and c_i represents the cost of each imperialist. After obtaining the normalised cost of each imperialist, the normalised power can be calculated as in equation (5.11).

$$p_n = \left| \frac{C_n}{\sum_{i=1}^{N_{imp}} C_i} \right| \quad (5.11)$$

The initial number of the colonies associated to the n^{th} imperialist can be obtained from equation (5.12). N_{col} is the initial number of colonies defined by the user.

$$N.C_n = round(p_n, N_{col}) \quad (5.12)$$

After distributing the colonies among the imperialists, the colonies start moving towards their corresponding imperialists. The mathematical representation of this movement is given in equation (5.13).

$$x_i^{t+1} = x_i^t + U(0, \beta \times d) \times V_1 \quad (5.13)$$

In equation (5.13), d is the distance between the colony and its corresponding imperialist, $\beta > 1$ ensures that the colonies move towards the imperialist from all directions. V_1 is a vector that its starting point is the previous location of the colony, and its direction is towards the imperialist. During the movement transition, if there exists a colony that is more powerful (lower cost value) than its imperialist, that colony becomes the new imperialist. In the imperialist competition stage, the power of each empire is calculated as the total power of each imperialist plus a percentage of the average power of its colonies. During the competition, the weakest empires that cannot increase their power will be eliminated from the imperialist competition. The ideal result of the optimisation is achieved when only one empire is left, and all its colonies have the same power as the imperialist. A simple pseudo-code for ICA can be written as follows:

- 1) create a random initial population (countries);
- 2) evaluate the fitness values of each country and select the best n individuals as the imperialists, and the rest of candidates as their colonies (number of countries, imperialists, and colonies are initialised before the optimisation starts);
- 3) move the colonies towards their corresponding imperialist (assimilating algorithm);

- 4) evaluate the fitness value of each individual in the empires, and if there exists a colony with higher power than its imperialist, exchange the position of the colony and the imperialist;
- 5) the empire that has the most likelihood to possess a colony can acquire the weakest colony from the weakest empire (imperialistic competition);
- 6) the weakest empires get eliminated;
- 7) iteration continues until only one empire is left, or other stopping criteria are reached.

5.4 Choice of an Objective Function

In order to design an optimal controller, both time- and frequency-domain characteristics can be utilised for the closed-loop system analysis. However, only time-domain analysis is available for the design of nonlinear fuzzy logic controllers. Several objective functions can be utilised for the time-domain optimisation of fuzzy logic controllers using meta-heuristic algorithms. For instance, mean absolute of error (MAE), integral absolute of error (IAE), mean squared of error (MSE), integral squared of error (ISE), and integral time absolute of error (ITAE) are the most common objective functions. The time-domain characteristics of the system, such as the settling-time and the percent-overshoot of the system to a unit-step input can also be used in conjunction with other time-domain objective functions. In the next

example, it is shown that unless there is enough information about the lower/upper bounds of the search-domain, the common time-domain objective functions may result in undesirable solutions. Subsequently, an alternative objective function is presented, and its effectiveness is verified by simulation and experimental studies.

5.4.1 Example: Stabilisation of a Time-Varying System Using the PID-Type Fuzzy Logic Controller

Suppose a standard PID-type fuzzy logic controller is to be designed for the time-varying system presented in equation (5.14) [134]. A Sugeno-type two-input PID-type fuzzy logic controller is first designed as shown in Figs. 5.2 and 5.3. In the first level of tuning, the membership functions are uniformly distributed, and the scaling factors $T_{1,2,3,4}$ need to be tuned using the meta-heuristic algorithms. At this stage, only PSO is used to find the optimal scaling factors ($T_{1,2,3,4}$). The optimisation process is carried out several times with different objective functions, and the optimisation search-domain is kept unchanged in the range of $[0, 10]$. This implies that the input/output membership functions can vary within the range of $[-10, 10]$. Several common time-domain objective functions, namely mean absolute of error (MAE), integral absolute of error (IAE), mean squared of error (MSE), integral squared of error (ISE), and integral time absolute of error (ITAE) are utilised to be minimised via the optimisation algorithm. The optimal scaling factors using these time-domain objective functions are shown in Table 5.2. The step response of the time-varying system using the tuned PID-type fuzzy logic

controllers, along with the required control signals are depicted in Fig. 5.4.

$$\begin{cases} \dot{x}_1(t) = x_2(t) \\ \dot{x}_2(t) = -e^{-0.2t}x_2(t) - e^{-5t} \sin(2t + 6)x_1(t) + u(t) \end{cases} \quad (5.14)$$

Table 5.2: Optimal scaling factors using different objective functions

Objective	T_1	T_2	T_3	T_4
IAE	1.01	2.78	10	4.96
MAE	1.01	2.97	10	5.28
ISE	1.01	3.61	9.95	6.52
MSE	1.01	4.19	10	1.71
ITAE	1.01	2.07	9.97	9.9

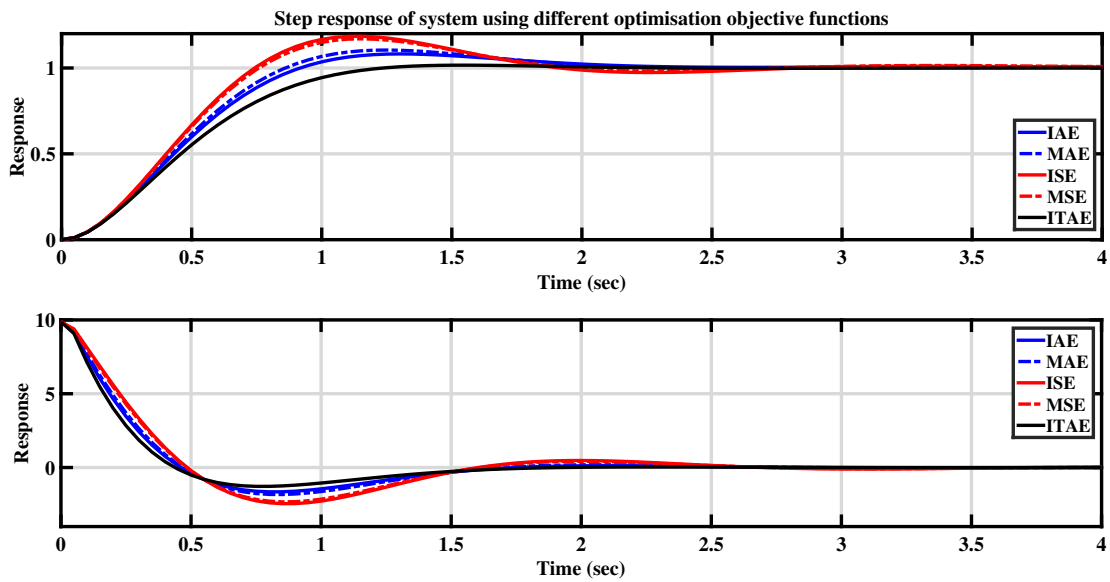


Figure 5.4: Closed-loop step responses of the system using different objective functions (Table 5.2).

It can be deduced from Fig. 5.4 that relatively similar behaviours are expected from these objective functions, as long as similar range of search-domain is chosen for the optimisation process. Nevertheless, ITAE shows a slightly better performance in terms of the percent overshoot and the settling time, and hence it is preferred in the remaining of this paper. In the sequel, only ITAE is used as the optimisation objective function while the optimisation search-domain is altered. The resulting scaling factors ($T_{1,2,3,4}$) are given in Table 5.3. The resulting step responses of the system and the control signals are depicted in Fig. 5.5, respectively. It is clear from the results that the bound on the search-domain has a critical impact on the final solution. This implies that unless an accurate knowledge is available about the size of search-domain, the common time-domain objective functions could result in a controller with excessively large control output signals and it could lead to actuators saturation.

Table 5.3: Optimal scaling factors using ITAE as the objective function and different bounds on the optimisation search-domain

Objective	T_1	T_2	T_3	T_4
ITAE [0,10]	1.01	2.07	9.97	9.9
ITAE [0,100]	1.00	7.13	97.62	50.39
ITAE [0,1000]	1.00	22.80	812.77	1.00

This problem can be alleviated by taking into account the magnitude of the control signal in the objective function. Since relatively similar results are expected from most of the time-domain objective functions, combining the magnitude of control signal with the common time-domain objective functions should result in

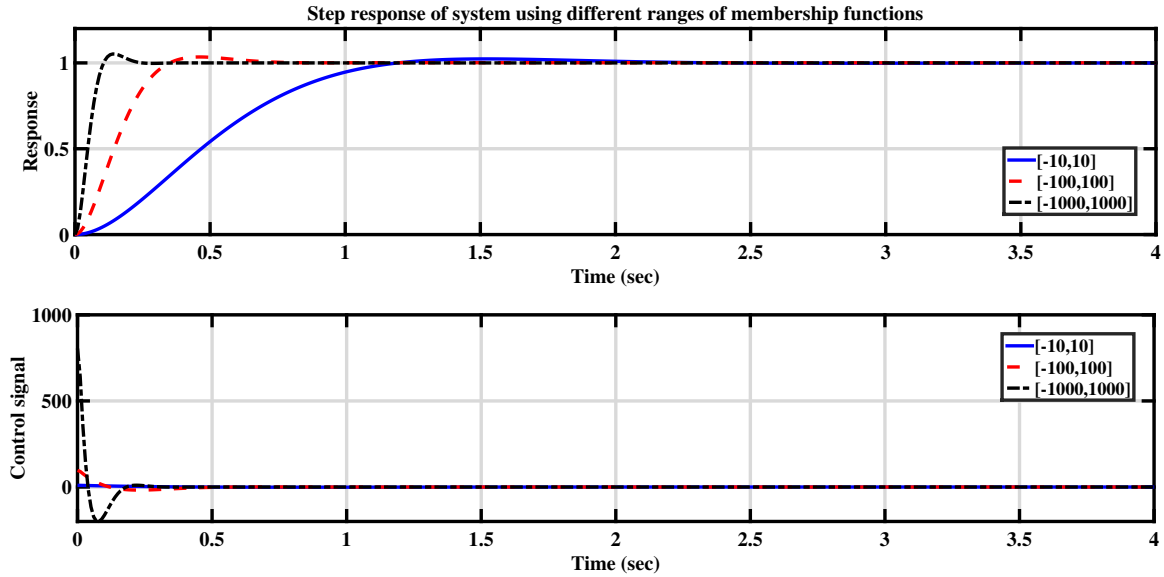


Figure 5.5: Closed-loop step responses of the system using ITAE as the objective function with different optimisation search-domains (Table 5.3).

relatively similar results. From extensive simulation studies, the following three objective functions have shown to result in satisfactory closed-loop behaviours:

$$J = \text{minimise} \left(\int_0^\infty Q|e(t)|tdt + \int_0^\infty R|u(t)|tdt \right) \quad (5.15)$$

OR:

$$J = \text{mininise} \left(\int_0^\infty Qe(t)^2dt + \int_0^\infty Ru(t)^2dt \right) \quad (5.16)$$

OR:

$$J = \text{minimise} \left(\int_0^\infty Q|e(t)|dt + \int_0^\infty R|u(t)|dt \right) \quad (5.17)$$

where Q and R in equations (5.15)-(5.17) are the weighting factors on the error and the control signals, and can be chosen such that:

$$0 \leq R < 1, \quad 0 < Q \leq 1, \quad Q + R = 1$$

Note the resemblance of equations (5.15)-(5.17) to the objective function used in the design of linear quadratic regulator (LQR) controllers. The weighting factors Q and R are chosen by the user to give the right trade-off between making the error small while keeping the control signal not too big. The step response of the system using equation (5.15) as the optimisation objective function with various bounds on the search-domain are depicted in Fig. 5.6. The results indicate that regardless of the size of search-domain, similar results are obtained when equation (5.15) is used as the optimisation objective function (see Table 5.4). Note that integral time absolute of the control signal is represented as (ITAU) in short in the table.

Table 5.4: Optimal scaling factors using the presented objective function (ITAE+ITAU) in equation (5.15)

Objective	T_1	T_2	T_3	T_4
ITAE+ITAU [0,10]	1.00	1.11	5.98	3.86
ITAE+ITAU [0,100]	29.23	30.12	100	74.48
ITAE+ITAU [0,1000]	332.80	234.26	1000	806.72

In order to better visualise the effect of the weighting factors Q and R on the optimal scaling factors $T_{1,2,3,4}$ and the performance of the closed-loop system, the optimisation process is repeated with several values of Q and R . The obtained

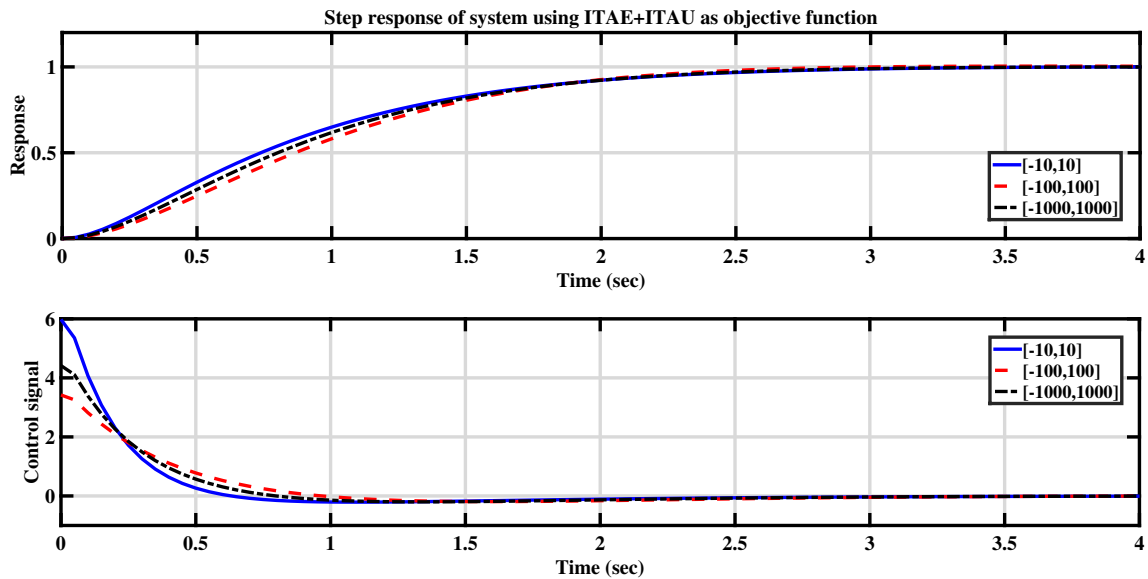


Figure 5.6: Closed-loop step responses of the system by using equation (5.15) as the objective function (Table 5.4).

scaling factors are given in Table 5.5, and the step responses of the system are also depicted in Fig. 5.7.

Table 5.5: Effect of Q and R on the optimal scaling factors

Values of Q and R	T_1	T_2	T_3	T_4
1,0	1.00	7.13	97.62	50.39
0.9,0.1	4.62	10.58	76.07	56.04
0.8,0.2	12.79	19.32	83.64	75.08
0.5,0.5	19.74	21.24	80.30	63.20
0.2,0.8	15.52	12.12	100.00	55.38
0.1,0.9	70.89	38.15	87.01	49.48

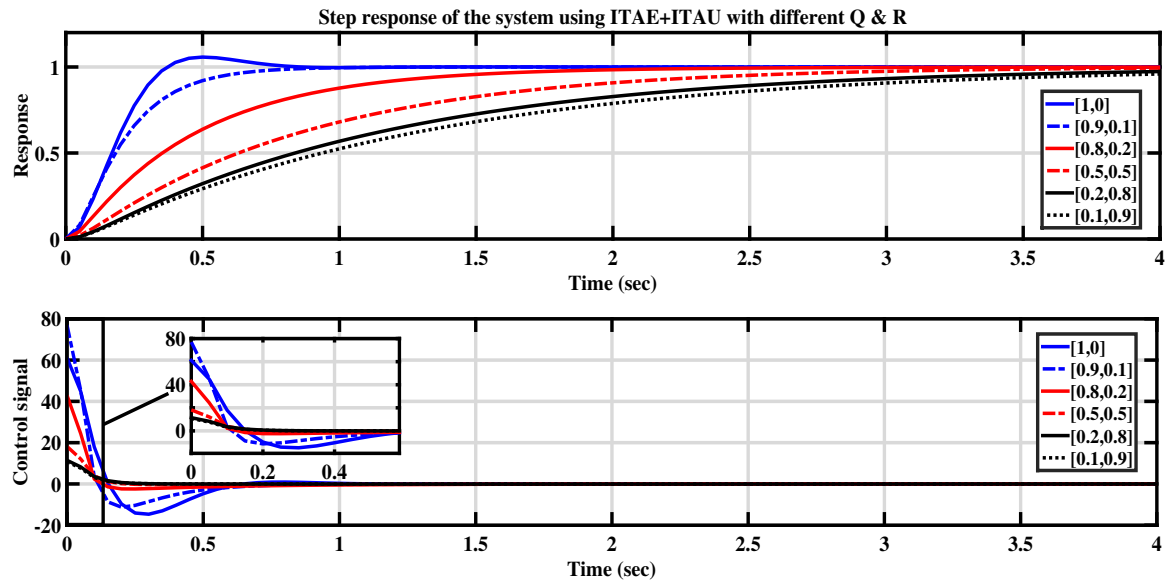


Figure 5.7: Closed-loop step responses of the system by using equation (5.15) as the objective function and different Q and R (Table 5.5).

5.5 Two-Level Tuning of the PID-Type Fuzzy Logic Controller and Application to Robust Stabilisation of Active Magnetic Bearing System

It is shown in the example in Section 5.4 that the proper tuning of the scaling factors ($T_{1,2,3,4}$) is crucial, and it has to be performed in the first level of tuning. Then, the optimisation can be further carried out on the distribution of the input/output membership functions to improve the performance of the final controller. In the sequel, the multi-level tuning procedure is carried out on the optimal design of a PID-type fuzzy logic controller for the robust stabilisation of the AMB system. In order to examine the performance of the PID-type fuzzy logic controller on partially

known systems, it is assumed that only a rough model of the system is available and hence the controller is designed on the basis of a reduced-order model of the first channel (i.e. based on equation (2.31)).

Similar to the Example in Section 5.4, a two-input Sugeno-type PID-FLC is first designed for the reduced-order model of the system. Next, different optimisation algorithms are employed to find the scaling factors ($T_{1,2,3,4}$) that minimise the objective function given in equation (5.15). It should be noted that the values of Q and R in equation (5.15) are assigned to be 0.5 throughout the optimisation process to ensure that large control signals are not produced. The simulations are executed for 0.2 seconds, and a unit-step disturbance is introduced to the system after 0.1 seconds to investigate the disturbance rejection capabilities of the designed controller. The obtained scaling factors ($T_{1,2,3,4}$) using different optimisation algorithms are listed in Table 5.6. The resulting closed-loop step responses of the system are depicted in Fig. 5.8.

Table 5.6: Optimal scaling factors using ITAE+ITAU equation (5.15) as the objective function and different optimisation algorithms

Algorithm	T_1	T_2	T_3	T_4
PSO	2.54	0.10	9.56	953.48
GA	9.83	0.10	7.876	745.9
GWO	2.02	0.10	5.82	1000
ICA	3.13	0.10	10.00	1000

It is clear from Fig. 5.8 that the step response of the system using GA is not satisfactory. On the other hand, the system shows similar performance in terms of

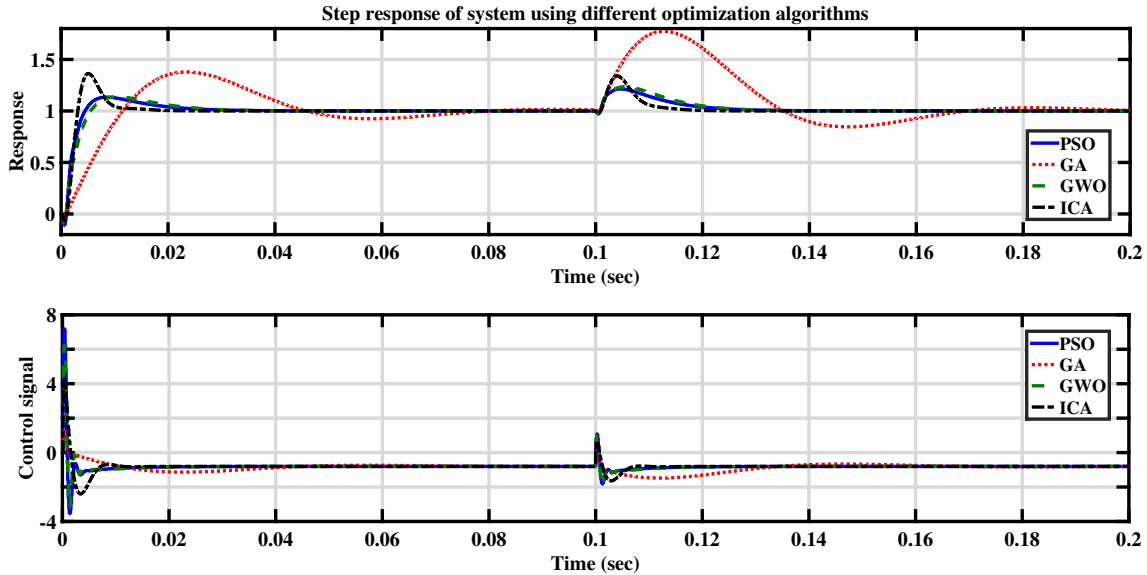


Figure 5.8: Closed-loop step responses of the system using different scaling factors $T_{1,2,3,4}$ (Table 5.6).

the percent overshoot and the settling-time by using the parameters obtained by PSO and GWO algorithms. To strive for a better performance, the distribution of the input-output membership functions is varied in the second level of tuning. It should be noted that the tuning of the membership functions distribution is much more challenging than the tuning of the scaling factors. This is due to the fact that the membership functions can be arbitrarily placed at any location in the universe of discourse. However, as it is shown in Fig. 5.3, some assumptions are made to reduce the number of design parameters and hence simplify the optimisation process. As it is desired to have a smooth transition between the rules when they are fired up, the distribution of the input/output membership functions are expected to vary arbitrarily while keeping a symmetrical partitioning of the input/output universe of discourse about the origin. Hence, eleven variables ($S_{1,2,\dots,11}$) are chosen to alter the distribution of the membership functions using the optimisation algorithms. Note

that some linear inequalities need to be satisfied during the optimisation process in order for MATLAB to successfully construct the FLC structure. For instance, $(S_2 < S_3 < S_4)$, and $(S_7 < S_8 < S_9)$ which imply that the left side of each triangle has to be less than its centroid and less than its right side. An additional inequality of $0 \leq S_{1,2,\dots,11} \leq 1$ is also required to ensure that the membership functions are within the range of $[-1, 1]$. After some simulations, the best objective function values and the optimisation run-times using different optimisation algorithms are obtained and listed in Table 5.7. It should be noted that the lowest objective value is obtained by employing the PSO algorithms, and the optimal distributions of the membership functions using PSO are depicted in Figs. 5.9a-5.9c. Furthermore, the closed-loop step responses of the system using different optimisation algorithms are depicted in Fig. 5.9d. The results from the second level of tuning are also compared with the results obtained from the first level of tuning (uniformly distributed membership functions) in Fig. 5.9d. It is clear from the results that the first level of tuning (tuning the scaling factors) has a significant impact on the closed-loop behaviour of the system. Nevertheless, the performance of the system can be slightly improved by altering the distribution of the membership functions. Please note that the MATLAB codes of the presented optimisation algorithm of the PID-type fuzzy logic controller is freely available¹.

Table 5.7: The optimisations runtime and the best objective function values

Optimisation Parameter	PSO Gbest	PSO Runtime (s)	GA Gbest	GA Runtime (s)	GWO Gbest	GWO Runtime (s)	ICA Gbest	ICA Runtime (s)
$T_{1,2,3,4}$	0.112	1164.16	0.131	1114.86	0.111	1075.86	0.1111	1131.11
$S_{1,\dots,11}$	0.1088	1100.66	0.126	1078.98	0.10911	1019.93	0.1110	1078.29

¹<http://www.mathworks.com/matlabcentral/fileexchange/52230-optimal-fuzzy-logic-controller-using-pso>

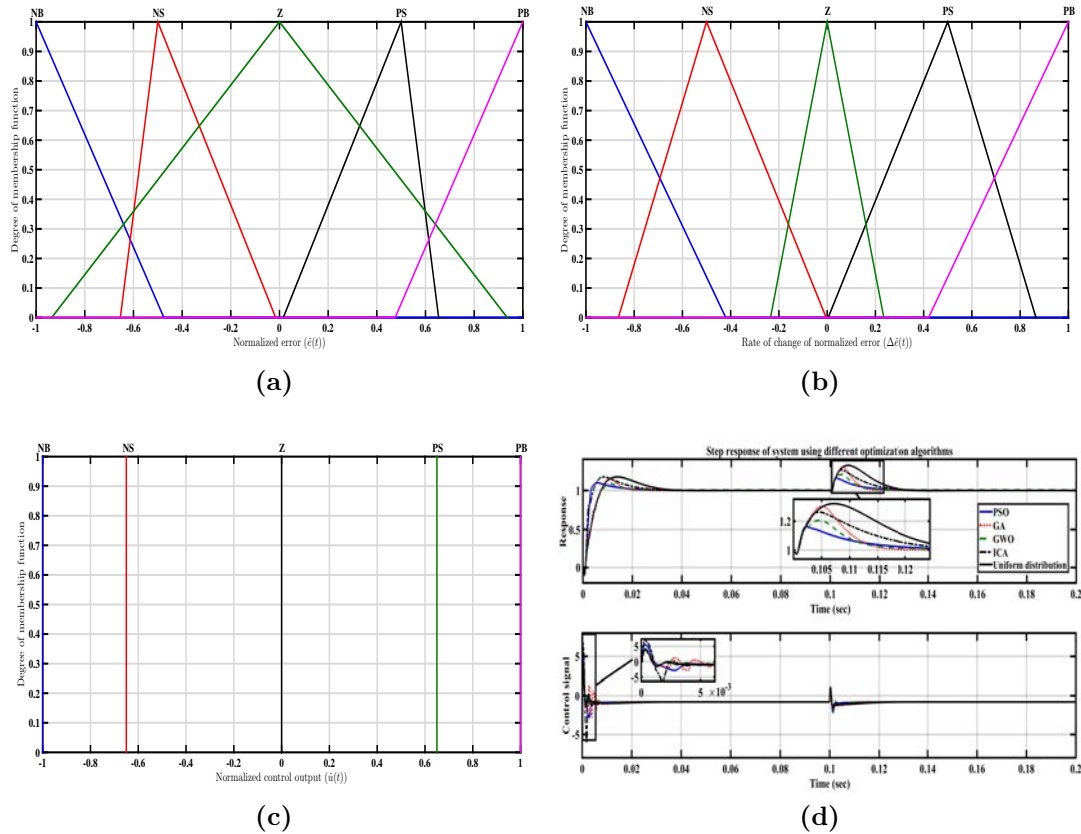


Figure 5.9: (a) Optimal distribution of error input membership function, (b) Optimal distribution of rate of change of error input membership function, (c) Optimal distribution of output membership function, (d) The closed-loop response of the system using different optimisation algorithms.

5.6 Real-Time Implementation of the Optimal PID-type Fuzzy Logic Controller on AMB System

This section is devoted to the real-time implementation of the designed PID-type fuzzy logic controller on the laboratory AMB system. After obtaining the optimal

scaling factors and the membership functions distributions, the designed PID-type fuzzy logic controllers are coded in C . The input/output of the controllers are connected to the AMB system via a digital signal processing board (DSPACE DS1104), and the measured data are collected through the DSPACE ControlDesk software package. In the first step of the experiment, the transient response of the first channel of the AMB system in real-time is compared with the simulation results of the high-order model of the first channel in Fig. 5.10. The comparison between the simulation response of the model and the real-time response of the actual system to a unit-step input shows the fidelity of the model obtained from the system identification and the behaviour of the actual closed-loop system.

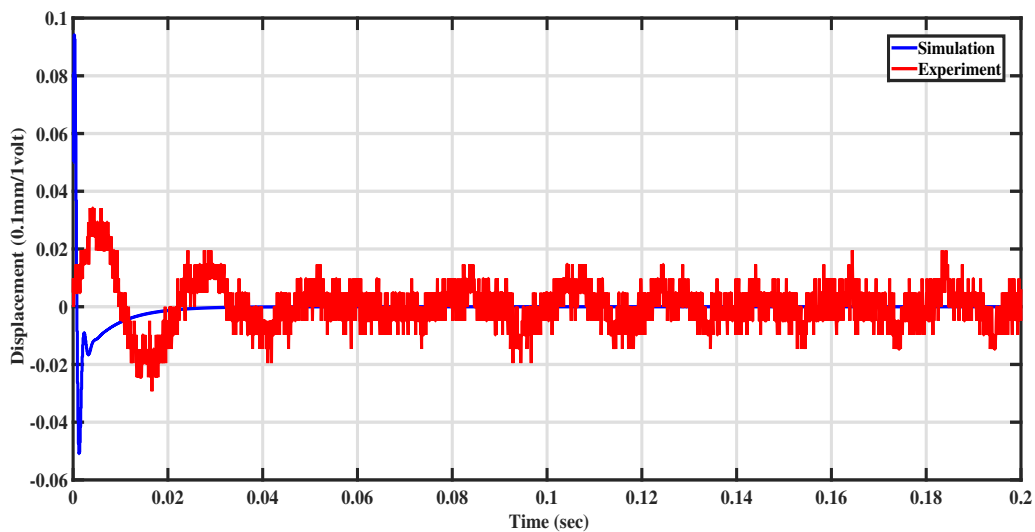


Figure 5.10: Closed-loop step response of the simulation model and the actual AMB system.

Next, the other three on-board controllers are replaced with the digital PID-type fuzzy logic controllers to have the MIMO system controlled by the digital

fuzzy logic controllers. It should be noted that the model of other three channels are slightly different from the model of the first channel and hence final fine-tuning is required before the successful implementation of the fuzzy logic controllers on the other three channels. After the system is stabilised by the designed PID-type fuzzy logic controllers, the performance of the closed-loop system is further investigated by rotating the shaft with the help of an attached air-turbine to one end of the rotor. As the speed of the rotor increases over time, the displacements of the geometrical centres of the rotor at both ends are recorded. The data are taken for 120 *seconds* to ensure that the steady-state speed of the rotor is achieved, and the obtained results are depicted in Figs. 5.11 and 5.12. For the completion of study, the results obtained from the PID-type fuzzy logic controllers are compared with those of PD-type fuzzy logic controllers and the analog on-board controllers. It is clear from the results that the performance of the PID-type fuzzy logic controllers are certainly better than those of PD-type fuzzy logic controllers and the analog on-board controllers. More interestingly, the control signals required at each channel in Fig. 5.13 reveals that lower profiles of control signals are retained by the PID-type fuzzy logic controllers than the analog on-board controllers.

In order to compare the performance of the designed fuzzy logic controller to a digital controller that is designed based on classical methods, the real-time step response of the system using the designed PID-type fuzzy logic controller and the lead-lag type compensator in equation (3.37) is depicted in Fig. 5.14. A unit-step disturbance is introduced to the system after 1.5 seconds to investigate the constant disturbance rejection capabilities of the system. It should be noted that in the conventional controller, the designed lead-lag compensator should be cascaded to two

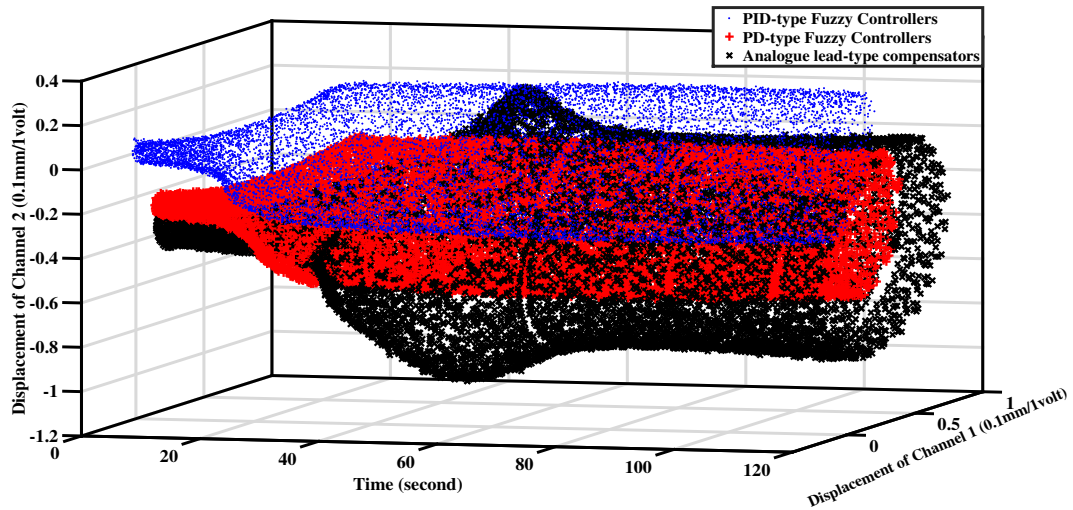


Figure 5.11: Displacement of the geometrical centres of the rotor over 120 *seconds* (left end).

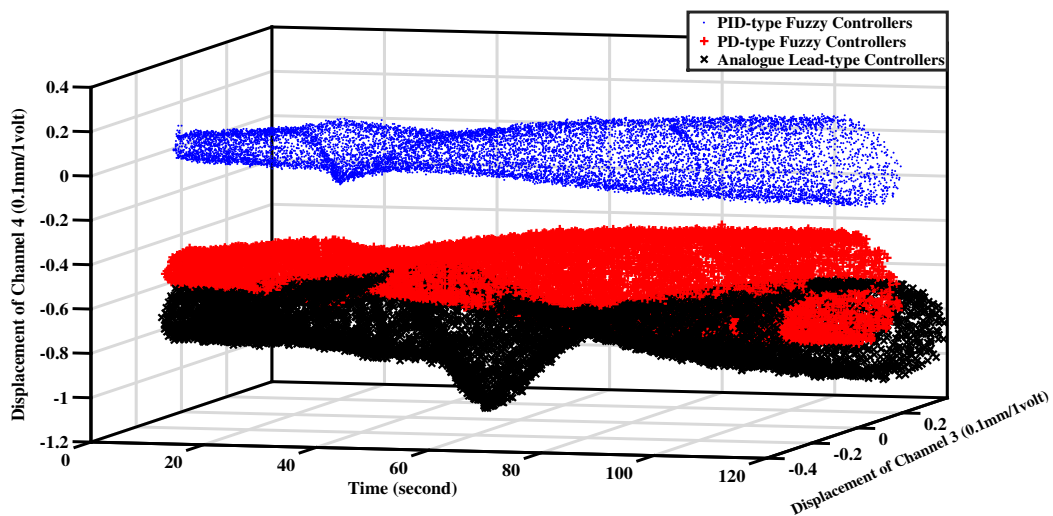


Figure 5.12: Displacement of the geometrical centres of the rotor over 120 *seconds* (right end).

notch filters in order to attenuate the effect of the structural resonance frequencies (at approximately $775Hz$ and $2059Hz$). The final conventional controller should also be cascaded with a low-pass filter in order to attenuate the high-frequency

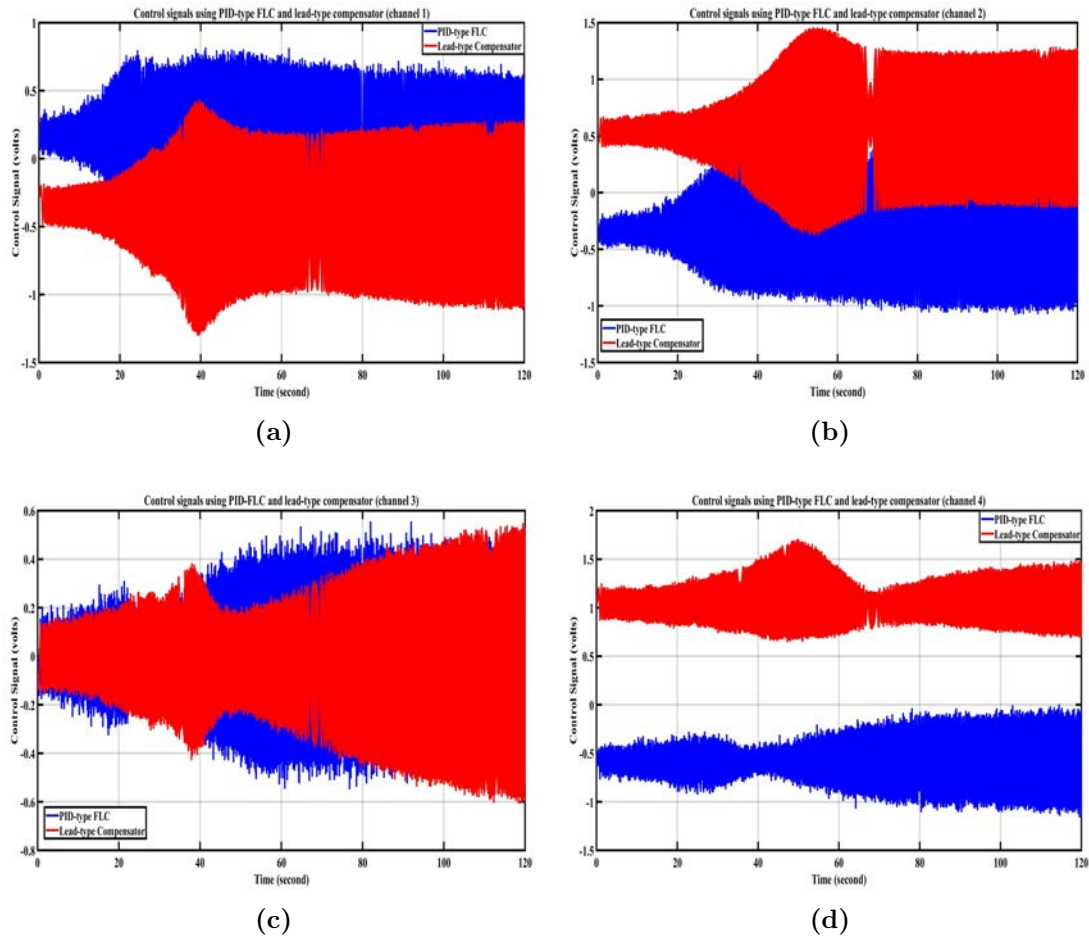


Figure 5.13: Control signals using the optimal PID-type fuzzy logic controllers and the analog on-board controllers over 120 seconds, (a) Control signal on channel Y_1 , (b) Control signal on channel Y_2 , (c) Control signal on channel Y_3 , (d) Control signal on channel Y_4 .

measurement noise. In contrast, the designed PID-FLC can be implemented on the AMBs without employing any notch filters and low-pass filters.

The disturbance rejection capabilities of the PID-type fuzzy logic controller is also compared with the analog on-board controller in Fig. 5.15. The results show

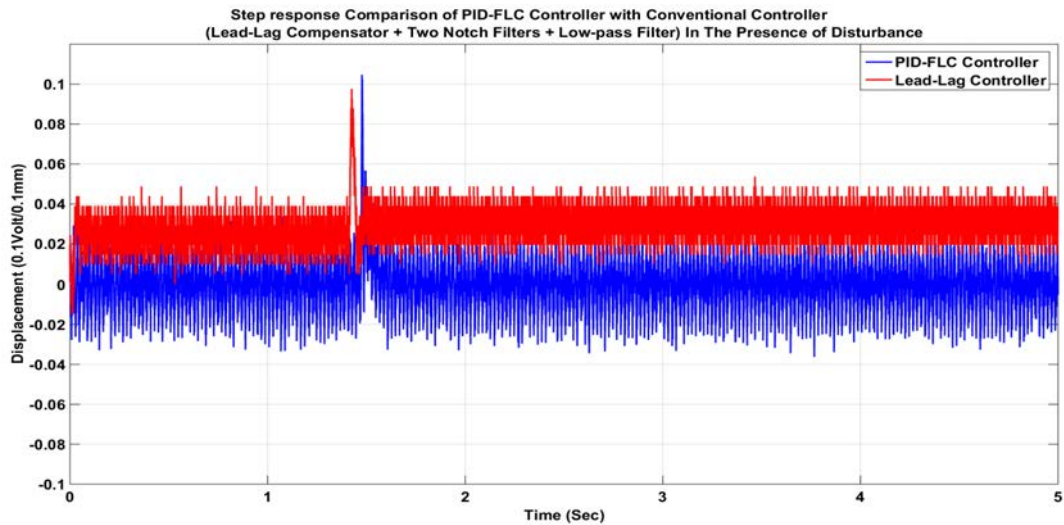


Figure 5.14: Step response of the system using the PID-FLC controller and the lead-lag compensator in the presence of disturbance.

that the performance performance of the system is dramatically improved by using the PID-FLC compared to the on-board analogue controller.

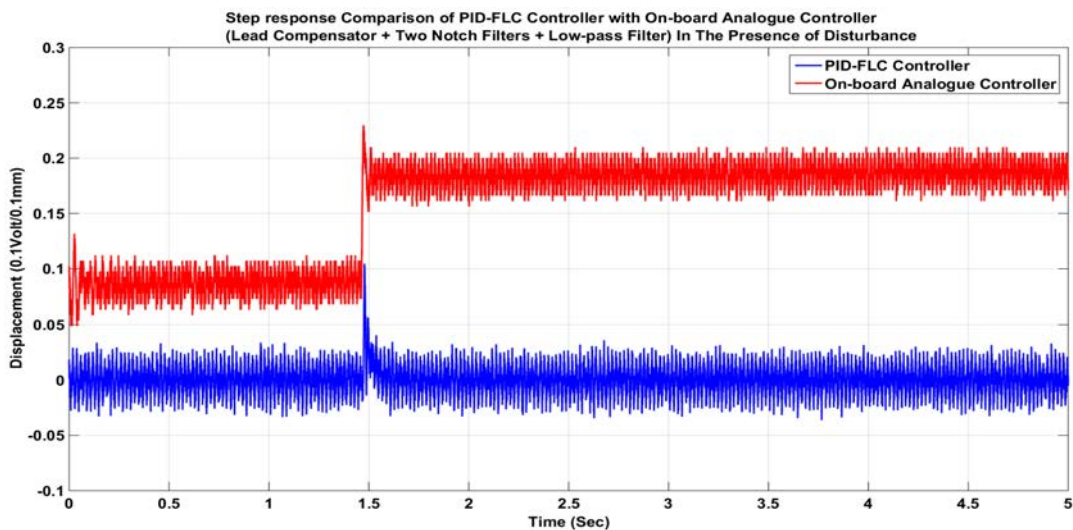


Figure 5.15: Step response of the system using the PID-FLC controller and the on-board analog controller in the presence of disturbance.

The results obtained from the PID-type fuzzy logic controllers are further compared with other controllers while the system is in rotation at low speed ($2500rpm$) as well as at high speed ($8000rpm$). For a fair comparison, controller that do not have an integrator in them compared with each other. In fact, the linear quadratic Gaussian (LQG) controllers are also designed for the system, and the performance of the PD-type fuzzy logic controllers is compared with those of LQG controllers and the analog on-board controllers. The system is tested while a constant air-pressure is supplied to the air-turbine for all controllers. The trajectories of the geometrical center of the rotor under the designed controllers are depicted in Figs. 5.16 and 5.17.

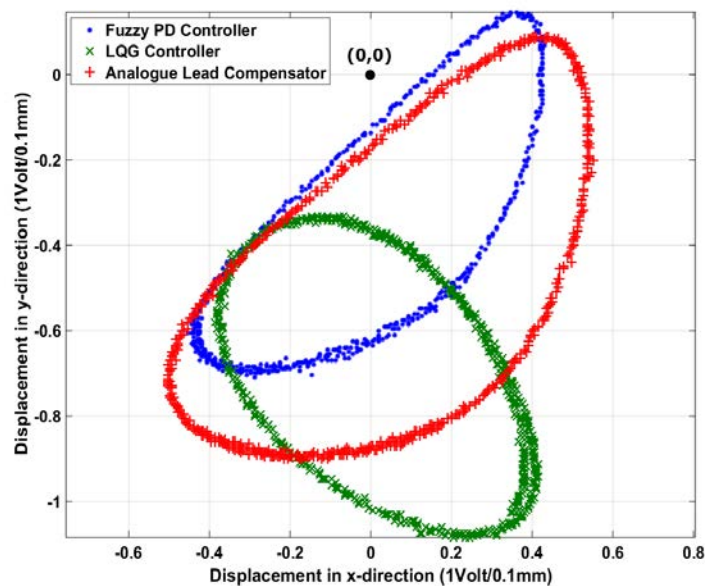


Figure 5.16: Trajectory of the rotor using PD-FLC, LQG, and the on-board analog controllers at $2500rpm$.

Furthermore, controller that include integrators, i.e., the PID-type fuzzy logic controllers are compared with the H_∞ -optimal controllers (obtained in equations

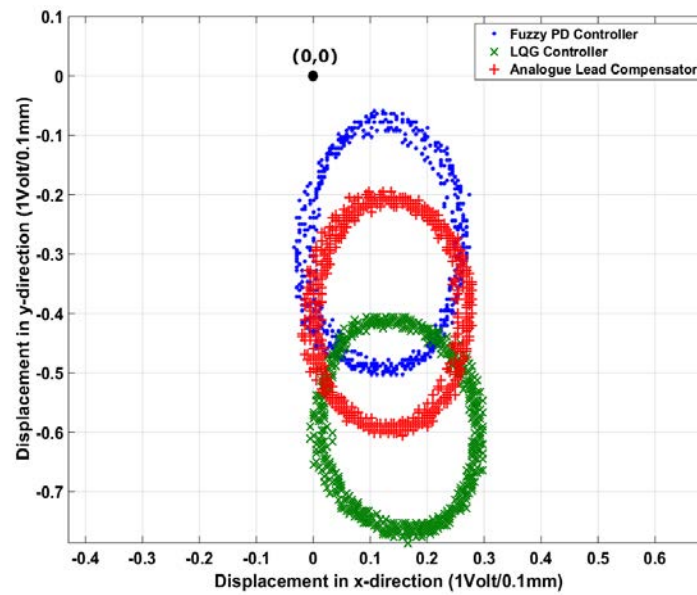


Figure 5.17: Trajectory of the rotor using PD-FLC, LQG, and the on-board analog controllers at $8000rpm$.

(3.27)-(3.30)) in Figs. 5.18 and 5.19. The minimum offset from the origin is achieved with the PID-FLCs and the H_∞ controllers compared to the other three controllers. Interestingly, at lower speeds the H_∞ controllers performed markedly better than all the other controllers with the minimum steady-state offset.

It is also found that the system under the H_∞ controllers and the PID-FLC controllers achieve higher steady-state rotational speed than the other three controllers. This may be due to the non-zero steady state errors produced by the analog on-board controllers, LQG, and PD-FLCs which cause the center of rotor to be misaligned. The transient response of the rotational speed between the PID-type FLCs and the PD-type FLCs are presented in Fig. 5.20.

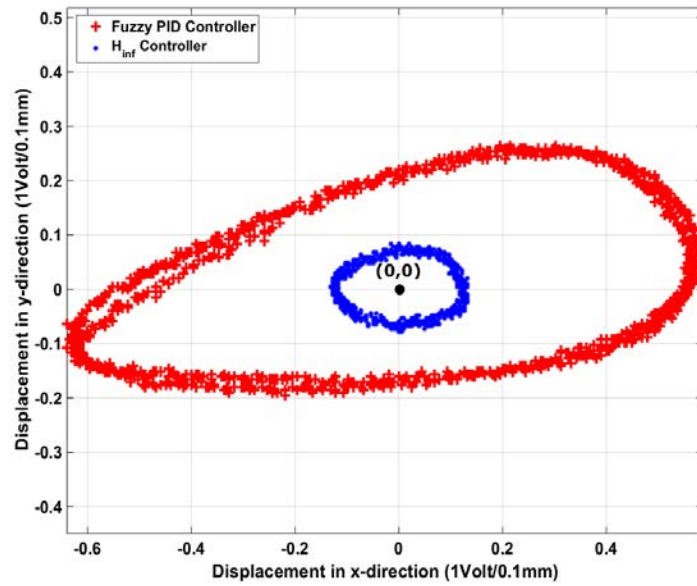


Figure 5.18: Trajectory of the rotor using PID-FLC and H_{∞} controllers at 2500rpm.

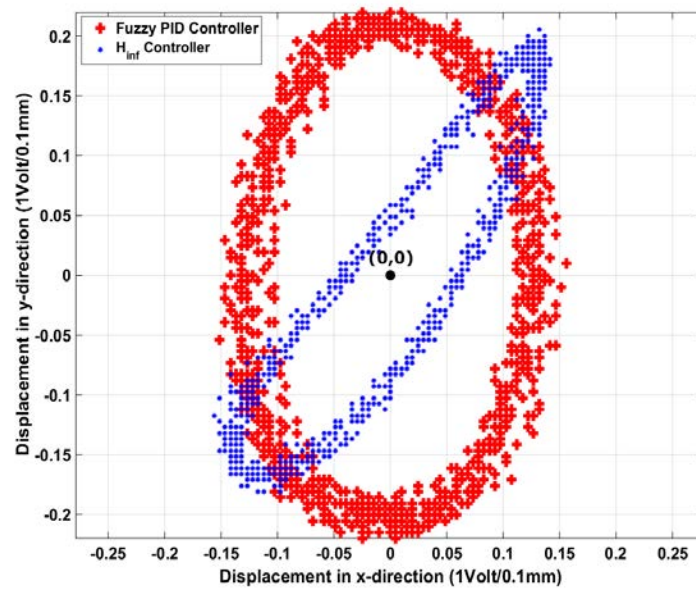


Figure 5.19: Trajectory of the rotor using PID-FLC and H_{∞} controllers at 8000rpm.

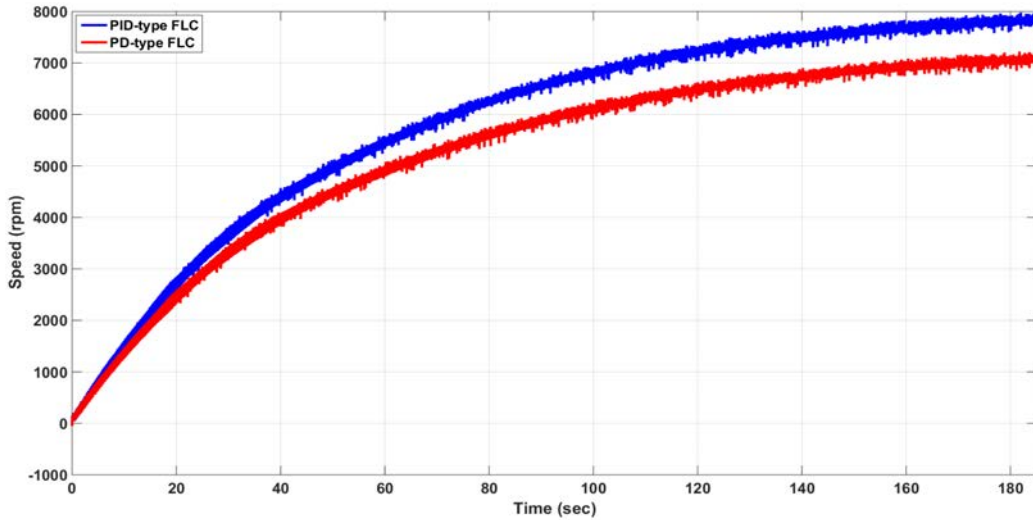


Figure 5.20: Rotational speed of the rotor under PD-FLCs and PID-FLCs.

5.7 Conclusion

A practical objective function was presented for the time-domain optimisation of the fuzzy logic controllers to secure an optimal trade-off between conflicting performance measures such as the time-domain characteristics of the system and the magnitude of control signal. Next, several meta-heuristic algorithms, namely Genetic Algorithm (GA), Particle Swarm Optimisation (PSO), Grey Wolf Optimisation (GWO), and Imperialist Competitive Algorithm (ICA) were utilised to find the optimal design parameters of the PID-type fuzzy logic controller in two levels. Interestingly, PSO and GWO showed the best performance compared to the other two algorithms. Moreover, several runs were required for GA and ICA, as these two algorithms failed to find the optimal values on the first attempt. Ultimately, an optimal PID-type fuzzy logic controller was designed and successfully implemented on the active magnetic bearing system. The experimental results were compared

with those of the PD-type fuzzy logic controllers, LQG controllers, lead-lag type compensators, and the analog on-board controllers while the system was stationary as well as while it was operating at different rotational speeds. In comparison to the linear controllers, the presented PID-type fuzzy logic controllers showed remarkably superior performances while retaining lower profiles of control signals.

Chapter 6

Disturbance Observer-Based Control of AMB System

6.1 Introduction

In the previous Chapters, the controllers were designed while the system was stationary, but the performance of the designed controllers were evaluated while the system was stationary, as well as while it was rotating. It is clear that AMBs are often subject to disturbances in the form of synchronous vibrations due to unmodelled dynamics such as the rotor mass-imbalance and centrifugal forces while the rotor is in rotation. In the early attempts to remove the effects of the harmonic disturbances while the rotor is in rotation, the AMB rotor was first levitated with

a feedback stabiliser. Then, an additional feed-forward variable narrow-band notch filter was inserted into the loop to reject the harmonic disturbances [93, 135, 136]. It is important to note that the parameters of the notch filter depend strongly on the rotational speed of the system. Furthermore, analytical verification of the closed-loop stability has to be performed *a priori*, because there are no guarantees on stability of the overall system with this approach. In the more recent developments, the underlying imbalance dynamics are first modelled as a linear parameter varying (LPV) system. Then, gain-scheduling or LPV controllers can be designed on the basis of the LPV model of the system. The advantage of this approach is that the stability and robustness of the closed-loop system can be analysed before the real-time implementation of the controllers. Although gain-scheduling and LPV controllers show appealing results in several simulation studies [137, 138], the real-time implementation of such controllers appear to have many practical issues. For instance, the experiments reported in references [31, 32] were carried out for a limited range of operation ($[4000, 5000]$ rpm), because the optimisation problem was found to be infeasible for other operating speeds. It should also be noted that these methods are practical only if the frequencies of these sinusoidal-like disturbances are directly measurable or accurately known in advance.

Disturbance observer-based controller (DOBC) scheme is an effective approach for disturbance estimation and it can be combined with any other available control methods to result in a two-degrees-of-freedom (2DOF) controller and hence improve the overall performance of the system in the presence of unknown but bounded disturbances. DOBC has been applied successfully in various practical areas, mostly in motion control systems [139, 140], robotic systems [141], flight control systems

[142], and process control systems [143]. The successful application of a hybrid DOBC-LQR on robust control of nonlinear magnetic levitation (MAGLEV) systems has been reported in references [144, 145]. The obtained results from the designed DOBC-LQR have been compared with LQR plus an Integrator (LQR+I) and LQR alone. A compound control scheme consisting of a DOBC as a disturbance rejector in combination with model predictive control (MPC) has been proposed in reference [143] for disturbance rejection of ball mill grinding circuits. A time-domain nonlinear DOBC has been developed and combined with sliding mode control (SMC) for attenuation of mismatched uncertainties and disturbances in reference [146]. A similar approach for rejection of unknown disturbances can also be found in the literature [147, 148, 149]. One of the advantages of using DOBC is that the inner-loop controller always achieves a faster dynamic response than the outer-loop feedback controller and hence is more effective than those of single-loop control structures in handling disturbances. It is well known that the DOBC structure cannot be used alone as a single-loop structure, and an outer-loop feedback controller is required for the stabilisation of an unstable system. In other words, the DOBC can be considered as an add-on to the existing feedback controller that ultimately results in a hybrid structure. Hence, a hybrid control scheme comprising a feedback H_∞ controller and an inner-loop DOBC is proposed for stabilisation of the AMB system and rejection of unknown but bounded disturbances. Stability analysis are provided and some useful guidelines are given for design of DOBC loop for non-minimum phase systems. The effectiveness of this control scheme is verified by simulation and real-time experiments on an AMB system. Both constant and sinusoidal disturbances are taken into consideration while the rotor is stationary as well as while it is rotating at different speeds. The results demonstrate that

the proposed hybrid control scheme exhibits significantly improved performance in comparison to single-loop controllers in the presence of unknown but bounded disturbances.

6.2 Disturbance Observer-Based Control (DOBC)

A basic framework of the disturbance observer-based controller (DOBC) is depicted in Fig. 6.1. Consider a SISO linear time-invariant system $G(s)$ with a nominal model of $G_n(s)$, the behaviour of the DOBC loop for the transfer functions from u_a , d , ξ to the output of the DOBC loop y can be analysed as in equation (6.1). In Fig. 6.1, u_a is the input to the DOBC, d the external disturbance, ξ the sensor noise, and y is the output from the system [150, 151].

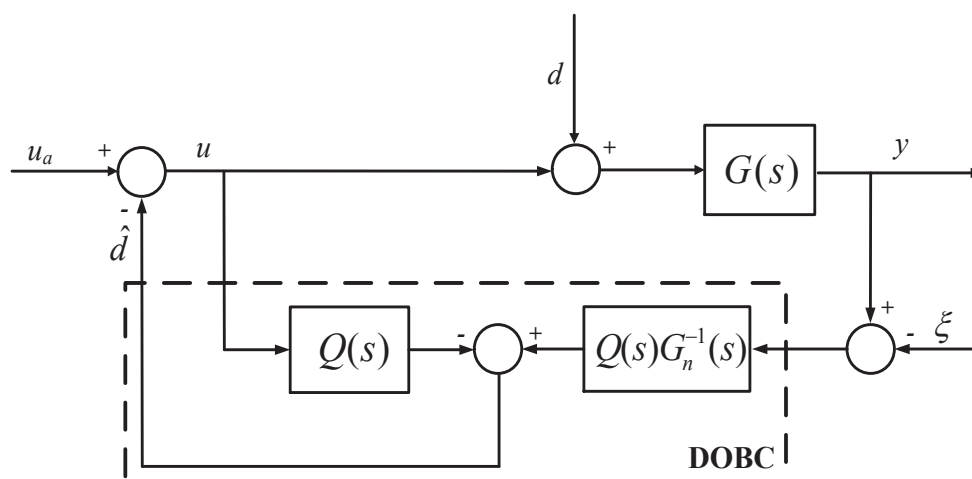


Figure 6.1: Standard framework of the disturbance observer-based controller.

$$Y(s) = G_{uay}(s)U_a(s) + G_{dy}(s)D(s) + G_{\xi y}(s)\xi(s) \quad (6.1)$$

where,

$$G_{uay}(s) := \frac{Y(s)}{U_a(s)} = \frac{G(s)G_n(s)}{Q(s)[G(s) - G_n(s)] + G_n(s)} \quad (6.2)$$

$$G_{dy}(s) := \frac{Y(s)}{D(s)} = \frac{G(s)G_n(s)(1 - Q(s))}{Q(s)[G(s) - G_n(s)] + G_n(s)} \quad (6.3)$$

$$G_{\xi y}(s) := \frac{Y(s)}{\xi(s)} = \frac{G(s)Q(s)}{Q(s)[G(s) - G_n(s)] + G_n(s)} \quad (6.4)$$

If the nominal model is close enough to the actual system, i.e. $G_n(s) \approx G(s)$, it can be deduced from equations (6.2)-(6.4) that:

$$G_{uay}(s) \approx G(s) \quad (6.5)$$

$$G_{dy}(s) \approx G(s)[1 - Q(s)] \quad (6.6)$$

$$G_{\xi y}(s) \approx Q(s) \quad (6.7)$$

It is clear from equations (6.5)-(6.7) that if $G_n(s) \approx G(s)$, the outer-loop controller does not notice the presence of the inner-loop DOBC. It also implies that the two loops can be designed independently, as long as the nominal system is close to the actual system. On the other hand, equation (6.6) suggests that when $|Q(s)| \approx 1$, the output of the system due to the disturbances becomes zero ($G_{dy} \approx 0$). It indicates that the DOBC rejects the disturbances and compensates for the model uncertainties, when $|Q(s)| \approx 1$. Furthermore, equation (6.7) implies that at frequencies where $|Q(s)| \approx 0$, the DOBC is essentially cut, and the sensor noise has no effect on the system. This indicates that the disturbance rejection properties of the DOBC depends solely on the bandwidth of so-called *Q-filter*. Since disturbances normally have low-frequency properties, whereas sensor noise is dominant at high frequencies, it implies that $Q(s)$ can be designed as a low-pass filter with a DC gain of one. The beauty of the described structure is that the DOBC can estimate not only the external disturbances, but also the internal model uncertainties. In fact, it can be seen from equation (6.2) that even if the actual system $G(s) \neq G_n(s)$, the DOBC loop nominalises the dynamics of the plant to be controlled, i.e. $G_{uay} \approx G_n(s)$, when $|Q(s)| \approx 1$.

6.3 Stability Analysis of the Closed-loop System Using Hybrid H_∞ – DOBC Scheme

It can be seen from Fig. 6.1 that the operators $Q(s)$ and $Q(s)G_n^{-1}(s)$ need to be stable transfer functions for internal stability of the DOBC-loop. However, it is

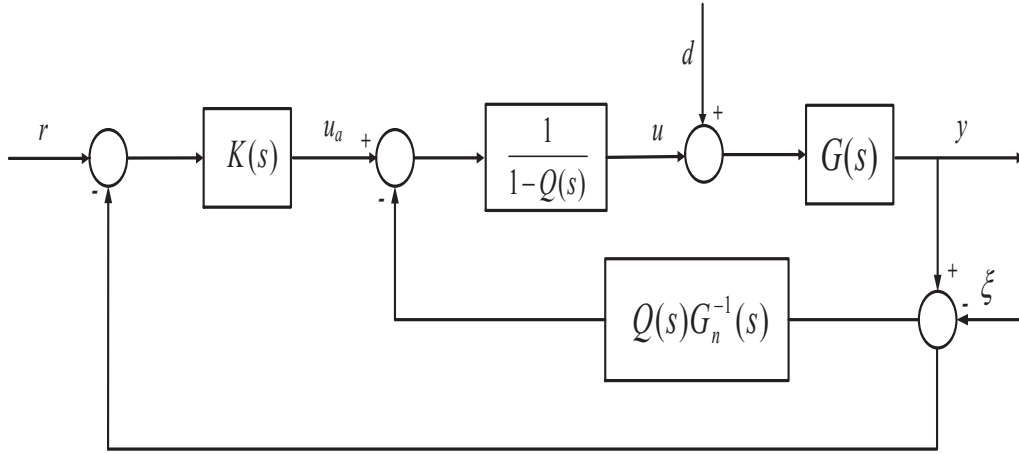
important to note that the DOBC loop is part of the overall feedback. Therefore, the stability analysis need to be performed for the overall system including both the DOBC loop and the feedback stabiliser. This section provides the stability analysis of the hybrid ($H_\infty - DOBC$) controller and the effect of the inner-loop DOBC on the overall closed-loop system. Without loss of generality, assuming that the uncertainties are modelled as input multiplicative uncertainties, the uncertain system can be written as in equation (6.8):

$$G(s) = G_n(1 + \Delta(s)) \quad (6.8)$$

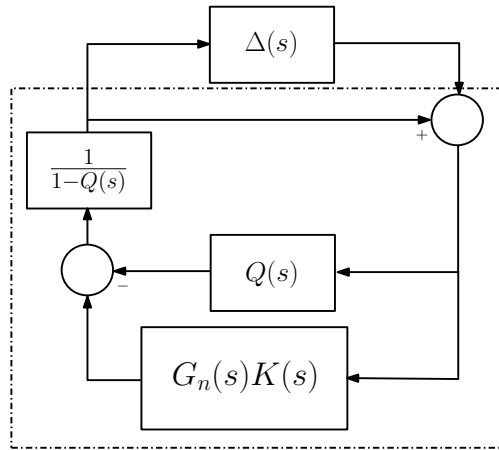
where the stable proper transfer function $\Delta(s)$ represents the uncertainties in the system. A proper rearrangement of DOBC (to avoid undesired algebraic loops) and combining it with the outer-loop controller $K(s)$ gives the final combined $H_\infty - DOBC$ scheme as depicted in Fig. 6.2a. By replacing $G(s)$ by $G_n(s)(1 + \Delta(s))$ and proper loop transformations, the transfer function from the output of the uncertainty to its input can be obtained as Fig. 6.2b.

The overall closed-loop transfer function is found to be in the form of:

$$T_{cl}(s) = \frac{G_n(s)K(s) + Q(s)}{1 + G_n(s)K(s)} \quad (6.9)$$



(a)



$$T_{cl}(s) = \frac{G_n(s)K(s)+Q(s)}{1+G_n(s)K(s)}$$

(b)

Figure 6.2: (a) Equivalent DOBC structure with the outer-loop controller $K(s)$, (b) robust stability analysis.

According to the small-gain theorem, the overall closed-loop system in equation (6.9) is robustly stable against uncertainties if equation (6.10) is satisfied:

$$|W_T(s)T_{cl}(s)| < 1 \quad \forall s = j\omega$$

where,

$$(6.10)$$

$$|\Delta(s)| \leq |W_T(s)|, \quad \forall s = j\omega \text{ (for robust stability)}$$

The weight $W_T(s)$ is designed to be the upper limit on the system uncertainties $\Delta(s)$. Equations (6.9) and (6.10) suggest that the robust stability of the overall closed-loop system depend not only on the proper selection of $Q(s)$, but also on the outer-loop feedback controller $K(s)$. Although the feedback stabiliser is designed first, the inner-loop DOBC has to be designed in such a way that the robust stability of the overall closed-loop system to parameter variations is satisfied. In order to check the robust stability condition, equation (6.10) can be rewritten as:

$$\left| W_T(s)T_{cl}(s) \right| < 1 := \left| W_T(s) \frac{G_n(s)K(s)+Q(s)}{1+G_n(s)K(s)} \right| < 1, \\ \forall s = j\omega \quad (6.11)$$

Equation (6.11) can be rearranged into:

$$\left| Q(s) \right| < \left| W_T^{-1}(s)(1 + G_n(s)K(s)) \right| - \left| G_n(s)K(s) \right|, \\ \forall s = j\omega \quad (6.12)$$

The operator $Q(s)$ should be designed in such a way that the DOBC loop achieves maximal disturbance suppression. Moreover, the inequality in equation (6.12) can be used as a sufficient condition for the robust stability check of the overall closed-loop system with the designed $Q(s)$. Several methods on the design of the DOBC Q -filter can be found in the literature. For instance, [152] transforms the DOBC design problem into another standard H_∞ control framework. In this method, the structure of the Q -filter is not preassigned, and the H_∞ optimisation

procedure results in a $Q(s)$ that ensures the inequality in equation (6.12) is satisfied. In this thesis, the structure in equation (6.13) is adopted for the design of the Q -filter, and the parameters of the filter are obtained such that the overall closed-loop transfer function in equation (6.12) is minimised in the H_∞ -norm sense.

$$Q(s) = \frac{1 + \sum_{k=1}^{N-r} a_k (\tau s)^k}{1 + \sum_{k=1}^N a_k (\tau s)^k} \quad (6.13)$$

In equation (6.13), N is the order of $Q(s)$, r is the relative degree of $Q(s)$, $\omega_c = 1/\tau$ is the cut-off frequency of $Q(s)$, and a_k can be selected to be a binomial model or Butterworth low-pass filter.

As it was mentioned before, the overall closed-loop sensitivity and complementary sensitivity functions can be found as in equations (6.14) and (6.15).

$$S_{cl}(s) = \frac{1 - Q(s)}{1 + G_n(s)K(s)} \quad (6.14)$$

$$T_{cl}(s) = \frac{G_n(s)K(s) + Q(s)}{1 + G_n(s)K(s)} \quad (6.15)$$

6.4 DOBC Design for Non-minimum Phase Systems

This section describes the design of DOBC loop for non-minimum phase systems. Since the inverse dynamics of the system ($G_n^{-1}(s)$) is used in the DOBC loop (see Fig. 6.2), it limits the application of the classical DOBC approach to systems with no right-half plane zeros (minimum-phase systems). It is clear that the inverse of non-minimum phase systems is unstable and cannot be used in the DOBC loop. It is further proved in references [152, 153] that the minimum phaseness of the system is a necessary condition for internal stability of the DOBC approach. In order to overcome the problem, an alternative DOBC filter is proposed in reference [139] to cancel the *RHP*-pole of the inverse dynamics by the *RHP*-zero in the proposed $Q(s)$ filter. However, exact pole-zero cancellations are not always possible in practice, and it could lead to instability of the system. In this Chapter, since the *RHP*-zero of the system under study is located relatively far from the dominant low-frequency poles, another alternative is presented to design the DOBC for the non-minimum phase AMB system. The non-minimum phase unstable system $G_n(s)$ can be factorised into a minimum-phase and an all-pass factor. The term $G_{n-mp}(s)$ includes all the poles of $G_n(s)$ (stable and unstable poles), while $G_{n-ap}(s)$ contains all the zeros of $G_n(s)$ in the open right half plane, i.e.:

$$G_n(s) = G_{n-mp}(s)G_{n-ap}(s) \quad (6.16)$$

The minimum-phase factor of the model $G_{n-mp}(s)$ can be used for the design of the DOBC loop. The designed DOBC loop can then be combined with the main feedback stabilising controller $K(s)$ to construct the overall hybrid controller. The final $H_\infty - DOBC$ controller is depicted in Fig. 6.3.

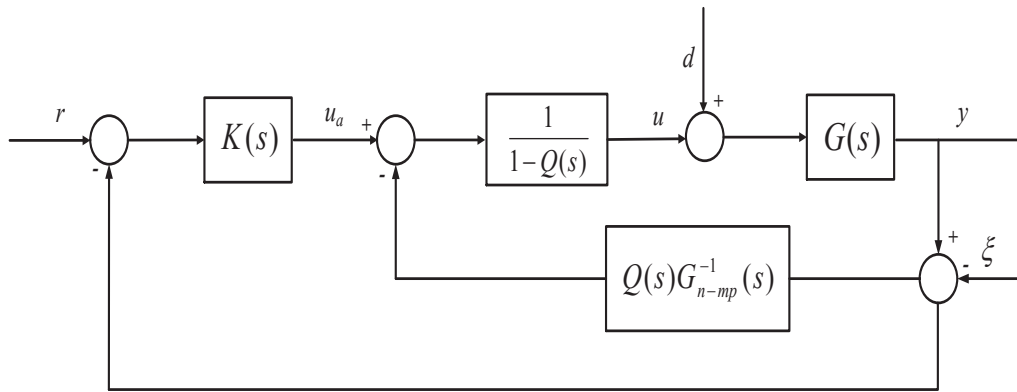


Figure 6.3: Overall $H_\infty - DOBC$ control structure.

6.4.1 Design Procedure of $H_\infty - DOBC$

The design procedure of $H_\infty - DOBC$ scheme can be broken down into the following steps:

- (i) select the required weighting functions ($W_P(s)$, $W_T(s)$, and $W_U(s)$) for mixed-sensitivity H_∞ controller design. The weightings $W_P(s)$, $W_T(s)$, and $W_U(s)$ are chosen to shape the closed-loop sensitivity functions in the frequency-domain.

- (ii) synthesise the H_∞ controller and ensure that the open-loop unstable system is robustly stable using the designed controller.
- (iii) design the DOBC inner-loop for the desired bandwidth of the disturbance rejection loop. The minimum-phasesness of the model is a necessary condition for the internal stability of the DOBC loop. In the case of non-minimum phase system, some alternatives such as approximate inversion of the system provided in the previous section can be used to ensure the stability of the inverse of the model.
- (iv) check if equation (6.12) is satisfied in the H_∞ -norm sense. Otherwise, re-design the outer-loop feedback controller and/or the inner DOBC loop by relaxing/limiting the design requirements.

6.5 Simulation and Experimental Validations

This section provides the simulation and experimental verification of the presented hybrid $H_\infty - DOBC$ scheme on the robust stabilisation of the active magnetic bearing system. The ultimate goal is to stabilise the rotor of the AMB system at its geometrical center both in horizontal and vertical directions. As the model of the system is obtained while the system is stationary, the effects caused by the rotor mass-imbalance and other disturbances are not taken into consideration at the system identification stage. Thus, the DOBC is designed to ensure the rejection

of unknown but bounded disturbances while the system is in rotation. The analysis for the first channel is presented in the sequel. However, a similar procedure is used to design the controllers for the other three channels. A multiplicative uncertainty is designed based on several measurements that were taken during the system identification process. An uncertainty of less than 20% is expected for the low frequencies (below 500 *rad/s*) where noise to signal ratio is negligible and relatively accurate measurements can be recorded. The uncertainties reach upto more than 400% at high frequencies around and beyond the rotor flexible modes (above 4000 *rad/s*). Subsequently, a first order $W_T(s)$ is designed to be an upper bound on the model uncertainties and is presented in equation (6.17). The weighting $W_T(s)$ is designed to ensure the attenuation of the closed-loop complementary sensitivity function at high frequencies where the measurement noise is significant. Similarly, a first order performance weighting function $W_P(s)$ is designed based on the expected closed-loop bandwidth of the system, and it is shown in equation (6.18).

$$W_T(s) = \frac{1.6(s + 500)}{(s + 4000)} \quad (6.17)$$

$$W_P(s) = \frac{0.3333(s + 500)}{(s + 0.00333)} \quad (6.18)$$

The sub-optimal continuous-time H_∞ controller for channel 1 is given in equation (6.19). It can be clearly seen from equation (6.19) that the proper selection of the weighting functions ($W_P(s)$ and $W_T(s)$) results in a controller that

automatically includes two notch filters.

$$K_1(s) = \frac{7986.2(s + 3 \times 10^5)^2}{(s + 4.822 \times 10^5)(s + 1.717 \times 10^4)} \frac{(s + 374.4)(s + 77.94)}{(s + 0.003333)(s^2 + 6429s + 2.328 \times 10^7)} \frac{(s^2 + 0.96s + 2.344 \times 10^7)(s^2 + 0.37s + 1.668 \times 10^8)}{(s^2 + 5087s + 2.191 \times 10^7)(s^2 + 5297s + 1.637 \times 10^8)} \quad (6.19)$$

In order to design the DOBC loop, the order of the original model of the unstable system is first reduced by removing the terms corresponding to the flexible modes of the rotor while keeping their DC gain contribution. The reduced order model is then factorised into a minimum-phase ($G_{n-mp}(s)$) and an all-pass ($G_{n-ap}(s)$) factor. The reduced-order model of the first channel after removing the terms corresponding to the flexible modes is found to be as in equation (6.20).

$$G_n(s) = \frac{-0.0040509(s + 1.72 \times 10^4)(s - 2075)}{(s + 374.4)(s - 310.2)} \quad (6.20)$$

The non-minimum phase model can be factorised into a minimum-phase part and an all-pass factor as in equation (6.21).

$$G_n(s) = G_{n-mp}(s) G_{n-ap}(s) = \frac{-0.0040509(s + 1.72 \times 10^4)(s + 2075)}{(s + 374.4)(s - 310.2)} \times \frac{(s - 2075)}{(s + 2075)} \quad (6.21)$$

The minimum-phase factor $G_{n-mp}(s)$ is used for the design of the inner-loop DOBC and $Q(s)$ is selected to be in the form of equation (6.22).

$$Q(s) = \frac{3\tau s + 1}{\tau^3 s^3 + 3\tau^2 s^2 + 3\tau s + 1}, \quad \tau = 1/1500 \quad (6.22)$$

After combining the inner-loop DOBC with the outer-loop H_∞ controller, the obtained sensitivity and complementary sensitivity functions of the closed-loop system using the single-loop H_∞ controller ($S(s)$ and $T(s)$), the inner-loop DOBC ($1 - Q(s)$ and $Q(s)$), and the combined $H_\infty - DOBC$ structure ($S_{cl}(s)$ and $T_{cl}(s)$) are illustrated in Fig. 6.4. It should be mentioned that an optimal value of $\gamma_1 = 0.86$ is obtained for the H_∞ optimised feedback controller. From the overall closed-loop complementary sensitivity functions $T_{cl}(s)$, it is observed that the introduction of the DOBC loop preserves the robust stability bounds compared to the single-loop H_∞ controller. The maximum peak of 5.2dB at 1497 rad/s implies that the uncertainties should not be larger than 54.95% of the nominal values at this frequency.

The hybrid controller scheme is implemented in real-time on the first channel (Y_1) using an ADC/DAC converter and the DS1104 DSP board. To investigate the constant disturbance rejection properties of the system while the rotor is stationary, two constant disturbances are introduced to the system at two separate instances of time. The first disturbance is introduced to the system after approximately 0.4 seconds, followed by the second disturbance after 1.4 seconds. The system response to the constant disturbances using the two structures are depicted in Fig. 6.5a.

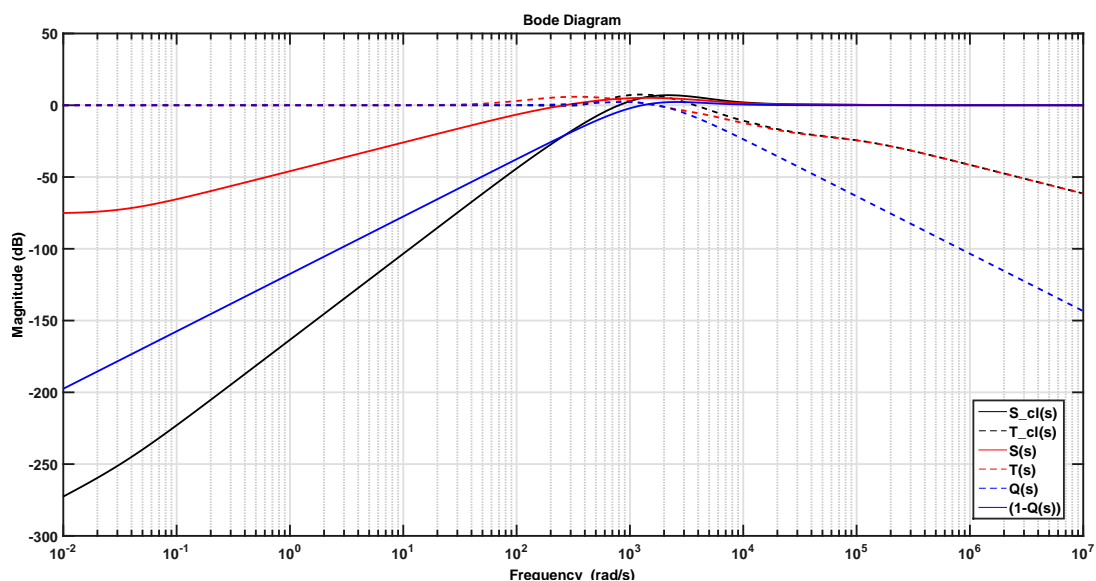
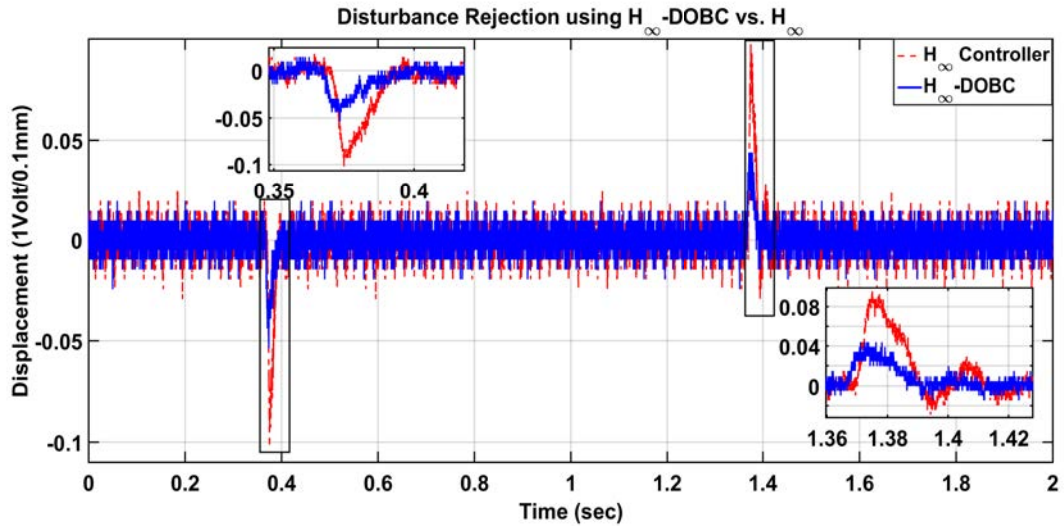


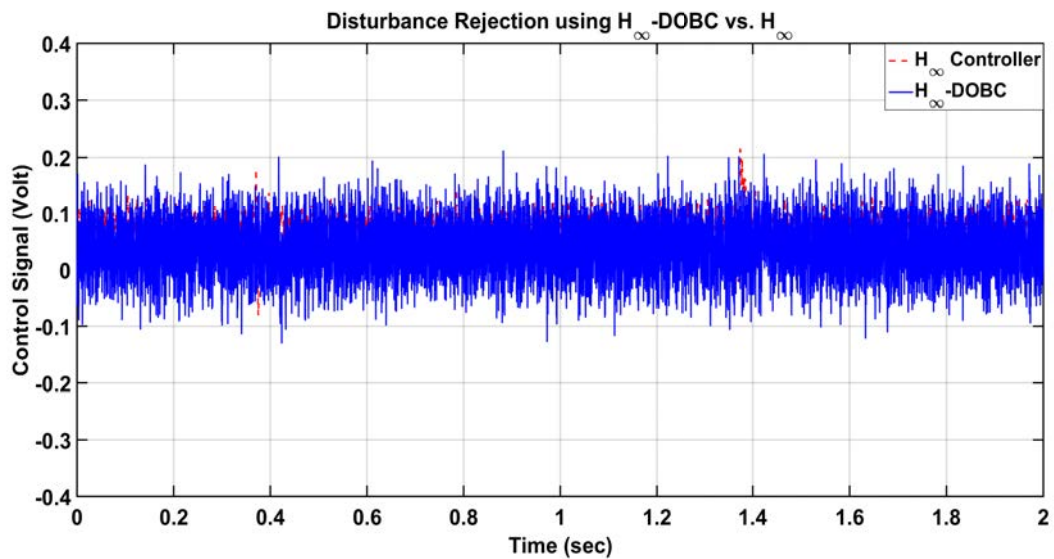
Figure 6.4: Sensitivity and complementary sensitivity functions of the DOBC ($1 - Q(s)$ and $Q(s)$), single-loop H_∞ controller ($S(s)$, $T(s)$), and the hybrid $H_\infty - DOBC$ ($S_{cl}(s)$, $T_{cl}(s)$).

The control signals are also illustrated in Fig. 6.5b. It is clear from the results that the proposed hybrid structure is much more efficient in rejecting constant disturbances compared to the single-loop H_∞ controller.

The AMB system under study operates within the range of $[0, 10000]rpm$ which corresponds to $[0, (10000 \times \frac{2\pi}{60})]rad/s$, and it is known that the rotor mass-imbalance manifests as a harmonic force with frequency synchronous to the rotor speed. In order to investigate the harmonic disturbance rejection capabilities of the two control structures, several sinusoidal disturbances in the form of $d(t) = 0.2 \sin(\omega t)$ with $\omega = 10\pi$, 40π , and $200\pi rad/s$ are applied to the first channel while the rotor is stationary. The obtained results using the $H_\infty - DOBC$ and the single-loop H_∞ controller are illustrated in Figs. 6.6-6.8. It can be deduced from the results that as the frequency of the disturbance increases, the single-loop H_∞ controller



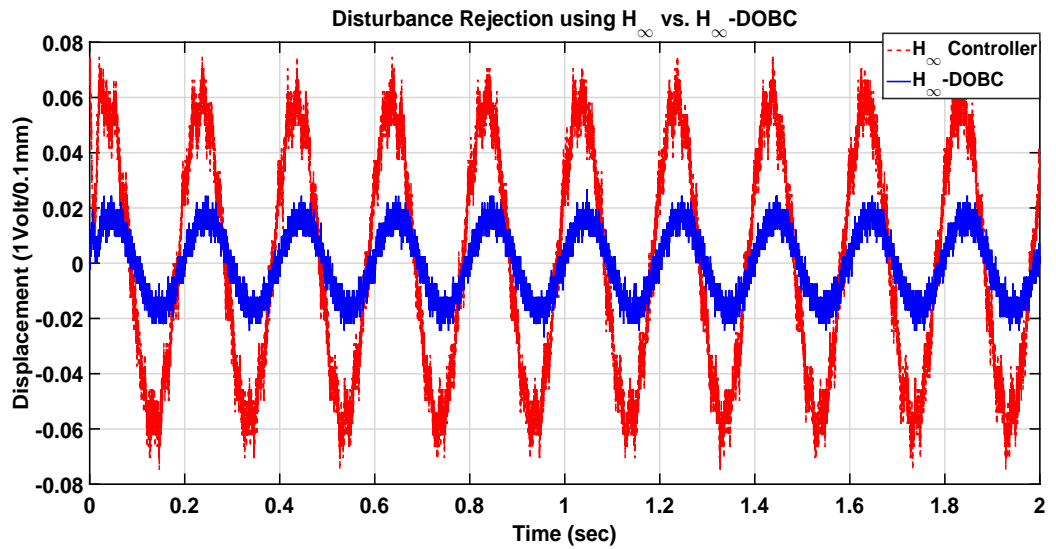
(a)



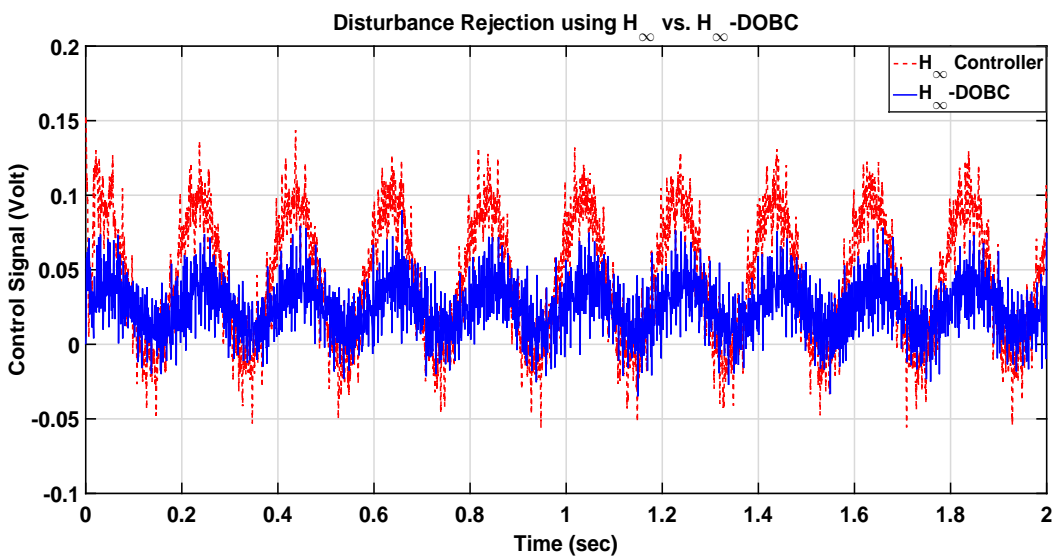
(b)

Figure 6.5: Displacement and control signal in the presence of step disturbance, (a) Displacement, (b) Control signal.

fails to remove the introduced disturbances. On the other hand, the combined H_{∞} – DOBC scheme significantly reduces the effect of the introduced sinusoidal disturbances.



(a)



(b)

Figure 6.6: Displacement and control signal in the presence of sinusoidal disturbance, $d(t) = 0.2 \sin(10\pi t)$, (a) Displacement, (b) Control signal.

In order to investigate the disturbance rejection capabilities of the system over the entire operating range $[0, 10000] \text{ rpm} \approx [0, 1047] \text{ rad/s}$, the experiment is repeated (while the rotor is stationary) and this time the results are compared in

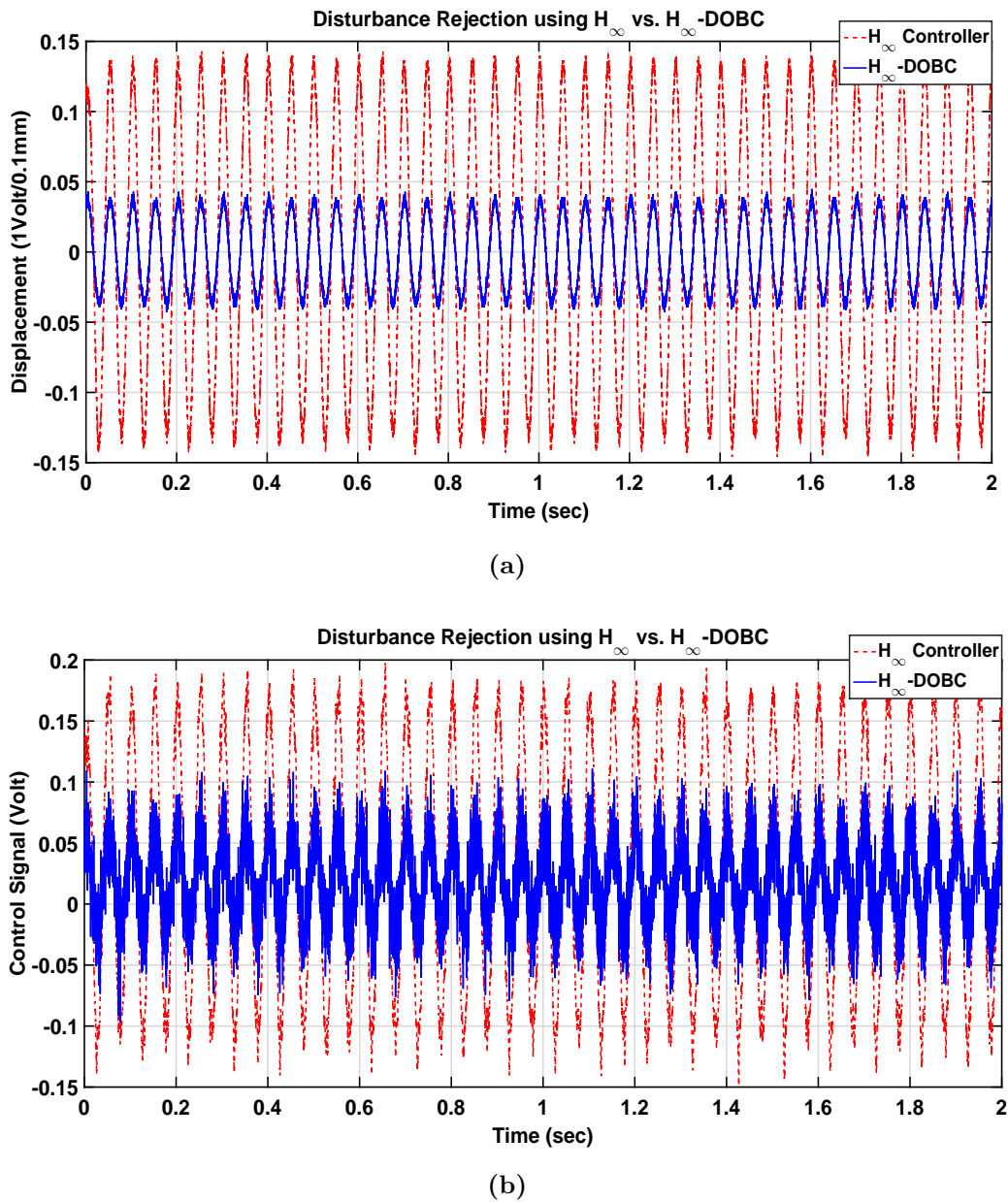
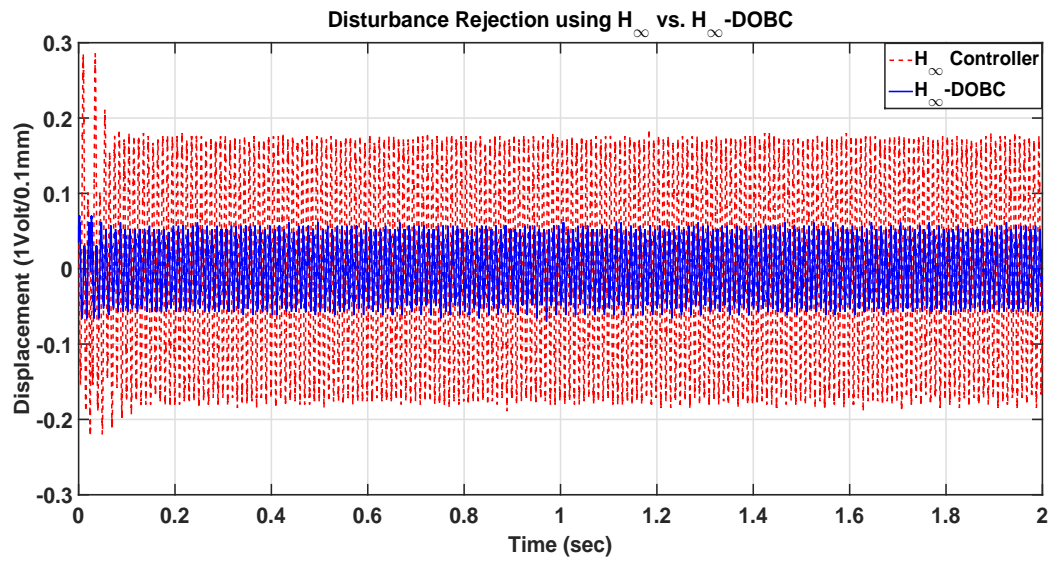
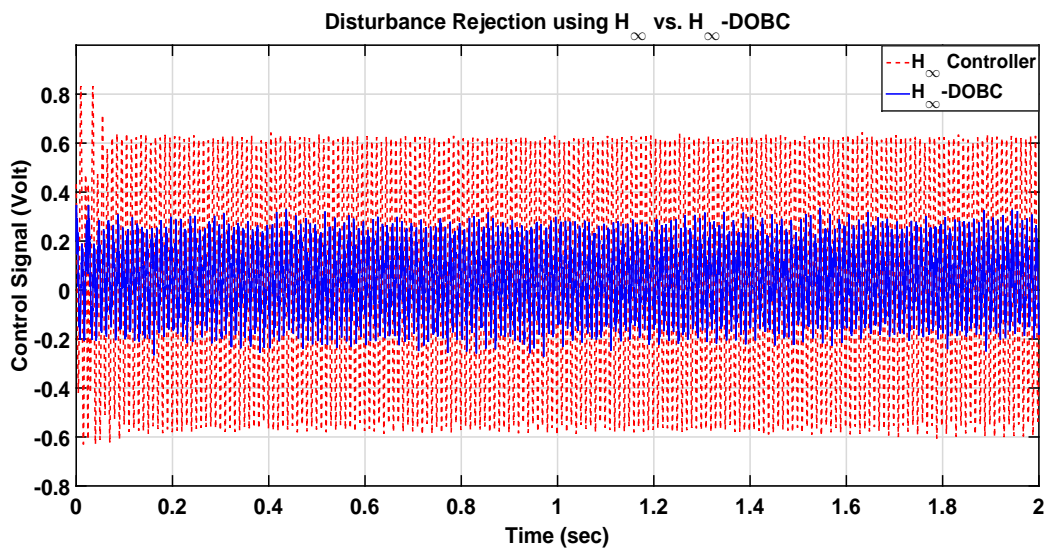


Figure 6.7: Displacement and control signal in the presence of sinusoidal disturbance, $d(t) = 0.2 \sin(40\pi t)$, (a) Displacement, (b) Control signal.

the frequency-domain. A chirp signal with an initial frequency of 0.001 Hz and the final frequency of 3000 Hz is introduced as a time-varying disturbance to the system, and the output response of the system is collected using the DSP board. Next,



(a)



(b)

Figure 6.8: Displacement and control signal in the presence of sinusoidal disturbance, $d(t) = 0.2 \sin(200\pi t)$, (a) Displacement, (b) Control signal.

the time-domain signals are transported into MATLAB for DFT analysis, and the experimental sensitivity functions for the single-loop H_∞ controller and the hybrid $H_\infty - DOBC$ structure are depicted in Fig. 6.9. It is clear from the results that for

the frequency range of interest ($[0, 1047] \text{ rad/s}$), the hybrid $H_\infty - DOBC$ structure exhibits a much steeper slope in the low-frequency range than the single-loop H_∞ controller. This shows that the hybrid $H_\infty - DOBC$ scheme is much more effective in rejecting low-frequency disturbances compared to the single-loop H_∞ controller.

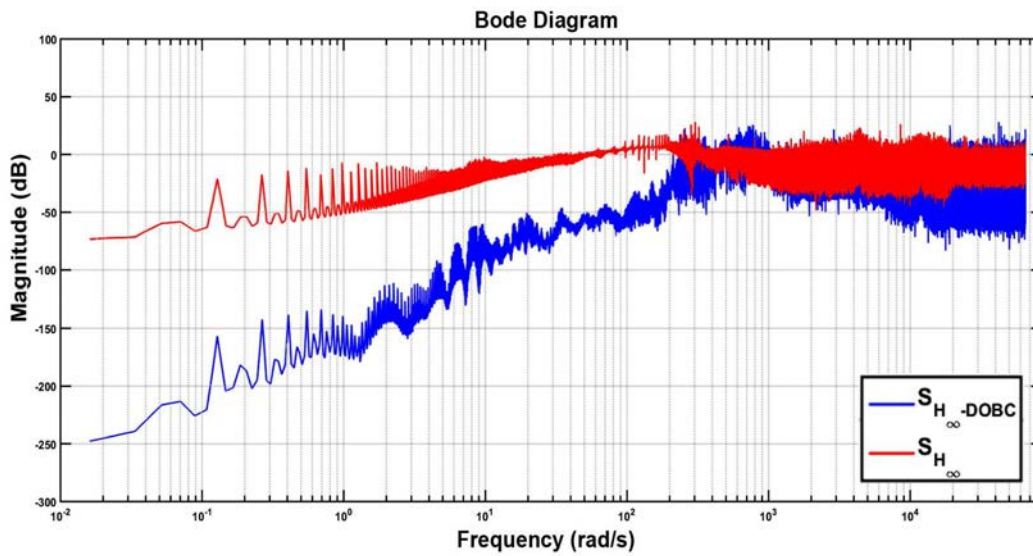


Figure 6.9: Closed-loop sensitivity functions of the single-loop H_∞ controller and hybrid $H_\infty - DOBC$.

Ultimately, three other $H_\infty - DOBC$ controllers are designed and implemented on the other three channels (Y_2, Y_3, Y_4), and the experiment is carried out while the rotor is in rotation. Again, to verify the performance of the designed controllers over the entire operating range, the air pressure supplied by the air compressor is set to 100 *psi*, and the displacements of the rotor at all four channels are recorded as the speed of the rotor increases over time (in a time span of 180 seconds). The obtained results are depicted in Figs. 6.10a - 6.10d. For a fair comparison, the performance

of the designed $H_\infty - DOBC$ controllers and the H_∞ controllers are also compared with the analog on-board controllers. It is clear that the designed $H_\infty - DOBC$ controllers exhibit significantly better performance in terms of rejecting unknown disturbances compared to the single-loop H_∞ controllers and the analog on-board controllers while the speed of the rotor increases over time. It should be noted that the maximum magnitude of vibration remains below $10 \mu m$ over the entire operating range by using the presented $H_\infty - DOBC$, allowing the system to operate much more safely in high rotational speeds compared to the single-loop controllers.

6.6 Conclusion

This Chapter presented a hybrid control scheme based on an outer-loop H_∞ optimal controller and an inner-loop disturbance observer-based controller. The effectiveness of the hybrid $H_\infty - DOBC$ structure was verified via simulations and real-time experiments on the laboratory AMB system. Several experimental studies were conducted on the performance of the designed controllers by taking into account both constant and harmonic disturbances while the rotor was stationary, as well as disturbances caused by the rotor mass-imbalance while the rotor was in rotation. In comparison to the analog on-board controllers, the experimental results clearly demonstrated that the vibrations were better attenuated by properly designed H_∞ controllers, and no additional notch filters were required in order to remove the effects of the resonant frequencies. In fact, not only the rotor remained at its geometric center over the entire operating range, the maximum magnitude of

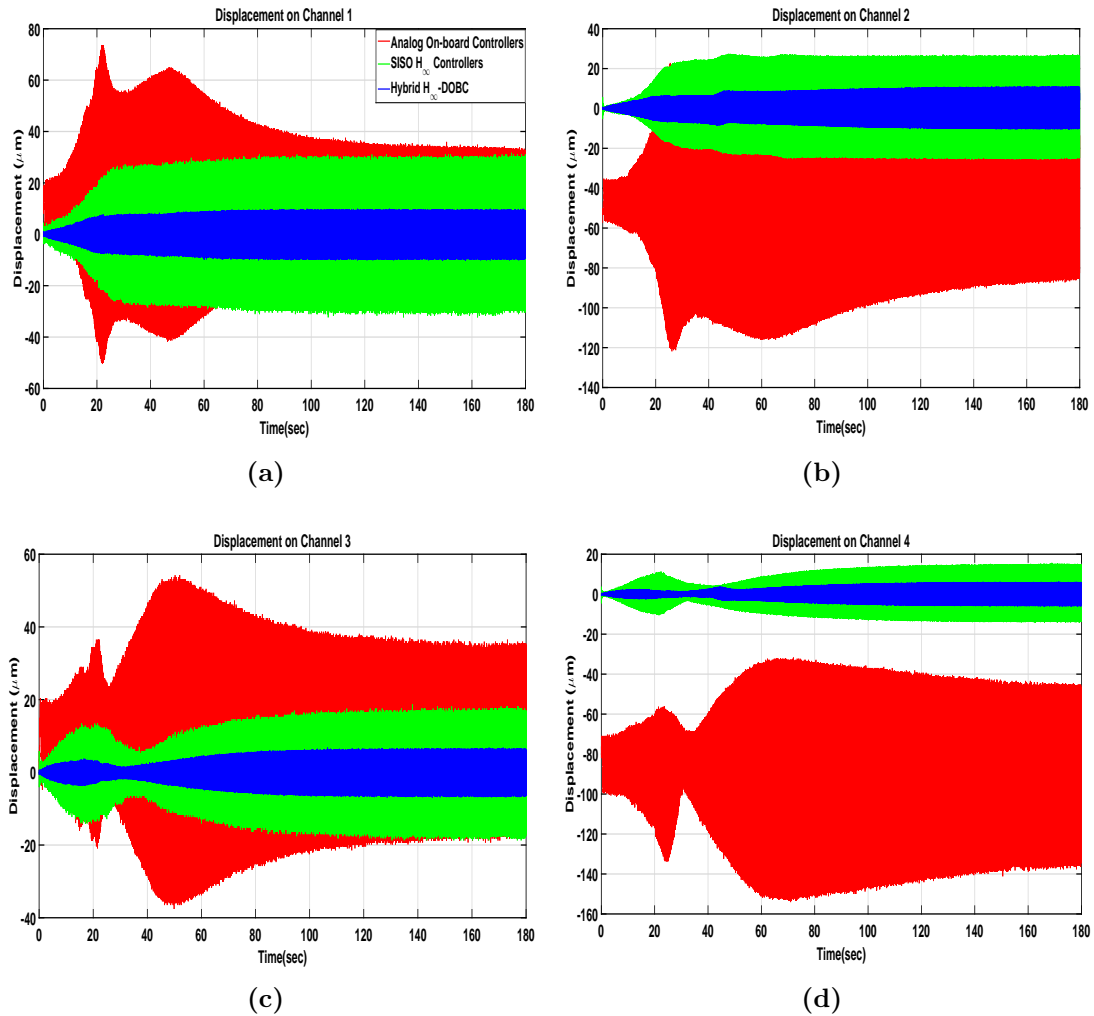


Figure 6.10: Trajectory of the geometrical centres of the rotor at different speeds using $H_\infty - DOBC$, H_∞ , and the analog on-board controllers, (a) Channel Y_1 , (b) Channel Y_2 , (c) Channel Y_3 , (d) Channel Y_4 .

vibrations reduced to less than $30\mu\text{m}$ compared to more than $70\mu\text{m}$ in the case of analog on-board controllers. The introduction of the DOBC loop into the feedback, further improved the disturbance rejection and vibration attenuation capabilities of the system. The maximum magnitude of vibrations remained below $10\mu\text{m}$ over the entire operating range by using the hybrid $H_\infty - DOBC$ structure. The

performance obtained from the presented hybrid structure was not achievable by a single-loop controller.

Chapter 7

Repetitive Disturbance

Observer-Based Controller of AMB System

7.1 Introduction

It was mentioned in the previous Chapter that vibrations with time-varying frequencies significantly affect the performance of the AMBs at high rotational speeds. It is well-known that these vibrations manifest as harmonic forces with frequencies synchronous to the rotor speed. In the previous Chapter, it was observed that the proposed 2DOF control structure significantly reduces the effects

of unknown but bounded disturbances compared to the single-loop structures while the rotor shaft is rotating. However, if there exists a repetitive disturbance with a known fundamental frequency, it turns out that the well-known repetitive control (RC) scheme provides significant improvement in rejecting the repetitive disturbance. Yet, the main drawback of the repetitive controllers is that along with the rejection of periodic disturbances, there will be undesirable gain amplifications of non-periodic disturbances. In this Chapter, the common repetitive control scheme is reformulated using the structure of disturbance observer. The new structure is called repetitive disturbance observer-based control (RDOBC) throughout the thesis and it is shown that the presented structure not only greatly reduces the gain amplification of repetitive disturbances, but also significantly reduces the effects caused by non-repetitive disturbances. This control scheme is very useful for repetitive disturbance rejection of systems that are also subject to non-repetitive disturbances. The stability analysis of the overall 2DOF control scheme is provided and some guidelines are given for designing RDOBC scheme for systems with non-minimum phase behaviour (systems with right half-plane zeros) [154].

7.2 Repetitive Disturbance Observer-based Control

This section aims to combine the features of the repetitive controllers and the disturbance observer-based control structures. Repetitive control is a well-known control design tool for systems subject to periodic disturbances. In recent years,

the repetitive control has attracted a great deal of attentions due to its design simplicity and capabilities in rejecting periodic disturbances. The versatility of the repetitive control has been reported in several practical applications [140, 155, 156, 157, 158, 159]. The main idea of the conventional repetitive controls is to include a term $1 - e^{-Ts}$ (T is the period of the repetitive disturbance) in continuous-time or $1 - z^{-N}$ (N denotes the period of the repetitive disturbance) in discrete-time into the overall feedback loop. This creates high-gain control at the repetitive frequencies. The significant problem with the conventional repetitive control is that along with the rejection of periodic disturbances, there will be undesired gain amplifications of non-periodic disturbances. The DOBC structures, on the other hand, add high-gains at low-frequency regions by including one or more integrators in the loop. The schematic diagram of the combined repetitive disturbance observer-based control is given in Fig. 7.1. $G(s)$ represents the system's model, $K(s)$ is the feedback stabiliser that can be designed by any methods to achieve the desired performance and robustness of the main feedback loop. The signals $d(t)$, $u(t)$, $y(t)$, and $r(t)$ are the input disturbance, control input, plant output, and the reference input to the system. There are three terms to be designed in the presented repetitive control:

- 1) $G_n^{-1}(s)$ is inverse of the nominal model.
- 2) $Q(s)$ is the RDOBC filter to be designed
- 3) e^{-ms} denotes m -step time-delay

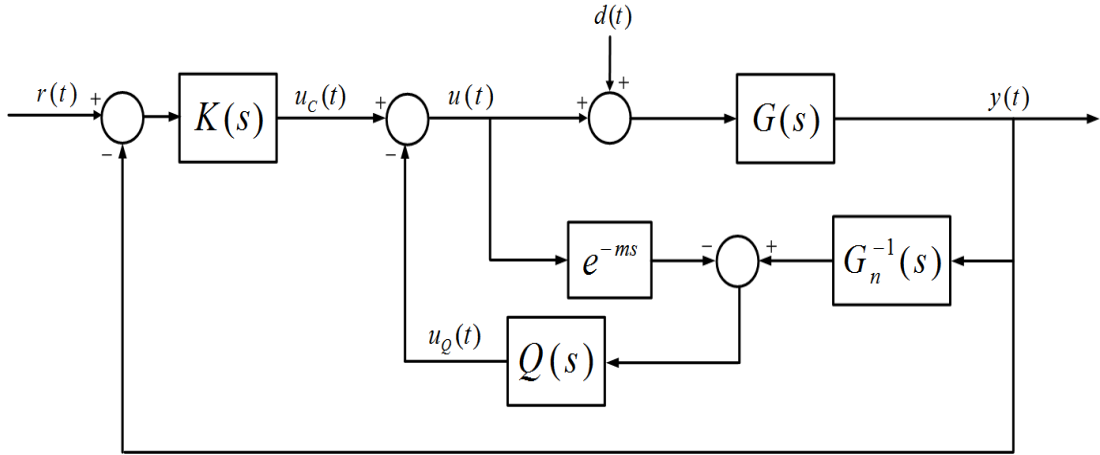


Figure 7.1: Schematic diagram of the repetitive disturbance observer-based control.

Note the resemblance of the structure to the common disturbance observer-based control (DOBC) structure [140]. If the filter $Q(s)$ is designed as a low-pass filter, the structure becomes identical to the DOBC structure that was introduced in the previous Chapter. On the other hand, if the term $G_n^{-1}(s)$ is removed from the loop and the filter $Q(s)$ is designed to be e^{-Ts} , the open-loop transfer function reduces to the repetitive controller $(G(s)K(s)/(1 - e^{-Ts}))$. It can also be inferred from the structure of the RDOBC that the central component $Q(s)$ is a repetitive-signal extractor rather than a low-pass filter in the standard DOBC structures. From Fig. 7.1, the equivalent controller $K_{eq}(s)$ from the error signal $e(t)$ to the control input $u(t)$ can be obtained as:

$$K_{eq}(s) = \frac{K(s) + Q(s)G_n^{-1}(s)}{1 - e^{-ms}Q(s)} \quad (7.1)$$

The overall closed-loop sensitivity function $S(s) = 1/(1 + G(s)K_{eq}(s))$ can be obtained as in equation (7.2).

$$S(s) = \frac{1 - e^{-ms}Q(s)}{1 + G(s)K(s) + (G(s)G_n^{-1}(s) - e^{-ms})Q(s)} \quad (7.2)$$

Suppose that the system is subject to repetitive components that need to be rejected by the feedback loop:

$$(1 - e^{-Ts})d(t) = 0 \quad (7.3)$$

From equations (7.2) and (7.3), to reject the repetitive disturbance $d(t)$, it suffices to have $S(s)d(t)$ to converge asymptotically to zero. This implies that the numerator in equation (7.2) should contain the term $1 - e^{-Ts}$. In this paper, the infinite impulse response (IIR) Q filter proposed by references [140, 159] is employed:

$$Q(s) = \frac{(1 - \alpha^T)e^{-(T-m)s}}{1 - \alpha^T e^{-Ts}} \quad (7.4)$$

or in discrete-time:

$$Q(z^{-1}) = \frac{(1 - \alpha^N)z^{-(N-m)}}{1 - \alpha^N z^{-N}} \quad (7.5)$$

Consider the discrete-time Q -filter. It can be shown that $1 - z^{-m}Q(z^{-1}) = (1 - z^{-N})/(1 - \alpha^N z^{-N})$ with an $\alpha(\in [0, 1])$. If $\alpha = 0$, the filter $Q(z^{-1})$ becomes a finite impulse response (FIR) filter. On the other hand, $\alpha = 1$ cuts off the repetitive compensation. Since there always exists large modelling uncertainties in the high-frequency region, it is necessary to incorporate a low-pass filter in the Q filter.

7.2.1 Robust Stability of the Repetitive Disturbance Observer-based Control

Suppose that the plant $G(s)$ is perturbed with an uncertainty. Without loss of generality, assume that the uncertainties are modelled as input multiplicative uncertainties. The uncertain system can be written as:

$$G(s) = G_n(s)(1 + \Delta(s)) \tag{7.6}$$

From the small gain theorem, the overall closed-loop system is robustly stable if and only if the following condition holds:

$$\|\Delta(s)T(s)\|_\infty < 1 \tag{7.7}$$

where, $T(s)$ is the closed-loop complementary sensitivity function:

$$T(s) = \frac{K(s)G(s) + G_n^{-1}(s)G(s)Q(s)}{1 + K(s)G(s) + Q(s)(G_n^{-1}(s)G(s) - e^{-ms})} \quad (7.8)$$

7.2.2 Design of RDOBC for Non-minimum Phase Systems

Since the inverse dynamics of the system $G_n^{-1}(s)$ is used in the RDOBC loops, it limits the application of the RDOBC approach to systems with no right-half plane zeros (minimum-phase systems). To overcome the problem, some alternatives have been reported in the application of DOBC which can be extended in design of RDOBC loop [139, 157]. In this study, since the *RHP*-zero of the system under study is located relatively far from the dominant low-frequency poles the non-minimum phase unstable system $G_n(s)$ is factorised into a minimum-phase and all-pass factors. The term $G_{n-mp}(s)$ includes all the poles of $G_n(s)$ (stable and unstable poles), while $G_{n-ap}(s)$ contains all the zeros of $G_n(s)$ in the open right half plane. The minimum-phase factor of the model $G_{n-mp}(s)$ is used for the design of the RDOBC loop. The designed RDOBC loop can then be combined with the main feedback stabilising controller $K(s)$ to construct the overall hybrid scheme.

$$G_n(s) = G_{n-mp}(s)G_{n-ap}(s) \quad (7.9)$$

7.3 Simulation and Experimental Validations

This section provides the simulation and experimental verification of the presented hybrid $H_\infty - RDOBC$ structure on the robust stabilisation of the AMB system. The ultimate goal is to stabilise the rotor at its geometrical center both in horizontal and vertical directions. As the model of the system is obtained while the system is stationary, the effects caused by the rotor mass-imbalance and other disturbances are not taken into consideration at the system identification stage. Thus, the RDOBC is designed to ensure the rejection of unknown but bounded disturbances while the system is in rotation. Due to the page limitation, the analysis for the first channel is presented in the sequel. However, similar procedures are used to design the controllers for the other three channels. A multiplicative uncertainty is designed based on several measurements that were taken during the system identification process. An uncertainty of less than 20% is expected for the low frequencies (below 500 rad/s) where noise to signal ratio is negligible and relatively accurate measurements can be recorded. The uncertainties reach up to more than 400% at high frequencies around and beyond the rotor flexible modes (above 4000 rad/s). Subsequently, a first order $W_T(s)$ is designed to be an upper bound on the model uncertainties and is presented in equation (7.10). The weighting $W_T(s)$ is designed to ensure the attenuation of the closed-loop complementary sensitivity function at high frequencies where the measurement noise is significant. Similarly, a first order performance weighting function $W_P(s)$ is designed based on the expected

closed-loop bandwidth of the system, and it is shown in equation (7.11).

$$W_T(s) = \frac{1.6(s + 500)}{(s + 4000)} \quad (7.10)$$

$$W_P(s) = \frac{0.3333(s + 500)}{(s + 0.00333)} \quad (7.11)$$

The sub-optimal continuous-time H_∞ controller for the first channel is given in equation (7.12). It can be clearly seen from equation (7.12) that the proper selection of the weighting functions $W_P(s)$ and $W_T(s)$ results in a controller that automatically includes two notch filters.

$$K_1(s) = \frac{7986.2(s + 3 \times 10^5)^2}{(s + 4.822 \times 10^5)(s + 1.717 \times 10^4)} \frac{(s + 374.4)(s + 77.94)}{(s + 0.003333)(s^2 + 6429s + 2.328 \times 10^7)} \frac{(s^2 + 0.96s + 2.344 \times 10^7)(s^2 + 0.37s + 1.668 \times 10^8)}{(s^2 + 5087s + 2.191 \times 10^7)(s^2 + 5297s + 1.637 \times 10^8)} \quad (7.12)$$

In order to design the RDOBC loop, the order of the original unstable system is first reduced by removing the terms corresponding to the flexible modes of the rotor while keeping their DC gain contribution. The reduced order model is then factorised into a minimum-phase ($G_{n-mp}(s)$) and an all-pass ($G_{n-ap}(s)$) factor. The reduced-order model of the first channel after removing the terms corresponding to

the flexible modes is found to be as in equation (7.13).

$$G_n(s) = \frac{-0.0040509(s + 1.72 \times 10^4)(s - 2075)}{(s + 374.4)(s - 310.2)} \quad (7.13)$$

The non-minimum phase model can be factorised into a minimum-phase part and an all-pass factor as in equation (7.14). The minimum-phase factor $G_{n-mp}(s)$ is used for the design of the inner-loop RDOBC.

$$\begin{aligned} G_n(s) &= G_{n-mp}(s) G_{n-ap}(s) \\ &= \frac{-0.0040509(s + 1.72 \times 10^4)(s + 2075)}{(s + 374.4)(s - 310.2)} \times \frac{(s - 2075)}{(s + 2075)} \end{aligned} \quad (7.14)$$

To show the effect of the design parameters, the RDOBC-loop is designed in such a way that the notches appear at multiple frequencies of 200 rad/s . The parameter N of the RDOBC loop (see equation (7.5)) is chosen to be 200, and the Bode diagram (magnitude) of the closed-loop sensitivity functions using the H_∞ controller and the hybrid H_∞ -RDOBC are depicted in Figs. 7.2 and 7.3. For the results in Fig. 7.2, α is chosen to be 0.999. Whereas, an α of 0.995 results in the closed-loop sensitivity function as shown in Fig. 7.3. It can be deduced from the two figures that reducing the value of α to zero is equivalent to the common plugin repetitive control. Although smaller α results in a wider notch filters in the sensitivity function, but the transient behaviour of the system will be unsatisfactory and it could threaten the robust stability of the closed-loop system. It can also be seen that the inclusion of the RDOBC loop successfully preserves the overall loop

shapes at the non-repetitive frequencies and the Integral Bode theorem is satisfied.

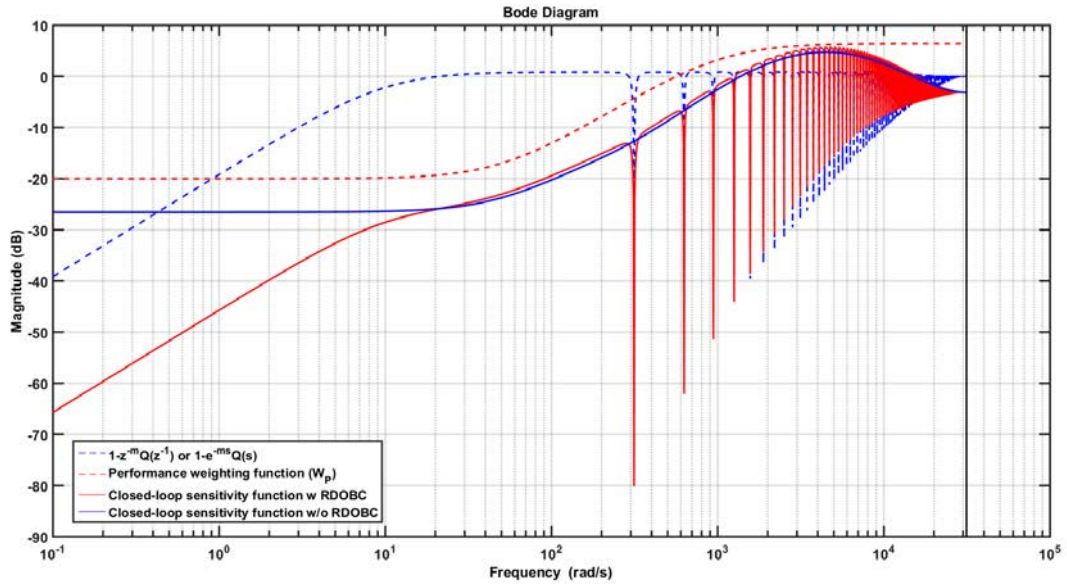


Figure 7.2: Closed-loop sensitivity functions using the single-loop H_∞ controller and the hybrid H_∞ -RDOBC with $\alpha = 0.999$.

The designed outer-loop H_∞ controller and the inner-loop RDOBC are discretised using the Bilinear transformations with a sampling frequency of $20kHz$. The discrete-time controllers are successfully implemented on the AMB system and the results are depicted in Figs. 7.4 - 7.7. The results in Fig. 7.4 show the performance of the single-loop H_∞ controller and the transient behavior of the hybrid H_∞ -RDOBC structure. It is clear that the displacement of the rotor is significantly reduced by introduction of the RDOBC inner-loop to the overall feedback system.

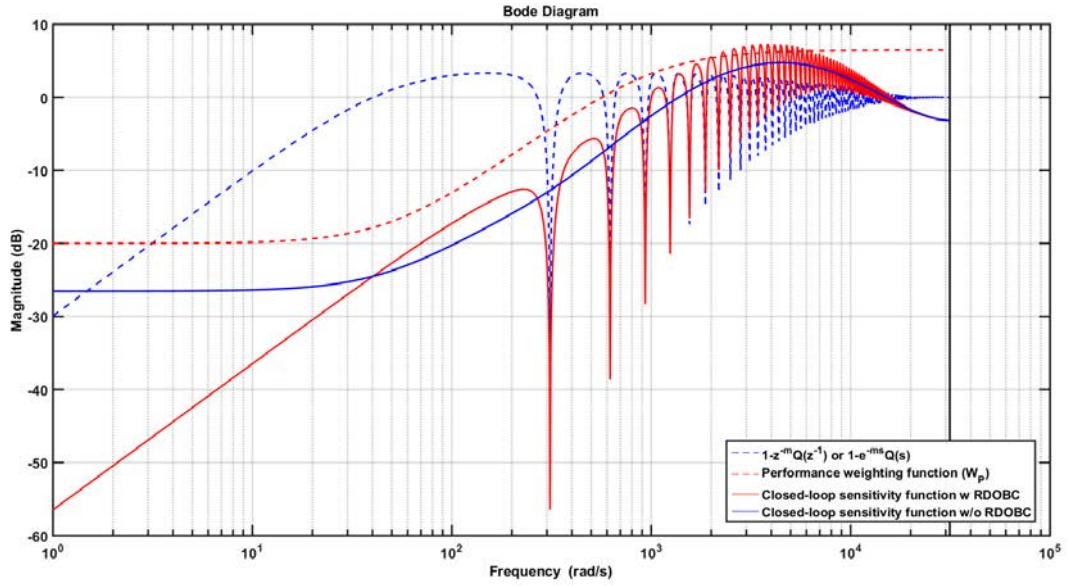


Figure 7.3: Closed-loop sensitivity functions using the single-loop H_∞ controller and the hybrid H_∞ -RDOBC with $\alpha = 0.995$.

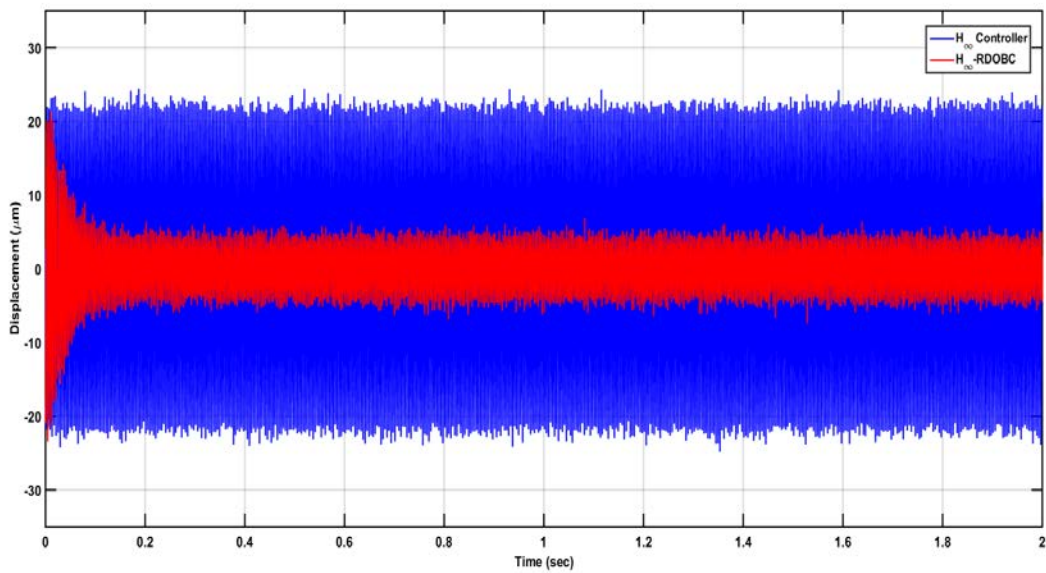


Figure 7.4: Rotor Displacement at 3000 rpm.

Fig. 7.5 represents the spectra of the rotor displacement using the single-loop H_∞ controller and the hybrid H_∞ -RDOBC structure. Compared to the single-loop H_∞ controller, using the H_∞ -RDOBC not only reduces the vibration of the system at the fundamental frequency, but also the effect of repetitive frequencies has been substantially reduced.

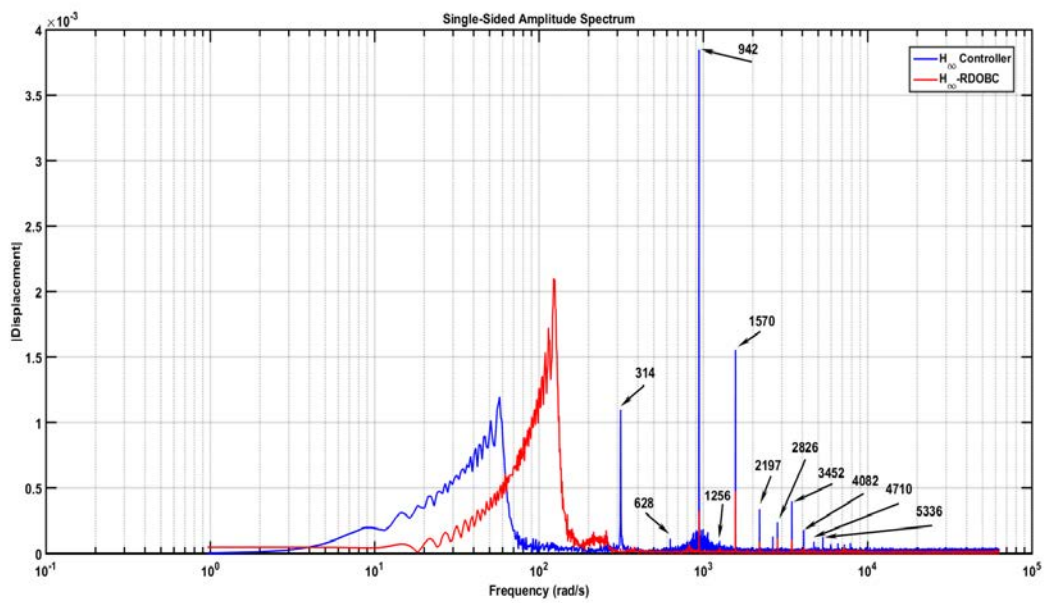


Figure 7.5: Spectra of the rotor displacement with and without RDOBC loop.

The AMB system under study operates within the range of $[0, 10000]$ rpm which corresponds to $[0, (10000 \times \frac{2\pi}{60})]$ rad/s. It is known that the rotor mass-imbalance manifests as a harmonic force with frequency synchronous to the rotor speed. In order to investigate the harmonic disturbance rejection of the two control structures, the experiment is carried out while the rotor is in rotation at various rotational speeds. To verify the performance of the designed controllers over the entire operating range, the air-pressure supplied by the air-compressor

is set to 100 psi , and the displacement of the rotor is recorded as the speed of the rotor increases over time (in a time span of 180 seconds). Fig. 7.6 shows the displacement of the geometrical center of the rotor as the rotational speed of the rotor increases over-time (from stationary). It should be noted that the RDOBC loop is turned on after five seconds. It is clear from Fig. 7.6 that the initial response of the hybrid structure is not satisfactory. This can be resolved by the dynamic switching algorithm proposed in reference [140]. However, the vibration of the rotor is significantly reduced over the entire operating range of the system. It should be noted that the maximum magnitude of vibration remains below $10\ \mu\text{m}$ over the entire operating range by using the presented H_∞ -RDOBC, allowing the system to operate much safer in high rotational speeds compared to the single-loop controller. The same approach is used to design the controllers for all four channels. Interestingly enough, the rotor achieves different steady-state rotational speeds using the designed controllers while constant air-pressure (100 psi) is supplied to the system (see Fig. 7.7). The rotational speed that is achieved by the hybrid H_∞ -RDOBC was neither achievable by the single-loop H_∞ controller, nor by the control methods used in the previously published works (see for example [53, 67, 117, 121], AminAupec20151).

7.4 Conclusion

This Chapter showed that the repetitive controllers can be reformulated into disturbance observer-based controller structure. The hybrid control structure was

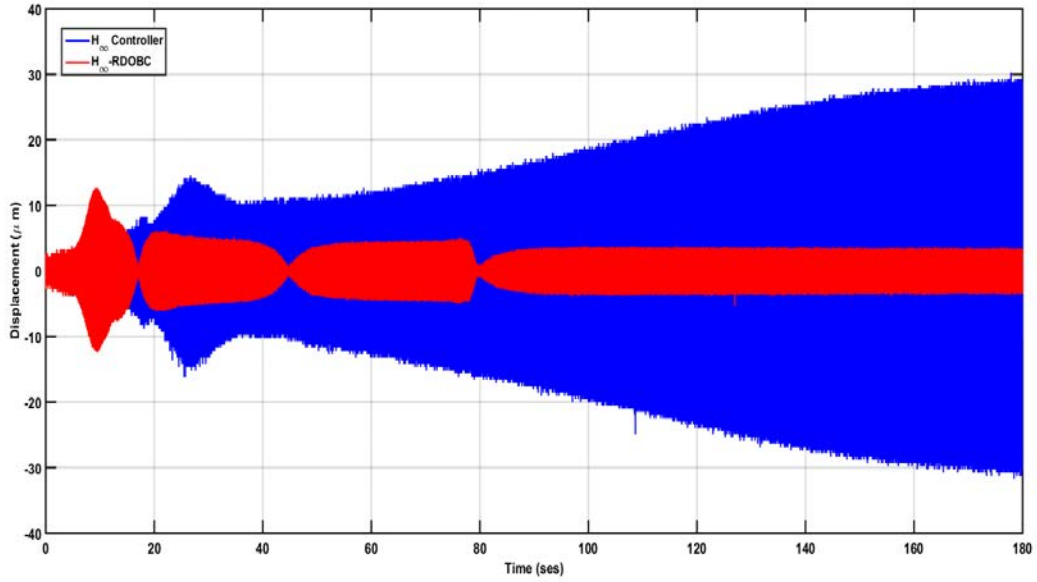


Figure 7.6: Displacement of the rotor on first channel over 180 seconds.

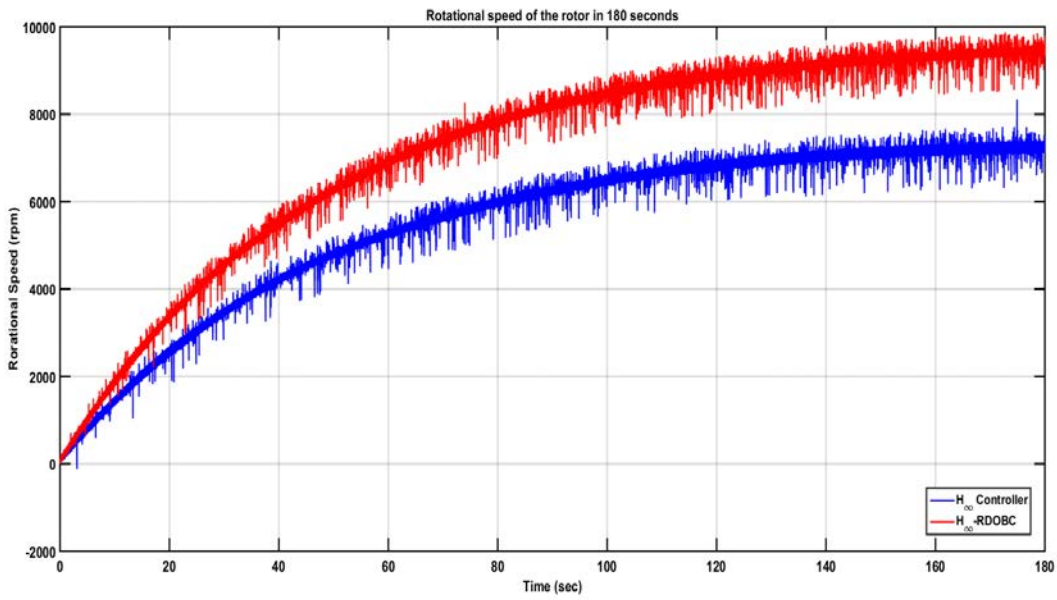


Figure 7.7: Rotational speed of the rotor over 180 seconds.

based on an outer-loop H_∞ controller and an inner-loop repetitive disturbance observer-based controller (RDOBC). The experimental results clearly demonstrated that the hybrid H_∞ -RDOBC structure provides much better performance than a single-loop H_∞ controller in term of rejection of harmonic disturbances and overall vibration attenuation. In comparison to the results demonstrated in the previous Chapter, the advantage of using the RDOBC over the DOBC is that not only the gain amplification of the harmonic disturbances at their fundamental frequencies is reduced, but also the amplification of the repetitive frequencies are also reduced substantially.

Chapter 8

Two-Step Controller Design for AMB System

8.1 Introduction

A key element to the successful design of “model-based” controllers is to have sufficiently accurate models of the system to be controlled. In order to obtain an accurate model experimentally, the system needs to be excited with sufficiently large probing signals. However, it is not always possible to excite the system with large probing signals over wide ranges of frequencies, where there is not much information available about the dynamic behaviour of the system. In fact, overly exciting the system may even lead to system instability. In the case of AMB system

for instance, exciting the resonant frequencies would endanger the closed-loop stability of the AMB system. Therefore, with the information that is obtained from the mathematical model of the system, the identification process is conducted in several steps. In fact, the magnitude of the chirp signals are reduced around the resonant frequencies, because large magnitude would destabilise the system. This is achieved by having *a priori* information about the location of the resonant frequencies. However, in practice this *a priori* information is not always available and the experimental system identification needs to be conducted very cautiously. The main idea of iterative identification and control procedure is to excite the system with a relatively narrow bandwidth probing signal and obtain a rough model of the system in the low frequency region. Next, design a controller on the basis of the identified model of the system. The bandwidth of the controller is increased progressively and cautiously until the closed-loop bandwidth of the system cannot be increased with the current controller. At this stage, more information is required from the system that is not available in the initial model. Therefore, the identification process needs to be repeated to find a better model of the system over a wider range of frequencies, and new controllers can be designed on the basis of the re-identified model. The iteration can stop when the desired performance is achieved. This iterative identification and control process is sometimes also called the “*windsurfer approach*” [160, 161, 162, 163].

For open-loop stable systems, the internal model control (IMC) method is found to be very convenient to use for the control design stage [38, 39]. This is because in the IMC method the closed-loop bandwidth of the system can be altered by a single design parameter (known as λ of the IMC filter). It is desirable to have a

control method in which a single parameter can be used to describe the bandwidth of the closed-loop system. However, if the plant is open-loop unstable, the standard IMC design is not very straightforward and sometimes becomes cumbersome for the purpose of iterative identification and control design [34, 40, 164]. To overcome this difficulty, several design alternatives have been reported in the literature. In reference [164], a new IMC filter is proposed for situations where the system has one or two unstable poles. However, this limits the application of the proposed approach only to limited types of systems. The work in reference [165] introduces an H_∞ control method to generalise the control design algorithm for the iterative identification and control of both stable and unstable systems. In the described algorithm, the controller is synthesised to minimise the H_∞ -norm between the obtained closed-loop system and a reference model with a prescribed bandwidth. The method reported in reference [34] breaks down the controller design process of unstable systems into two separate steps. In the first step, a feedback controller is designed to stabilise the unstable plant. In the second step, the standard IMC method is employed on the basis of the stabilised system for the purposes of iterative identification and control. This Chapter can be considered as an improvement to the idea of two-step controller design of unstable systems for iterative identification and control. It provides a systematic two-step control design approach for open-loop unstable systems for iterative identification and control purposes. In the first step of the proposed algorithm, a minor-loop is designed to stabilise the open-loop unstable system with minimum required energy (“expensive energy control strategy”). It is desirable to stabilise the system without exciting the high-frequency ranges where the model of the plant is highly uncertain. Next, a major-loop is designed on the basis of the stabilised system. In order to progressively increase the bandwidth of the

overall closed-loop system in the second step, a mixed-sensitivity H_∞ optimisation procedure is applied to the closed-loop stable system. The advantage of using the mixed-sensitivity H_∞ controller is that the bandwidth of the closed-loop system can be expanded by proper selection of the weighting functions and re-synthesising the H_∞ controller. Furthermore, special attention can be paid to the magnitude of control signal and the high-frequency roll-off at the design stage. Therefore, this design method addresses the shortcomings of the standard IMC method specially for open-loop unstable systems. The effectiveness of the proposed design approach is verified by a numerical example and real-time experiments on the AMB system. It should be emphasised that the focus of this Chapter is not on the identification stage, but rather on the control design of open-loop unstable systems for the purpose of iterative identification and control.

8.2 Two-Step Controller Design Approach

Motivated by the properties of 2DOF structures [69, 166, 167, 168, 169], a two-step controller design scheme is formulated by combining the properties of minimum energy LQR controllers and the frequency-domain properties of the H_∞ controllers. Furthermore, it is shown that the proposed design structure is suitable for the purpose of iterative identification and control design of open-loop unstable systems.

8.2.1 First Step: Linear Quadratic Regulator (LQR)

In this step, a feedback controller is designed to stabilise the open-loop unstable system shown in equation (8.1) with the minimum (weighted) energy. An “expensive energy” LQR control strategy is employed to achieve the minimum energy stabiliser [170]. In a continuous-time linear time-invariant (LTI) system of the form:

$$\begin{cases} \dot{x}(t) = Ax(t) + Bu(t), & x \in R^n, u \in R^k \\ y = Cx(t), & y \in R^m \end{cases} \quad (8.1)$$

The LQR controller employs a gain matrix K_{reg} in the control law in equation (8.2) such that the closed-loop system becomes stable and the quadratic cost function in equation (8.3) is minimised:

$$u(t) = -K_{reg}x(t) \quad (8.2)$$

$$J_{LQR} = \int_0^{\infty} \left(x(t)^T Q x(t) + u(t)^T R u(t) \right) dt \quad (8.3)$$

In equation (8.3), Q and R are symmetric positive semi-definite and positive definite weighting matrices of appropriate sizes on state variables and control signals, respectively. The optimal value of the controller K_{reg} can be found as:

$$K_{reg} = R^{-1} B^T P \quad (8.4)$$

In equation (8.4), P is the unique solution of the Algebraic Riccati Equation (ARE):

$$A^T P + PA - PBR^{-1}B^T P + Q = 0 \quad (8.5)$$

The state-space representation of the closed-loop system incorporating the optimal linear state-feedback control law can be written as in equation (8.6).

$$\begin{cases} \dot{x}(t) = (A - BK_{reg})x(t) \\ y = Cx(t) \end{cases} \quad (8.6)$$

The equivalent transfer function of the closed-loop stable system can be also represented as in equation (8.7).

$$G_{closed-loop} = C(sI - A + BK_{reg})^{-1}B \quad (8.7)$$

For situations where not all states are available for measurement, a state estimator can be designed to estimate the internal states of the system from the inputs and outputs measurements. The output feedback controller can be written as in equations (8.8) and (8.9).

$$\hat{\dot{x}}(t) = A\hat{x}(t) + L(y(t) - \hat{y}(t)) + Bu(t) \quad (8.8)$$

$$\hat{y}(t) = C\hat{x}(t) \quad (8.9)$$

The overall closed-loop system is obtained as in equation (8.10).

$$\begin{bmatrix} \dot{x}(t) \\ \dot{\hat{x}}(t) \end{bmatrix} = \begin{bmatrix} A & -BK_{reg} \\ LC & A - BK_{reg} - LC \end{bmatrix} \begin{bmatrix} x(t) \\ \hat{x}(t) \end{bmatrix} \quad (8.10)$$

In general, the proper selection of Q and R is important for achieving the desired performance and robustness in the closed-loop LQR controller design. However, the LQR controller is only used here to stabilise the system with minimum weighted energy (“expensive energy control strategy”), while the desired overall closed-loop performance will be achieved in the second step via H_∞ control design. To reflect the fact that control signal is “expensive”, the output from K_{reg} should be made as small as possible and hence a large R should be assigned to penalise the control signal heavily.

8.2.2 Second Step: Mixed-Sensitivity H_∞ Controller

In the second step of the design, a mixed-sensitivity H_∞ controller is designed on the basis of the closed-loop stable plant (G_{stable}) to shape the closed-loop sensitivity functions (in the frequency-domain) and gradually increase the closed-

loop bandwidth of the system. The structure of the overall closed-loop system based on the proposed two-step controller design method is depicted in Fig. 8.1.

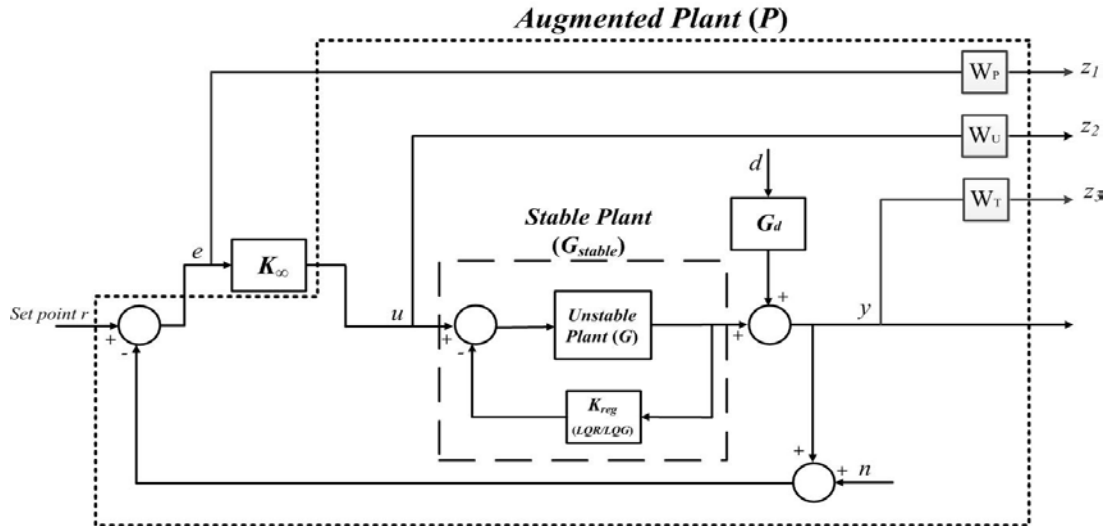


Figure 8.1: Proposed two-step controller design structure.

In a standard H_∞ configuration the feedback control system can be rearranged as a linear fractional transformation (LFT). Plant P in the figure represents the stabilised system (G_{stable}) augmented with the weighting functions ($W_P(s)$, $W_U(s)$, and $W_T(s)$). These weighting functions can be easily absorbed into the interconnected system $P(s)$. The generalised plant $P(s)$ can be partitioned as shown in equation (8.11).

$$P = \begin{bmatrix} P_{11} & P_{12} \\ P_{21} & P_{22} \end{bmatrix} \quad (8.11)$$

where,

$$P_{11} = \begin{bmatrix} W_P \\ 0 \\ 0 \end{bmatrix}, P_{12} = \begin{bmatrix} -W_P P \\ W_U \\ W_T P \end{bmatrix}, P_{21} = I, P_{22} = -G_{stable} \quad (8.12)$$

The closed-loop transfer function (T_{zw}) from exogenous inputs w (set-point and disturbances) to the exogenous outputs z (outputs that need to be minimised) can be found as:

$$T_{zw} =: \mathcal{F}_l(P, K_\infty) = P_{11} + P_{12}K_\infty(I - P_{22}K_\infty)^{-1}P_{21} \quad (8.13)$$

Again, the $\mathcal{F}_l(P, K_\infty)$ is the lower linear fractional transformation (LFT) of P with respect to K_∞ . The mixed-sensitivity H_∞ synthesis problem is to find a controller K_∞ which minimises the H_∞ - norm of the closed-loop transfer function of the augmented plant:

$$\min_{K_{stabilising}} \|\mathcal{F}_l(P, K_\infty)\|_\infty \quad (8.14)$$

where:

$$\|\mathcal{F}_l(P, K_\infty)\|_\infty = \left\| \begin{array}{c} W_P S \\ W_U K_\infty S \\ W_T T \end{array} \right\|_\infty \quad (8.15)$$

In equation (8.15), $S(s) = (I + G_{stable}(s)K_\infty(s))^{-1}$ is the closed-loop sensitivity function, while $T(s) = G_{stable}(s)K_\infty(I + G_{stable}(s)K_\infty(s))^{-1}$ represents the closed-loop complementary sensitivity function. For detailed description of the H_∞ optimal controller design, please refer to Section 3.2.

8.3 Numerical Example and Experimental

Validation

8.3.1 Difficulties with One-Step Control Design Approach

Example 1: Assume a second-order model of the system being controlled is available as in equation (8.16). An initial controller needs to be designed based on this model, and the bandwidth of the closed-loop system is gradually increased until a more accurate model is required. Note that the model is open-loop unstable and contains a non-minimum phase zero. The system does not possess the parity

interlacing property, and an unstable controller is required for stabilisation of the system. To better illustrate the difficulties with one-step control design approach, an IMC controller is designed based on the model, and the step response of the closed-loop system is compared with the proposed two-step design approach. It should be emphasised that the aim of this example is not to compare the performance of the two structures, but rather to show the difficulties that may occur in the one-step design approach.

$$G(s) = \frac{(s - 1)}{(s + 0.5)(s - 2)} \quad (8.16)$$

The IMC controller is designed based on the IMC filter proposed in reference [164]. According to the reference [164], the IMC filter should take the form:

$$F(s) = \frac{\mu(s + \alpha)}{(s + \gamma)(s + \lambda)(s + 10\lambda)} \quad (8.17)$$

In equation (8.17), the parameters μ and α are determined from two interpolation constraints, i.e., $F(s = p) = 1$, where $p = 2$ is the unstable pole of the model, and $F(s = 0) = 1$ for tracking a step reference input. From the guidelines, λ needs to be chosen in such a way that $\lambda \in [4p, 10p]$. The other parameter γ needs to be designed for securing the robust stability of the system against model uncertainties. It is found that $\gamma \in [0.1p, 0.25p]$ to give the minimum possible overshoot. If the model uncertainty is small, larger value of γ can be chosen to reduce the peak overshoot of the closed-loop step response. The final IMC controller is found to be

in the form of equation (8.18).

$$K_{IMC}(s) = \frac{9.1742 \times 10^5 (s - 0.2857)(s + 0.3815)}{s(s - 34.64)(s + 0.3651)} \times \frac{(s + 0.5)}{(s^2 + 249.8s + 2.174 \times 10^4)} \quad (8.18)$$

The unit-step response of the closed-loop system and the required control signal using the one-step IMC controller are depicted in Fig. 8.2. The excessive overshoot in the step response resulting from the one-step IMC control design approach clearly demonstrates the difficulty in achieving the desired performance using this design approach.

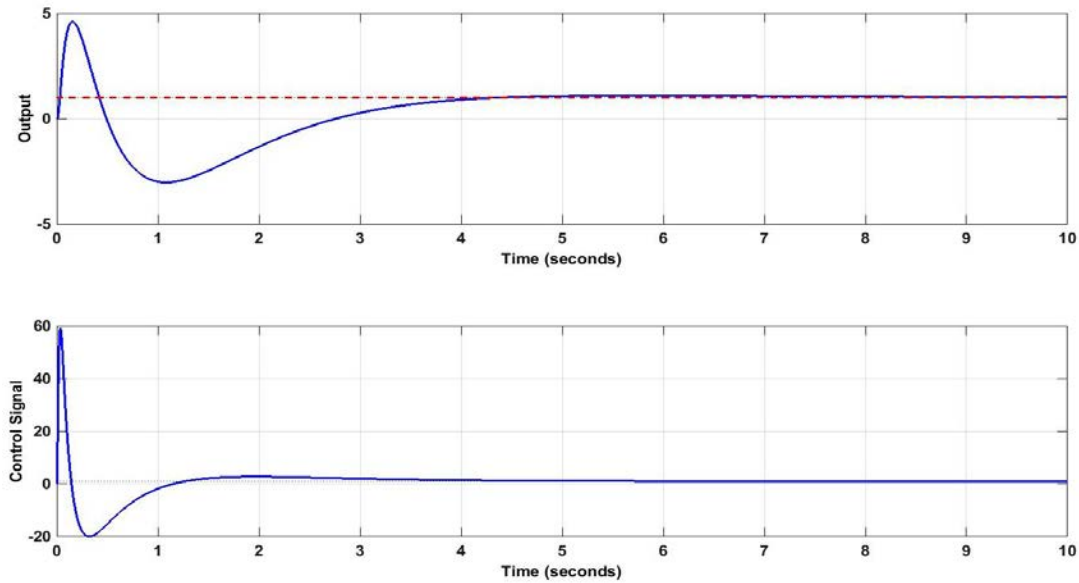


Figure 8.2: Step response of the system and the control signal using 1DOF IMC.

On the other hand, in the proposed two-step design approach, the unstable plant is first stabilised using an “expensive energy” LQR control strategy. At this

stage, the aim is to stabilise the system with the minimum possible energy and hence a large value of R needs to be assigned for the design of the LQR controller. It is worth noting that in the case of SISO systems, assigning a large value on the controller weighting R shifts the unstable poles of the system to their stable mirror images about the imaginary axis [171]. The resulting closed-loop transfer function of **Example 1** by assigning an identity matrix of Q and $R = 100$ is shown in equation (8.19).

$$G_{stable}(s) = \frac{(s - 1)}{(s + 0.5079)(s + 2.008)} \quad (8.19)$$

In the second step, a mixed sensitivity H_∞ optimisation is used to obtain the desired time-domain and frequency-domain behaviour. A first-order $W_P(s)$ is designed to be an upper-bound on the closed-loop sensitivity function ($S(s)$):

$$W_P(s) = \frac{0.333(s + 1.05)}{(s + 3.5 \times 10^{-5})} \quad (8.20)$$

From the designed $W_P(s)$, it is clear that the pure integrator is replaced by $(s + 3.5 \times 10^{-5})$ to avoid the numerical issues. A maximum sensitivity peak of $(1/0.333)$ is allowed (see reference [67]) and a closed-loop bandwidth of $(0.333 \times 1.05 \text{ rad/s})$ is desired (similar to the closed-loop bandwidth of the system using one-step IMC method). Another weighting function $W_T(s)$ is designed in equation (8.21) to ensure the robust stability of the system at high frequencies where the

model uncertainties are significant, and the measurement noise is dominant:

$$W_T(s) = \frac{2(s+1)}{(s+20)} \quad (8.21)$$

The transfer function (output-feedback) representation of the H_∞ optimised controller is found to be:

$$K_\infty(s) = \frac{-206.27(s+10)(s+2.008)(s+0.5079)}{(s+39.57)(s+19.45)(s+6.251)(s+3.5 \times 10^{-5})} \quad (8.22)$$

The designed weighting functions ($W_P(s)$ and $W_T(s)$), and the resulting closed-loop sensitivity and complementary sensitivity functions ($S(s)$ and $T(s)$) are illustrated in Fig. 8.3. It can be seen from the figure that the weighting functions are designed in such a way that $1/W_P(s)$ and $1/W_T(s)$ to be the upper bounds on $S(s)$ and $T(s)$, respectively.

The resulting unit-step response of the closed-loop system with the two-step controller design approach is depicted in Fig. 8.4. In comparison to the obtained results from the one-step approach (see Fig. 8.2), it is clear that the system has achieved the desired performance using the presented two-step structure, and the magnitude of control signal to the plant is significantly smaller than the control signal using the one-step design approach. The closed-loop bandwidth of the system can then be increased by increasing the bandwidth of the weighting function W_P in equation (8.20) and resynthesising the controller using the available H_∞ optimisation algorithms.

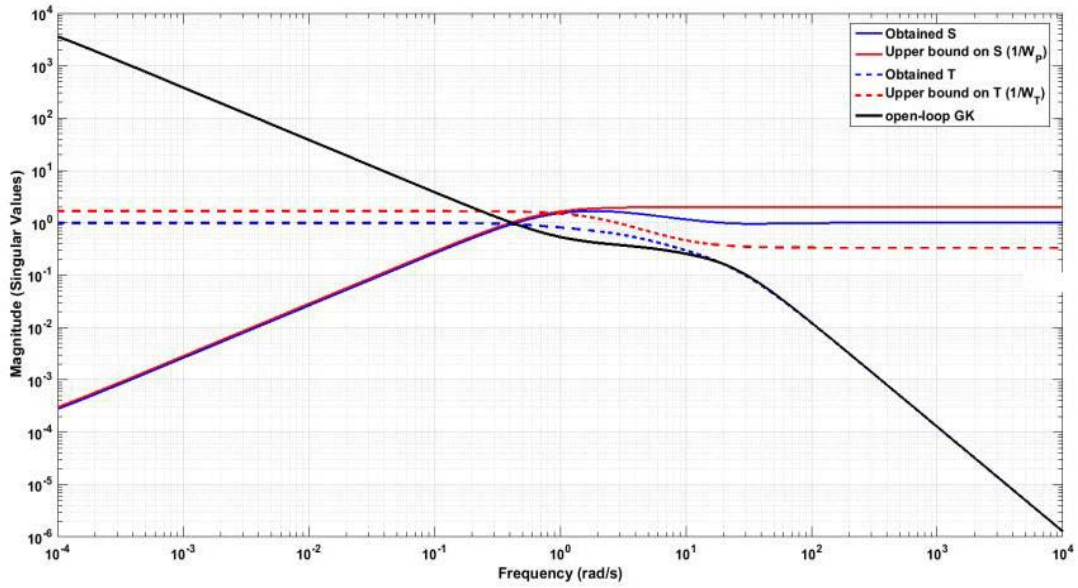


Figure 8.3: Magnitude of $1/W_P$, S , $1/W_T$, T , and $G_{stable}K_{\infty}$.

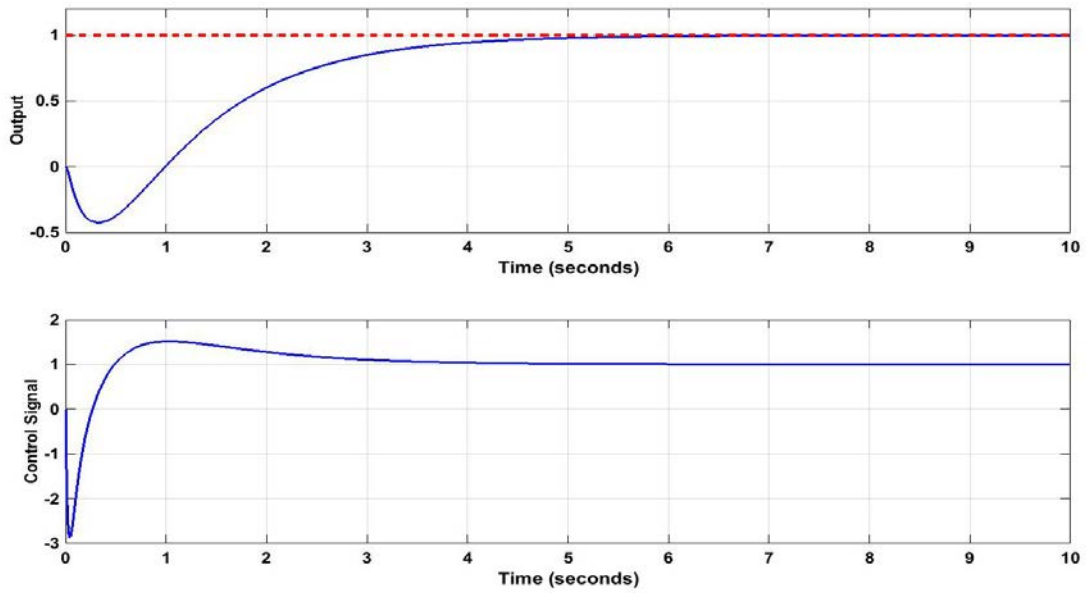


Figure 8.4: Step response of the system and the control signal (input signal to the plant) using the proposed controller.

8.3.2 Verification by Experiment: Time-domain Response of Non-Minimum Phase AMB System

The controller design process is started with the assumption that no information is available from the true plant, other than the mathematical description of the electromagnetic force, hall-effect sensors, and the current amplifiers, as described in the system manuals [172, 173]. The non-linear electromagnetic force of the bearings is a function of the distance between the bearings and the rotor (x_i), and the control current into the bearings ($i_{control}$):

$$F_i = k \frac{(i_{control} + 0.5)^2}{(x_i - 0.0004)^2} - k \frac{(i_{control} - 0.5)^2}{(x_i + 0.0004)^2} \quad (8.23)$$

In equation (8.23), $k = 2.8 \times 10^{-7} Nm^2/A^2$. The air-gap between the bearings and the rotor is $0.4 mm$, and the bias current is $0.5 A$. The linearised model of the equation (8.23), by taking into account the linear model of the hall-effect sensor and the current amplifier is shown in equation (8.24).

$$G_{initial}(s) = \frac{1.1346 \times 10^8}{(s - 129)(s + 129)(s + 4545)} \quad (8.24)$$

Similar to the previous example, the open-loop unstable system is first stabilised by using an “expensive energy strategy” LQR controller. The bandwidth of the closed-loop stable system is gradually expanded by synthesising the H_∞ controller based on the redesigned weighting functions $W_P(s)$ and $W_T(s)$. Eventually, the

designed controller destabilises the system due to the presence of the flexible modes of the rotor in higher frequencies. Therefore, a more accurate model of the system that includes the model of the first two flexible modes (around 770 Hz and 2053 Hz) is acquired through the closed-loop system identification process. The details of the closed-loop system identification can be found in reference [53]. The Bode diagram (magnitude) of the initial model and the re-identified model are depicted in Fig. 8.5, and the re-identified model for the first channel is found to be in the form of equation (8.25).

$$G_{re-identified}(s) = \frac{-1.9739 \times 10^5 (s + 2.657 \times 10^4)(s - 1637)}{(s + 1.2 \times 10^4)(s + 4612)(s + 390.1)(s - 261.3)} \quad (8.25)$$

$$\times \frac{(s^2 + 1352s + 2.127 \times 10^7)(s^2 + 1236s + 1.631 \times 10^8)}{(s^2 + 11.12s + 2.344 \times 10^7)(s^2 + 15.61s + 1.673 \times 10^8)}$$

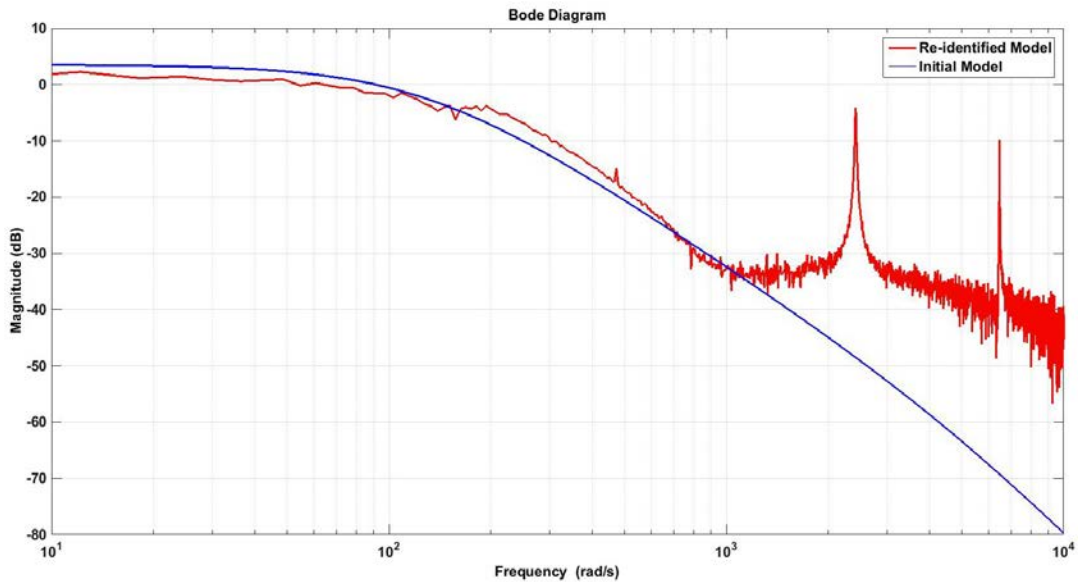


Figure 8.5: Initial and re-identified model of AMB system.

Similarly, the re-identified model is stabilised by an “expensive energy” LQR controller. Then, the closed-loop stable model is used in the second step to improve the overall performance of the system. The bandwidth of the closed-loop system is gradually increased, until the sensor noise becomes dominant, and hence the process is stopped. The designed H_∞ controller based on the closed-loop stable system is shown in equation (8.26).

$$\begin{aligned}
K_\infty(s) = & \frac{5.9901 \times 10^6 (s + 1.2 \times 10^4)(s + 4612)(s + 390.1)(s + 261.3)}{(s + 2.408 \times 10^4)(s + 0.00333)(s^2 + 3674s + 8.129 \times 10^6)} \\
& \times \frac{(s^2 + 11.12s + 2.344 \times 10^7)(s^2 + 1.364 \times 10^4s + 1.623 \times 10^8)}{(s + 6.633 \times 10^4)(s^2 + 1347s + 2.129 \times 10^7)(s^2 + 1232s + 1.631 \times 10^8)} \\
& \times \frac{(s^2 + 15.61s + 1.673 \times 10^8)}{(s^2 + 4.515 \times 10^4s + 1.33 \times 10^9)}
\end{aligned} \tag{8.26}$$

Finally, the closed-loop step response of the proposed 2DOF controller structure is compared with a 1DOF H_∞ controller (designed on the basis of the re-identified model), and a 2DOF servo LQR controller in Fig. 8.6. Two unit-step disturbances are added into the system, and the control signals are depicted in Fig. 8.7.

As the system identification is conducted while the rotor is stationary, the effects caused by the centrifugal forces and the rotor mass-imbalance are not taken into account at the identification stage. To further investigate the performance of the proposed algorithm while the system is in rotation, a similar procedure is repeated for the second channel. The performance of the final designed controllers is investigated while the rotor is in rotation with the maximum rotational speed of 10000 *rpm*. The displacement of the geometrical center of the rotor using the

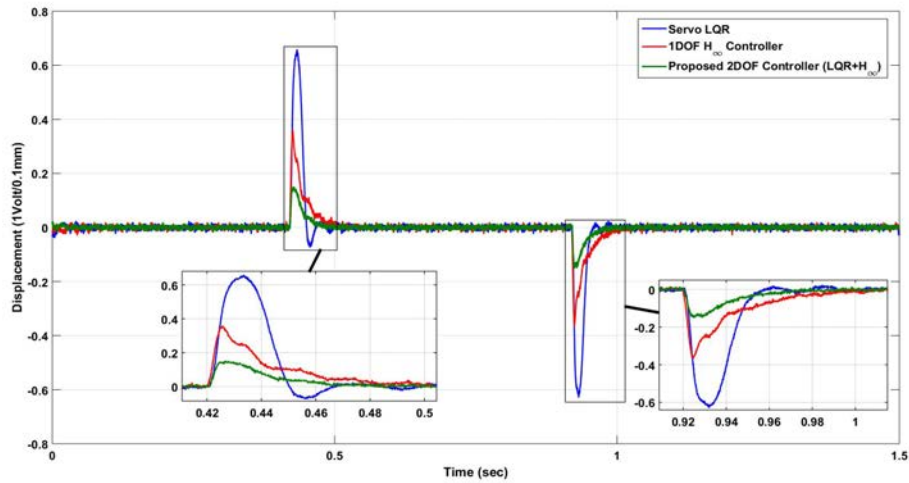


Figure 8.6: Step response of the system using the proposed 2DOF controller, 1DOF H_∞ controller, and servo LQR.

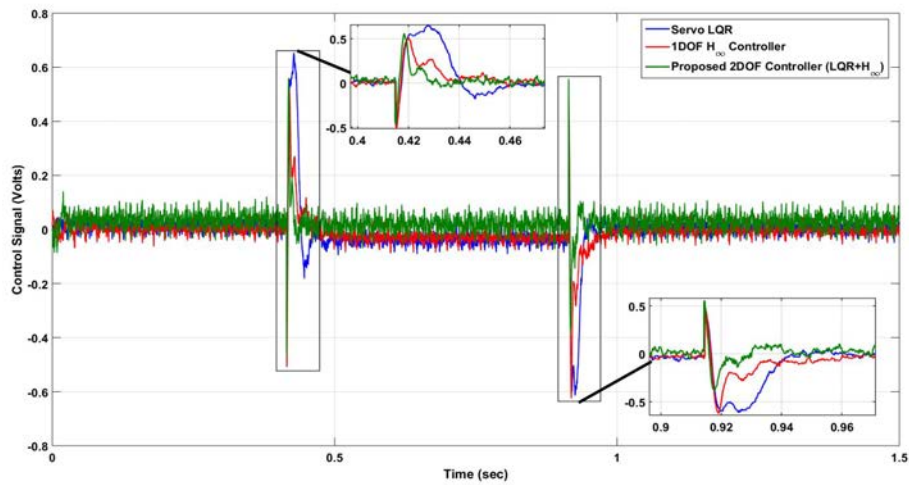


Figure 8.7: Control signal using the proposed 2DOF controller, 1DOF H_∞ controller, and servo LQR.

final 2DOF controller is depicted in Fig. 8.8, and the results are compared with the 1DOF H_∞ controller and the servo LQR controller.

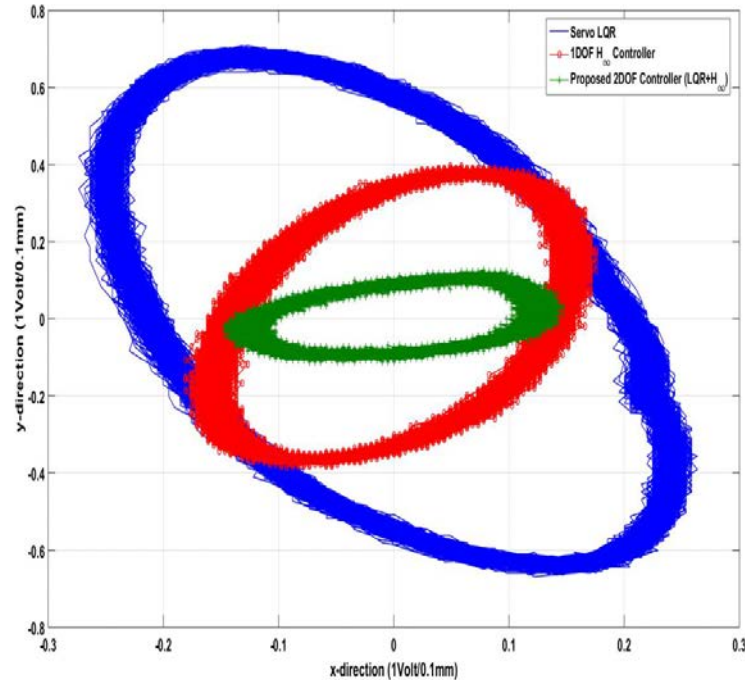


Figure 8.8: Trajectory of the geometrical center of the rotor at 10000 *rpm* using the proposed 2DOF controller, 1DOF H_{∞} controller, and servo LQR.

8.4 Conclusion

In this Chapter, the difficulties with the one-step control design of open-loop unstable systems for iterative identification and control purposes are discussed. To overcome these difficulties, a systematic two-step control design structure is presented. In the proposed approach, the unstable plant is first stabilised with the minimum required energy (“expensive energy” LQR controller). The overall bandwidth of the closed-loop stable system can then be expanded in the second step by proper selection of the weighting functions in the mixed-sensitivity H_{∞} controller design. The effectiveness of the proposed approach was verified by a

numerical example and a real-time experiment on the open-loop unstable AMB system.

Chapter 9

Summary and Future Work

9.1 Summary

The main focus of this thesis was on analytical modelling, system identification, and high-performance controllers of active magnetic bearing systems. The aim was to address the gaps between control theory and its application to active magnetic bearing systems. In Chapter 2, an analytical model of the laboratory scale AMB system was derived using the first principles. The derived model provided invaluable insights into the underlying system dynamics. For instance, the mathematical model suggested that the first two flexible modes of the rotor (approximately at $770Hz$ and $2050Hz$) are within the bandwidth of the system and special attentions need to be paid to these flexible modes at the system identification and control

design stages. It is clear that overly exciting these frequencies at the system identification stage may lead to system instability and hence the amplitude of the probing chirp signals was reduced near these resonant frequencies to avoid the danger of the system instability at the identification stage. Furthermore, inclusion of two notch-filters is inevitable for robust stabilisation of the systems. Furthermore, the analytical model of the system suggested that the cross-coupling effects between the channels are negligible at low-frequency regions (dc-gain contribution of $-20dB$) and hence the MIMO system can be considered as four decoupled SISO subsystems, if low-complexity controllers are to be designed for the system.

In the system identification stage, the time-domain responses of the system to the input chirp signals were captured and converted into frequency-domain by using the Discrete Fourier Transformation. Next, both SISO and MIMO models of the system were obtained from the frequency-domain response of the system. A novel GA-based iterative weighted least squares method was proposed for SISO and MIMO modelling of the system. Unlike most of the identification methods in the literature, it was shown that the presented algorithm was capable of accurately modelling the high-frequency flexible modes as well as the low-frequency regions. The advantage of obtaining the decoupled SISO models was that low-order controllers could be designed on the basis of the SISO models. The SISO controllers were able to successfully stabilise the AMB system, as the cross-coupling effects between the channels were negligible at low-frequency regions (dc-gain of $-20dB$). However, it was observed from the experimental frequency response of the system that the cross-coupling effects between the channels become more significant at high-frequency regions. Hence, the cross-coupling effects between the channels need

to be modelled accurately if higher performance controllers are to be designed for the system (i.e., to increase the closed-loop bandwidth of the system). Therefore, a similar iterative system identification algorithm was extended for high-order MIMO modelling of the system by taking into account the cross-couplings between the channels.

In Chapter 3, several SISO and MIMO controllers were designed for stabilisation of the AMB system, namely, decoupled PID controllers, SISO H_∞ controllers, MIMO H_2 , and MIMO H_∞ controllers. Extensive experimental studies were conducted on the robust performance of the SISO and MIMO controllers (in terms of transient performance, steady-state error, and disturbance rejection capabilities) for the AMB system while the rotor was stationary, as well as while it was rotating. The performance of the classically designed PID controllers (including two notch filters and a low-pass filter) were compared with their SISO H_∞ -optimal counterparts. Also, MIMO H_2 and H_∞ optimal controllers were synthesised on the basis of the MIMO model of the system. The experimental results showed that the SISO H_∞ controllers provide a better performance compared to the conventional PID controllers. Moreover, the H_∞ optimisation algorithms automatically introduce all the required components (two notch filters, low-pass filter, lead-lag compensators) into the controller without the need of any manual intervention on the part of the designer. The MIMO H_∞ controllers performed much better than their SISO counterparts while the rotor was rotating, although they were found to be excessively high in order. The real-time implementation of such high-order controllers could become challenging, unless advanced hardware is available. Last but not least, the

results obtained from the H_2 optimal control theory were not satisfactory while the rotor was rotating (when the unstructured modelling uncertainty was significant).

Chapter 4 attempted to design controllers that not only provide robust stability of the nominal system, but also guarantee the robust performance of all possible systems in the uncertainty set. It was shown that the main drawback of the common robust control synthesis algorithms is that they result in exceedingly high-order controllers that are difficult to implement on the actual system. In fact, the presence of the high-frequency resonant modes in the model caused the numerical issues at the synthesis stage and hence resulted in excessively high-order controller. In order to alleviate the problem of synthesising high-order controllers, some alternative approaches were presented. In the first approach, the rigid-body model of the system was considered as the nominal model for the control synthesis procedure. Whereas, the flexible modes of the system were treated as structured modelling uncertainties and their model were included in the design weighting functions. The advantage of the presented approach was that a much lower-order controller was synthesised. Furthermore, unlike the first approach where the controller was synthesised on the basis of the full-order model of the system, two notch-filters were appeared in the final controller. This was because of the inclusion of the resonant modes in the design weighting functions. The second approach was to design fixed-order robust controllers using non-smooth optimisation algorithms. The shortcoming of the latter method was that there was no guarantee in the global convergence of the optimisation problem. However, the obtained locally optimal controller successfully stabilised the AMB system under study. Another drawback of the latter method was that the order of the controller needed to be predefined before the

optimisation process is initialised. A trial and error process was required to find the minimum controller's order that satisfies the robust performance requirements (the closed-loop structured singular value $\mu_{\Delta} < 1$). The controller that was synthesised based on the full-order model of the system failed to stabilise the experimental AMB system. Furthermore, the controllers that were synthesised based on the two presented approaches successfully stabilised the MIMO AMB system. The system remained stable by the controllers that were obtained by full-order and fixed-order H_{∞} -optimisation and μ -synthesis algorithms. The lowest amount of vibration was achieved by using the full order μ synthesised controllers while the shaft was rotating at different speeds.

Chapter 5 provided a “model-free” PID-type fuzzy logic controller for the stabilisation of the AMB system under study. It is well-known that the performance of fuzzy logic controllers depends highly on the proper selection of the input/output tuning parameters of the controller. Meta-heuristic optimisation algorithms can be utilised to obtain these parameters more systematically. Usually, time-domain objective functions such as integral absolute of error (IAE) or integral time absolute of error (ITAE) are utilised for optimisation of the tuning parameters in fuzzy logic controllers. It is clear that by choosing time-domain objective functions, the optimisation algorithms try to find optimal values of the tuning parameters such that the minimum error between the time-domain response of the system to a predefined input signal is obtained. The larger the optimisation search domain, the larger the “optimal values” and hence the faster the closed-loop transient performance will be. This is not always desirable, as it may lead to large control signals and the saturation of actuators. To alleviate this problem, an alternative

objective function was proposed for the time-domain optimisation of the design parameters of fuzzy logic controllers. It was further demonstrated that by using the presented objective function, most of the global optimisation algorithms converge to similar values regardless of the size of the optimisation search-domain. A similar approach was utilised to obtain the optimal tuning parameters of the fuzzy logic controllers for stabilisation of the AMB system and the tuned fuzzy logic controllers were coded in *C* for the real-time implementation.

In Chapters 6 and 7, the performance of the system was further improved (in terms of disturbance rejection and vibration reduction) while the rotor was rotating at various speeds. In order to reduce the vibrations caused by the rotor imbalance, centrifugal forces, and other unknown dynamics, an additional inner-loop disturbance-observer based controller (DOBC) was included into the overall feedback loop resulting in a 2DOF control scheme. One of the advantages of using the inner-loop disturbance observer-based controller was that the inner-loop was designed to have a faster dynamic response than the outer-loop feedback stabiliser and hence was more effective in rejecting disturbances than those of single-loop control structures. In Chapter 6, a 2DOF control structure comprising an outer-loop feedback stabiliser and an inner-loop disturbance observer was presented and implemented successfully on the AMB system. It was demonstrated via experimental studies that the presented 2DOF control scheme was much more effective than single-loop control structures in reducing the overall vibration of the system while the system was rotating. The DOBC loop is capable of reducing the effects caused by unknown but bounded disturbances. However, if there exist repetitive disturbances with known fundamental frequencies, the repetitive control (RC) scheme is known to be more

effective in rejecting these types of disturbances. Nevertheless, the major drawback of the RC schemes is that while the repetitive disturbances are perfectly rejected with this scheme, the magnitude of non-repetitive disturbances is amplified by using this scheme and this is not desirable. An algorithm was described in Chapter 7 to reformulate the repetitive controller into the disturbance observer-based structure. The presented structure was called repetitive disturbance observer-based controller (RDOBC) and its performance was evaluated via simulation and experimental studies. It was shown that the RDOBC scheme was able to perfectly reject the effects caused by harmonic disturbances, as well as it significantly reduced the effects of non-repetitive disturbances. Interestingly, the experimental results revealed that, with a constant supplied air-pressure, the highest steady-state rotational speed was achieved by the proposed control scheme compared to all our previously applied methods. This was because the overall vibration of the system was reduced substantially while the system was rotating.

Finally, Chapter 8 was an extension to the idea of iterative identification and control. In order to obtain the model of a system experimentally, chirp or multi-sine signals could be employed as probing signals for system identification purposes. The probing signals need to be strong enough to sufficiently excite the system in the frequency range of interest. On the one hand, in practice, it is not always possible to overly excite the system over a wide range frequencies, where there is not clear information about the behaviour of the system. This could be very dangerous in industrial applications and it may lead to system instability. On the other hand, weak probing signals will result in poor signal to noise ratios and hence may fail to provide enough information about the system dynamics. In iterative

identification and control scheme, a controller is first designed on the basis of a low-order model of the plant that is only known in the low-frequency regions. An initial controller is designed on the basis of this possibly low-order model of the system. Then, the closed-loop bandwidth of the system is expanded gradually until the closed-loop bandwidth cannot be increased any further by the current controller. At this stage, a more accurate model of the plant in a wider range of frequencies is required for the control design stage. Hence, the identification process can be repeated to find a better model of the plant in higher ranges of frequencies and new controllers can be designed based on the re-identified model. This iterative process can stop when the desired performance (or closed-loop bandwidth) is achieved. The internal model control (IMC) method is the most commonly used method in the literature for iterative identification and control purposes. The IMC is a simple but effective method for iterative identification and control of open-loop stable systems. However, controller design based on IMC method for open-loop unstable systems may become challenging and not efficient for the iterative identification and control purposes. Therefore, an alternative strategy was proposed in Chapter 8 for control design of open-loop unstable systems for iterative identification and control procedure. In this method, the system was first stabilised by using a minor stabilising loop that was based on minimum weighted energy LQG/LTR methods. This minor-loop ensures the closed-loop stability of the system with minimum weighted energy and without exciting the high-frequency regions where the model of the system is unknown. Then, a major-loop controller based on mixed-sensitivity H_∞ optimisation method was employed on the closed-loop stable system to increase the closed-loop bandwidth of the system progressively and cautiously. It should be noted that we favour the use of mixed-sensitivity H_∞ controller over the LQG/LTR

controllers for the major-loop controller, because the closed-loop bandwidth of the system can be altered by proper selection of a single parameter in the design weighting function. The effectiveness of the proposed algorithm was investigated via simulation and experimental studies on the iterative identification and control of the AMB system. It was assumed that no information was available about the dynamics of the system other than the attractive forces of the electromagnets governed by the Maxwell's theorem. It was shown that the closed-loop performance of the system was improved significantly via the presented iterative identification and control approach.

9.2 Future Works

The scope of this work was limited to the control design of an AMB system with radial type magnetic bearings. In fact, the radial electromagnets were spaced with 90° angle from each other. Three-pole AMBs with three electromagnets that are distributed around the rotor with an angle of 120° has been proposed recently [174, 175, 176]. It appears that the three pole AMBs are more power efficient than the four pole AMBs. However, the control design of these three-poles AMBs is much more difficult. The future work could focus on the application of the presented control methods on the three-pole AMB arrangements.

The MIMO model of the system was found to be exceedingly high-order and hence the synthesised robust controllers were found to be very high-order and

difficult to implement. The implementation of such high-order controllers require expensive hardware and they are not efficient for product commissioning. The problem of arriving at a lower-order MIMO model that is capable of capturing the dynamic behaviour of the system over a wide range of frequencies needs to be further investigated.

The Takagi-Sugeno (TS) fuzzy modelling and control of the AMB system could be the focus of the future work. In recent works, It is shown that the TS fuzzy modelling and control approach can handle nonlinearities in modelling physical plants by approximating the nonlinear terms to any specified accuracy with a family of fuzzy sets and rules [177]. Then, fuzzy state-feedback and output-feedback controllers can be designed on the basis of the TS fuzzy model of the system [178]. The advantage of the TS fuzzy modelling and control design over the “model-free” fuzzy logic controllers is that the closed-loop stability of the system can be analysed systematically [179, 180, 181, 182]. The recent interval type 2 (IT2) fuzzy logic controllers are claimed to be more robust than the type 1 fuzzy logic controllers to modelling uncertainties [177, 183]. The application of the interval type 2 (IT2) fuzzy logic controllers on stabilisation of AMBs can be investigated in the future.

In Chapters 6 and 7 the DOBC and RDOBC loops were implemented on all four channels as decentralised SISO controllers. An interesting but challenging future work can focus on reformulating the DOBC and RDOBC loops as an MIMO structure. In the case of AMBs, the periodic disturbances are slow varying type disturbances with frequencies that vary in accordance to the rotor speed. Hence, the future work can also investigate the implementation of the RDOBC scheme

in a linear parameter varying or gain-scheduling form in which the fundamental frequency of the repetitive disturbances can be estimated online with the real-time rotor speed measurements and the controllers parameters can be modified accordingly [184].

The introduction of iterative identification and control has led to several robust adaptive control methods such as multi-model adaptive control, safe adaptive control, and unfalsified adaptive control methods [185, 186, 187, 188, 189, 190]. The iterative identification and control appears to be a systematic method for performance improvement of partially known system without having to perform any online system identification while the controller is in the loop (unlike the adaptive control structures). Hence, it prevents the several issues that the adaptive control methods face in practice, such as the difficulty of online system identification which itself has numerous challenges that need to be addressed, poor transient performance, the danger of including destabilising controllers in the loop, and the uncertainty about the dwell-time (the required time before the current controller is switched to another one). Further insight into the advantages and disadvantages of these methods and a systematic approach to improve the performance of these algorithms is an open research area.

References

- [1] J. X. Shen, K. J. Tseng, D. M. Vilathgamuwa, and W. K. Chan, “A novel compact PMSM with magnetic bearing for artificial heart application,” *IEEE Transactions on Industry Applications*, vol. 36, no. 4, pp. 1061–1068, 2000.
- [2] M. Morshuis, A. El-Banayosy, L. Arusoglu, R. Koerfer, R. Hetzer, G. Wieselthaler, A. Pavie, and C. Nojiri, “European experience of dura-heart TM magnetically levitated centrifugal left ventricular assist system,” *European Journal of Cardio-Thoracic Surgery*, vol. 35, no. 6, pp. 1020–1028, 2009.
- [3] K. C. Lee, Y. H. Jeong, D. H. Koo, and H. J. Ahn, “Development of a radial active magnetic bearing for high speed turbo-machinery motors,” in *the Proceedings of International Joint Conference of SICE-ICASE*, pp. 6090–6095, 2006.
- [4] S. Y. Yoo, H. I. Lee, and M. D. Noh, “Comparative study of power minimiz-

- ing control algorithms for active magnetic bearings,” in *the Proceedings of IEEE/ASME International Conference on Advanced Intelligent Mechatronics*, pp. 155–159, 2012.
- [5] G. Shrestha, H. Polinder, D. J. Bang, and J. A. Ferreira, “Direct drive wind turbine generator with magnetic bearing,” in *the Proceedings of European Wind Energy Assosiation Offshore Wind Conference and Exhibition*, 2007.
- [6] G. Shrestha, H. Polinder, D. Bang, A. K. Jassal, and J. A. Ferreira, “Investigation on the possible Use of magnetic bearings in large direct drive wind turbines,” in *the Proceedings of Europe’s Premier Wind Energy Event*, 2009.
- [7] J. Kumbernuss, J. Chen, W. Junhua, H. X. Yang, and W. N. Fu, “A novel magnetic levitated bearing system for Vertical Axis Wind Turbines,” *Applied Energy*, vol. 90, no. 1, pp. 148–153, 2012.
- [8] T. Tezuka, N. Kurita, and T. Ishikawa, “Design and Simulation of a five degrees of freedom active control magnetic levitated motor,” *IEEE Transactions on Magnetics*, vol. 49, no. 5, pp. 2257–2262, 2013.
- [9] S. Y. Yoon, Z. L. Lin, and P. E. Allaire, “Experimental evaluation of a surge controller for an AMB supported compressor in the presence of piping acoustics,” *IEEE Transactions on Control Systems Technology*, vol. 22, no. 3, pp. 1215–1223, 2014.

-
- [10] N. J. M. Van Dijk, N. van de Wouw, E. J. J. Doppenberg, H. A. J. Oosterling, and H. Nijmeijer, “Robust active chatter control in the high-speed milling process,” *IEEE Transactions on Control Systems Technology*, vol. 20, no. 4, pp. 901–917, 2012.
- [11] B. C. Han, S. Q. Zheng, X. Wang, and Q. Yuan, “Integral design and analysis of passive magnetic bearing and active radial magnetic bearing for agile satellite application,” *IEEE Transactions on Magnetics*, vol. 48, no. 6, pp. 1959–1966, 2012.
- [12] J. Shi and W. S. Lee, “An experimental comparison of a model based controller and a fuzzy logic controller for magnetic bearing system stabilization,” in *the Proceedings of International Conference on Control and Automation*, pp. 379–384, 2009.
- [13] J. Shi, X. Yu, Y. Yan, and S. Yu, “Comparison of two types of nonlinear controllers for magnetic bearing system stabilization: An experimental approach,” in *the Proceedings of Third International Conference on Intelligent Control and Information Processing*, pp. 167–173, 2012.
- [14] H. M. N. K. Balini, *Advanced systems theory applied to AMB systems*. PhD thesis, TU Delft, Delft University of Technology, 2011.
- [15] J. Lundh, *Model predictive control for active magnetic bearings*. PhD thesis, Linköpings University, Sweden, 2012.

-
- [16] A. Smirnov, *AMB system for high-speed motors using automatic commissioning*. PhD thesis, Lappeenranta University of Technology, Finland, 2012.
- [17] A. H. Pesch, *Development of chatter attenuation robust control for an AMB machining spindle*. PhD thesis, Cleveland State University, USA, 2013.
- [18] R. P. Jastrzebski, K. M. Hynynen, and A. Smirnov, “ H_∞ control of active magnetic suspension,” *Mechanical Systems and Signal Processing*, vol. 24, no. 4, pp. 995–1006, 2010.
- [19] Z. Gosiewski and A. Mystkowski, “Robust control of active magnetic suspension: Analytical and experimental results,” *Mechanical Systems and Signal Processing*, vol. 22, no. 6, pp. 1297–1303, 2008.
- [20] H. M. N. K. Balini, I. Houtzager, J. Witte, and C. Scherer, “Subspace identification and robust control of an AMB system,” in *the Proceedings of the American Control Conference*, pp. 2200–2205, 2010.
- [21] J. Witte, H. M. N. K. Balini, and C. W. Scherer, “Robust and LPV control of an AMB system,” in *the Proceedings of the American Control Conference*, pp. 2194–2199, 2010.
- [22] H. M. N. K. Balini, C. W. Scherer, and J. Witte, “Performance enhancement for AMB systems using unstable H_∞ controllers,” *IEEE Transactions on Control Systems Technology*, vol. 19, no. 6, pp. 1479–1492, 2011.

- [23] H. M. N. K. Balini, J. Witte, and C. Scherer, "Synthesis and implementation of gain-scheduling and LPV controllers for an AMB system," *Automatica*, vol. 48, no. 3, pp. 521–527, 2012.
- [24] J. C. Doyle, B. A. Francis, and A. R. Tannenbaum, *Feedback Control Theory*. Macmillan, New York, 1992.
- [25] S. E. Mushi, Z. Lin, and P. E. Allaire, "Design, construction, and modeling of a flexible rotor active magnetic bearing test rig," *IEEE/ASME Transactions on Mechatronics*, vol. 17, no. 6, pp. 1170–1182, 2012.
- [26] A. H. Pesch, A. Smirnov, O. Pyrhonen, and J. T. Sawicki, "Magnetic bearing spindle tool tracking through μ -synthesis robust control," *IEEE/ASME Transactions on Mechatronics*, vol. 20, no. 3, pp. 1448–1457, 2015.
- [27] G. Mann, B.-G. Hu, and R. Gosine, "Analysis of direct action fuzzy PID controller structures," *IEEE Transactions on Systems, Man, and Cybernetics, Part B: Cybernetics*, vol. 29, no. 3, pp. 371–388, 1999.
- [28] "The MathWorks, Global Optimization Toolbox 3.3, Matlab R2014b," 2014.
- [29] J. Shi, R. Zmood, and L. Qin, "The direct method for adaptive feed-forward vibration control of magnetic bearing systems," in *the Proceedings of International Conference on Control, Automation, Robotics and Vision*, vol. 2, pp. 675–680, 2002.

-
- [30] J. Shi, R. Zmood, and L. Qin, “Synchronous disturbance attenuation in magnetic bearing systems using adaptive compensating signals,” *Control Engineering Practice*, vol. 12, no. 3, pp. 283 – 290, 2004.
- [31] A. S. Ghersin, R. S. Smith, and R. S. S. Peña, “Classical, robust and LPV control of a magnetic-bearing experiment,” in *Identification and Control*, pp. 277–325, Springer, 2007.
- [32] A. S. Ghersin, R. S. Smith, and R. S. Sánchez, “LPV control of a magnetic bearing experiment,” *Latin American applied research*, vol. 40, no. 4, pp. 303–310, 2010.
- [33] D. Luong, *Advanced digital controls*. PhD thesis, University of California, USA, 2008.
- [34] W. S. Lee, I. M. Mareels, and B. Anderson, “Iterative identification and two step control design for partially unknown unstable plants,” *International journal of control*, vol. 74, no. 1, pp. 43–57, 2001.
- [35] W. S. Lee, B. D. O. Anderson, R. L. Kosut, and I. M. Y. Mareels, “New approach to adaptive robust control,” *International Journal of Adaptive Control and Signal Processing*, vol. 7, no. 3, pp. 183–211, 1993.
- [36] W. S. Lee, B. D. O. Anderson, I. M. Y. Mareels, and R. L. Kosut, “On some key issues in the windsurfer approach to adaptive robust control,” *Automatica*,

- vol. 31, no. 11, pp. 1619–1636, 1995.
- [37] A. Dehghani, A. Lanzon, and B. Anderson, “An H_∞ algorithm for the windsurfer approach to adaptive robust control,” *International Journal of Adaptive Control and Signal Processing*, vol. 18, no. 8, pp. 607–628, 2004.
- [38] M. Morari, *Robust process control*. Englewood Cliffs: Prentice-Hall, 1989.
- [39] I. G. Horn, J. R. Arulandu, C. J. Gombas, J. G. VanAntwerp, and R. D. Braatz, “Improved filter design in internal model control,” *Industrial and Engineering Chemistry Research*, vol. 35, pp. 3437–3441, 1996.
- [40] M. Campi, W. S. Lee, and B. D. O. Anderson, “Filters for internal model control design for unstable plants,” in *the Proceedings of the 32nd IEEE Conference on Decision and Control*, pp. 1343–1348, 1993.
- [41] A. Noshadi, W. S. Lee, J. Shi, P. Shi, and A. Kalam, “On Two-Step Controller Design for Partially Unknown Unstable Systems,” in *the Proceedings of the European Control Conference*, pp. 485–490, 2015.
- [42] L. Ljung, *System identification: Theory for the User*. Springer, 1998.
- [43] P. Van Overschee and B. De Moor, “N4SID: subspace algorithms for the identification of combined deterministic-stochastic systems,” *Automatica*, vol. 30, no. 1, pp. 75–93, 1994.

-
- [44] S. J. Qin, “An overview of subspace identification,” *Computers & chemical engineering*, vol. 30, no. 10, pp. 1502–1513, 2006.
- [45] M. Viberg, “Subspace-based methods for the identification of linear time-invariant systems,” *Automatica*, vol. 31, no. 12, pp. 1835–1851, 1995.
- [46] Y. Todo and T. Mitsui, “A learning multiple-valued logic network using genetic algorithm,” *International Journal of Innovative Computing, Information and Control*, vol. 10, no. 2, pp. 565–574, 2014.
- [47] J. Yang, H. Gao, and W. Liu, “Hybrid method of chaotic genetic algorithm and boundary simulation for constrained optimization,” *International Journal of Innovative Computing, Information and Control*, vol. 11, no. 3, pp. 1059–1073, 2015.
- [48] K. Kristinsson and G. A. Dumont, “System identification and control using genetic algorithms,” *IEEE Transactions on Systems, Man and Cybernetics*, vol. 22, no. 5, pp. 1033–1046, 1992.
- [49] A. Ghaffari, A. R. Mehrabian, and M. Mohammad-Zaheri, “Identification and control of power plant de-superheater using soft computing techniques,” *Engineering Applications of Artificial Intelligence*, vol. 20, no. 2, pp. 273–287, 2007.
- [50] A. R. Tavakolpour, I. Z. M. Darus, O. Tokhi, and M. Mailah, “Genetic

- algorithm-based identification of transfer function parameters for a rectangular flexible plate system,” *Engineering Applications of Artificial Intelligence*, vol. 23, no. 8, pp. 1388–1397, 2010.
- [51] I. Daubechies, R. DeVore, M. Fornasier, and C. S. Güntürk, “Iteratively reweighted least squares minimization for sparse recovery,” *Communications on Pure and Applied Mathematics*, vol. 63, no. 1, pp. 1–38, 2010.
- [52] G. Baselli and P. Bolzern, *Closed-loop system identification*. John Wiley & Sons, Inc., 2006.
- [53] A. Noshadi, J. Shi, W. S. Lee, P. Shi, and A. Kalam, “Genetic algorithm-based system identification of active magnetic bearing system: a frequency-domain approach,” in *the Proceedings of the 11th IEEE International Conference on Control & Automation*, pp. 1281–1286, 2014.
- [54] K. Michalski, “On the low-order partial-fraction fitting of dielectric functions at optical wavelengths,” *IEEE Transactions on Antennas and Propagation*, vol. 61, no. 12, pp. 6128–6135, 2013.
- [55] D. Lee, J. Park, Y. Joo, K. Lin, and C. Ham, “Robust H_∞ control for uncertain nonlinear active magnetic bearing systems via Takagi-Sugeno fuzzy models,” *International Journal of Control, Automation and Systems*, vol. 8, no. 3, pp. 636–646, 2010.

-
- [56] K. Hoshik, O. Sang-Yong, and S. Ohseop, “ H_∞ Control of a rotor-magnetic bearing System based on linear matrix inequalities,” *Journal of Vibration and Control*, vol. 17, no. 2, pp. 291–300, 2011.
- [57] I. S. Kuseyri, “Robust control and unbalance compensation of rotor-active magnetic bearing systems,” *Journal of Vibration and Control*, vol. 18, no. 6, pp. 817–832, 2011.
- [58] G. Barbaraci and G. V. Mariotti, “Performances comparison for a rotating shaft suspended by 4-axis radial active magnetic bearings via μ -synthesis, loop-shaping design, and H_∞ with uncertainties,” *Modelling and Simulation in Engineering*, vol. 2011, pp. 1–10, 2011.
- [59] R. P. Jastrzebski, A. Smirnov, O. Pyrhnen, and A. K. Piat, *Discussion on robust control applied to active magnetic bearing rotor system*. InTech, 2011.
- [60] J. Chen, K. Liu, and K. Xiao, “ H_∞ control of active magnetic bearings using closed loop identification model,” in *the Proceedings of International Conference on Mechatronics and Automation*, pp. 349–353, 2011.
- [61] A. Noshadi, J. Shi, W. S. Lee, P. Shi, and A. Kalam, “Optimal PID-type fuzzy logic controller for a multi-input multi-output active magnetic bearing system,” *Neural Computing and Applications*, DOI: 10.1007/s00521-015-1996-7, 2015.
- [62] A. Noshadi, J. Shi, W. S. Lee, P. Shi, and A. Kalam, “Robust control of an

- active magnetic bearing system using H_∞ and disturbance observer-based control,” *Journal of Vibration and Control*, DOI: 10.1177/1077546315602421, 2015.
- [63] A. Noshadi, J. Shi, W. S. Lee, P. Shi, and A. Kalam, “System identification and robust control of multi-input multi-output active magnetic bearing systems,” *IEEE Transactions on Control Systems Technology*, DOI: 10.1109/TCST.2015.2480009, 2015.
- [64] B. A. Francis, *A Course in H_∞ Control Theory*. Springer-Verlag, 1987.
- [65] K. Zhou, *Essentials of Robust Control*. Prentice Hall, 1999.
- [66] P. Gahinet and P. Apkarian, “A linear matrix inequality approach to H_∞ control,” *International journal of robust and nonlinear control*, vol. 4, no. 4, pp. 421–448, 1994.
- [67] A. Noshadi, J. Shi, W. S. Lee, and A. Kalam, “PID-type fuzzy logic controller for active magnetic bearing system,” in *the Proceedings of the 40th Annual Conference of IEEE Industrial Electronics*, pp. 241–247, 2014.
- [68] J. C. Doyle, K. Glover, P. P. Khargonekar, and B. A. Francis, “State-space solutions to standard H_2 and H_∞ control problems,” *IEEE Transactions on Automatic Control*, vol. 34, no. 8, pp. 831–847, 1989.
- [69] S. Skogestad and I. Postlethwaite, *Multivariable feedback control: analysis*

- and design*, vol. 2. Wiley New York, 2007.
- [70] D. C. McFarlane and K. Glover, “Robust controller design using normalized coprime factor plant descriptions,” 1990.
- [71] D. McFarlane and K. Glover, “A loop-shaping design procedure using H_∞ synthesis,” *IEEE Transactions on Automatic Control*, vol. 37, no. 6, pp. 759–769, 1992.
- [72] M. A. Dahleh and I. J. Diaz-Bobillo, *Control of uncertain systems: a linear programming approach*. Prentice-Hall, Inc., 1994.
- [73] T. Iwasaki and R. E. Skelton, “All controllers for the general H_∞ control problem: LMI existence conditions and state space formulas,” *Automatica*, vol. 30, no. 8, pp. 1307–1317, 1994.
- [74] J. Doyle, K. Lenz, and A. Packard, “Design examples using μ -synthesis: Space shuttle lateral axis FCS during reentry,” in *Modelling, Robustness and Sensitivity Reduction in Control Systems*, pp. 127–154, 1987.
- [75] G. J. Balas, *Robust control of flexible structures: Theory and experiments*. PhD thesis, California Institute of Technology, 1989.
- [76] D. Bernstein, W. Haddad, and C. Nett, “Minimal complexity control law synthesis, part 2: Problem solution via H_2/H_∞ optimal static output feedback,” in *Proceedings of the American Control Conference*, pp. 2506–2511, 1989.

-
- [77] C. Nett, D. Bernstein, and W. Haddad, “Minimal complexity control law synthesis, part 1: Problem formulation and reduction to optimal static output feedback,” in *Proceedings of the American Control Conference*, pp. 2056–2064, 1989.
- [78] D. C. Hyland and D. S. Bernstein, “The optimal projection equations for model reduction and the relationships among the methods of wilson, skelton, and moore,” *IEEE Transactions on Automatic Control*, vol. 30, no. 12, pp. 1201–1211, 1985.
- [79] W. M. Haddad and V. Kapila, “Fixed-architecture controller synthesis for systems with input-output time-varying nonlinearities,” in *Proceedings of the American Control Conference*, vol. 6, pp. 4396–4400, 1995.
- [80] J. R. Corrado and W. M. Haddad, “Static output feedback controllers for systems with parametric uncertainty and controller gain variation,” vol. 2, pp. 915–919, 1999.
- [81] W. M. Haddad, V. Chellaboina, J. R. Corrado, and D. S. Bernstein, “Robust fixed-structure controller synthesis using the implicit small-gain bound,” *Journal of the Franklin Institute*, vol. 337, no. 1, pp. 85–96, 2000.
- [82] J. R. Corrado and W. M. Haddad, “Improving robust controller performance via multi-objective fixed-structure controller design,” vol. 1, pp. 487–492, 2002.

-
- [83] W. M. Haddad, J. R. Corrado, and A. Leonessa, “Fixed-order dynamic compensation for axial flow compression systems,” *IEEE Transactions on Control Systems Technology*, vol. 10, no. 5, pp. 727–734, 2002.
- [84] P. Apkarian and N. Dominikus, “Nonsmooth H_∞ synthesis,” *IEEE Transactions on Automatic Control*, vol. 51, no. 1, pp. 71–86, 2006.
- [85] P. Apkarian and D. Noll, “Nonsmooth optimization for multidisk H_∞ synthesis,” *European Journal of Control*, vol. 12, no. 3, pp. 229 – 244, 2006.
- [86] V. Bompard, P. Apkarian, and D. Noll, “Non-smooth techniques for stabilizing linear systems,” in *the Proceedings of the American Control Conference*, pp. 1245–1250, 2007.
- [87] P. Apkarian, D. Noll, and A. Rondepierre, “Mixed H_2/H_∞ control via nonsmooth optimization,” *SIAM Journal on Control and Optimization*, vol. 47, no. 3, pp. 1516–1546, 2008.
- [88] A. S. Lewis and M. L. Overton, “Behavior of BFGS with an exact line search on nonsmooth examples.”
- [89] A. S. Lewis and M. L. Overton, “Nonsmooth optimization via quasi-Newton methods,” *Mathematical Programming*, vol. 141, no. 1-2, pp. 135–163, 2013.
- [90] J. Burke, D. Henrion, A. Lewis, and M. Overton, “HIFOO—a MATLAB package for fixed-order controller design and H_∞ optimization,” in *the Proceedings*

- of the fifth IFAC Symposium on Robust Control Design, Toulouse, 2006.*
- [91] J. V. Burke, D. Henrion, A. S. Lewis, and M. L. Overton, “Stabilization via nonsmooth, nonconvex optimization,” *IEEE Transactions on Automatic Control*, vol. 51, no. 11, pp. 1760–1769, 2006.
- [92] S. Gumussoy, D. Henrion, M. Millstone, and M. L. Overton, “Multiobjective robust control with HIFOO 2.0,” *arXiv preprint arXiv:0905.3229*, 2009.
- [93] R. Herzog, P. Buhler, C. Gahler, and R. Larsonneur, “Unbalance compensation using generalized notch filters in the multivariable feedback of magnetic bearings,” *IEEE Transactions on Control Systems Technology*, vol. 4, no. 5, pp. 580–586, 1996.
- [94] P. Schroder, B. Green, N. Grum, and P. J. Fleming, “On-line evolution of robust control systems: an industrial active magnetic bearing application,” *Control Engineering Practice*, vol. 9, no. 1, pp. 37 – 49, 2001.
- [95] J. Shi, R. Zmood, and L. Qin, “Synchronous disturbance attenuation in magnetic bearing systems using adaptive compensating signals,” *Control Engineering Practice*, vol. 12, no. 3, pp. 283 – 290, 2004.
- [96] J. Shi and W. S. Lee, *Design and Implementation of Conventional and Advanced Controllers for Magnetic Bearing System Stabilization*. Bostjan Polajzer (Ed.), 2010.

-
- [97] A. Mystkowski, “ μ -synthesis control of flexible modes of AMB rotor,” in *Conference on Smart Materials, Adaptive Structures and Intelligent Systems*, pp. 357–363, 2009.
- [98] H. L. Chang and T.-C. Tsao, “Repetitive control of a levitated shaft-FPGA implementation based on Powell-Chau filters,” in *the Proceedings of International Symposium on Flexible Automation*, pp. 1–8, 2010.
- [99] I. Arredondo and J. Jugo, “2-DOF controller design for precise positioning a spindle levitated with active magnetic bearings,” *European Journal of Control*, vol. 18, no. 2, pp. 194 – 206, 2012.
- [100] L. Di and Z. Lin, “Control of a flexible rotor active magnetic bearing test rig: a characteristic model based all-coefficient adaptive control approach,” *Control Theory and Technology*, vol. 12, no. 1, pp. 1–12, 2014.
- [101] C. Wei and D. Soffker, “Optimization strategy for PID-controller design of AMB rotor systems,” *IEEE Transactions on Control Systems Technology*, DOI: 10.1109/TCST.2015.2476780, 2015.
- [102] S. E. Mushi, Z. Lin, and P. E. Allaire, “Stability analysis for a flexible rotor on active magnetic bearings subject to aerodynamic loads,” in *the Proceedings of the 12th international symposium on magnetic bearings*, pp. 22–25, 2010.
- [103] A. C. Wroblewski, J. T. Sawicki, and A. H. Pesch, “Rotor model updating

- and validation for an active magnetic bearing based high-speed machining spindle,” *Journal of Engineering for Gas Turbines and Power*, vol. 134, no. 12, pp. 1–6, 2012.
- [104] B. J. E. Misgeld, D. Rschen, S. Schwandtner, S. Heinke, M. Walter, and S. Leonhardt, “Robust decentralised control of a hydrodynamic human circulatory system simulator,” *Biomedical Signal Processing and Control*, vol. 20, pp. 35–44, 2015.
- [105] Z. Chen, B. Yao, and Q. Wang, “ μ -synthesis-based adaptive robust control of linear motor driven stages with high-frequency dynamics: A case study,” *IEEE/ASME Transactions on Mechatronics*, vol. 20, no. 3, pp. 1482–1490, 2015.
- [106] A. Falcoz, C. Pittet, S. Bennani, A. Guignard, C. Bayart, and B. Frapard, “Systematic design methods of robust and structured controllers for satellites,” *CEAS Space Journal*, vol. 7, no. 3, pp. 319–334, 2015.
- [107] G. Stein and J. C. Doyle, “Beyond singular values and loop shapes,” *Journal of Guidance, Control, and Dynamics*, vol. 14, no. 1, pp. 5–16, 1991.
- [108] A. Packard, J. Doyle, and G. Balas, “Linear, multivariable robust control with a μ perspective,” *Journal of dynamic systems, measurement, and control*, vol. 115, no. 2B, pp. 426–438, 1993.

-
- [109] M. K. H. Fan, A. L. Tits, and J. C. Doyle, "Robustness in the presence of mixed parametric uncertainty and unmodeled dynamics," *IEEE Transactions on Automatic Control*, vol. 36, no. 1, pp. 25–38, 1991.
- [110] A. Packard and J. Doyle, "The complex structured singular value," *Automatica*, vol. 29, no. 1, pp. 71–109, 1993.
- [111] P. Shi, X. Luan, and C. Liu, " H_∞ filtering for discrete-time systems with stochastic incomplete measurement and mixed delays," *IEEE Transactions on Industrial Electronics*, vol. 59, no. 6, pp. 2732–2739, 2012.
- [112] J. Wu, H. R. Karimi, and P. Shi, "Network-based H_∞ output feedback control for uncertain stochastic systems," *Information Sciences*, vol. 232, pp. 397 – 410, 2013.
- [113] M. Liu, L. Zhang, P. Shi, and H. R. Karimi, "Robust control of stochastic systems against bounded disturbances with application to flight control," *IEEE Transactions on Industrial Electronics*, vol. 61, no. 3, pp. 1504–1515, 2014.
- [114] D.-W. Gu, P. H. Petkov, and M. M. Konstantinov, *Robust control design with MATLAB®*, vol. 1. Springer Science & Business Media, 2005.
- [115] P. Apkarian, "Nonsmooth μ -synthesis," *International Journal of Robust and Nonlinear Control*, vol. 21, no. 13, pp. 1493–1508, 2011.

-
- [116] P. Apkarian and D. Noll, "Nonsmooth H_∞ synthesis," *IEEE Transactions on Automatic Control*, vol. 51, no. 1, pp. 71–86, 2006.
- [117] A. Noshadi, J. Shi, W. S. Lee, P. Shi, and A. Kalam, "High performance H_∞ control of non-minimum phase active magnetic bearing system," in *the Proceedings of the 40th Annual Conference of IEEE Industrial Electronics*, pp. 183–189, 2014.
- [118] "The MathWorks, Robust Control Toolbox Version 3.5, Matlab R2010b," 2010.
- [119] "The MathWorks, Robust Control Toolbox 5.2, Matlab R2014b," 2014.
- [120] G. Mann, B.-G. Hu, and R. Gosine, "Two-level tuning of fuzzy PID controllers," *IEEE Transactions on Systems, Man, and Cybernetics, Part B: Cybernetics*, vol. 31, no. 2, pp. 263–269, 2001.
- [121] A. Noshadi, J. Shi, S. Poolton, W. Lee, and A. Kalam, "Comprehensive experimental study on the stabilization of active magnetic bearing system," in *the Proceedings of Australasian Universities Power Engineering Conference*, pp. 1–7, 2014.
- [122] E. Harinath and G. Mann, "Design and tuning of standard additive model based fuzzy PID controllers for multivariable process systems," *IEEE Transactions on Systems, Man, and Cybernetics, Part B: Cybernetics*, vol. 38, no. 3,

- pp. 667–674, 2008.
- [123] A. Vick and K. Cohen, “Longitudinal stability augmentation using a fuzzy logic based PID controller,” in *the Proceedings of Annual Meeting of the North American Fuzzy Information Processing Society*, pp. 1–6, 2009.
- [124] D. Wolpert and W. Macready, “No free lunch theorems for optimization,” *IEEE Transactions on Evolutionary Computation*, vol. 1, pp. 67–82, Apr 1997.
- [125] J. Shi, A. Kalam, A. Noshadi, and P. Shi, “Genetic algorithm optimised fuzzy control of DSTATCOM for improving power quality,” in *the Proceedings of Australasian Universities Power Engineering Conference*, pp. 1–6, 2014.
- [126] A. Zolfagharian, A. Noshadi, M. R. Khosravani, and M. Z. M. Zain, “Unwanted noise and vibration control using finite element analysis and artificial intelligence,” *Applied Mathematical Modelling*, vol. 38, no. 9, pp. 2435–2453, 2014.
- [127] J. Kennedy and R. Eberhart, “Particle swarm optimization,” in *the Proceedings of IEEE International Conference on Neural Networks*, pp. 1942–1948, 1995.
- [128] Y. Shi and R. Eberhart, “A modified particle swarm optimizer,” in *the Proceedings of IEEE International Conference on Evolutionary Computation*,

- pp. 69–73, 1998.
- [129] S. Mirjalili, S. M. Mirjalili, and A. Lewis, “Grey wolf optimizer,” *Advances in Engineering Software*, vol. 69, pp. 46 – 61, 2014.
- [130] S. Saremi, S. Mirjalili, and S. Mirjalili, “Evolutionary population dynamics and grey wolf optimizer,” *Neural Computing and Applications*, pp. 1–7, 2014.
- [131] J. Shi, A. Noshadi, A. Kalam, and P. Shi, “Fuzzy logic control of DSTATCOM for improving power quality and dynamic performance,” in *the Proceedings of Australasian Universities Power Engineering Conference*, pp. 1–6, 2015.
- [132] E. Atashpaz-Gargari and C. Lucas, “Imperialist competitive algorithm: an algorithm for optimization inspired by imperialistic competition,” in *the Proceedins of IEEE Congress of Evolutionary Computation*, pp. 4661–4667, 2007.
- [133] R. Rajabioun, E. Atashpaz-Gargari, and C. Lucas, “Colonial competitive algorithm as a tool for nash equilibrium point achievement,” in *Computational Science and its Applications*, pp. 680–695, Springer, 2008.
- [134] D. Xue, Y. Chen, and D. P. Atherton, *Linear feedback control: analysis and design with MATLAB*, vol. 14. Siam, 2007.
- [135] C. R. Knospe, R. Hope, S. J. Fedigan, and R. D. Williams, “Experiments in the control of unbalance response using magnetic bearings,” *Mechatronics*,

- vol. 5, no. 4, pp. 385 – 400, 1995.
- [136] J. Fang, X. Xu, and J. Xie, “Active vibration control of rotor imbalance in active magnetic bearing systems,” *Journal of Vibration and Control*, vol. 21, no. 4, pp. 648–700, 2013.
- [137] F. Wu, “Switching LPV control design for magnetic bearing systems,” in *the Proceedings of IEEE International Conference on Control Applications*, pp. 41–46, 2001.
- [138] Y. Lee, S.-H. Lee, D. Shin, W. Kim, and C. C. Chung, “Position control of active magnetic bearings using linear parameter varying synthesis,” in *the Proceedings of 13th International Conference on Control, Automation and Systems*, pp. 5–10, 2013.
- [139] E. Schrijver and J. Van Dijk, “Disturbance observers for rigid mechanical systems: Equivalence, stability, and design,” *Journal of Dynamic Systems Measurement and Control*, vol. 124, no. 4, pp. 539–548, 2002.
- [140] X. Chen and M. Tomizuka, “New repetitive control with improved steady-state performance and accelerated transient,” *IEEE Transactions on Control Systems Technology*, vol. 22, no. 2, pp. 664–675, 2014.
- [141] Y. I. Son, G. J. Jeong, and I. H. Kim, “Disturbance observer based position control of a one-link manipulator under input time delay,” *International*

- Journal of Innovative Computing, Information and Control*, vol. 8, no. 2, pp. 1371–1384, 2012.
- [142] R. Zhang, T. Li, and L. Guo, “Disturbance observer based H_∞ control for flexible spacecraft with time-varying input delay,” *Advances in Difference Equations*, pp. 1–12, 2013.
- [143] J. Yang, S. H. Li, X. S. Chen, and Q. Li, “Disturbance rejection of ball mill grinding circuits using DOB and MPC,” *Powder Technology*, vol. 198, no. 2, pp. 219–228, 2010.
- [144] J. Yang, A. Zolotas, W. Chen, K. Michail, and S. Li, “Disturbance observer based control for nonlinear MAGLEV suspension system,” in *the Proceedings of 2010 Conference on Control and Fault-Tolerant Systems*, pp. 281–286, 2010.
- [145] J. Yang, A. Zolotas, W. H. Chen, K. Michail, and S. H. Li, “Robust control of nonlinear MAGLEV suspension system with mismatched uncertainties via DOBC approach,” *ISA Transactions*, vol. 50, no. 3, pp. 389–396, 2011.
- [146] J. Yang, S. H. Li, and X. H. Yu, “Sliding-mode control for systems with mismatched uncertainties via a disturbance observer,” *IEEE Transactions on Industrial Electronics*, vol. 60, no. 1, pp. 160–169, 2013.
- [147] A. Noshadi, M. Mailah, and A. Zolfagharian, “Active force control of 3-RRR

- planar parallel manipulator,” in *the Proceedings of the 2nd International Conference on Mechanical and Electrical Technology*, pp. 77–81, 2010.
- [148] A. Noshadi, M. Mailah, and A. Zolfagharian, “Intelligent active force control of a 3-RRR parallel manipulator incorporating fuzzy resolved acceleration control,” *Applied Mathematical Modelling*, vol. 36, no. 6, pp. 2370–2383, 2012.
- [149] A. Noshadi and M. Mailah, “Active disturbance rejection control of a parallel manipulator with self learning algorithm for a pulsating trajectory tracking task,” *Scientia Iranica*, vol. 19, no. 1, pp. 132–141, 2012.
- [150] C. C. Wang and M. Tomizuka, “Design of robustly stable disturbance observers based on closed loop consideration using H_∞ optimization and its applications to motion control systems,” in *the Proceedings of American Control Conference*, pp. 3764–3769, 2004.
- [151] B. A. Guvenc, L. Guvenc, and S. Karaman, “Robust MIMO disturbance observer analysis and design with application to active car steering,” *International Journal of Robust and Nonlinear Control*, vol. 20, no. 8, pp. 873–891, 2010.
- [152] J. N. Yun, J. B. Su, Y. I. Kim, and Y. C. Kim, “Robust disturbance observer for two-inertia system,” *IEEE Transactions on Industrial Electronics*, vol. 60, no. 7, pp. 2700–2710, 2013.

- [153] H. Shim and N. H. Jo, “An almost necessary and sufficient condition for robust stability of closed-loop systems with disturbance observer,” *Automatica*, vol. 45, no. 1, pp. 296–299, 2009.
- [154] A. Noshadi, J. Shi, W. S. Lee, P. Shi, and A. Kalam, “Repetitive disturbance observer-based control for an active magnetic bearing system,” in *the Proceedings of Australian Control Conference*, 2015.
- [155] K. Chew and M. Tomizuka, “Digital control of repetitive errors in disk drive systems,” *IEEE Control Systems Magazine*, vol. 10, no. 1, pp. 16–20, 1990.
- [156] X. Chen and M. Tomizuka, “An enhanced repetitive control algorithm using the structure of disturbance observer,” in *the Proceedings of IEEE/ASME International Conference on Advanced Intelligent Mechatronics*, pp. 490–495, 2012.
- [157] C. Kang and T. C. Tsao, “Control of magnetic bearings with plug-in time-varying harmonic resonators,” in *the Proceedings of American Control Conference*, pp. 4237–4242, 2014.
- [158] L. Zhou, J. She, M. Wu, Y. He, and S. Zhou, “Estimation and rejection of aperiodic disturbance in a modified repetitive-control system,” *IET Control Theory and Applications*, vol. 8, no. 10, pp. 882–889, 2014.
- [159] X. Chen and M. Tomizuka, “Overview and new results in disturbance observer

- based adaptive vibration rejection with application to advanced manufacturing,” *International Journal of Adaptive Control and Signal Processing*, 2015.
- [160] A. Lanzon, A. Lecchini, A. Dehghani, and B. D. Anderson, “Checking if controllers are stabilizing using closed-loop data,” in *the Proceedings of 45th IEEE Conference on Decision and Control*, pp. 3660–3665, 2006.
- [161] A. Dehghani, A. Lecchini-Visintini, A. Lanzon, and B. D. Anderson, “Validating controllers for internal stability utilizing closed-loop data,” *IEEE Transactions on Automatic Control*, vol. 54, no. 11, pp. 2719–2725, 2009.
- [162] A. Dehghani, B. D. Anderson, and S. H. Cha, “Verifying closed-loop performance before inserting a new controller,” in *the Proceedings of American Control Conference*, pp. 4022–4027, 2010.
- [163] S. H. Cha, A. Dehghani, W. Chen, and B. Anderson, “Verifying stabilizing controllers for performance improvement using closed-loop data,” *International Journal of Adaptive Control and Signal Processing*, vol. 28, no. 2, pp. 121–137, 2014.
- [164] M. Campi, W. S. Lee, and B. Anderson, “New filters for internal model control design,” *International Journal of Robust and Nonlinear Control*, vol. 4, no. 6, pp. 757–775, 1994.

- [165] A. Dehghani, A. Lanzon, and B. D. Anderson, “An H_∞ model referencing design utilizing a two degree of freedom controller scheme,” in *the Proceedings of the 44th IEEE Conference on Decision and Control*, pp. 2302–2307, 2005.
- [166] D. Hoyle, R. Hyde, and D. Limebeer, “An H_∞ approach to two degree of freedom design,” in *the Proceedings of the 30th IEEE Conference on Decision and Control*, pp. 1581–1585, 1991.
- [167] D. McFarlane and K. Glover, “A loop-shaping design procedure using H_∞ synthesis,” *IEEE Transactions on Automatic Control*, vol. 37, no. 6, pp. 759–769, 1992.
- [168] D. J. Limebeer, E. Kasenally, and J. Perkins, “On the design of robust two degree of freedom controllers,” *Automatica*, vol. 29, no. 1, pp. 157–168, 1993.
- [169] E. Lavretsky and K. Wise, *Robust and adaptive control with aerospace applications*. Springer Science & Business Media, 2012.
- [170] J. P. Hespanha, *Linear systems theory*. Princeton university press, 2009.
- [171] B. Zhou, Z. Lin, and G.-R. Duan, “A parametric lyapunov equation approach to low gain feedback design for discrete-time systems,” *Automatica*, vol. 45, no. 1, pp. 238 – 244, 2009.
- [172] N. Morse, R. Smith, and B. Paden, *Analytical modeling of a magnetic bearing system, MBC500 magnetic system operating instructions*. 1996.

-
- [173] L. Matthias, *Solutions to Magnetic Bearing Lab, University of Calgary*. 2004.
- [174] S.-L. Chen, “Nonlinear smooth feedback control of a three-pole active magnetic bearing system,” *IEEE Transactions on Control Systems Technology*, vol. 19, pp. 615–621, May 2011.
- [175] S. Darbandi, M. Behzad, H. Salarieh, and H. Mehdigholi, “Linear output feedback control of a three-pole magnetic bearing,” *IEEE/ASME Transactions on Mechatronics*, vol. 19, pp. 1323–1330, Aug 2014.
- [176] S. Mahdi Darbandi, M. Behzad, H. Salarieh, and H. Mehdigholi, “Harmonic disturbance attenuation in a three-pole active magnetic bearing test rig using a modified notch filter,” *Journal of Vibration and Control*, DOI: 10.1177/1077546315586494, 2015.
- [177] J. Mendel, R. John, and F. Liu, “Interval type-2 fuzzy logic systems made simple,” *IEEE Transactions on Fuzzy Systems*, vol. 14, no. 6, pp. 808–821, 2006.
- [178] L. Wu, X. Su, and P. Shi, “Model approximation of continuous-time T-S fuzzy stochastic systems,” in *Fuzzy Control Systems with Time-Delay and Stochastic Perturbation*, vol. 12 of *Studies in Systems, Decision and Control*, pp. 269–286, Springer International Publishing, 2015.
- [179] M. Narimani and H. Lam, “Relaxed LMI-based stability conditions for Takagi-

- Sugeno fuzzy control systems using regional-membership-function-shape-dependent analysis approach,” *IEEE Transactions on Fuzzy Systems*, vol. 17, no. 5, pp. 1221–1228, 2009.
- [180] M. Narimani and H. Lam, “SOS-based stability analysis of polynomial fuzzy-model-based control systems via polynomial membership functions,” *IEEE Transactions on Fuzzy Systems*, vol. 18, no. 5, pp. 862–871, 2010.
- [181] M. Narimani, H. Lam, R. Dilmaghani, and C. Wolfe, “LMI-based stability analysis of fuzzy-model-based control systems using approximated polynomial membership functions,” *IEEE Transactions on Systems, Man, and Cybernetics, Part B: Cybernetics*, vol. 41, no. 3, pp. 713–724, 2011.
- [182] H. Lam, M. Narimani, H. Li, and H. Liu, “Stability analysis of polynomial-fuzzy-model-based control systems using switching polynomial Lyapunov function,” *IEEE Transactions on Fuzzy Systems*, vol. 21, no. 5, pp. 800–813, 2013.
- [183] H. Li, C. Wu, P. Shi, and Y. Gao, “Control of nonlinear networked systems with packet dropouts: Interval type-2 fuzzy model-based approach,” *IEEE Transactions on Cybernetics*, vol. 45, no. 11, pp. 2378–2389, 2015.
- [184] M. Abusara, S. Sharkh, and P. Zanchetta, “Adaptive repetitive control with feedforward scheme for grid-connected inverters,” *IET Power Electronics*, vol. 8, no. 8, pp. 1403–1410, 2015.

-
- [185] S. Fekri, M. Athans, and A. Pascoal, “Issues, progress and new results in robust adaptive control,” *International Journal of Adaptive Control and Signal Processing*, vol. 20, no. 10, pp. 519–579, 2006.
- [186] M. Kuipers and P. Ioannou, “Multiple model adaptive control with mixing,” *IEEE Transactions on Automatic Control*, vol. 55, no. 8, pp. 1822–1836, 2010.
- [187] B. D. Anderson and A. Dehghani, “Challenges of adaptive control past, permanent and future,” *Annual Reviews in Control*, vol. 32, no. 2, pp. 123 – 135, 2008.
- [188] M. Stefanovic and M. Safonov, “Safe adaptive switching control: Stability and convergence,” *IEEE Transactions on Automatic Control*, vol. 53, no. 9, pp. 2012–2021, 2008.
- [189] S. Baldi, G. Battistelli, E. Mosca, and P. Tesi, “Multi-model unfalsified adaptive switching supervisory control,” *Automatica*, vol. 46, no. 2, pp. 249 – 259, 2010.
- [190] H. Jin, M. W. Chang, and M. G. Safonov, “Unfalsifying pole locations using a fading memory cost function,” *Asian Journal of Control*, vol. 16, no. 6, pp. 1583–1591, 2014.